MAGNETIC ANISOTROPY ENERGY

BY IMSEOK YANG

A dissertation submitted to the
Graduate School—New Brunswick
Rutgers, The State University of New Jersey
in partial fulfillment of the requirements
for the degree of
Doctor of Philosophy
Graduate Program in Physics and Astronomy
Written under the direction of
Professor Gabriel B. Kotliar
and approved by

_____

_____

_____

_____

_____

New Brunswick, New Jersey

June , 2001

ABSTRACT OF THE DISSERTATION

Magnetic Anisotropy Energy

by Imseok Yang

Dissertation Director: Professor Gabriel B. Kotliar

We calculate magnetic anisotropy energy of Fe and Ni by taking into account the effects of strong electronic correlations, spin-orbit coupling, and non-collinearity of intra-atomic magnetization. The LDA+U method is used and its equivalence to dynamical mean–field theory in the static limit is emphasized. Both experimental magnitude of MAE and direction of magnetization are predicted correctly near $U = 4\ eV$ for Ni and $U = 3.5\ eV$ for Fe. Correlations modify one–electron spectra which are now in better agreement with experiments.

Acknowledgements

I am grateful to my adviser, Gabriel Kotliar for providing guidance, direction for my research over the last few years, and his helps at every difficult time. Special thanks go also to Sergej Y. Savrasov whose help was crucial in bringing this work to conclusion.

I would moreover like to thank Willem Kloet, Peter Lindenfeld, Andrei Ruckenstein and Sergej Savrasov for acting as members of my Ph.D. committee.

Thanks to my many friends here at Rutgers, Milos Milosavljevic, Keunhyuk Ahn, Makoto Taniguchi, Venkateswara (Venky) Sarma Kancharla, Balakrishna Subramanian, Gunnar Palsson, Ekkehard Lange, Victor Oudovenko and Alexander Poteryaev for enjoyable, interesting, and at times fruitful discussions.

Special thanks go to people in Korea for their endless help over the difficult times.

To my parents, Jungho Yang and Pokryun Kim, whose support was an essential part in completing this thesis.

Special thanks go to my younger brother. Without his generous assumption of my duty, this thesis would not be able to see the light.

Finally my deepest love goes to my wonderful wife, Hyunyoung, whose loving care, wit and strength has been an endless source of inspiration and confidence.

Dedication

I dedicate this thesis to my father, a construction site worker.

Table of Contents

Part I

Study of Magnetic Anisotropy using Local Spin Density Approximation with Strong Correlation

Chapter 1

Introduction

One of the long-standing problems that are still short of detailed understanding is to explain the magneto-crystalline anisotropy energy of magnetic materials containing transition-metal elements, especially that of Fe, Co, and Ni. The magneto-crystalline anisotropy or magnetic anisotropy energy (MAE) is the energy difference of ground states with different directions of magnetic moments. This is the driving force determining the direction of magnetic moment of ground state without external magnetic fields. The primary difficulty toward investigating MAE has been attributed to the fact that the MAEs of the metals are as small as of the order of 1 μeV/atom. At low temperature ($T = 4.2K$), MAE is of the order of 60 μeV/atom for hcp Co, 2.7μeV/atom for fcc Ni, and 1.4 μeV/atom for bcc Fe.

With advances in the accurate total energy method combined with the development of faster computers, attempts have been made to calculate MAEs from first-principles for bulk crystalline Fe, Co, and Ni. While the magnitude of the MAEs have been predicted for all the three metals, the correct easy axis for Ni has not been predicted so far. Here we present new results that predict the correct easy axis for Ni as well as reproduce the previous results in relevant limits. We also suggest why the previous approaches have failed in obtaining the correct easy axis for Ni.

Magnetic anisotropy is the dependency of internal energy on the direction of spontaneous magnetization. Generally, the magnetic anisotropy energy term possesses the symmetry of the crystal. It is therefore called magneto-crystalline anisotropy or crystal magnetic anisotropy. In transition metals, most of the magnetic moment comes from spin polarization. Within the non-relativistic approach, there is no term coupling to the spin degrees of freedom. The magnetic moment, therefore, can points

to an arbitrary direction. The magnetic anisotropy energy is an relativistic phenomenon, say spin-orbit coupling. With spin-orbit coupling, the spin degrees of freedom interact with the spatial anisotropy through the coupling to the orbital degrees of freedom. This induces a preferred direction of spins. This happens even though the total angular momentum is completely quenched. Since spin-orbit coupling couples individual spin degrees of freedom to individual orbital degrees of freedom, the fact that total orbital magnetic moment is quenched does not affect the visibility of spatial anisotropy to magnetic moment.

Early attempts to explain magnetic anisotropy are based on the interaction between the magnetization and the lattice through spin-orbit coupling combined with band theory [1]. Later, Brooks [2] used an itinerant electron model and orbital angular momentum quenching in cubic crystals to explain MAE. Treating the spin-orbit coupling as a perturbation, the nontrivial magnetic anisotropy came out at the fourth-order. The correct directions of magnetization were obtained for Fe and Ni. The difference of these metals' easy axes was attributed to the different lattice structures of them. Based on the Ni-Fe alloy data, however, a much closer correlation between the anisotropy and the number of valence electrons was observed. What is the factor that determines the easy axis has been another unanswered question since then. In subsequent papers [3, 4, 5] the calculations became more and more refined. Finally the discussion centered around the importance of degenerate states along symmetry lines in the Brillouin zone and plausible explanations of the origin of magnetic anisotropy were provided [6, 7].

Contemporary studies of magnetic anisotropy energy have centered on first-principle calculations, using density functional theory [8] within the framework of local spin density approximation (LSDA). Eckardt, Fritsche, and Noffke [9] were able to get the values of the right order of magnitude for Fe and Ni, but with incorrect easy axis for Fe. Daalderop, Kelly, and Schuurmans [10] used the force theorem [11] to obtain correct order of magnitude of the MAEs for Fe, Co, and Ni, but incorrect easy axes were found for Co, and Ni. They also observed that changing the number of valence electrons would restore the correct easy axis. This observation is similar to Brooks'

observation of close correlation bewteen the direction of magnetic moment and the number of valence electrons. Trygg, Johansson, Eriksson, and Willis [12] improved the method while using fully self-consistent approach. Orbital polarization was also incorporated, which was suggested by Jansen [13]. While the correct easy axis was obtained for Co and Fe, in case of Ni the calculation still gave the wrong easy axis. This the best result before the current work. Schneider, Erickson, and Jansen [14] used torque instead of energy difference to obtain the same result as that of Trygg, Johansson, Eriksson, and Willis. They also treated the spin-orbit coupling constant as an adjustable parameter. They succeeded in restoring the correct easy axis for Ni with an unphysically large value of spin-orbit coupling. This work suggested a close relation between magnetic anisotropy energy and the strength of spin-orbit coupling.

We believe that the physics of transition metal compounds is intermediate between atomic limit where the localized d electrons are treated in the real space and fully itinerant limit when the electrons are described by band theory in k space. A many–body method incorporating these two important limits is the dynamical mean–field theory (DMFT) [15]. The DMFT approach has been extensively used to study model Hamiltonian of correlated electron systems in the weak, strong and intermediate coupling regimes. It has been very successful in describing the physics of realistic systems, like the transition metal oxides and, therefore, is expected to treat properly the materials with d or f electrons.

We take a new view that the correlation effects within the d shell are important for the magnetic anisotropy of $3d$ transition metals like Ni. These effects are not captured by the LDA but are described by Hubbard–like interactions presented in these systems and need to be treated by an extension of first principles methods such as LDA+U [16]. Since, DMFT reduces to LDA+U in static limit, we adopt LDA+U method to attack the problem of magnetic anosotropy of $3d$ transition metals.

The LDA+U method has been very successful compared with experiments at zero temperature in ordered compounds. By establishing its equivalence to the static limit of the DMFT we establish a sound theoretical ground for LDA+U. We also see clearly that dynamical mean–field theory is a way of improving upon it, which is crucial for

finite temperature properties.

Another effect which has not been investigated in the context of magnetic anisotropy calculations is the non-collinear nature of intra-atomic magnetization [17]. It is expected to be important when spin-orbit coupling and correlation effects come into play together. We show that when we include these new ingredients into the calculation we solve the long-standing problem of predicting the correct easy axis of Ni.

Chapter 2

Overview of Magnetic Anisotropy

2.1 Experiments

In this section, we briefly overview experimental methods and results. The simplest form of crystal magnetic anisotropy is uniaxial anisotropy, for example, in hexagonal cobalt with easy direction parallel to the c axis of the crystal at room temperature. As the internal magnetization rotates away from the c axis, the anisotropy energy increases with increase of ϕ, where ϕ is the angle between the c axis and the internal magnetization. We can expand this energy in a series of powers of $\sin^2\phi$:

$$E_a = K_1 \sin^2\phi + K_2 \sin^4\phi + \cdots , \tag{2.1}$$

where K_1 and K_2 are constants.

For cubic crystals such as iron and nickel, the anisotropy energy can be expressed in terms of the directional cosines $(\alpha_1, \alpha_2, \alpha_3)$ of the internal magnetization with respect to the three cubic edges. Because of the high symmetry of the cubic crystal, the anisotropy energy can be expressed in a fairly simple way:

$$E_a = K_1 \left(\alpha_1^2\alpha_2^2 + \alpha_2^2\alpha_3^3 + \alpha_3^2\alpha_1^2\right) + K_2 \left(\alpha_1^2\alpha_2^2\alpha_3^2\right) + \cdots , \tag{2.2}$$

where K_1 and K_2 are constants.

In experiment, torque is measured instead of total energy. The torque measured at various angles are interpolated to a corresponding analytic expression such as angular derivatives of Eqs. 2.1 and 2.2. The constants K_n obtained in this interpolation is substituted back to get the expression for the total energy. Magnetic anisotropy energy is calculated by subtracting energies at two different energy, e.g. [001] and [111] (See Fig. 2.1).

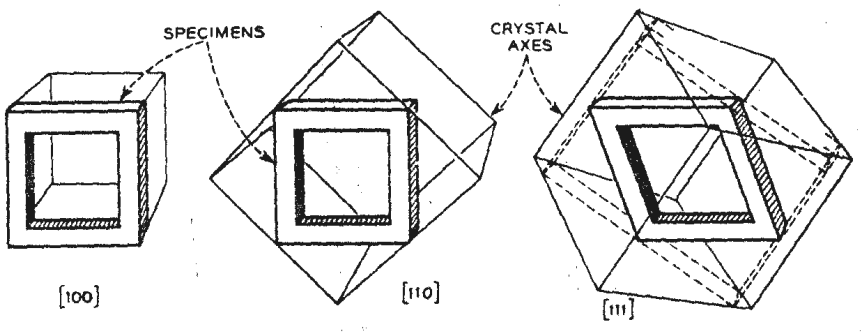

Figure 2.1: Three basic directions of magnetization in cubic crystal. The specimens are used to determine magnetization in [100]. [110], and [111] directions. Specimens are cut in the form of hollow parallelogram or "picture frame". The purpose of this form is to provide a closed magnetic circuit so that the uncertainty of a demagnetizing factor can be obviated. In a cubic crystal, a parallelogram can always be constructed so that each side is parallel to a direction of the form $< hkl >$, the sides being, for example, $[hkl]$, $[hlk]$, $[\bar{h}\bar{h}\bar{l}]$, and $[\bar{h}\bar{l}\bar{k}]$.

To measure torque, specimens are formed into short cylinders, and measurement of torque is made as shown in Fig. 2.2. The specimens are mounted in a carriage held by two torsion fibers that are fastened to a rigid support at the top and to a circular scale S at the bottom. When the field is excited in the electromagnet, the crystal tends to turn so that the direction of easy magnetization is parallel to the field. The torque so produced is balanced by turning the bottom of the lower fiber until the crystal regains its original orientation as determined by reflection of a light beam from the mirror. The scale reading S_2 is then compared with the original reading S_1 with $H = 0$. $S_2 - S_1$ is a measure of the torque. The orientation of the crystal axes with respect to the applied field is varied by turning the electromagnet, which is mounted on a heavy bearing, and noting its position on a suitable scale, S'. One then plots the torque against the crystal orientation and deduces from the curve the crystal anisotropy constant K_n.

2.2 Cubic Symmetry

We shall deal mainly with cubic crystal. A digression to cubic group is presented here. Cubic group has five irreducible representations with dimensions $l_1, \cdots, l_5$, where

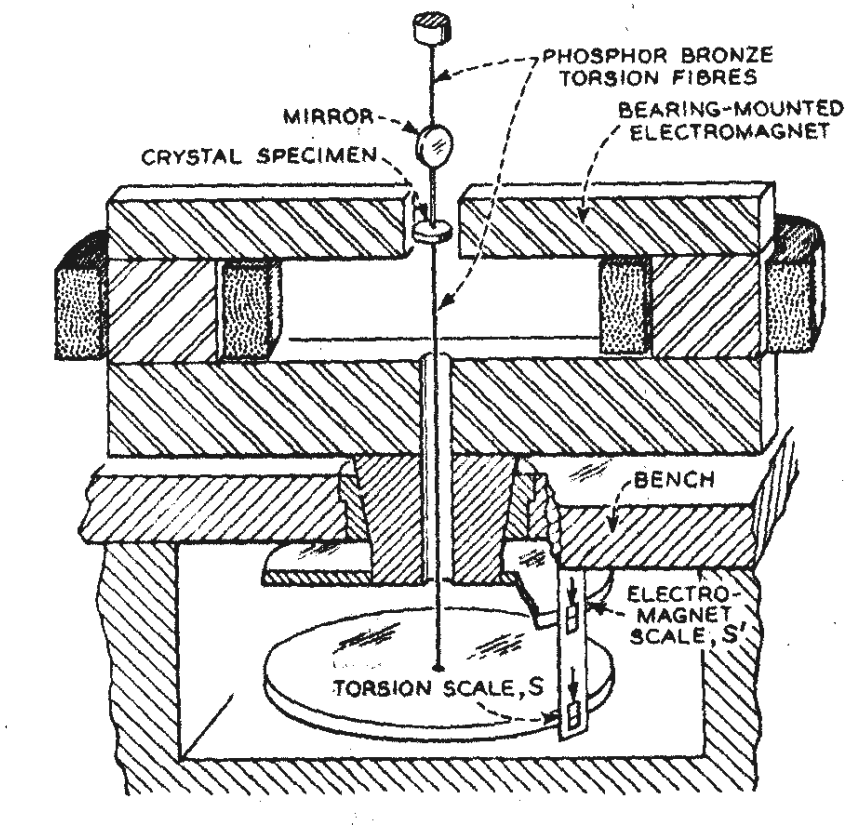

Figure 2.2: Torque magnetometer. Electromagnet can be rotated so that the field is in any desired direction in the crystal specimen. The torque induced in the crystal is balanced by twisting the fiber a measured amount by means of the scale S' at the bottom

$l_1 = l_2 = 1$, $l_3 = 2$, and $l_4 = l_5 = 3$. The corresponding representations are denoted by Γ_1, Γ_2, Γ_3, Γ_4, Γ_5 or A_1, A_2, E, T_1, T_2. Under rotations of cubic group, Γ_1 rotates as $\{1\}$, Γ_2 as $\{xyz\}$, Γ_3 as $\{x^2 - y^2,\ 3z^2 - r^2\}$, Γ_4 as $\{x,\ y,\ z\}$, and Γ_5 as $\{xy,\ yz,\ zx\}$. In analogy with half integral angular momentum representation, cubic group has double cubic group as its 'covering group'. Double cubic group has eight irreducible representation. Five of them are the five irreducible representation of cubic group. The other three with dimensions $l_6 = 2$, $l_7 = 2$, $l_8 = 4$ are denoted by Γ_6, Γ_7, Γ_8 or E', E'', U. Under rotations of cubic group, Γ_6 rotates as the $J = 1/2$ representation of angular momentum, Γ_8 as $J = 3/2$ representation of angular momentum. The direct product $\Gamma_2 \times \Gamma_6$ is Γ_7, hence Γ_7 rotates as the product of xyz and $J = 1/2$ representation of angular momentum.

The calculation of matrix elements $\langle\alpha|V|\beta\rangle$, where α belong to Γ'' and β to Γ', is facilitated by irreducible decomposition of the direct product $\Gamma''^* \times \Gamma'$, or of $\Gamma'' \times \Gamma'$ because Γ can be made real. Without loss of generality, we can assume that V belongs to Γ. Non-zero elements arise only when the decomposition of the direct product contains one or more representation Γ, say Γ^a, Γ^b, $\cdots$, where $a,\ b,\ \cdots$ are indices to distinguish multiple Γ's. All the matrix elements are uniquely determined by group theory within proportionality factors c_a, c_b, $\cdots$: The decomposition of a direct product of rotation group representations contains each representation at most once. Thus, there is only one proportionality factor, which is the basis of Wigner-Eckart theorem. In case of cubic group, $\Gamma_4 \times \Gamma_8$ breaks into $\Gamma_6 + \Gamma_7 + 2\Gamma_8$ and $\Gamma_8 \times \Gamma_8$ into $\Gamma_1 + \Gamma_2 + \Gamma_3 + 2\Gamma_4 + 2\Gamma_5$. All the other direct products decomposes into a sum of representation containing each representation at most once. In the context of cubic group, a version of Wigner-Wickart theorem can be re-casted as: the magnetic moment can be written as $\vec{\mu} = \mu_B g \vec{J}$ for representations other than Γ_8, as $\vec{\mu} = \mu_B(g_1\vec{J} + g_3\vec{J^3})$ for representation Γ_8. Two more application are worth mentioning.

The Decompositions of direct products $\Gamma_4 \times \Gamma_4$ and $\Gamma_5 \times \Gamma_5$ have Γ_4 only once, hence all the matrix elements of a vector quantity are determined within proportionality factor. Since angular momentum is a vector, we can introduce a fictitious angular moment $\alpha\tilde{\vec{I}}$ with $\tilde{I} = 1$ and use it calculating matrix elements of a vector quantity with the manifold. Also note that the decomposition of $\Gamma_3 \times \Gamma_3$ does not contain Γ_4, hence a vector quantity does not have non-zero matrix elements. This is usually expressed by saying that the doublet is non-magnetic.

Another application to note is another way to applying Wigner-Eckart theorem to rotation group. Namely

$$\langle j''j''_m|T^l_{l_m}|j'j'_m\rangle = \langle j''j''_m|T'^l_{l_m}|j'j'_m\rangle, \tag{2.3}$$

where $T'^l_{l_m}$ has the same transformation property as T'_{l_m}. Cubic crystal field can be written as $A(20x^4 + 20y^4 + 20z^4 - 12r^4)$, which in turn is $A(P^4_0 + 5P^4_4)$, where P^l_m's are unnormalized homogeneous polynomial proportional to $r^l(Y^l_m + Y^{l\,*}_m)$. Therefore

we can use any operator $O_0^4 + O_4^4$ transforms in the same way as $P_0^4 + 5P_4^4$ to calculate the matrix elements up to overall factor. In total angular momentum representation, the proper orators O_0^4 and O_4^4 read

$$O_0^4 = 35J_z^4 - 30J(J+1)J_z^2 + 25J_z^2 - 6J(J+1) + 3J^2(J+1)^2 \quad (2.4)$$

$$O_4^4 = \frac{1}{2}(J_+^4 + J_-^4). \quad (2.5)$$

In orbital angular momentum representation, one only need to change $\vec{J}$ by $\vec{L}$.

2.3 Origin of Magnetic Anisotropy

In this section, we overview basic theory of magnetic anisotropy. Theories relevant to transition metals will be expanded in later sections.

The ordinary exchange energy and super-exchange energy have the form of the scalar products of two spins, and do not give rise to magnetic anisotropy energy. Two kinds of anisotropic interactions can be considered: one is the dipolar interaction between magnetic moments and the other is the anisotropic exchange interaction. The latter interaction is a combined effect of the spin-orbit coupling and the exchange interaction. This interaction was proposed by van Vleck [1] as an origin of magnetic anisotropy and is particularly important in ferromagnetic metals.

In addition to these two anisotropic interactions, the crystalline field acting on each magnetic ion produces anisotropy energy. Anisotropy in the g-factor usually found in paramagnetic salts is also a product of the anisotropy of the crystalline field.

Thus, the anisotropy energy can be considered to stem from three sources: magnetic dipolar interaction, anisotropic exchange interaction, and the anisotropy of the crystalline field. However, the effects of these three parts are quite different in different substances.

A brief description of magnetic anisotropy based on the atomic picture will be presented in what follows.

2.4 Intermediate Crystalline Field

When a free magnetic ion is brought into the crystalline electric field arising from the surrounding ions, the directional degeneracy of the angular momentum is removed—completely or partially—due to the crystalline Stark effect. We shall assume that spin-orbit coupling is small compared to the crystalline Stark effect, just as in $3d$ ions, and that the ground state is a singlet. In this limit, we can treat the spin $\vec{S}$ as a parameter. The unperturbed ground states can be any of the five representations of the cubic group.

2.4.1 Singlet Ground State

Ions in $3d^2$ (V^{3+}, Cr^{4+} in tetrahedral field). $3d^3$ (V^{2+}, Cr^{3+}, Mn^{4+} in octahedral field), $3d^7$ (Fe^{+}, Co^{2+}, Ni^{3+} in tetrahedral field), and $3d^8$ (Co^{+}, Ni^{2+}, Cu^{3+} in octahedral field) configuration have singlet ground state Γ_2. Denoting energy of the ground state by E_0, the unperturbed Hamiltonian can be written as

$$H_0 = E_0 + 2\mu_B \vec{S} \cdot \vec{H}, \tag{2.6}$$

where H is an external field. The perturbing Hamiltonian is

$$V = \lambda \vec{L} \cdot \vec{S} + \mu_B \vec{L} \cdot \vec{H}. \tag{2.7}$$

Since angular moment operator is a complex operator and the energy is real, the expectation value of angular moment of a singlet state is zero. The first order perturbation energy is therefore zero. The second order perturbation energy is

$$E_2 = -\sum_{i \neq 0} \frac{1}{E_i - E_0} \left| \sum_{\mu} \{\lambda \langle i|L_\mu|0\rangle S_\mu + \mu_B \langle i|L_\mu|0\rangle H_\mu\} \right|^2, \tag{2.8}$$

where indices μ and ν represent Cartesian coordinates x, y, and z. This can be written

$$E_2 = -2\lambda\mu_B \sum_{\mu,\nu} \Lambda_{\mu\nu} S_\mu H_\nu - \lambda^2 \sum_{\mu,\nu} \Lambda_{\mu\nu} S_\mu S_\nu - \mu_B^2 \sum_{\mu,\nu} \Lambda_{\mu\nu} H_\mu H_\nu, \tag{2.9}$$

where

$$\Lambda_{\mu\nu} = \sum_{i \neq 0} \frac{\langle 0|L_\mu|i\rangle\langle i|L_\mu|0\rangle}{E_i - E_0}. \tag{2.10}$$

The effective Zeeman energy becomes

$$E_{\text{Zeeman}} = 2\mu_B \sum_{\mu,\nu} \left(\delta_{\mu\nu} - \lambda\Lambda_{\mu\nu}\right) S_\mu H_\nu. \tag{2.11}$$

Hence, the effective g-value is generally a tensor $2(\mathbf{1} - \lambda\Lambda)$ that can be made real and symmetric by choosing real unperturbed basis wave functions. Taking the principal axes of this tensor as the x-, y-, and z-axes, the anisotropic energy takes the form

$$-\lambda^2\Lambda_x S_x^2 - \lambda^2\Lambda_y S_y^3 - \lambda^2\Lambda_z S_z^2. \tag{2.12}$$

Thus, the anisotropy energy arising from the crystalline field is of the order of λ times $(g-2) = 2\lambda\Lambda$.

When the ion has cubic symmetry, the principal values of Λ are degenerate, and eq. 2.12 is isotropic.

$$E_2(H=0) = -\frac{2}{3}\lambda^2(\text{Tr}\Lambda)\vec{S}^2. \tag{2.13}$$

The third order perturbation energy is zero for the same reason as the first order perturbation energy is zero. The first nontrivial anisotropy energy arises from the fourth order perturbation as

$$A\left(S_x^4 + S_y^4 + S_z^4\right), \tag{2.14}$$

where A is a constant of the order of λ^4

An interesting point is that when $S = 1/2$, there is no anisotropy energy due to crystalline Stark effect. This is because $(S_\mu)^{2n} = 1/4$ for any positive integer n.

2.4.2 Doublet Ground States

Ions in $3d^1$ (Ti^{3+}, V^{4+} in tetrahedral field). $3d^4$ (Cr^{2+}, in octahedral field), $3d^6$ (Fe^{2+}, in tetrahedral field), and $3d^9$ (Ni^{+}, Cu^{2+} in octahedral field) configuration have doublet ground states Γ_3.

The double Γ_3 is 'non-magnetic' in the sense that any matrix element of a vector operator, including magnetic moment and orbital angular momentum, is zero. The same analysis as in the case of singlet ground state applies to double ground state.

2.4.3 Triplet Ground State

Ions in $3d^2$ (V^{3+}, Cr^{4+} in octahedral field). $3d^3$ (V^{2+}, Cr^{3+}, Mn^{4+} in tetrahedral field), $3d^7$ (Fe^{+}, Co^{2+}, Ni^{3+} in octahedral field), and $3d^8$ (Co^{+}, Ni^{2+}, Cu^{3+} in tetrahedral field) configuration have triplet ground state Γ_4. Ions in $3d^1$ (Ti^{3+}, V^{4+} in octahedral field). $3d^4$ (Cr^{2+}, in tetrahedral field), $3d^6$ (Fe^{2+}, in octahedral field), and $3d^9$ (Ni^{+}, Cu^{2+} in tetrahedral field) configuration have triplet ground states Γ_5.

We consider now orbital triplets Γ_4 and Γ_5. Within these manifold, every orbital vector can be replaced by an equivalent fictitious orbital momentum operator $\alpha\tilde{\vec{l}}$ with $\tilde{l} = 1$. The spin orbital coupling can be written within the manifold as $\alpha\lambda\tilde{\vec{l}} \cdot \vec{S}$.

Neglecting the admixture between the ground manifold Γ_i, where i is 4 or 5, and excited orbital multiplets Γ_j, through spin orbital coupling, we obtain $\tilde{\vec{J}}$ multiplets, where the fictitious total angular momentum $\tilde{\vec{J}}$ takes values $S+1$, S, or $|S-1|$. The magnetic moment operator can be written as $\vec{\mu} = \mu_B \tilde{g}_J \tilde{\vec{J}}$, where the effective orbital g factor reads

$$\tilde{g}_J = \frac{1}{2}\left(g_{\tilde{l}} + g_s\right) + \frac{\tilde{l}(\tilde{l}+1) - S(S+1)}{2\tilde{J}(\tilde{J}+1)}(g_{\tilde{l}} - g_s) \tag{2.15}$$

Spin-orbital interaction to excited orbital states can be took into account through perturbative analysis. Second order effects does not change the isotropy but the effective g-factor. They also give rise to small splitting of states with $\tilde{J} \geq 2$ in a manner consistent with group theoretic requirement. Fourth order perturbation would find anisotropy energy resulting in the form of $A(\tilde{J}_x^4 + \tilde{J}_y^4 + \tilde{J}_z^4)$.

For mutiplet ground state, it is convenient to use magnetic suceptibility to measure magnetic moment. Denoting the ground states by $|0;\alpha\rangle$ and the excited states by $|n\rangle$, the suceptibility reads

$$\chi^{\mu} = \sum_{\alpha} \rho_{\alpha} \left(\frac{|\langle 0;\alpha|\mu^{\mu}|0;\alpha\rangle|^2}{k_B T} + 2\sum_{n\neq 0} \frac{|\langle n|\mu^{\mu}|0;\alpha\rangle|^2}{E_n - E_0} \right), \tag{2.16}$$

where ρ_α is the fraction of α states in ground states and $\mu = x, y, z$.

2.5 Weak Crystal Field

When crystal field is weak compared to spin-orbital coupling, we can treat the crystal field as pertubation. The unperturbed ground state is the manifold with smallest totoal angular moment for less than half filled ions, largest totoal angular moment for more than half filled ions. The crystal field effect breaks this manifold into submanifolds consistent with group theoretic consideration. For non-Kramers ion, which has even the number of electrons, the totoal angular moment is integr and the analysis is similar to the case of intermediate crystal field. Kramers ion, having odd number of electrons, demands another analysis.

2.5.1 Non-Kramers Ions

The ground states are one of the five manifolds Γ_i, where i is 1 to 5. The three manifolds Γ_1, Γ_2, and Γ_3 are non-magnetic. The other two manifolds Γ_4 and Γ_5 can be dealt with fictitious momentum operator $\alpha\tilde{\vec{I}}$ with $\tilde{I} = 1$. Higher order effect to excited totoal angluar momentum states can be took into account.

2.5.2 Kramers Ions

The ground states are one of the three manifolds Γ_6, Γ_7, and Γ_8. The two manifolds Γ_6 and Γ_7 are Kramers douplets and does not have anisotropy in cubic crystal field. Γ_8 consists of four sates. Uimin and Brenig showed anisotropy arises via isotropic magnetic exchange [18].

Chapter 3

Density Functional Theory and Local Density Approximation

3.1 Density Functional Theory

Being a ground state property, the MAE should be accessible in principle via density functional theory (DFT) [8, 19]. Density functional theory is the basis of LDA+U that we employ to tackle the magnetic anisotropy of $3d$ transition metals. A brief description of density functional theory is presented here.

We condier a system couples to an external source $J(x)$ with an interaction Hamiltonian

$$H_I = \int dx^3 \rho(\vec{x}) J(\vec{x}), \tag{3.1}$$

where $\rho(\vec{x})$ is the density of particles, the Hohenberg-Kohn theorem [8] states that

- There exists density functional $E[\rho]$.
- The ground state energy can be obtained by minimizing this functional with respect to the density.

A derivation of Hohenberg-Kohn theorem can be easily done in functional integration formulation.

Consider a fermionic system with a fermi field $\psi(\vec{x})$ and Hamiltonian

$$H = H_0 + \int dx^3 \psi^\dagger(\vec{x}) J(\vec{x}) \psi(\vec{x}), \tag{3.2}$$

where H_0 is the Hamiltonian without the external source, i.e., the Hamiltonian when $J(\vec{x}) = 0$. The partition function

$$Z = \exp(-W[J]) = \langle 0 | T_\tau \exp(-\int d\tau H) | 0 \rangle, \tag{3.3}$$

where T_τ is the time ordering operator, can be written as

$$e^{-W[J]} = \int [D\psi^\dagger][D\psi] e^{- \quad dtL}, \tag{3.4}$$

where L is the Lagrangian and $\int [D\psi^\dagger][D\psi]$ is a Grassmannian functional integral. Explicit form of the Lagrangian is

$$L = \int dx^3 d\tau \psi^\dagger(\vec{x}) \frac{\partial \psi}{\partial \tau}(\vec{x}) - H. \tag{3.5}$$

For a system of electrons moving in a crystal potential $V_c(x)$ and interacting via Coulomb interactions V, in the presence of an external source J coupled to the electron density, the partition function can be written down explicitly as,

$$\begin{aligned} Z = \exp[-W[J]] &= \int D[\psi\psi^\dagger] \exp\left[- \int dx \psi^+(x)[\partial_\tau - \frac{\nabla^2}{2m} + V_c(x)]\psi(x) \right. \\ &- \frac{1}{2} \int dx dx' \psi^+(x)\psi^+(x') V(x-x')\psi(x')\psi(x) \\ &+ \left. \int dx J(x)\psi^\dagger(x)\psi(x) \right]. \end{aligned} \tag{3.6}$$

Here $x = (\mathbf{x}, \tau)$ denotes the space–imaginary time coordinates.

For time independent system, the effective action $W[J]$ can be written as a product of energy functional $E[J]$ and the total time, i.e., $W[J] = -E[J] \int d\tau$. Taking a functional derivative of the eq. 3.4, we obtain the function derivative of the energy functional with respect to the external source:

$$\frac{\delta E[J]}{\delta J(\vec{x})} = \rho(\vec{x}). \tag{3.7}$$

Invertibilty of eq. 3.7 is equivalent to the existence of density functional in Density Functional Theory. Assuming that the eq. 3.7 is invertible , we can express $v(\vec{x})$ in terms of $\rho(\vec{x})$. Using this relation between $v(\vec{x})$ and $\rho(\vec{x})$, we can express the energy functional as a functional of density, called density functional, $E[\rho]$. (Calling this energy functional of density as density functional is a convention. Note that the energy functional is not a functional of density but a functional of external source. The energy functional expressed in terms of density by inverting the eq. 3.7 is the density functional.)

To show that the ground state can be obtained by minimizing the density functional, we consider the free energy obtained by Legendre transformation (We can obtain the same conclusion using Legendre transformation of $W[J]$. This point of view will be taken when we are discussing Local Density Approximation and its extentions),

$$F[\rho, J] = E[\rho] - \int dx^3 \rho(\vec{x}) J(\vec{x}). \tag{3.8}$$

The functional derivative of $F[\rho]$ with respect to $v(\vec{x})$ is zero:

$$\begin{aligned} \frac{\delta F[\rho, J]}{\delta J} &= \frac{\delta E[\rho]}{\delta J} - \rho(\vec{x}), & (3.9) \\ &= \rho(\vec{x}) - \rho(\vec{x}) & (3.10) \\ &= 0. & (3.11) \end{aligned}$$

Therefore the free energy functional is a functional of density, i.e., $F[\rho, J] = F[\rho]$. The derivative of $F[\rho]$ with respect to $\rho(\vec{x})$ is

$$\frac{\delta F[\rho]}{\delta \rho(\vec{x})} = -J(\vec{x}). \tag{3.12}$$

Now, using the expression $E[\rho] = F[\rho] + \int dx^3 \rho(\vec{x}) v(\vec{x})$, we take the derivative of $E[\rho]$ with respect to $\rho(\vec{x})$

$$\frac{\delta E[\rho]}{\delta \rho(\vec{x})} = 0. \tag{3.13}$$

Equation 3.13 is the minimization condition. This equation together with the invertibility of the eq. 3.7 consists of the Density Functional Theory.

We can extend the Density Functional Theory to systems with magnetic moments. We add an external magnetic field $\vec{h}(\vec{x})$ such that the interaction Hamiltonian reads

$$H_I = \int dx^3 \psi^\dagger(\vec{x}) J(\vec{x}) \psi(\vec{x}) + 2 \int dx^3 \psi^\dagger(\vec{x}) \vec{S} \psi(\vec{x}) \cdot \vec{h}(\vec{x}), \tag{3.14}$$

where $\vec{S}$ is the spin operator. For simplicity we assumed that the orbital moment is quenched, $\langle \vec{L} \rangle = 0$. In the same vein as the case without an external magnetic field, we obtain

$$\frac{\delta E[J, h]}{\delta J(\vec{x})} = \rho(\vec{x}), \quad \frac{\delta E[J, h]}{\delta \vec{h}(\vec{x})} = -\vec{m}(\vec{x}), \tag{3.15}$$

where $\vec{m}(\vec{x}) = -\psi^\dagger(\vec{x})\vec{S}\psi(\vec{x})$. The free energy is

$$F[\rho, \vec{m}] = E[\rho, \vec{m}] - \int dx^3 \rho(\vec{x}) J(\vec{x}) + \int dx^3 \vec{m}(\vec{x}) \cdot \vec{h}(\vec{x}), \tag{3.16}$$

which in turn has the following functional derivatives,

$$\frac{\delta F[\rho, \vec{m}]}{\delta \rho(\vec{x})} = -v(\vec{x}), \quad \frac{\delta F[\rho, \vec{m}]}{\delta \vec{m}(\vec{x})} = h(\vec{x}), \tag{3.17}$$

Assuming the invertibility of eq. 3.15, we can devise "magnetic" density functional $E[\rho, \vec{m}]$. Taking derivatives of this functional with respect to density and magnetic moment density, we obtain minimization conditions:

$$\frac{\delta E[\rho, \vec{m}]}{\delta \rho(\vec{x})} = 0, \quad \frac{\delta E[\rho, \vec{m}]}{\delta \vec{m}(\vec{x})} = 0. \tag{3.18}$$

Therefore, the extension of Density Functional Theory to the case with magnetic moment is that

- There exists "magnetic" density functional $E[\rho, \vec{m}]$. and that
- The ground state energy can be obtained by minimizing this functional with respect to energy and magnetization, respectively.

3.2 Kohn-Sham Self-Consistency Equations

Density functional theory can be used in conjunction with functional integration. When non-trivial interaction is considered, the functional integration is performed using perturbation theory. In a year after the density functional theory is published, Kohn and Sham devised a method dealing with the density functional theory in a computationally implementable way, known as Kohn-Sham self-consistency equations. In this section, we describe Kohn-Sham self-consistency equations.

Kohn and Sham [19] rewrite the density functional as

$$\begin{aligned} E[\rho, \vec{m}] &= T_{\rm S}[\rho, \vec{m}] + \int d^3x V_{\rm ext}(\vec{x})\rho(\vec{x}) - \int d^3x \vec{h}(\vec{x}) \cdot \vec{m}(\vec{x}) \\ &+ \frac{1}{2} \int \int dx^3 dy^3 \frac{\rho(\vec{x})\rho(\vec{y})}{|\vec{x} - \vec{y}|} + E_{\rm XC}[\rho, \vec{m}], \end{aligned} \tag{3.19}$$

where $V_{\rm ext}(\vec{x})$ is the external potential, i.e., $V_{\rm c}(\vec{x}) + J(\vec{x})$. $T_{\rm S}[\rho, \vec{m}]$ is the kinetic energy of a noninteracting electron gas in its ground state with density $\rho(\vec{x})$.

Exchange correlation energy functional $E_{\rm XC}[\rho, \vec{m}]$ is implicitly defined by the above equation. In practice, the exchange correlation energy function is approximated by an analytic expression.

Applying the minimization conditions, the Kohn-Sham approach boils down to the Kohn-Sham self-consistent equations:

$$H_{\rm ks}\psi_i(\vec{x}) = \epsilon_i\psi_i(\vec{x}), \tag{3.20}$$

$$\rho(\vec{x}) = \sum_i f(\epsilon_i - \mu)\left|\psi(\vec{x})_i\right|^2, \tag{3.21}$$

$$\vec{m}(\vec{x}) = -\mu_0 \sum_i f(\epsilon_i - \mu)\psi_i^\dagger(\vec{x})\vec{\sigma}\psi(\vec{x})_i, \tag{3.22}$$

$$N = \sum_i f(\epsilon_i - \mu), \tag{3.23}$$

where f is the fermi distribution, N is the total number of particles, μ_0 is the Bohr magneton, μ is the chemical potential, and

$$H_{\rm ks} = -\frac{1}{2}\nabla^2 + V_{\rm ks} + \mu_0\vec{\sigma}\cdot\vec{h}_{\rm ks}, \tag{3.24}$$

$$\rho(\vec{x}) = \sum_i f(\epsilon_i - \mu)\left|\psi(\vec{x})_i\right|^2, \tag{3.25}$$

$$\vec{m}(\vec{x}) = -\mu_0 \sum_i f(\epsilon_i - \mu)\psi_i^\dagger(\vec{x})\vec{\sigma}\psi(\vec{x})_i, \tag{3.26}$$

$$V_{\rm ks}(\vec{x}) = V_{\rm ext}(\vec{x}) + \int dy^3 \frac{\rho(\vec{y})}{|\vec{x}-\vec{y}|} + \frac{\delta E_{\rm XC}[\rho,\vec{m}]}{\delta\rho(\vec{x})}, \tag{3.27}$$

$$\vec{h}_{\rm ks}(\vec{x}) = \vec{h}(\vec{x}) + \frac{\delta E_{\rm XC}[\rho,\vec{m}]}{\delta\vec{m}(\vec{x})}. \tag{3.28}$$

Kohn-Sham's approach calculates single-electron states ψ_i, called Kohn-Sham orbitals, using effective potential $V_{\rm ks}(\vec{x}) + \mu_0\vec{\sigma}\cdot\vec{h}_{\rm ks}$. The effective potential in turn depends on the Kohn-Sham orbitals through density and magnetization. When the self-consistency of the Kohn-Sham orbitals and the effective potential is reached, the ground state energy can be found by Eq. (3.19), where $T_{\rm S}$ is usually calculated by

$$T_{\rm S}[\rho,\vec{m}] = \sum_i f(\epsilon_i - \mu)\epsilon_i - \int dx^3\rho(\vec{x})V_{\rm ks}(\vec{x}) + \int dx^3\vec{m}(\vec{x})\cdot\vec{h}_{\rm ks}(\vec{x}). \tag{3.29}$$

In principle, the Kohn-Sham orbitals ψ_i are technical devices for generating total energy. In practice, however, they are used as a first step in perturbative calculations

of one-electron Green functions. This underscores the single-particle picture and small corrections around it upon which the standard model of solids is built.

The Kohn-Sham formulation of Density Functional Theory can be summarized to the following functional,

$$\begin{aligned}\Gamma(\rho, V_{ks}) &= -T\sum_{i\omega_n} tr\log[i\omega_n + \nabla^2/2 - V_{ks} - \mu_0\vec{\sigma}\cdot\vec{h}_{\rm ks}] \\ &- \int V_{KS}(\vec{x})\rho(\vec{x})dx^3 + \int dx^3\vec{m}(\vec{x})\cdot\vec{h}_{\rm ks}(\vec{x}) \\ &+ \frac{1}{2}\int\frac{\rho(\vec{x})\rho(\vec{y})}{|\vec{x}-\vec{y}|}dx^3dy^3 + \int V_{ext}(\vec{x})\rho(\vec{x})dx^3 - \int dx^3\vec{h}(\vec{x})\cdot\vec{m}(\vec{x}) \\ &+ E_{xc}[\rho].\end{aligned} \tag{3.30}$$

The sum of first three terms is the kinetic energy of a non-interacting electron gas in potential $V_{KS}(\vec{x})$ and magnetic field $\vec{h}_{\rm ks}$. Compared with the Eq. (3.19), the Eq. (3.30) can be identified with the density functional. Extremizing Eq. (3.30) with respect to $\rho(\vec{x})$ and $\vec{m}(\vec{x})$ gives

$$V_{\rm ks}(\vec{x}) = V_{\rm ext}(\vec{x}) + \int dy^3\frac{\rho(\vec{y})}{|\vec{x}-\vec{y}|} + \frac{\delta E_{\rm xc}[\rho,\vec{m}]}{\delta\rho(\vec{x})}, \tag{3.31}$$

$$\vec{h}_{\rm ks}(\vec{x}) = \vec{h}(\vec{x}) + \frac{\delta E_{\rm xc}[\rho,\vec{m}]}{\delta\vec{m}(\vec{x})}. \tag{3.32}$$

Therefore the functional (3.30) contains the prescription for Kohn-Sham potential and magnetic field. The equation of motion part of Kohn-Sham self consistency equations can be obtained by extremizing this function with respect to $\rho(\vec{x})$ and $\vec{m}(\vec{x})$.

Extremizing Eq. (3.30) with respect to $\rho(\vec{x})$ and $\vec{m}(\vec{x})$ leads to

$$\rho(\vec{x}) = T\sum_{i\omega_n}\left\langle\vec{x}\left|\frac{1}{i\omega_n + \nabla^2/2 - V_{\rm ks} - \mu_0\vec{\sigma}\cdot\vec{h}_{\rm ks}}\right|\vec{x}\right\rangle, \tag{3.33}$$

$$\vec{m}(\vec{x}) = -\mu_0 T\sum_{i\omega_n}\left\langle\vec{x}\left|\frac{\vec{\sigma}}{i\omega_n + \nabla^2/2 - V_{\rm ks} - \mu_0\vec{\sigma}\cdot\vec{h}_{\rm ks}}\right|\vec{x}\right\rangle. \tag{3.34}$$

These equations can be solved using Kohn-Sham orbitals:

$$\rho(\vec{x}) = \sum_i f(\epsilon_i - \mu)\left|\psi(\vec{x})_i\right|^2, \tag{3.35}$$

$$\vec{m}(\vec{x}) = -\mu_0\sum_i f(\epsilon_i - \mu)\psi_i^\dagger(\vec{x})\vec{\sigma}\psi(\vec{x})_i, \tag{3.36}$$

where $\psi(\vec{x})_i$ are Kohn-Sham orbitals obtained by solving effective one-electron problem,

$$H_{\rm ks}\psi_i(\vec{x}) = \epsilon_i\psi_i(\vec{x}). \tag{3.37}$$

Therefore the functional (3.30) contains all the pieces of Kohn-Sham self consistency equations. When the self consistency is reached, the energy is calculated by

$$\begin{aligned} E &= \sum_i f(\epsilon_i - \mu)\epsilon_i - \int V_{ks}(\vec{x})\rho(\vec{x})dx^3 + \int dx^3\vec{m}(\vec{x})\cdot\vec{h}_{\rm ks}(\vec{x}) \\ &+ \frac{1}{2}\int\frac{\rho(\vec{x})\rho(\vec{y})}{|\vec{x}-\vec{y}|}dx^3dy^3 + \int V_{ext}(\vec{x})\rho(\vec{x})dx^3 - \int dx^3\vec{h}(\vec{x})\cdot\vec{m}(\vec{x}) \\ &+ E_{xc}[\rho]. \end{aligned} \tag{3.38}$$

3.3 Local Density Approximation

Density Functional Theory is an exact theory as long as the invertibility condition holds. (Density Functional Theory is an effective field theory. All the effective field theory is exact at the ground state as long as the invertibility condition holds.) Since the exchange energy functional $E_{xc}[\rho]$ is not known, the usefulness of this approach is due to the existence of successful approximations to the exchange energy functional. Kohn and Sham proposed Local Density Approximation (LDA). In LDA, the exchange energy functional is assumed to be local:

$$E_{xc}[\rho] = \int dx^3\epsilon_{xc}[\rho(x)]\rho(x), \tag{3.39}$$

with $\epsilon_{xc}[\rho(x)]$ being the energy density of the uniform electron gas.

When nontrivial magnetic moment is present, the exchange energy functional is assumed to be dependent on magnetic moment density also:

$$E_{xc}[\rho,\vec{m}] = \int dx^3\epsilon_{xc}[\rho(\vec{x}),|\vec{m}(\vec{x})|]\rho(\vec{x}) + \int dx^3 f_{xc}[\rho(\vec{x}),|\vec{m}(\vec{x})|]|\vec{m}(\vec{x})|(\vec{x}). \tag{3.40}$$

It is a usual assumption that the magnetic moment density is collinear, in other words, that the direction of magnetic moment density is independent of position and aligns with the external magnetic moment. The magnitude of magnetic moment density is then $|\vec{m}(\vec{x})| = \rho(\vec{x})_+ - \rho(\vec{x})_-$, where $\rho(\vec{x})_\pm$ is the density of spin-up

(spin-down) electrons. Electron spin is quantized along the internal magnetization. Since the density is sum of spin-up and spin-down densities, the exchange energy is a functional of spin densities:

$$E_{xc}[\rho,\vec{m}] = E_{xc}[\rho_+,\rho_-] = \int dx^3 \epsilon_{xc}^{+}[\rho_+(\vec{x}),\rho_-(\vec{x})]\rho_+(\vec{x}) + \int dx^3 \epsilon_{xc}^{-}[\rho_+(\vec{x}),\rho_-(\vec{x})]\rho_-(\vec{x}). \tag{3.41}$$

This approximation is called local spin density approximation (LSDA) [20]. In this approximation, spin-up and spin-down wavefunctions are used. Then, the Kohn Sham equation reads

$$\left(-\frac{1}{2}\nabla^2 + V_{\rm ks}(\vec{x}) \pm \mu_0 h_{\rm ks}(\vec{x})\right)\psi_\pm(\vec{x}) = \epsilon_{i\pm}\psi_\pm(\vec{x}). \tag{3.42}$$

Spin densities are calculated as usual

$$\rho_\pm(\vec{x}) = \sum_i f(\epsilon_{i\pm} - \mu)\left|\psi_\pm(\vec{x})_i\right|^2. \tag{3.43}$$

When the magnetic moment density may not be collinear, Spinor, in place of spin-up and spin-down wavefunctions, should be used. For example, when spin-orbit coupling is incorporated, we can not assume collinear magnetic moment any more. Spin-orbit coupling is included by adding spin-orbit coupling term to the Kohn-Sham Hamiltonian [21]:

$$\left(-\frac{1}{2}\nabla^2 + V_{\rm ks}(\vec{x}) + \mu_0\vec{\sigma}\cdot\vec{h}_{\rm ks}(\vec{x}) + \xi(\vec{x})\vec{l}\cdot\vec{s}\right)\tilde{\psi}_i(\vec{x}) = \epsilon_i\tilde{\psi}_i(\vec{x}) \tag{3.44}$$

where $\vec{l}$ and $\vec{s}$ are one-electron orbital and spin angular moment operator, respectively. $\psi_i(\vec{x})$ is Kohn Sham spinor. ξ determines the strength of spin–orbit coupling and in practice is determined[22] by radial derivative of the $l = 0$ component of the Kohn–Sham potential inside an atomic sphere:

$$\xi(r) = \frac{2}{c^2}\frac{dV_{KS}(r)}{dr}. \tag{3.45}$$

The Kohn Sham equation in the form (3.44) can deal with intra-atomic non-collinearity as well as non-collinearity with the external magnetic field.

The Kohn–Sham parametrization of the density in terms of V_{KS} is extremely useful because it expresses uniquely $\rho(\vec{x})$ in terms of the Kohn–Sham orbitals $\psi_{\mathbf{k}j}(\vec{x})$. This is

a key point for understanding how DFT is truncated in practical implementations. There are two different philosophies in truncating Eqs.(3.20)–(3.26), one is via the introduction of pseudopotentials which we will not describe here. All–electron methods simply introduce a finite basis set $\chi_\alpha^{\mathbf{k}}(\vec{x})$ and expand

$$\psi_{\mathbf{k}j}(\vec{x}) = \sum_\alpha \chi_\alpha^{\mathbf{k}}(\vec{x}) A_\alpha^{\mathbf{k}j} \tag{3.46}$$

keeping a finite set of α. Note that this truncation immediately restricts the active part of the multiplicative operator associated with the Kohn–Sham potential to have a form

$$\hat{V} = \sum_{\mathbf{k}} |\chi_\alpha^{\mathbf{k}}\rangle V_{\alpha\beta} \langle\chi_\alpha^{\mathbf{k}}| \tag{3.47}$$

Of course, one can add to this contributions from the set which is orthogonal to the minimal basis set $|\chi_\alpha^{\mathbf{k}}\rangle$ without changing the truncated density. The requirement of locality presumably determines the Kohn–Sham potential and the component of ((3.47)) outside the space of$\chi_\alpha^{\mathbf{k}}(\mathbf{r})$ uniquely.

Linear muffin–tin orbitals (LMTO's) [21] are an optimal minimal basis set. For a known Kohn–Sham potential this construction can be done once and for all. However, since V_{ks} depends on the density, the basis $|\chi_\alpha^{\mathbf{k}}\rangle$ is adapted iteratively to the self–consistent solution.

Finally, it is worth pointing out that in practical implementations of DFT, one also needs to make a truncation of the degrees of freedom included in the functional. Since this formalism is based on Kohn–Sham orbitals, this is done by truncating the Hilbert space from which the Kohn–Sham orbitals are chosen. Truncations similar in spirit are involved in pseudopotential methods.

Chapter 4

Local Density Approximation with Strong Correlations

4.1 Introduction

The LDA method is very successful in many materials for which the standard model of solids works. However, in correlated electron system this is not always the case. In strongly correlated situations, the total energy is not very sensitive to the potential since the electrons are localized due to the interactions themselves, and the lack of sensitivity of the functional to the density, does not permit to device good approximations to the exact functional in this regime. Furthermore, when the Mott transition takes place the invertibility condition is not satisfied. Our view, is that this situation cannot be remedied by using more complicated exchange and correlation functionals in density functional theory.

4.2 Formulation

LDA+U method[23] is the method proposed to overcome this difficulty of LDA when strong correlations are present. We will deal with the spin unrestricted formulation for illustration. This allows us to choose a quantization axis along some direction, say z, since the total energy is now invariant with respect to its orientation.

The approach requires an introduction of a set of localized orbitals $\phi_a(\vec{x})$ which are used to build an "occupancy spin density matrix"

$$n^{\sigma}_{ab} = \sum_{\mathbf{k}j} f(\epsilon_{\mathbf{k}j\sigma}) \int \psi^{*}_{\mathbf{k}j\sigma}(\vec{x})\phi_a(\vec{x})dx^3 \int \psi_{\mathbf{k}j\sigma}(\vec{y})\phi^{*}_b(\vec{y})dy^3 \tag{4.1}$$

This intuitively represents the "correlated part of the electron density" as long as we associate our projectors ϕ_a with correlated electrons, say d orbitals. The total energy

now is represented as a functional of the spin densities $\rho^\sigma(\mathbf{r})$ and of n^σ_{ab}. We introduce spin-dependent Kohn Sham fields $V^\sigma_{\rm ks}(\vec{x}) \equiv V_{\rm ks}(\vec{x}) + \sigma\mu_0|\vec{h}_{\rm ks}(\vec{x})|$ and external potential $V^\sigma_{\rm ext}(\vec{x}) \equiv V_{\rm ext}(\vec{x}) + \sigma\mu_0|\vec{h}(\vec{x})|$. In complete analogy with Eq. (3.30), one introduces a Lagrange multipliers matrix λ^σ_{ab} to enforce (4.1). The LDA+U functional then read

$$\begin{aligned}\Gamma_{LDA+U}[n^\sigma_{ab},\lambda^\sigma_{ab},V^\sigma_{\rm ks},\rho^\sigma] &= -T\sum_{i\omega_n} tr\log[i\omega_n + \nabla^2/2 - V^\sigma_{\rm ks} - \sum_{ab}\lambda^\sigma_{ab}|\phi_a\rangle\langle\phi_b|] \\ &- \sum_\sigma\int V^\sigma_{\rm ks}(\vec{x})\rho^\sigma(\vec{x})dx^3 + \int V_{\rm ext}(\vec{x})\rho(\vec{x})dx^3 \\ &+ \frac{1}{2}\int\frac{\rho(\vec{x})\rho(\vec{y})}{|\vec{x}-\vec{y}|}dx^3dy^3 - \sum_\sigma\sum_{ab}\lambda^\sigma_{ab}n^\sigma_{ab} \\ &+ E^{\rm LDA}_{\rm xc}[\rho^\sigma] + E^{\rm Model}[n^\sigma] - E^{\rm Model}_{dc}[n^\sigma],\end{aligned} \tag{4.2}$$

where we have added a contribution from the Coulomb energy in the shell of correlated electrons

$$E^{\rm Model}[n^\sigma] = \frac{1}{2}\sum_\sigma\sum_{abcd}U_{abcd}n^\sigma_{ab}n^{-\sigma}_{cd} + \frac{1}{2}\sum_\sigma\sum_{abcd}(U_{abcd}-J_{abcd})n^\sigma_{ab}n^\sigma_{cd} \tag{4.3}$$

Since, part of this energy is already taken into account in LDA, we have to subtract a double-counting part denoted by $E^{\rm Model}_{dc}[n^\sigma]$.

4.3 Self-Consistency Equations

Extremizing the functional (4.2) with respect to $V_{KS}(\vec{x})$ and $\vec{h}_{KS}(\vec{x})$ yield

$$\rho^\sigma(\vec{x}) = T\sum_{i\omega_n}\left\langle\vec{x}\left|\frac{1}{i\omega_n + \nabla^2/2 - V^\sigma_{\rm ks} - \sum_{ab}\lambda^\sigma_{ab}|\phi_a\rangle\langle\phi_b|}\right|\vec{x}\right\rangle e^{i\omega_n 0^+}, \tag{4.4}$$

which is equivalnent to

$$\rho^\sigma(\vec{x}) = \sum_{\mathbf{k}j} f(\epsilon_{\mathbf{k}j\sigma})|\psi_{\mathbf{k}j\sigma}(\vec{x})|^2, \tag{4.5}$$

$$[-\nabla^2/2 + V^\sigma_{KS}(\vec{x})]\psi_{\mathbf{k}j\sigma}(\vec{x}) + \sum_{ab}\lambda^\sigma_{ab}\phi_a(\vec{x})\int dy^3\phi^*_b(\vec{y})\psi_{\mathbf{k}j\sigma}(\vec{y}) = \epsilon_{\mathbf{k}j\sigma}\psi_{\mathbf{k}j\sigma}(\vec{x}). \tag{4.6}$$

$V^\sigma_{\rm ks}(\vec{x})$ is obtained by extremizing the functional with respect to $\rho(\vec{x})^\sigma$:

$$V^\sigma_{\rm ks}(\vec{x}) = V^\sigma_{\rm ext}(\vec{x}) + \int dy^3\frac{\rho(\vec{y})}{|\vec{x}-\vec{y}|} + \frac{\delta E^{\rm LDA}_{\rm xc}[\rho^\sigma]}{\delta\rho^\sigma(\vec{x})}, \tag{4.7}$$

Extremizing with respect to λ^{σ}_{ab} yield the constraint (4.1). Extremizing with respect to n^{σ}_{ab} yield the correction to the potential λ^{σ}_{ab}

$$\lambda^{\sigma}_{ab} = \sum_{cd} U_{abcd} n^{-\sigma}_{cd} + \sum_{cd} (U_{abcd} - J_{abcd}) n^{\sigma}_{cd} - \frac{dE^{\rm Model}_{\rm dc}[n^{\sigma}]}{dn^{\sigma}_{ab}}. \tag{4.8}$$

The Eqs. (4.5)–(4.8) form self-consistency equations of LDA+U

4.4 Correlation Matrix

The LDA+U functional and the LDA+U equations are defined once a set of projectors $\{\phi_a(\vec{x})\}$ and a matrix of interactions U_{abcd} is prescribed. Formally, the matrices $\hat{U}$ and $\hat{J}$ have the following definitions:

$$U_{abcd} = \langle ac|v_C|bd\rangle = \int \phi^*_a(\vec{x})\phi^*_c(\vec{y}) v_C(\vec{x}-\vec{y})\phi_b(\vec{x})\phi_d(\vec{y}) dx^3 dy^3, \tag{4.9}$$

$$J_{abcd} = \langle ac|v_C|db\rangle = \int \phi_a(\vec{x})^* \phi^*_c(\vec{y}) v_C(\vec{x}-\vec{y})\phi_d(\vec{x})\phi_b(\vec{y}) dx^3 dy^3, \tag{4.10}$$

where the Coulomb interaction $v_C(\vec{x}-\vec{y})$ has to take into account the effects of screening by conduction electrons. In practice, one expresses these matrices via a set of Slater integrals. When l orbitals are used as the projection operators, the matrix is expressed in terms of Slater parameters F^k. For $a \equiv lm, b \equiv lk, c \equiv l'm', d \equiv l'k'$ and representing $\phi_{lm}(\mathbf{r}) = \phi_l(r) i^l Y_{lm}(\hat{r})$, we can express the matrices U and J in the following manner:

$$\langle lml'm'|\frac{1}{r}|lkl'k'\rangle = \sum_{l''=0,2,\ldots}^{\min(2l,2l')} \frac{4\pi}{2l''+1} F^{(u)l''}_{ll'} C^{l''m''=m-k}_{lklm} C^{l''m''=k'-m'}_{l'm'l'k'} \delta_{k'-m',m-k}$$

$$\langle lml'm'|\frac{1}{r}|l'k'lk\rangle = \sum_{l''=0,2,\ldots}^{\min(2l,2l')} \frac{4\pi}{2l''+1} F^{(j)l''}_{ll'} C^{l''m''=m-k'}_{l'k'lm} C^{l''m''=k-m'}_{l'm'lk} \delta_{m-k',k-m'}$$

where the quantitites $F^{(u)}$ and $F^{(j)}$ are given by the following radial integrals

$$F^{(u)l''}_{ll'} = \int \frac{r^{l''}}{r'^{l''+1}} \phi^2_l(r)\phi^2_{l'}(r') dr dr'$$

$$F^{(j)l''}_{ll'} = \int \frac{r^{l''}}{r'^{l''+1}} \phi_l(r)\phi_{l'}(r)\phi_l(r')\phi_{l'}(r') dr dr'$$

When $l \equiv l'$, the quantites $F^{(u)}$ and $F^{(j)}$ are equal and have a name of Slater integrals which for s–electrons are reduced to one constant $F^{(0)}$, for p–electrons there are two

constants: $F^{(0)}$, $F^{(2)}$, for d's: $F^{(0)}$, $F^{(2)}$, $F^{(4)}$, etc. In this case, the expressions for U and J reduces to

$$\langle m, m''|v_C|m', m'''\rangle = \sum_k a_k(m, m', m'', m''')F^k, \tag{4.11}$$

where $0 \leq k \leq 2l$

$$a_k(m, m', m'', m''') = \frac{4\pi}{2k+1}\sum_{q=-k}^{k}\langle lm|Y_{kq}|lm'\rangle\langle lm''|Y^*_{kq}|lm'''\rangle. \tag{4.12}$$

Slater integrals can be linked to Coulomb and Stoner parameters U and J obtained from LSDA supercell procedures via $U = F^0$ and $J = (F^2 + F^4)/14$. The ratio F^2/F^4 is to a good accuracy a constant ~ 0.625 for d electrons. For f electrons, the corresponding expression is $U = F^0$ and $J = (286F^2 + 195F^4 + 250F^6)/6435$.

4.5 Double Counting Term

When the electron distribution is orbitally symmetric, $n^\sigma_{ab} = n^\sigma_{aa}\delta_{ab}$,

$$\begin{aligned} E^{\text{Model}}[n^\sigma] &= \frac{1}{2}\sum_\sigma(2l+1)^2\bar{U}\,n^\sigma_{aa}n^{-\sigma}_{aa} + \frac{1}{2}2l(2l+1)\sum_\sigma(\bar{U}-\bar{J})n^\sigma_{aa}n^\sigma_{aa} && (4.13)\\ &= \frac{1}{2}\bar{U}\,\bar{n}\bar{n} - \frac{1}{2}\sum_\sigma\bar{J}\,\bar{n}^\sigma\bar{n}^\sigma - \frac{1}{2}\sum_\sigma(\bar{U}-\bar{J})(2l+1)n^\sigma_{aa}n^\sigma_{aa} && (4.14)\\ &= \frac{1}{2}\bar{U}\,\bar{n}\bar{n} - \frac{1}{2}\sum_\sigma\bar{J}\,\bar{n}^\sigma\bar{n}^\sigma - \text{self energy}. && (4.15)\end{aligned}$$

where

$$\begin{aligned} \bar{U} &= \frac{1}{(2l+1)^2}\sum_{ab}\langle ab|\frac{1}{r}|ab\rangle, && (4.16)\\ \bar{J} &= \bar{U} - \frac{1}{2l(2l+1)}\sum_{ab}(\langle ab|\frac{1}{r}|ab\rangle - \langle ab|\frac{1}{r}|ba\rangle), && (4.17)\\ \bar{n}^\sigma &= \sum_a n^\sigma_{aa}, \quad \bar{n} = \bar{n}^\uparrow + \bar{n}^\downarrow. && (4.18)\end{aligned}$$

For d electrons, $\bar{U} = F^0$ and $\bar{J} = F^2 + F^4$.

Part of the energy added by $E^{\text{Model}}[n^\sigma]$ is already included in LSDA functional. The double counting term $E^{\text{Model}}_{dc}[n^\sigma]$ is added to subtract this already included part of $E^{\text{Model}}[n^\sigma]$. This is done by imposing that LDA+U reduces to LSDA when the electon

distribution is orbitally symmaetric. It was proposed [24] that the form for $E_{dc}^{Model}[n^\sigma]$ is

$$E_{\rm dc}^{\rm Model} = \frac{1}{2}\bar{U}\,\bar{n}(\bar{n}-1) - \frac{1}{2}\bar{J}[\bar{n}^\uparrow(\bar{n}^\uparrow - 1) + \bar{n}^\downarrow(\bar{n}^\downarrow - 1)], \tag{4.19}$$

where the subtraction by 1 is made to take the self-interaction into account. This generates the correction to the potential in the form:

$$\lambda_{ab}^\sigma = \sum_{cd} U_{abcd} n_{cd}^{-\sigma} + \sum_{cd}(U_{abcd} - J_{abcd}) n_{cd}^\sigma - \delta_{ab}\bar{U}(\bar{n} - \frac{1}{2}) + \delta_{ab}\bar{J}(\bar{n}^\sigma - \frac{1}{2}) \tag{4.20}$$

As an example, when only the effect of U is under investigation, the U and J matrices are $U_{abcd} = \delta_{ab}\delta_{cd}U$, $J_{abcd} = \delta_{ad}\delta_{cd}U$, $\bar{U} = U$, and $\bar{J} = 0$. This simple U and J matrices make it possible to write down corrections to LSDA functional and LSDA kohn-sham potential:

$$E^{\rm Model}[n^\sigma] - E_{\rm dc}^{\rm Model} = -\frac{1}{2}\sum_\sigma \sum_{ab} U n_{ab}^\sigma n_{bc}^\sigma + \frac{1}{2}\bar{U}\,\bar{n} \tag{4.21}$$

$$\begin{aligned}
\lambda_{ab}^\sigma &= \sum_{cd} U_{abcd} n_{cd}^{-\sigma} + \sum_{cd}(U_{abcd} - J_{abcd}) n_{cd}^\sigma - \delta_{ab}U(\bar{n} - \frac{1}{2}) && (4.22)\\
&= \delta_{ab}U\sum_d (n_{dd}^{-\sigma} + n_{dd}^\sigma) - n_{ba}^\sigma - \delta_{ab}\bar{U}(\bar{n} - \frac{1}{2}) && (4.23)\\
&= U(\frac{1}{2}\delta_{ab} - n_{ba}^\sigma) && (4.24)
\end{aligned}$$

The question now arises whether double–counting term should include self-interaction effects or not. In principle, if the LSDA functional contains this spirituous term, the same should be taken into account in the double–counting expression. Judged by the experience that the LSDA total energy is essentially free of self-interaction. For example, the total energy of the hydrogen atom is very close to -1 Ry, while the Kohn–Sham eigenvalue is only about -0.5 Ry. The construction of $E_{\rm dc}^{\rm Model}$ is made in order to be free of self-interaction. However this statement cannot be considered seriously in general, and alternative form of the double counting may include the effects of self-interaction.

4.6 Interpretation of LDA+U Functional

LDA+U can be viewed in several aspects. Frist, Γ_{LDA+U} could perhaps be viewed as an approximation to a functional of a projected density matrix. Second, If one uses the Eqs.(4.7), (4.8) and (4.1) to eliminate V^{σ}_{KS}, n^{σ}_{ab}, and λ^{σ}_{ab} as functions of ρ^{σ}, and substitutes these into (4.2), one obtains a functional of the density alone. In this way, LDA+U could viewed simply as a different density functional where in addition to dividing the density into spin up and spin down as in LSDA, one introduced a correlated component n_{ab} of the density and an uncorrelated one. Third, a different point of view is to introduce a "correlated part of the one-particle density matrix"

$$\int\int \phi_a(\mathbf{r})\langle\psi^{+}(\mathbf{r})\psi(\mathbf{r}')\rangle\phi_b(\mathbf{r}')d\mathbf{r}d\mathbf{r}' \tag{4.25}$$

and to consider a functional of this quantity and of the total density by effective action methods and view Eq. (4.2) as an approximation to this exact functional.

However, the interpretation of

$$T\sum_{i\omega_n}\left\langle \mathbf{r}'\left|[i\omega_n+\nabla^2/2-V^{\sigma}_{KS}-\sum_{ab}\lambda^{\sigma}_{ab}\phi_a(\mathbf{r})\phi^{*}_b(\mathbf{r}')]^{-1}\right|\mathbf{r}\right\rangle e^{i\omega_n 0^{+}} \tag{4.26}$$

as a density matrix is not consistent when interactions are present. This is because Eq. (4.25) describes a density matrix with eigenvalues one or zero, which is characteristic of a non-interacting density matrix. The density matrix of an interacting system has eigenvalues less than one. Therefore, Eq.(4.1) can not represent an interacting density matrix. Last, we have suggested to interpret the LDA+U method as a static limit of the more powerful DMFT method which we describe later. The static limit of DMFT is going to be most accurate as more symmetries are broken. Removing local degeneracies by spontaneous symmetry breaking is the simplest way of minimizing the energy, hence reducing the correlations [25].

It was argued[24] that the Green function

$$\left\langle \mathbf{r}'\left|[i\omega_n+\nabla^2/2-V^{\sigma}_{KS}-\sum_{ab}\lambda_{ab}\phi_a(\mathbf{r})\phi^{*}_b(\mathbf{r}')]^{-1}\right|\mathbf{r}\right\rangle \tag{4.27}$$

can be viewed as a limiting case of the GW approximation but this is again not clear since an interacting Green's function has poles with residues less than one, and this is

not the case in expression (4.27) except for the uncorrelated situation where Hartree Fock theory is exact.

4.7 Extension to Relativistic Cases

Relativistic effects, for example spin-orbit coupling, can be considered. These effects are important for such applications as magnetic anisotropy calculations. We have described the extended DFT in the previous section, and here we only discuss the LDA+U corrections. If spin–orbit coupling is taken into account, the occupancy matrix becomes non–diagonal with respect to spin index:

$$n_{ab}^{\sigma\sigma'} = n_{ab}^{\sigma} = \sum_{\mathbf{k}j} f(\epsilon_{\mathbf{k}j}) \int \psi_{\mathbf{k}j}^{*\sigma}(\mathbf{r})\phi_a(\mathbf{r})d\mathbf{r} \int \psi_{\mathbf{k}j}^{\sigma'}(\mathbf{r}')\phi_b^*(\mathbf{r}')d\mathbf{r}' \tag{4.28}$$

The correction to the functional has the form similar to Eq(4.3), and it is given by

$$E^{Model}[n^{\sigma\sigma'}] = \frac{1}{2}\sum_{abcd\sigma} U_{abcd} n_{ab}^{\sigma\sigma} n_{cd}^{-\sigma-\sigma} + \frac{1}{2}\sum_{abcd\sigma} (U_{abcd} - J_{abcd}) n_{ab}^{\sigma\sigma} n_{cd}^{\sigma\sigma} - \frac{1}{2}\sum_{abcd\sigma} J_{abcd} n_{ab}^{\sigma-\sigma} n_{cd}^{-\sigma\sigma} \tag{4.29}$$

which can be figured out by considering a Hartree–Fock averaging of the original expression for the Coulomb interaction

$$\frac{1}{2}\sum_{\sigma\sigma'}\sum_{abcd} \langle a\sigma b\sigma'|\frac{e^2}{r}|c\sigma d\sigma'\rangle c_{a\sigma}^{+} c_{b\sigma'}^{+} c_{d\sigma'} c_{c\sigma} \tag{4.30}$$

The correction to the potential takes the same form as Eq.(4.20) when $\sigma \equiv \sigma'$, i.e.,

$$\lambda_{ab}^{\sigma\sigma} = \sum_{cd} U_{abcd} n_{cd}^{-\sigma-\sigma} + \sum_{cd} (U_{abcd} - J_{abcd}) n_{cd}^{\sigma\sigma} - \bar{U}(\bar{n} - \frac{1}{2}) + J(\bar{n}^{\sigma\sigma} - \frac{1}{2}) \tag{4.31}$$

and for off–diagonal elements it is given by

$$\lambda_{ab}^{\sigma-\sigma} = -\sum_{cd} J_{abcd} n_{cd}^{-\sigma\sigma} \tag{4.32}$$

To make it more physically transparent we can introduce magnetic moments at the given shell by

$$m_{ab}^{\mu} = \sum_{\sigma\sigma'} s_{\sigma\sigma'}^{\mu} n_{ab}^{\sigma\sigma'} \tag{4.33}$$

where μ runs over x, y, z for Cartesian coordinates, or over, $-1, 0, +1$ $(z, \pm)$ for spherical coordinates. Relativistic correction to the LDA+U energy can be written in physically transparent form

$$\frac{1}{2}\sum_{abcd\sigma} J_{abcd} n_{ab}^{\sigma-\sigma} n_{cd}^{-\sigma\sigma} \equiv \frac{1}{2}\sum_{abcd} m_{ab}^{(+)} J_{abcd} m_{cd}^{(-)} + \frac{1}{2}\sum_{abcd} m_{ab}^{(-)} J_{abcd} m_{cd}^{(+)} \tag{4.34}$$

and in principle assumes further generalization of exchange matrix J_{abcd} to be anisotropic, i.e depend on $\mu\mu'$: $J_{abcd}^{\mu\mu'}$.

To summarize, since the density uniquely defines the Kohn–Sham orbitals, and they in turn, determine the occupancy matrix of the correlated orbitals, once a choice of correlated orbital in Eq. (4.28) is made, we still have a functional of the density alone. However it is useful to proceed by analogy with Eq. (4.2), and think of the LDA + U functional as a functional of ρ^σ, n^σ V_{KS}^σ and λ^σ, whose minimum gives better approximations to the ground–state energy in strongly correlated situations. Allowing the functional to depend on the projection of the Kohn–Sham energies onto a given orbital, allows the possibility of orbitally ordered states. This is a major advance over LDA in situations where this orbital order is present. As recognized many years ago, this is a very efficient way of gaining energy in correlated situations, and is realized in a wide variety of systems.

Those are the formal difficulties of the LDA+U method. From a practical point of view, despite the great successes of the LDA+U theory in predicting materials properties of correlated solids (for a review, see book of Anisimov [16]) there are obvious problems of this approach when applied to metals or to systems where the orbital symmetries are not broken. The most noticeable is that it only describes spectra which has Hubbard bands. A correct treatment of the electronic structure of strongly correlated electron systems has to treat both Hubbard bands and quasiparticle bands on the same footing. Another problem occurs in the paramagnetic phase of Mott insulators, in the absence of any broken symmetry the LDA + U method reduces to the LDA, and the gap collapses. In systems like NiO where the gap is of the order of eV, but the Neel temperature is a few hundred Kelvin, it is unphysical to assume that the gap and the magnetic ordering are related. For this

reason the LDA+U predicts magnetic order in cases that it is not observed, as, e.g., in the case of Pu [26].

Chapter 5

Perturbative Analysis

5.1 Introduction

An analytic insight can be gained by treating the spin-orbit coupling as a perturbation. This section is presented to show how a perturbative calculation can be performed to find magnetic anisotropy energy. With a perturbative calculation scheme, we may calculate torque directly avoiding comparing large numbers (total energies) to get a small number (magnetic anisotropy energy). We divide the contribution to magnetic anisotropy into two pieces. One is the contribution from degenerate states and the other is the contribution from non-degenerate states. When the spin-orbit coupling is taken as a perturbation, the first order correction to the dispersion relation $\epsilon_{\vec{k}\lambda\sigma}$ equals $\langle\vec{k}\lambda\sigma|\lambda\vec{s}\cdot\vec{l}|\vec{k}\lambda\sigma\rangle$. The matrix elements under consideration do not vanish only when the corresponding wave vectors are equal to each other due to the periodicity of the system. Degeneracy enters the perturbation scheme only when the matrix elements are non-zero. In this context, states with different wavevectors will be called "non-degenerate". For generic $\vec{k}$ the unperturbed state $|\vec{k}\lambda\sigma\rangle$ is a singlet, hence its wavefunction is real. Since the angular momentum operator is imaginary and the matrix element must be real, the matrix element must be zero for singlet states.

When the wave vector points to a symmetric direction, the system contains a subset of the original symmetry. The states are degenerate, which reflects the residual symmetry. Also there is an accidental degeneracy when the states with the same wave vector come to within the magnitude of spin-orbit coupling. In these subsets, the states are to be diagonalized at the first order. When all these perturbed states are occupied, their net effect of them is zero since the original matrix is traceless.

Interesting situations occurs when some of the degenerate states are occupied, while the other are unoccupied. In this case, the first order perturbation is proportional to the direction of the magnetization. We will call these states *degenerate fermi surface crossing* (DFSC) states.

5.2 Torque and Magnetic Anisotropy Energy

In computational view point, LDA+U self-consistency equations form a set of fixed point equations. With an appropriate initial guess, the standard fixed point iteration converges to a solution. We depend on physics for the existence of solution and for the uniqueness of solution. When the convergence is reached, we get magnetic moment in direction $[klm]$, total energy with the magnetic moment $E[klm]$, Kohn Sham orbitals $\psi_{\vec{k}i\sigma}$ with eigenvalues $\epsilon_{\vec{k}i\sigma}$, and occupancy spin density matrix $n_{ab}^{\sigma\sigma'}$. Magnetic anisotropy energy is calculated by taking difference of total energies with different direction of magnetic moment, e.g., $E_{\text{ani}} = E[111] - E[001]$. For high symmetry directions, the direction of magnetic moment can be set by a guess configuration with a magnetic moment aligned in the direction. When the guess direction of magnetic moment is not a high symmetry direction, the magnetic moment rotates to a direction of a nearby local minimum over iterations. For a magnetic moment pointing to a generic direction, we need to turn on a external magnetic moment. In general, the magnetic moment is not collinear with the magnetic moment. The desired direction of magnetic moment, however, can be obtained by adjusting the external magnetic field.

For Fe and Ni, the total energy is of the order of $10^4 eV$, where the magnetic anisotropy energy is of the order of $10^{-6} eV$. Finding magnetic anisotropy energy by the difference of two total energy, we are dealing with a quantity of the order of 10^{-11}. In modern 32bit computers, double precision has 17 digit mantissa. Since there are 6 digits to absorb numerical noise, calculating total energy to this precision is a demanding but doable job. The computational load for this precision calculation is huge with runtime over a week on 600MHz Alpha machines.

We may calculate torque instead of total energy. In this way, we don't need to compare two huge numbers to find a tiny number. Torque method, therefore, may reduce computing overhead. Here, we first formulate a prescription of calculating magnetic anisotropy in terms of torque.

The magnetic anisotropy energy equals,

$$E_{\text{aniso}} = E(\vec{\theta_2}) - E(\vec{\theta_1}), \tag{5.1}$$

where $\vec{\theta_1}$ and $\vec{\theta_2}$ are directions of the magnetic moment. The magnetic anisotropy can also be found by integrating torque. Consider changing direction of the constant external magnetic fields from $\vec{\theta_1}$ to $\vec{\theta_2}$ while keeping its magnitude constant. The anisotropy energy can be calculated according to what follows.

$$\begin{aligned} E(\theta_2) - E(\theta_1) &= \int_1^2 \int dx^3 \delta E[v, \vec{h}] \\ &= \int_1^2 \int dx^3 \delta \vec{h} \cdot \frac{\delta E[v, \vec{h}]}{\delta \vec{h}} \\ &= \int_1^2 \delta \vec{\theta} \cdot \vec{h} \times \int dx^3 \vec{m}(\vec{x}) \\ &= \int_1^2 \delta \vec{\theta} \cdot \vec{h} \times \vec{M} \end{aligned} \tag{5.2}$$

where $\vec{M}$ is total magnetic moment equal to $\int dx^3 \vec{m}(\vec{x})$.

A similar expression can be obtained using the free energy. In this case we roate the magnetization from angle $\vec{\theta}_1$ to $\vec{\theta}_2$. Assuming that the magnitude of the external magnetic field does not change, we can express the difference of free energy

$$\begin{aligned} F(\theta_2) - F(\theta_1) &= \int_1^2 \int dx^3 \delta F[\rho, \vec{m}] \\ &= \int_1^2 \int dx^3 \delta \vec{m}(\vec{x}) \cdot \frac{\delta F[\rho, \vec{m}]}{\delta \vec{m}} \\ &= \int_1^2 \delta \vec{\theta} \cdot \vec{h} \times \int dx^3 \vec{m}(\vec{x}) \\ &= \int_1^2 \delta \vec{\theta} \cdot \vec{h} \times \vec{M}, \end{aligned} \tag{5.3}$$

Note that in eq. (5.2) the angle is that of the external magnetic field, while in eq. (5.3) it is that of the magnetic field. We also get a relation of the magnetic anisotropy energy and the magnetic anisotropy free energy.

$$\Delta E = \Delta F - \Delta \int dx^3 \vec{m}(\vec{x}) \cdot \vec{h}. \tag{5.4}$$

Taking high symmetry directions as the initial and the final direction, where the external magnetic field and the magnetic moment are parallel, we can force the second term in eq. (5.4) vanish.

We can do LDA+U calculations with several external magnetic fields, say, from [111] direction to [001] direction. With the resulting magnetic moments, the calculation of torque is straightforward, and the integration will give the magnetic anisotropy energy. The question is, now, how much precision we need to get the magnetic anisotropy to desired precision. Jansen [13] studied this question to find out that we need to calculate the total energy to the precision needed for direct subtraction method even when torque method is used.

5.3 Non-Degenerate Perturbation

The analysis for non-degenerate states and fully occupied degenerate states are the same in perturbative analysis. In this section, we study these states.

We solve the following self consistent equations perturbatively.

$$H_{\rm ks}\psi_{\mathbf{k}i\sigma} = \epsilon_i\psi_{\mathbf{k}i\sigma}, \tag{5.5}$$

$$\rho(\vec{x}) = \sum_i f(\epsilon_i - \mu)\left|\psi_{\mathbf{k}i\sigma}(\vec{x})\right|^2, \tag{5.6}$$

$$\vec{m}(\vec{x}) = -\mu_0\sum_i f(\epsilon_i - \mu)\psi^\dagger_{\mathbf{k}i\sigma}(\vec{x})\vec{\sigma}\psi_{\mathbf{k}i\sigma}(\vec{x}), \tag{5.7}$$

$$H_{\rm ks} = H^0_{\rm ks} + H'. \tag{5.8}$$

Taking the spin orbit coupling as perturbation, we denote the unperturbed Kohn Sham Hamiltonian at self-consistence $H^0_{\rm ks}$:

$$H^0_{\rm ks}\psi_{\lambda\vec{k}\sigma} = \epsilon^0_{\lambda\vec{k}\sigma}\psi_{\lambda\vec{k}\sigma}. \tag{5.9}$$

When the spin-orbit coupling is turned on, the eigenvalues and eigenfunctions change, leading to changes of all quantities including Kohn Sham potential $v_{\rm ks}$, Kohn Sham magnetic field $\vec{h}_{\rm ks}$, and LDA+ band correction λ. The perturbation can be written as

$$H' = \delta v_{\rm ks} + \mu_0\sigma\cdot\delta h_{\rm ks} + \xi\vec{s}\cdot\vec{l} + \delta\lambda, \tag{5.10}$$

where $\lambda = \sum_{ab} \lambda_{ab} \phi_a^* \phi_b$. Due to the self-consistency of the Kohn-Sham equations, to perform a rigorous perturbative calculation would be a formidable task. With the self-consistent solutions obtained without spin-orbit coupling, we may turn on the spin-orbit coupling in a non self-consistent fashion. This approach has been widely used and can be justified to a certain degree as an application of the force theorem [11]. Also, for the shake of discussion, we use spin-orbit coupling constant. To attack the self consistent equations, we first regard the spin-orbit coupling as the only perturbation. Expanding the eigenstates upto fourth order in ξ, we obtain the perturbed eigenstates (The formula is at the end of this section) .

The correction to energy ΔE^n can be calculated from the above perturbed wave functions. For example

$$\Delta E^{(2)} = \langle \vec{k} i\sigma | \xi \vec{s} \cdot \vec{l} | \vec{k} i\sigma \rangle + \sum_{j\sigma_a}{}' \frac{\left| \langle \vec{k} j\sigma_a | \xi \vec{s} \cdot \vec{l} | \vec{k} i\sigma \rangle \right|^2}{\epsilon^0_{\vec{k}i\sigma} - \epsilon^0_{\vec{k}j\sigma_a}}. \tag{5.11}$$

There is no first order correction in case of non-degenerate states. The second order correction equals

$$E^{(2)} = \sum_{\vec{k}\lambda\sigma}^{\text{occ}} \sum_{\lambda'\sigma'}{}' \frac{\langle \vec{k}\lambda\sigma | \lambda \vec{s} \cdot \vec{l} | \vec{k}\lambda'\sigma' \rangle \langle \vec{k}\lambda'\sigma' | \lambda \vec{s} \cdot \vec{l} | \vec{k}\lambda\sigma \rangle}{\Big(\epsilon(\vec{k}\lambda\sigma) - \epsilon(\vec{k}\lambda'\sigma') \Big)}, \tag{5.12}$$

where "occ" denotes occupied states and the primed sum excludes states with vanishing denominator. With occupied intermediate states, the summation is odd under the exchange of primed states and unprimed states. The contribution from occupied intermediate states adds to zero total effect. The second order contribution can be written as

$$E^{(2)} = \sum_{\vec{k}\lambda\sigma}^{\text{occ}} \sum_{\lambda'\sigma'}^{\text{unocc}} \frac{\langle \vec{k}\lambda\sigma | \lambda \vec{s} \cdot \vec{l} | \vec{k}\lambda'\sigma' \rangle \langle \vec{k}\lambda'\sigma' | \lambda \vec{s} \cdot \vec{l} | \vec{k}\lambda\sigma \rangle}{\Big(\epsilon(\vec{k}\lambda\sigma) - \epsilon(\vec{k}\lambda'\sigma') \Big)}, \tag{5.13}$$

where "unocc" means unoccupied states. Now that we exclude the DFSC states, all $\vec{k}$ points related by single group symmetry are occupied when one of them is occupied. The summation must reflects this symmetry and we can write down the form of anisotropy energy consistent with the symmetry. In this subset of states, the energy would be analytic with respect to the direction of the magnetization as long as the

subset does not change. In case of cubic symmetry, on which we shall focus henceforth, symmetry considerations restrict the summation to the form

$$E^{(2)}_{\text{aniso}} = a_2(m_x^2 + m_y^2 + m_z^2), \tag{5.14}$$

where a_2 is a constant of the order of λ^2. The second order term turns out to be spherically symmetric. Hence the anisotropy is of the fourth order. Since the magnetization comes from spin and the spin enters into the Hamiltonian through spin-orbit coupling, the magnetic anisotropy energy is apparently of the fourth order. The term which will generate anisotropy energy at the fourth order is

$$\sum_{\vec{k}\lambda\sigma}^{\text{occ}} \sum_{\lambda_a\sigma_a\lambda_b\sigma_b\lambda_c\sigma_c}^{\text{unocc}} \frac{\langle\vec{k}\lambda\sigma|\lambda\vec{s}\cdot\vec{l}|\vec{k}\lambda_a\sigma_a\rangle\langle\vec{k}\lambda_a\sigma_a|\lambda\vec{s}\cdot\vec{l}|\vec{k}\lambda_b\sigma_b\rangle\langle\vec{k}\lambda_b\sigma_b|\lambda\vec{s}\cdot\vec{l}|\vec{k}\lambda_c\sigma_c\rangle\langle\vec{k}\lambda_c\sigma_c|\lambda\vec{s}\cdot\vec{l}|\vec{k}\lambda\sigma\rangle}{\Big(\epsilon(\vec{k}\lambda\sigma)-\epsilon(\vec{k}\lambda_a\sigma_a)\Big)\Big(\epsilon(\vec{k}\lambda\sigma)-\epsilon(\vec{k}\lambda_b\sigma_b)\Big)\Big(\epsilon(\vec{k}\lambda\sigma)-\epsilon(\vec{k}\lambda_c\sigma_c)\Big)}. \tag{5.15}$$

The cubic symmetry in this term is realize in the same way as in the second order term. After diagonalization the anisotropic energy term appears to be

$$E^{(4)}_{\text{aniso}} = a_4(m_x^4 + m_y^4 + m_z^4), \tag{5.16}$$

where a_4 is a constant of the order of λ^4. This term is not spherically symmetric and generates anisotropy energy.

We concentrate on systems with cubic symmetry such as Fe and Ni. Using cubic symmetry, the magnetic moment perpendicular to the external field is simplified to

$$\begin{aligned} M_\perp \;=\; -\mu_0 \sum_{\vec{k}i\sigma}^{\text{occ}} \sum_{j\sigma_a}{}' \sum_{k\sigma_b}{}' \sum_{l\sigma_c}{}' \sum_{m\sigma_d}{}' \langle\vec{k}i\sigma|\vec{\sigma}_{||}|\vec{k}j\sigma_a\rangle \frac{\langle\vec{k}j\sigma_a|\xi\vec{s}\cdot\vec{l}|\vec{k}k\sigma_b\rangle}{\epsilon^0_{\vec{k}i\sigma}-\epsilon^0_{\vec{k}j\sigma_a}} \frac{\langle\vec{k}k\sigma_b|\xi\vec{s}\cdot\vec{l}|\vec{k}l\sigma_c\rangle}{\epsilon^0_{\vec{k}i\sigma}-\epsilon^0_{\vec{k}k\sigma_b}} \times \\ \frac{\langle\vec{k}l\sigma_c|\xi\vec{s}\cdot\vec{l}|\vec{k}m\sigma_d\rangle}{\epsilon^0_{\vec{k}i\sigma}-\epsilon^0_{\vec{k}l\sigma_c}} \frac{\langle\vec{k}m\sigma_d|\xi\vec{s}\cdot\vec{l}|\vec{k}i\sigma\rangle}{\epsilon^0_{\vec{k}i\sigma}-\epsilon^0_{\vec{k}m\sigma_d}}. \end{aligned} \tag{5.17}$$

The torque can be calculated by $\vec{\tau} = \vec{H} \times \vec{M}_\perp$, and the MAE by integrating the torque over the expanede angle.

5.4 Torque and Perturbation

At this stage, the torque is calculated disregarding the self consistency of Kohn Sham equations. Also the cubic symmetry is used on an weak ground. We will discuss these issues in what following.

1. The existence of an external magnetic field destroys the cubic symmetry. The expression for magnetic moment 5.17 is not correct then. Without cubic symmetry we need to evaluate the magnetic moment from the perturbed eigenfunctions 5.31 and there is no simplification. This problem can be relieved considering the situation with small external magnetic field compared to the spin orbit coupling.

2. Since the magnitude of the external magnetic field is too small to determine the direction of magnetic moment, the direction of magnetic moment must be determined independently. This brings the need to evaluate the parallel component of magnetic moment also. The perturbative correction to the parallel component is of the second order and does not allow any more simplification beyond the vanishing of first order correction. Moreover, it is uncertain whether such a small external magnetic moment is able to rotate the magnetic moment from the easy axis to a hard axis.

3. At this stage, we did not take the self consistency of Kohn Sham equation into consideration. Change of eigenfunctions results in changes of Kohn Sham potential and magnetic field. Though the magnetic moment gets correction at the second order, the magnetic moment density, $\vec{m}(\vec{x})$ gets correction at the first order, so does the Kohn Sham potential and magnetic field. To incorporate the change of these fields, we need to calculate the new fields using the new wave functions and redo the perturbation theory again with changed perturbation:
$\xi\vec{s}\cdot\vec{l} \to \delta v_{\mathrm{ks}} + \mu_0\sigma\cdot\delta h_{\mathrm{ks}} + \xi\vec{s}\cdot\vec{l} + \lambda$. At first order, this leads to the following equation.

$$\delta\vec{m}(\vec{x}) = -\mu_0 \sum_{i\vec{k}\sigma}^{\mathrm{occ}} \sum_{j\sigma'} \left[\langle i\vec{k}\sigma|\vec{\sigma}|j\vec{k}\sigma'\rangle \frac{\langle j\vec{k}\sigma'|\xi\vec{s}\cdot\vec{l} + \delta v_{\mathrm{ks}} + \vec{\sigma}\cdot\delta\vec{h}_{\mathrm{ks}} + \lambda|i\vec{k}\sigma\rangle}{\epsilon^0_{\lambda\vec{k}\sigma} - \epsilon^0_{j\vec{k}\sigma'}} \right.$$
$$\left. \langle j\vec{k}\sigma'|\vec{\sigma}|\lambda\vec{k}\sigma\rangle \frac{\langle i\vec{k}\sigma|\lambda\vec{s}\cdot\vec{l} + \delta v_{\mathrm{ks}} + \vec{\sigma}\cdot\delta\vec{h}_{\mathrm{ks}} + \lambda|j\vec{k}\sigma'\rangle}{\epsilon^0_{i\vec{k}\sigma} - \epsilon^0_{j\vec{k}\sigma'}} \right]. \tag{5.18}$$

Even though the change of magnetic moment obtained from this equation does not generate torque, this equation must be solved self-consistently before considering higher order perturbation. Only after that, the perturbation Hamiltonian is known exactly up to the first order and higher order perturbation is possible. In short, the perturbative treatment of spin-orbit coupling is prohibitive when self-consistency is taken into account.

4. There is a possibility that the eq. 5.17 is a good approximation for the purpose of calculating MAE. This is called "force theorem". We may check the validity of the force theorem numerically. First we calculated the energy without the spin orbit theorem. Then we calculated the energy with spin orbit coupling starting from the solutions of the case without spin orbit coupling. When there is no on-site interaction, the new solutions converge very fast hinting that the force theorem is valid. The new solutions, however, converge very slowly for the case with on-site interaction suggesting that we can not depend on the force theorem.

5. As has been studied by Mori and Kondorskii, degenerate states have significant contribution to MAE at the fourth order, the same order as non-degenerate states. This is discussed in the next section.

5.5 Degenerate Fermi Surface Crossing States

In this section, we consider states that are DFSC states. Behavior of the other subset involving DFSC states is quite different. Mori, Fukuda, and Ukai [7] investigated this subset and concluded that the subset dominates the magnetic anisotropy. In case of Ni, based on the tight binding model, they found two points on the fermi surface where degenerate bands cross. One is along the ΓX ([001]) direction,

$$\phi_2 = \sqrt{\frac{15}{4\pi}} yz f(r), \tag{5.19}$$

$$\phi_3 = \sqrt{\frac{15}{4\pi}} zx f(r), \tag{5.20}$$

$$\phi_5 = \sqrt{\frac{5}{16\pi}} (3z^2 - r^2) f(r). \tag{5.21}$$

Here, $\{\phi_2,\ \phi_3\}$ are exact degenerate states and $\{\phi_5\}$ is a state accidentally passing the same same point. The other lies along the ΓL ([111]) direction,

$$\frac{1}{2}(\phi_1 - \phi_2) + \frac{1}{2\sqrt{2}}(\phi_4 - \sqrt{3}\phi_5), \tag{5.22}$$

$$\frac{1}{2\sqrt{3}}(\phi_1 + \phi_2 - 2\phi_3) - \frac{1}{2\sqrt{2}}(\sqrt{3}\phi_4 - \phi_3), \tag{5.23}$$

where

$$\phi_1 = \sqrt{\frac{15}{4\pi}} xyf(r), \tag{5.24}$$

$$\phi_4 = \sqrt{\frac{5}{16\pi}} (x^2 - y^2) f(r). \tag{5.25}$$

With the direction of magnetization being (l, m, n), the degeneracy along ΓX generates a splitting of energy with magnitude

$$\delta E^{\Gamma X} = \lambda \left(3 - 2l^2\right)^{1/2}, \tag{5.26}$$

and the degeneracy along ΓL direction generates,

$$\delta E^{\Gamma L} = \frac{2\sqrt{2} - 1}{\sqrt{3}} \lambda |l + m + n|. \tag{5.27}$$

The volume in the Brillouin zone, where the splitting of the degenerate energy level, can be considered to be proportional to the third power of the splitting. Summing over the symmetric points yields a contribution to the anisotropy energy is

$$E^{\Gamma X}_{\text{aniso}} = -C^{\Gamma X} \lambda^4 \left(\left(3 - 2l^2\right)^2 - \left(3 - 2l^2\right)^2 - \left(3 - 2l^2\right)^2 \right), \tag{5.28}$$

due to degeneracy around the crossing point along the ΓX direction, where $C^{\Gamma X}$ is a constant, and

$$E^{\Gamma L}_{\text{aniso}} = -C^{\Gamma L} \lambda^4 \left(|l + m + n|^4 + | - l + m + n|^4 + |l - m + n|^4 + |l + m - n|^4 \right) \tag{5.29}$$

due to degeneracy around the crossing point along the ΓL direction, where $C^{\Gamma L}$ is a constant.

Neglecting the contributions from non-DFSC states, the difference of energies between $(0, 0, 1)$ and $(1, 1, 1)$ directions of magnetization is

$$\Delta E = E(1, 1, 1) - E(0, 0, 1) = -\frac{8}{3} (2C^{\Gamma L} - C^{\Gamma X}) \lambda^4. \tag{5.30}$$

It would be reasonable to assume that the coefficients $C^{\Gamma L}$ and $C^{\Gamma X}$ would be equal. This assumption brings the correct easy axis. A similar analysis has been done for Fe. The easy axis was found to be $(0, 0, 1)$ direction

The important message in this section is that the contribution of DFSC states to magnetic anisotropy is of the same order as that of non-degenerate states. Since the contribution of DFSC states are sensitive to the relative location of band and Fermi surface, a small change of band structure may affect the magetic anosotropy energy. In this respect, a proper treatment of bands are of utmost important in predicting magnetic anisotropy. When strongly correlated electrons are present, LDA+U is the only known method that treats strongly correlated bands properly.

Here follows the perturbed eigenstate at fourth order

$$
\begin{aligned}
|\vec{k}i\sigma\rangle' &= |\vec{k}i\sigma\rangle + \sum_{j\sigma_a}{}' |\vec{k}j\sigma_a\rangle \frac{\langle \vec{k}j\sigma_a|\xi\vec{s}\cdot\vec{l}|\vec{k}i\sigma\rangle}{\epsilon^0_{\vec{k}i\sigma} - \epsilon^0_{\vec{k}j\sigma_a}} \\
&+ \sum_{j\sigma_a}{}' \sum_{k\sigma_b}{}' |\vec{k}j\sigma_a\rangle \frac{\langle \vec{k}j\sigma_a|\xi\vec{s}\cdot\vec{l}|\vec{k}k\sigma_b\rangle}{\epsilon^0_{\vec{k}i\sigma} - \epsilon^0_{\vec{k}j\sigma_a}} \frac{\langle \vec{k}k\sigma_b|\xi\vec{s}\cdot\vec{l}|\vec{k}i\sigma\rangle}{\epsilon^0_{\vec{k}i\sigma} - \epsilon^0_{\vec{k}k\sigma_b}} \\
&- \Delta E^{(3)} \sum_{j\sigma_a}{}' |\vec{k}j\sigma_a\rangle \frac{\langle \vec{k}j\sigma_a|\xi\vec{s}\cdot\vec{l}|\vec{k}i\sigma\rangle}{(\epsilon^0_{\vec{k}i\sigma} - \epsilon^0_{\vec{k}j\sigma_a})^2} \\
&+ \sum_{j\sigma_a}{}' \sum_{k\sigma_b}{}' \sum_{l\sigma_c}{}' |\vec{k}j\sigma_a\rangle \frac{\langle \vec{k}j\sigma_a|\xi\vec{s}\cdot\vec{l}|\vec{k}k\sigma_b\rangle}{\epsilon^0_{\vec{k}i\sigma} - \epsilon^0_{\vec{k}j\sigma_a}} \frac{\langle \vec{k}k\sigma_b|\xi\vec{s}\cdot\vec{l}|\vec{k}l\sigma_c\rangle}{\epsilon^0_{\vec{k}i\sigma} - \epsilon^0_{\vec{k}k\sigma_b}} \frac{\langle \vec{k}l\sigma_c|\xi\vec{s}\cdot\vec{l}|\vec{k}i\sigma\rangle}{\epsilon^0_{\vec{k}i\sigma} - \epsilon^0_{\vec{k}l\sigma_c}} \\
&+ (\Delta E^{(2)})^2 \sum_{j\sigma_a}{}' |\vec{k}j\sigma_a\rangle \frac{\langle \vec{k}j\sigma_a|\xi\vec{s}\cdot\vec{l}|\vec{k}i\sigma\rangle}{(\epsilon^0_{\vec{k}i\sigma} - \epsilon^0_{\vec{k}j\sigma_a})^2} \\
&- \Delta E^{(2)} \sum_{j\sigma_a}{}' \sum_{k\sigma_b}{}' |\vec{k}j\sigma_a\rangle \frac{\langle \vec{k}j\sigma_a|\xi\vec{s}\cdot\vec{l}|\vec{k}k\sigma_b\rangle}{(\epsilon^0_{\vec{k}i\sigma} - \epsilon^0_{\vec{k}j\sigma_a})^2} \frac{\langle \vec{k}k\sigma_b|\xi\vec{s}\cdot\vec{l}|\vec{k}i\sigma\rangle}{\epsilon^0_{\vec{k}i\sigma} - \epsilon^0_{\vec{k}k\sigma_b}} \\
&- \Delta E^{(2)} \sum_{j\sigma_a}{}' \sum_{k\sigma_b}{}' |\vec{k}j\sigma_a\rangle \frac{\langle \vec{k}j\sigma_a|\xi\vec{s}\cdot\vec{l}|\vec{k}k\sigma_b\rangle}{\epsilon^0_{\vec{k}i\sigma} - \epsilon^0_{\vec{k}j\sigma_a}} \frac{\langle \vec{k}k\sigma_b|\xi\vec{s}\cdot\vec{l}|\vec{k}i\sigma\rangle}{(\epsilon^0_{\vec{k}i\sigma} - \epsilon^0_{\vec{k}k\sigma_b})^2} \\
&+ \sum_{j\sigma_a}{}' \sum_{k\sigma_b}{}' \sum_{l\sigma_c}{}' \sum_{i_d\sigma_d}{}' |\vec{k}j\sigma_a\rangle \frac{\langle \vec{k}j\sigma_a|\xi\vec{s}\cdot\vec{l}|\vec{k}k\sigma_b\rangle}{\epsilon^0_{\vec{k}i\sigma} - \epsilon^0_{\vec{k}j\sigma_a}} \frac{\langle \vec{k}k\sigma_b|\xi\vec{s}\cdot\vec{l}|\vec{k}l\sigma_c\rangle}{\epsilon^0_{\vec{k}i\sigma} - \epsilon^0_{\vec{k}k\sigma_b}} \times \\
&\qquad \frac{\langle \vec{k}l\sigma_c|\xi\vec{s}\cdot\vec{l}|\vec{k}i_d\sigma_d\rangle}{\epsilon^0_{\vec{k}i\sigma} - \epsilon^0_{\vec{k}l\sigma_c}} \frac{\langle \vec{k}i_d\sigma_d|\xi\vec{s}\cdot\vec{l}|\vec{k}i\sigma\rangle}{\epsilon^0_{\vec{k}i\sigma} - \epsilon^0_{\vec{k}i_d\sigma_d}} \\
&- (\Delta E^{(1)})^3 \sum_{j\sigma_a}{}' |\vec{k}j\sigma_a\rangle \frac{\langle \vec{k}j\sigma_a|\xi\vec{s}\cdot\vec{l}|\vec{k}i\sigma\rangle}{(\epsilon^0_{\vec{k}i\sigma} - \epsilon^0_{\vec{k}j\sigma_a})^4} \\
&+ (\Delta E^{(1)})^2 \sum_{j\sigma_a}{}' \sum_{k\sigma_b}{}' |\vec{k}j\sigma_a\rangle \frac{\langle \vec{k}j\sigma_a|\xi\vec{s}\cdot\vec{l}|\vec{k}k\sigma_b\rangle}{(\epsilon^0_{\vec{k}i\sigma} - \epsilon^0_{\vec{k}j\sigma_a})^3} \frac{\langle \vec{k}k\sigma_b|\xi\vec{s}\cdot\vec{l}|\vec{k}i\sigma\rangle}{\epsilon^0_{\vec{k}i\sigma} - \epsilon^0_{\vec{k}k\sigma_b}} \qquad (5.31) \\
&+ (\Delta E^{(1)})^2 \sum_{j\sigma_a}{}' \sum_{k\sigma_b}{}' |\vec{k}j\sigma_a\rangle \frac{\langle \vec{k}j\sigma_a|\xi\vec{s}\cdot\vec{l}|\vec{k}k\sigma_b\rangle}{\epsilon^0_{\vec{k}i\sigma} - \epsilon^0_{\vec{k}j\sigma_a}} \frac{\langle \vec{k}k\sigma_b|\xi\vec{s}\cdot\vec{l}|\vec{k}i\sigma\rangle}{(\epsilon^0_{\vec{k}i\sigma} - \epsilon^0_{\vec{k}k\sigma_b})^3} \\
&+ (\Delta E^{(1)})^2 \sum_{j\sigma_a}{}' \sum_{k\sigma_b}{}' |\vec{k}j\sigma_a\rangle \frac{\langle \vec{k}j\sigma_a|\xi\vec{s}\cdot\vec{l}|\vec{k}k\sigma_b\rangle}{(\epsilon^0_{\vec{k}i\sigma} - \epsilon^0_{\vec{k}j\sigma_a})^2} \frac{\langle \vec{k}k\sigma_b|\xi\vec{s}\cdot\vec{l}|\vec{k}i\sigma\rangle}{(\epsilon^0_{\vec{k}i\sigma} - \epsilon^0_{\vec{k}k\sigma_b})^2} \\
&- \Delta E^{(1)} \sum_{j\sigma_a}{}' \sum_{k\sigma_b}{}' \sum_{l\sigma_c}{}' |\vec{k}j\sigma_a\rangle \frac{\langle \vec{k}j\sigma_a|\xi\vec{s}\cdot\vec{l}|\vec{k}k\sigma_b\rangle}{(\epsilon^0_{\vec{k}i\sigma} - \epsilon^0_{\vec{k}j\sigma_a})^2} \frac{\langle \vec{k}k\sigma_b|\xi\vec{s}\cdot\vec{l}|\vec{k}l\sigma_c\rangle}{\epsilon^0_{\vec{k}i\sigma} - \epsilon^0_{\vec{k}k\sigma_b}} \frac{\langle \vec{k}l\sigma_c|\xi\vec{s}\cdot\vec{l}|\vec{k}i\sigma\rangle}{\epsilon^0_{\vec{k}i\sigma} - \epsilon^0_{\vec{k}l\sigma_c}} \\
&- \Delta E^{(1)} \sum_{j\sigma_a}{}' \sum_{k\sigma_b}{}' \sum_{l\sigma_c}{}' |\vec{k}j\sigma_a\rangle \frac{\langle \vec{k}j\sigma_a|\xi\vec{s}\cdot\vec{l}|\vec{k}k\sigma_b\rangle}{\epsilon^0_{\vec{k}i\sigma} - \epsilon^0_{\vec{k}j\sigma_a}} \frac{\langle \vec{k}k\sigma_b|\xi\vec{s}\cdot\vec{l}|\vec{k}l\sigma_c\rangle}{(\epsilon^0_{\vec{k}i\sigma} - \epsilon^0_{\vec{k}k\sigma_b})^2} \frac{\langle \vec{k}l\sigma_c|\xi\vec{s}\cdot\vec{l}|\vec{k}i\sigma\rangle}{\epsilon^0_{\vec{k}i\sigma} - \epsilon^0_{\vec{k}l\sigma_c}} \\
&- \Delta E^{(1)} \sum_{j\sigma_a}{}' \sum_{k\sigma_b}{}' \sum_{l\sigma_c}{}' |\vec{k}j\sigma_a\rangle \frac{\langle \vec{k}j\sigma_a|\xi\vec{s}\cdot\vec{l}|\vec{k}k\sigma_b\rangle}{\epsilon^0_{\vec{k}i\sigma} - \epsilon^0_{\vec{k}j\sigma_a}} \frac{\langle \vec{k}k\sigma_b|\xi\vec{s}\cdot\vec{l}|\vec{k}l\sigma_c\rangle}{\epsilon^0_{\vec{k}i\sigma} - \epsilon^0_{\vec{k}k\sigma_b}} \frac{\langle \vec{k}l\sigma_c|\xi\vec{s}\cdot\vec{l}|\vec{k}i\sigma\rangle}{(\epsilon^0_{\vec{k}i\sigma} - \epsilon^0_{\vec{k}l\sigma_c})^2}.
\end{aligned}
$$

Chapter 6

LDA+U as a Computational Method

6.1 Introduction

Being a ground state property, the MAE should be accessible in principle via density functional theory (DFT) [8, 19]. Despite the primary difficulty related to the smallness of MAE ($\sim 1\ \mu eV$/atom), great efforts to compute the quantity with advanced total energy methods based on local density approximation (LDA) combined with the development of faster computers, have seen success in predicting its correct orders of magnitudes [9, 27, 13, 12, 10]. However, the correct easy axis of Ni has not been predicted by this method and the fundamental problem of understanding MAE is still open.

In this article we take a new view that the correlation effects within the d shell are important for the magnetic anisotropy of $3d$ transition metals like Ni. These effects are not captured by the LDA but are described by Hubbard–like interactions presented in these systems and need to be treated by first principles methods[16]. Another effect which has not been investigated in the context of magnetic anisotropy calculations is the non-collinear nature of intra-atomic magnetization [17]. It is expected to be important when spin-orbit coupling and correlation effects come into play together. In this article we show that when we include these new ingredients into the calculation we solve the long-standing problem of predicting the correct easy axis of Ni.

We believe that the physics of transition metal compounds is intermediate between atomic limit where the localized d electrons are treated in the real space and fully itinerant limit when the electrons are described by band theory in k space. A

many–body method incorporating these two important limits is the dynamical mean–field theory (DMFT) [15]. The DMFT approach has been extensively used to study model Hamiltonian of correlated electron systems in the weak, strong and intermediate coupling regimes. It has been very successful in describing the physics of realistic systems, like the transition metal oxides and, therefore, is expected to treat properly the materials with d or f electrons.

6.2 LDA+U as a static limit of DMFT

Electron-electron correlation matrix $U_{\gamma_1\gamma_2\gamma_3\gamma_4} = \langle m_1 m_3 \,|v_C|\, m_2 m_4\rangle \,\delta_{s_1 s_2}\delta_{s_3 s_4}$ for d orbitals is the quantity which takes strong correlations into account. This matrix can be expressed via Slater integrals $F^{(i)}$, $i = 0, 2, 4, 6$ in the standard manner. The inclusion of this interaction generates self–energy $\Sigma_{\gamma_1\gamma_2}(i\omega_n, \vec{k})$ on top of the one–electron spectra. Within DMFT it is approximated by momentum independent self–energy $\Sigma_{\gamma_1\gamma_2}(i\omega_n)$.

A central quantity of the dynamical mean–field theory is the one–electron on–site Green function

$$\begin{aligned} G_{\gamma_1\gamma_2}(i\omega_n) = \quad & \sum_{\vec{k}} \quad \Big[(i\omega_n + \mu)O_{\gamma_1\gamma_2}(\vec{k}) - H^0_{\gamma_1\gamma_2}(\vec{k}) \\ & + \quad v_{dc} - \Sigma_{\gamma_1\gamma_2}(i\omega_n)\Big]^{-1} . \end{aligned} \tag{6.1}$$

where $H^0_{\gamma_1\gamma_2}(\vec{k})$ is the one-electron Hamiltonian standardly treatable within the LDA. Since the latter already includes the electron-electron interactions in some averaged way, we subtract the double counting term v_{dc} [28]. The use of realistic localized orbital representation such as linear muffin–tin orbitals [21] leads us to include overlap matrix $O_{\gamma_1\gamma_2}(\vec{k})$ into the calculation.

The DMFT reduces the problem to solving effective impurity model where the correlated d orbitals are treated as an impurity level hybridized with the bath of conduction electrons. The role of hybridization is played by the so–called bath Green function defined as follows:

$$[\mathcal{G}_0^{-1}]_{\gamma_1\gamma_2}(i\omega_n) = {G_{\gamma_1\gamma_2}}^{-1}(i\omega_n) + \Sigma_{\gamma_1\gamma_2}(i\omega_n). \tag{6.2}$$

Solving this impurity model gives access to the self–energy $\Sigma_{\gamma_1\gamma_2}(i\omega_n)$ for the correlated electrons. The one–electron Green function (6.1) is now modified with new $\Sigma_{\gamma_1\gamma_2}(i\omega_n)$, which generates a new bath Green function. Therefore, the whole problem requires self–consistency.

In this paper we confine ourselves to zero temperature and make an additional assumption on solving the impurity model using the Hartree–Fock approximation. In this approximation the self–energy reduces to

$$\Sigma_{\gamma_1\gamma_2} = \sum_{\gamma_3\gamma_4} (U_{\gamma_1\gamma_2\gamma_3\gamma_4} - U_{\gamma_1\gamma_2\gamma_4\gamma_3})\bar{n}_{\gamma_3\gamma_4} \tag{6.3}$$

where $\bar{n}_{\gamma_1\gamma_2}$ is the average occupation matrix for the correlated orbitals. The off-diagonal elements of the occupancy matrix are not zero when spin-orbit coupling is included [29]. The latter can be implemented following the prescription of Andersen [21] or more recent one by Pederson [30].

In the Hartree–Fock limit the self–energy is frequency independent and real. The self–consistency condition of DMFT can be expressed in terms of the average occupation matrix: Having started from some $\bar{n}_{\gamma_1\gamma_2}$ we find $\Sigma_{\gamma_1\gamma_2}$ according to (6.3). Fortunately, the computation of the on–site Green function (6.1) needs *not* to be performed. Since the self–energy is real, the new occupancies can be calculated from the eigenvectors of the one–electron Hamiltonians with $\Sigma_{\gamma_1\gamma_2} - v_{dc}$ added to its *dd* block. The latter can be viewed as an orbital–dependent potential which has been introduced by the LDA+U method [16].

The LDA+U method has been very successful compared with experiments at zero temperature in ordered compounds. By establishing its equivalence to the static limit of the DMFT we see clearly that dynamical mean–field theory is a way of improving upon it, which is crucial for finite temperature properties.

6.3 Precision of the calculation

In this work we study the effect of the Slater parameters F_0, F_2 and F_4 on the magnetic anisotropy energy. The latter is calculated by taking the difference of two total energies with different directions of magnetization (MAE=$E(111) - E(001)$).

The total energies are obtained via fully self consistent solutions. Since the total energy calculation requires high precision, full potential LMTO method [31] has been employed. For the $\vec{k}$ space integration, we follow the analysis given by Trygg and co–workers [12] and use the special point method [32] with a Gaussian broadening [33] of 15 mRy.

The validity and convergence of this procedure has been tested in their work [12]. For convergence of the total energies within desired accuracy, about 15000 k-points are needed. We used 28000 k-points to reduce possible numerical noise, where the convergency is tested up to 84000k-points.

Our calculations include non-spherical terms of the charge density and potential both within the atomic spheres and in the interstitial region [31]. All low-lying semi-core states are treated together with the valence states in a common Hamiltonian matrix in order to avoid unnecessary uncertainties.

These calculations are spin polarized and assume the existence of long-range magnetic order. Spin-orbit coupling is implemented according to the suggestions by Andersen [21]. We also treat magnetization as a general vector field, which realizes non-collinear intra-atomic nature of this quantity. Such general magnetization scheme has been recently discussed in [17].

Chapter 7

The Effect of Coulomb Parameter

7.1 Introduction

The effect of strong correlations is captured in the Coulomb parameter $U = F^0$. When only the Coulomb parameter U is considered, the correction to LSDA functional is

$$E^{\text{Model}}[n^\sigma] - E^{\text{Model}}_{\text{dc}} = -\frac{1}{2}\sum_\sigma \sum_{ab} U n^\sigma_{ab} n^\sigma_{bc}, \tag{7.1}$$

and the correction to the LSDA Kohn-Sham potential is

$$\lambda^\sigma_{ab} = -U n^\sigma_{ba}. \tag{7.2}$$

In this chapter, we study the effect of strong correlations using only the Coulomb parameter U

7.2 Magnetic Anisotropy Energy

We now discuss our calculated MAE. We first test our method in case of LDA ($U = 0$). To compare with previous calculations, we turn off the non-collinearity of magnetization which makes it collinear with the quantization axis. The calculation gives correct orders of magnitude for both fcc Ni and bcc Fe but with the wrong easy axis for Ni, which is the same result as the previous result [12].

Turning on the non-collinearity results in a a larger value of the absolute value of the MAE for Ni but the easy axis predicted to be (001), which is still wrong. The magnitude of the experimental MAE of Ni is 2.8 μeV aligned along (111) direction [34].

We now describe the effect of strong correlations, which is crucial in predicting the correct axis of Ni (see Fig. 7.1). As U increases, the MAE of Ni smoothly increases

until U reaches 2.5 eV and then smoothly decreases up to the value 3.8 μeV. Around $U = 3.9\ eV$, the MAE decreases abruptly to negative value. Around $U = 4.0\ eV$, the experimental order of magnitude and the correct easy axis (111) are restored. The change from the wrong easy axis to the correct easy axis occurs over the range of $\delta U \sim 0.2eV$, which is the order of spin-orbit coupling constant ($\sim 0.1eV$).

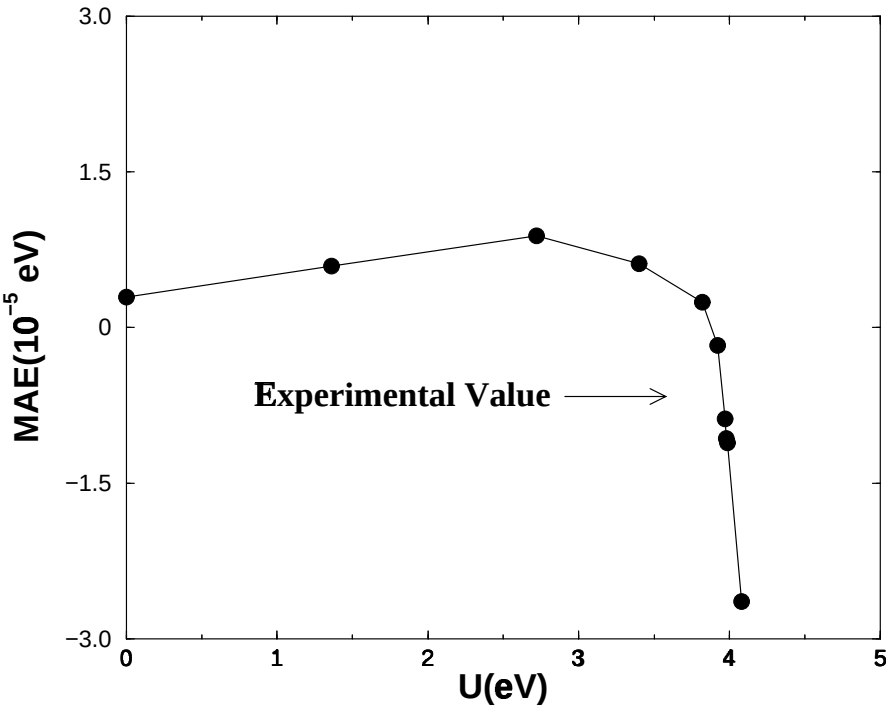

Figure 7.1: Experimental and calculated magnetocrystalline anisotropy energy MAE = $E(111) - E(001)$ for Ni. Experimental MAEs are marked by arrows for Ni ($-2.8\ \mu eV$).

For Fe (see Fig. 7.2), the MAE decreases on increasing U to negative values, where the magnetization takes the wrong axis. From $U = 2.7\ eV$, it increases back to the correct direction of easy axis (positive MAE). Around $U = 3.5\ eV$, it restores the correct easy axis and the experimental value of MAE is reproduced.

It is remarkable that the values of U necessary to reproduce the correct magnetic anisotropy energy are very close (within 1.2 eV) to the values which are needed to describe photoemission spectra of these materials [35, 36]. The correct estimation of U is indeed a serious problem. Different estimates based on different methods give a range of values from 1 eV to 6 eV. The work of Katsnelson and coworkers used a

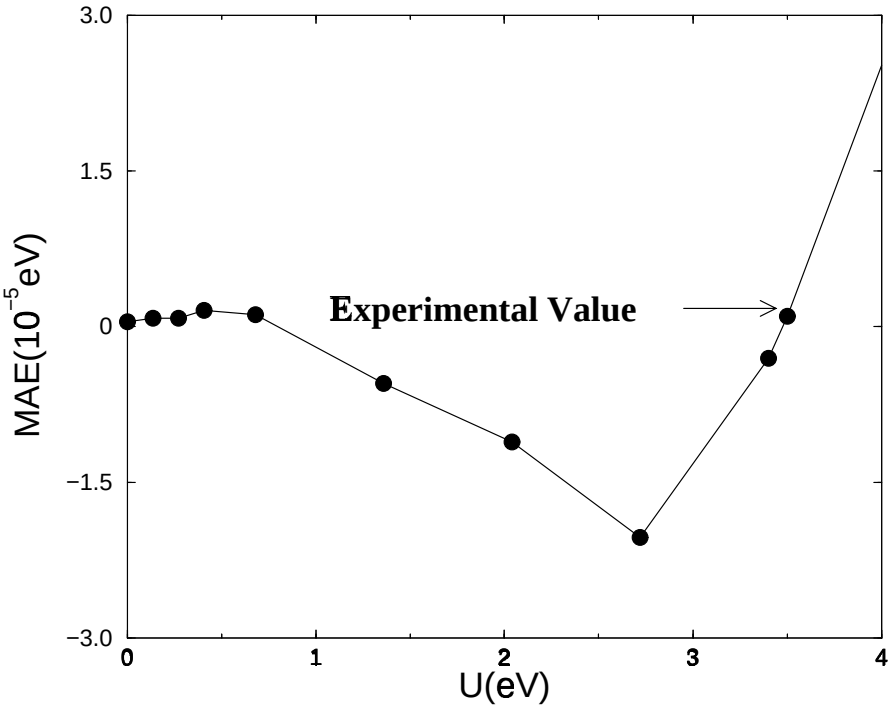

Figure 7.2: Experimental and calculated magnetocrystalline anisotropy energy MAE = $E(111) - E(001)$ (square) for Fe. Experimental MAEs are marked by arrows for Fe ($1.4\ \mu eV$).

dynamic approach utilizing finite temperature Quantum Monte Carlo method whereas we use a static approach at zero temperature. Considering this discrepancy, an agreement within $1.2eV$ shows an internal consistency of our approach and emphasizes the importance of correlations.

7.3 Correlation between MAE and the difference of magnetic moments

We find direct correlation between the dependency of the MAE as a function of U and the difference of magnetic moments ($\Delta M = -(M(111) - M(001))$ behaving similarly. For Ni (see Fig. 7.3, the difference of magnetic moments is nearly U independent up to $U = 3\ eV$. For large U, it smoothly decreases from the positive value to the negative one. It also decreases rapidly around $U = 3.9\ eV$ in accord with MAE. For Fe (see Fig. 7.4 , the difference is positive at $U = 0$. It decreases slightly to the

negative values and then increases to the positive value over the range of $U < 2.7\ eV$ where MAE decreases. For larger U's, where MAE is coming back to positive value, its slope is significantly larger than that at smaller U's.

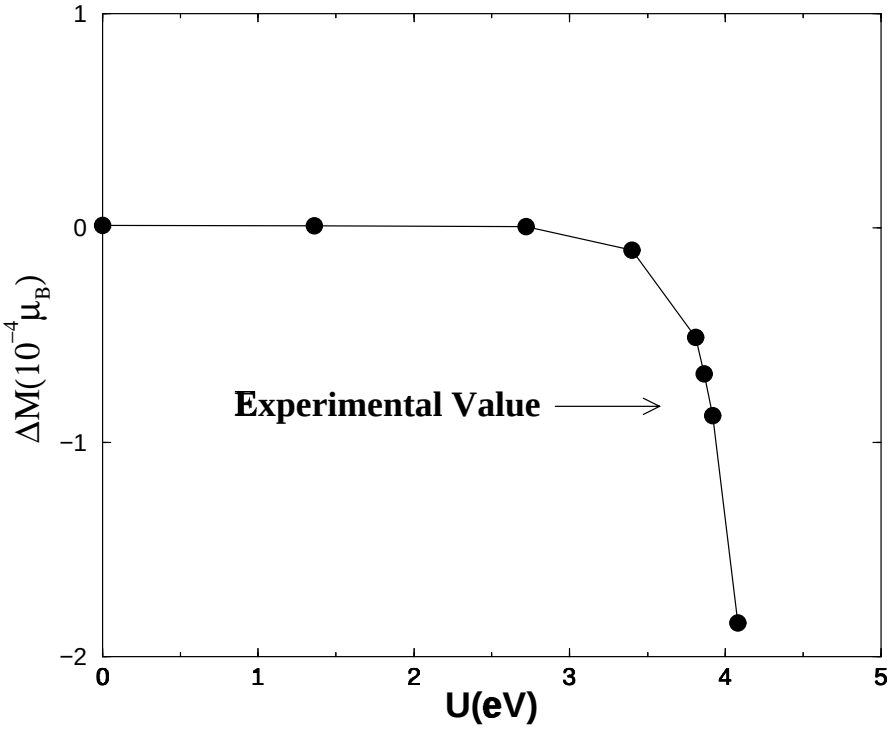

Figure 7.3: Calculated the difference of magnetic moment $\Delta M = M(001) - M(111)$ for Ni(bottom).

This concurrent change of MAE and the difference of magnetic moments suggests why some previous attempts based on force theorem [10] failed in predicting the correct easy axes. Force theorem replaces the difference of the total energies by the difference of one–electron energies. In this approach, the contribution from the slight difference in magnetic moments does not appear and, therefore, is not counted in properly. Unfortunately, we could not find any experimental data of magnetic moments to the desired precision ($10^{-4}\mu_B$) to compare with. We also have problems in reaching the convergence of the total energy with desired accuracy for large values of U in both Fe and Ni.

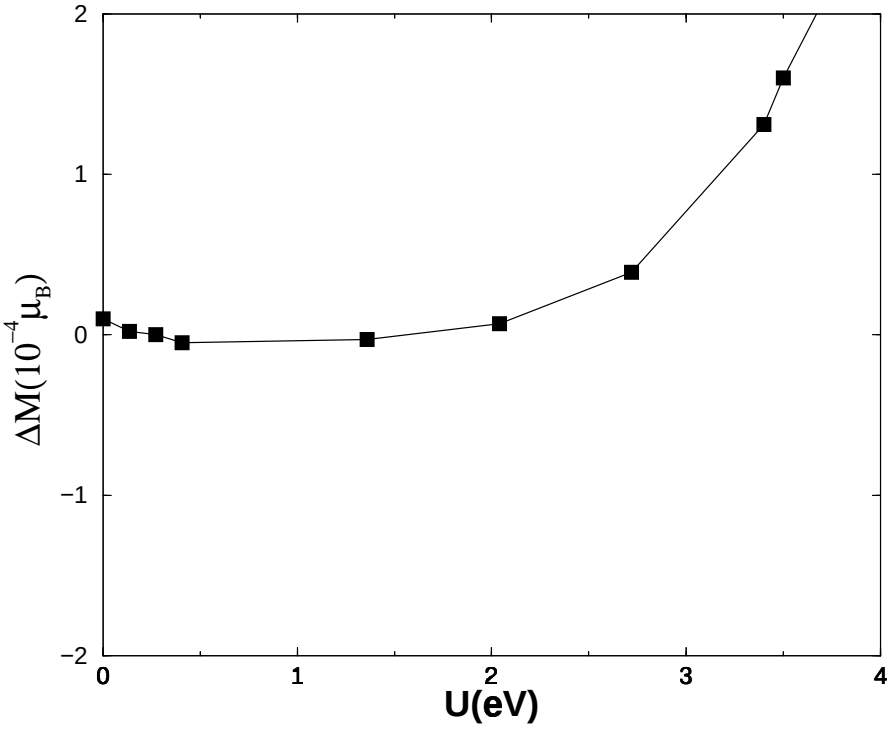

Figure 7.4: Calculated the difference of magnetic moment $\Delta M = M(001) - M(111)$ for Fe.

7.4 X pockets

We now present implications of our results on the calculated electronic structure for the case of Ni. One important feature which emerges from the calculation is the absence of the X_2 pocket (see Fig. 7.5). Notice that the band candidate for X_2 pocket is way below the Fermi surface. This X_2 pocket has been predicted by LDA but has not been found experimentally [37]. The band corresponding to the pocket is pushed down well below the Fermi level. This is expected since correlation effects are more important for slower electrons and the velocity near the pocket is rather small. It turns out that the whole band is submerged under the Fermi level.

There has been some suspicions that the incorrect position of the X_2 band within LDA was responsible for the incorrect prediction of the easy axis within this theory. Daalderop and coworkers [10] removed the X_2 pocket by increasing the number of valence electrons and found the correct easy axis. We therefore conclude that the

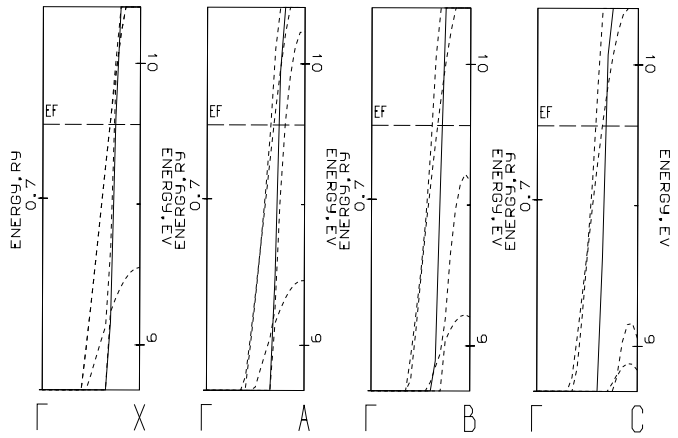

Figure 7.5: The X pockets of LDA+U at $U = 4\ eV$ and $J = 0\ eV$. Inspecting the figures, we see that there is X_5 pocket. Note that the X_2 pocket is not present. The solid lines represent bands with dominating up-spin. The dotted lines represent bands with dominating down-spin. $X = (0, 0, 1)$, $A = (1/16, 1/16, 1)$, $B = (2/16, 2/16, 1)$, $C = (3/16, 3/16, 1)$. .

absence of the pocket is one of the central elements in determining the magnetic anisotropy, and there is no need for any ad-hoc adjustment within a theory which takes into account the correlations.

Notice that as we move away from the ΓX direction, we see that one band, which is above the Fermi surface in ΓX is submerged below the Fermi level. The is the experimentally confirmed X_5 pocket.

7.5 L neck

Experiments found a a spin-down dominated L neck. From the Fig. 7.6, we see a spin-down dominated band is below the Fermi level in ΓL direction. As we mover away from the ΓL direction, we see that the band is surfacing up above the Fermi level. This is the experimentally confirmed L neck.

Unlike LDA, we have found two extra very tiny L pockets in LDA+U. Both of them are dominated by *sp* orbital with opposite spins. Being small, these extra pockets may be artifacts of LDA+U. As U increases L-neck appears first and then X-pocket disappears. There no such U at which X pocket disappears without presence of L necks.

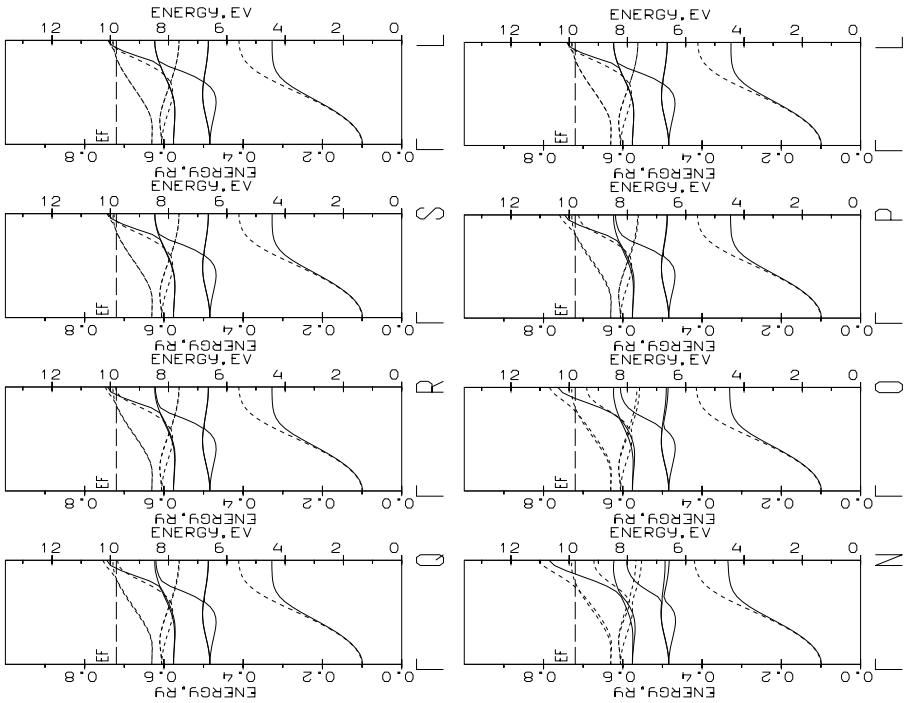

Figure 7.6: The L neck and pockets of LDA+U. Inspecting the figures, we see that there is a L neck and two L pockets. The pockets are dominated by s orbital and spin up and spin down respectively. The points are: $N = (29/64, 29/64, 19/32)$, $O = (30/64, 30/64, 18/32)$, $P = (31/64, 31/64, 17/32$, $Q = (125/256, 125/256, 67/128)$, $R = (126/256, 126/256, 66/128)$, $S = (127/256, 127/256, 65/128)$, $L = (128/256, 128/256, 64/128)$.

7.6 Band structure near the Fermi level

We now describe the effects originated from (near) degenerate states close to the Fermi surface. These have been of primary interest in past analytic studies [6, 7]. We will call such states *degenerate Fermi surface crossing* (DFSC) states. The contribution to MAE by non-DFSC states comes from the fourth order perturbation. Hence it is of the order of λ^4.

The energy splitting between DFSC states due to spin-orbit coupling is of the order of λ because the contribution comes from the first order perturbation. Using linear approximation of the dispersion relation $\epsilon(\vec{k}\lambda)$, the relevant volume in k-space was found of the order λ^3. Thus, these DFSC states make contribution of the order of λ^4. However, there may be accidentally DFSC states appearing along a line on the Fermi

surface, rather than at a point. We have found this case in our LDA calculation for Ni. Therefore the contribution of DFSC states is as important as the bulk non-DFSC states though the degeneracies occur only in small portion of the Brillouin zone.

For Ni, the change from the wrong easy axis to the correct easy axis occurs over the range of $\delta U \sim 0.2eV$, which is the order of spin-orbit coupling constant ($\sim 0.1eV$).This suggests that the easy axis depends on a quantity linearly proportional to spin-orbit coupling constant rather than on the higher order bulk effects.

The only quantity which changes linearly in spin-orbit coupling constant is the magnitudes of energy splitting of DFSC states by spin-orbit coupling. When the on-site repulsion changes by amount of the order of spin-orbit coupling constant, a state formerly just below the fermi surface would cross the surface making the splitting effective.

This rapid change of MAE with respect to spin-orbit coupling constant would explain why previous attempts failed to get the correct easy axis for Ni. Since non-magnetic DFSC states exert their contribution at a higher order, another criterion for the crossing band to be effective is their band character to be magnetic. We tracked down the band character to find that the crossing bands are magnetic bands. Since all the states are combinations of various orbital states, we draw a kind of fat band as darkened area when the crossing band contains substantial amount of t_{2g} band, which is shown in Fig.'s A.1–A.6.

The importance of the DFSC states leads us to comparative analysis of the LDA and LDA+U band structures near the Fermi level. In LDA (see Fig. 7.7), five bands are crossing the Fermi level at nearly the same points along the ΓX direction. Two of the five bands are degenerate for the residual symmetry and the other three bands accidentally cross the Fermi surface at nearly the same points. There are two sp bands with spin up and spin down, respectively. The other three bands are dominated by d orbitals. In LDA+U (see Fig. 7.5), one of the d bands is pushed down below the Fermi surface. The other four bands are divided into two degenerate pieces at the Fermi level (see Fig. 7.8): Two symmetry related degenerate $d_\downarrow$ bands and two near degenerate $sp_\uparrow$ and $sp_\downarrow$ bands. In sum the correlation weakens the effect of degenerate

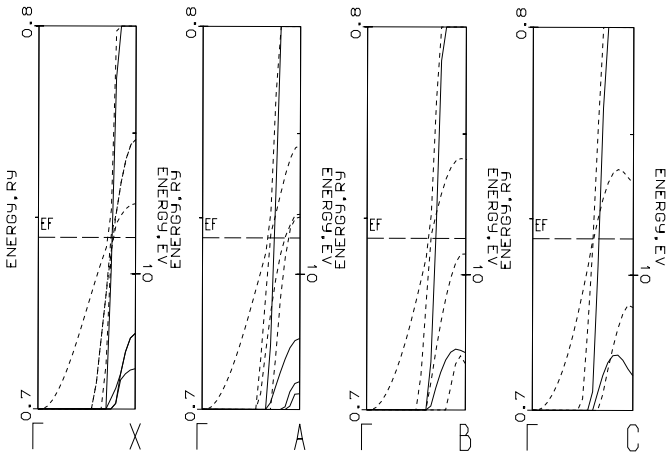

Figure 7.7: The X pockets. Inspecting the figures, we see that there are X_5 and X_2 pockets. The solid lines represent bands with dominating up-spin. The dotted lines represent bands with dominating down-spin. Notice that as we move away from the ΓX direction, we see that two bands, which are above the Fermi surface in ΓX, are submerged below the Fermi level. One of them is the experimentally confirmed X_5 pocket. The other is the LDA artificial X_2 pocket that has not been confirmed experimentally. $X = (0, 0, 1)$, $A = (1/16, 1/16, 1)$, $B = (2/16, 2/16, 1)$, $C = (3/16, 3/16, 1)$. .

bands along ΓX direction.

In LDA (see Fig. 7.7), we found that two bands are accidentally near degenerate along the line on the Fermi surface within the plane ΓXL. One band is dominated by $d_\downarrow$ orbitals. The other is dominated by $s_\downarrow$ orbitals near X and by $d_\downarrow$ orbitals off X. This accidental DFSC states persist from ΓX direction to ΓL direction. (Along ΓL direction, the degeneracy is for the residual symmetry). In LDA+U, these accidental DFSC states disappear(see Fig. 7.8). With the correlation effect U, this accidental DFCS states along a line on fermi surface move away from the fermi surface leaving only the states along ΓL direction DFSC. This degenerate states' moving away from fermi surface makes the first order perturbation effect sums up to zero as described above. Instead, there is new two-fold DFSC states along ΓL direction, both of which are dominated by $d_\downarrow$ orbitals.

Comparing the bands of LDA and LDA+U, we see that turning on of U removes five-fold degeneracy to two two-fold degeneracy along the ΓX direction, and generates a two-fold degeneracy and an effective two-fold degeneracy along the ΓL direction. In other words, the on-site repulsion U reduces the effect of splitting along ΓX direction

while increase the effect of splitting along ΓL direction. Based on the tight binding model of Mori and coworkers [7], degenerate bands along ΓL direction prefer $(1,1,1)$ direction of magnetic moment and that along ΓX direction prefer $(0,0,1)$. Therefore we can conclude that the change of DFSC states, induced by the strong correlation effect, makes the magnetic moment prefer $(1,1,1)$ direction to $(0,0,1)$ direction.

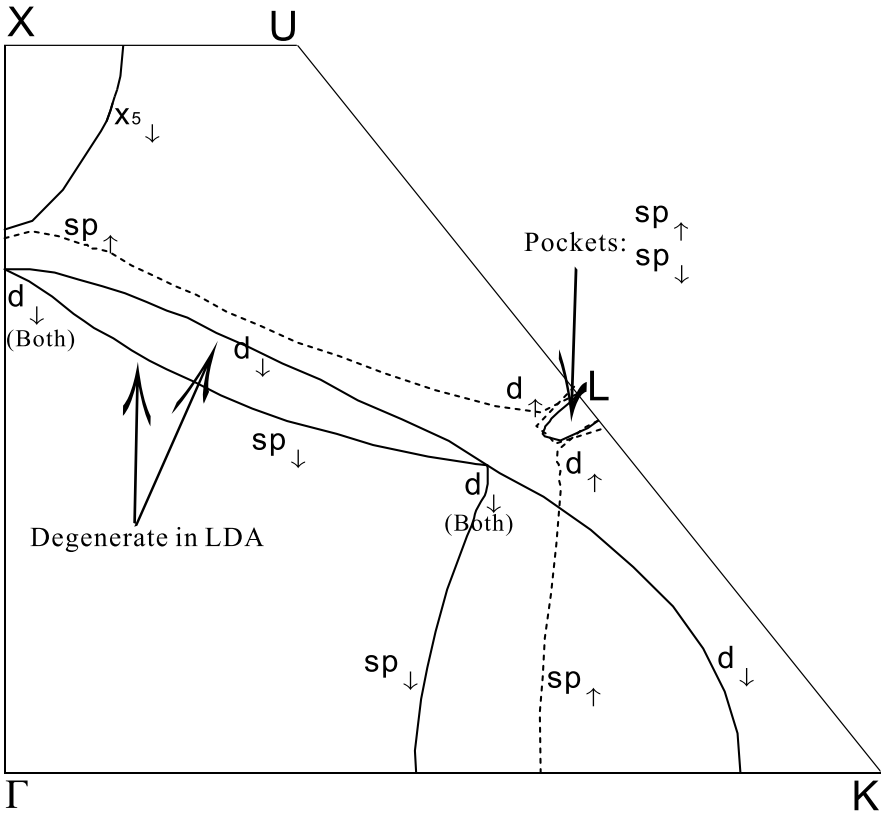

Figure 7.8: Calculated Fermi Surface of Ni with the correlation effects taken into account. The solid and dotted lines correspond to majority and minority dominant spin carriers. Dominant orbital characters are expressed. Both experimentally confirmed X_5 pocket and L neck can be seen. The X_2 pocket is missing, which is in agreement with experiments. There are two small L pockets, which has not been found by experiments.

As we have seen, the on-site repulsion U reduces the number of DFSC states along ΓX direction while increasing that of DFSC states along ΓL direction. Based on the tight–binding model, Mori and coworkers [7] have shown that DFSC states along ΓL direction result in the magnetization aligned along $(1,1,1)$ direction and DFSC states along ΓX direction result in the magnetization aligned along $(0,0,1)$ direction. Since the strong correlation does precisely this, we conclude that disappearance of DFSC

states along ΓX direction and their appearance along ΓL direction is another important element that determines the easy axis of Ni.

Chapter 8

The effect of double counting term

8.1 Introduction

We discussed an ambiguity of double counting term in section 4.5. This ambiguity is associated with the self energy in double counting term

$$E_{\rm dc}^{\rm Model}[n^\sigma] = \frac{1}{2}\bar{U}\,\bar{n}\bar{n} - \frac{1}{2}\sum_\sigma \bar{J}\,\bar{n}^\sigma\,\bar{n}^\sigma - \text{self energy}. \tag{8.1}$$

Normally the self energy term is assumed to be

$$\text{self energy} = \frac{1}{2}\bar{U}\,\bar{n} + \frac{1}{2}\sum_\sigma \bar{J}\,\bar{n}^\sigma. \tag{8.2}$$

Double counting term is designed so that the strong correlation effects already included in LSDA functional is not added by LDA+U correction. Judged by experience, LSDA functional is essentially free of self-interaction. Taking the self energy term (8.2) makes sure that this non-existent self energy is not subtracted by the double counting term.

There is, however, no theoretical ground guaranteeing that the LSDA functional is free of self-interaction. Since double counting term is spherically symmetric, change of double counting term would not change magnetic anisotropy energy, but will change other quantities such as magnetic moment. The study of the effect of Coulomb parameter in chapter 7, did not predicts magnetic moments within desired accuracy. Change of double counting term resolved this problem for Ni. In this section, we discuss the effect of double counting term. For the purpose of discussion, we call this double counting term as the new double counting term while the double counting term in chapter 7 as the old double counting term.

For simplicity, we consider only the Coulomb parameter U. The correction to LSDA

functional is then

$$E^{\mathrm{Model}}[n^\sigma] - E^{\mathrm{Model}}_{\mathrm{dc}} = -\frac{1}{2}\sum_\sigma \sum_{ab} U n^\sigma_{ab} n^\sigma_{bc}, \tag{8.3}$$

and the correction to the LSDA Kohn-Sham potential is

$$\lambda^\sigma_{ab} = -U n^\sigma_{ba}. \tag{8.4}$$

8.2 Fe

We now discuss the calculated MAE of Fe (see Fig. 8.1). The MAE at $U = 0$ is the same as in the case with the old double counting term (0.5 μeV). The change of MAE as U is turned on is very similar to the case with the old double counting term. This confirms our motivation that change of double counting term would not change MAE much. As U increases to 2 μeV till $U = 0.5$ eV. Then MAE decreases, changing the easy axis to (111) direction at $U = 1$ eV, till $U = 2.5$ eV. Around $U = 2.5eV$, MAE increase back, changing the easy axis to (001) direction at $U = 3.1$ eV. The experimental value of MAE with the correct easy axis is predicted at 3.4 eV.

The difference of magnetic moments (m[001]-m[111]) again shows close relationship with MAE (see Fig. 8.3). It increases till $U = 0.5$ ev. Then it decreases to negative value till $U = 2.5$ eV. It goes back to positive value and increases rapidly as MAE. This concurrent change of MAE and the difference of magnetic moments confirms our claim explaining why previous attempts using force theorem has failed in predicting magnetic anisotropy energy.

We found that the magnetic moment is still outside a desired accuracy (see Fig. 8.3). On increasing U, magnetic moment rapidly increaes till $U = 1.5$ eV. Then it converges to 2.7 μ_{B}. At $U = 3.5$ eV, the magnetic moment is 2.7 μ_{B}, which is 23% off from the experimental value. We correct this problem in later sections by considering the effect of Stoner parameter J as well as the Coulomb parameter U.

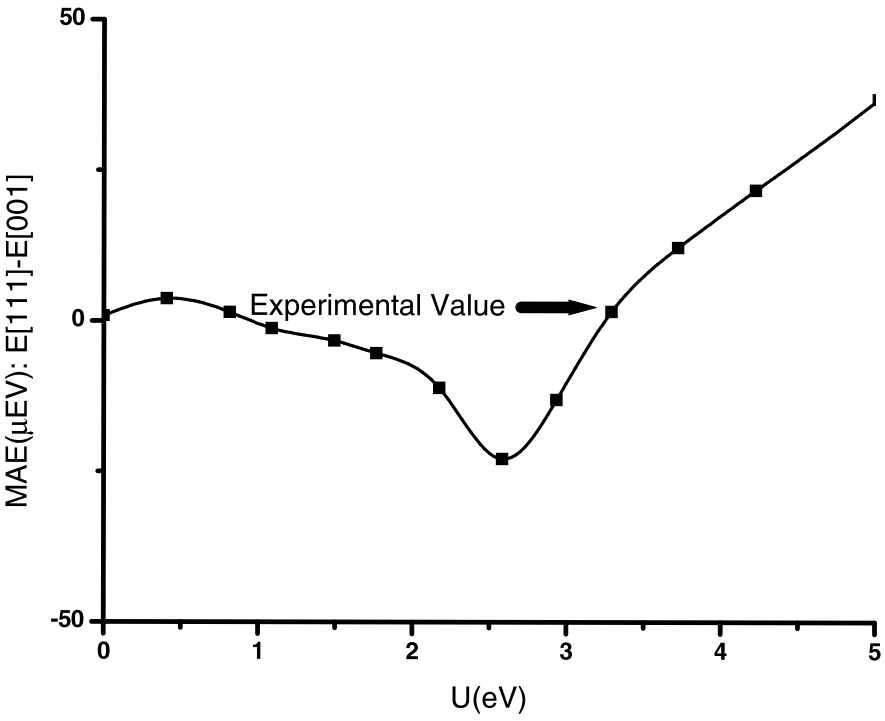

Figure 8.1: Experimental and calculated magnetocrystalline anisotropy energy MAE = $E(111) - E(001)$ for Fe. Experimental MAEs are marked by arrows for Fe (1.4 μeV).

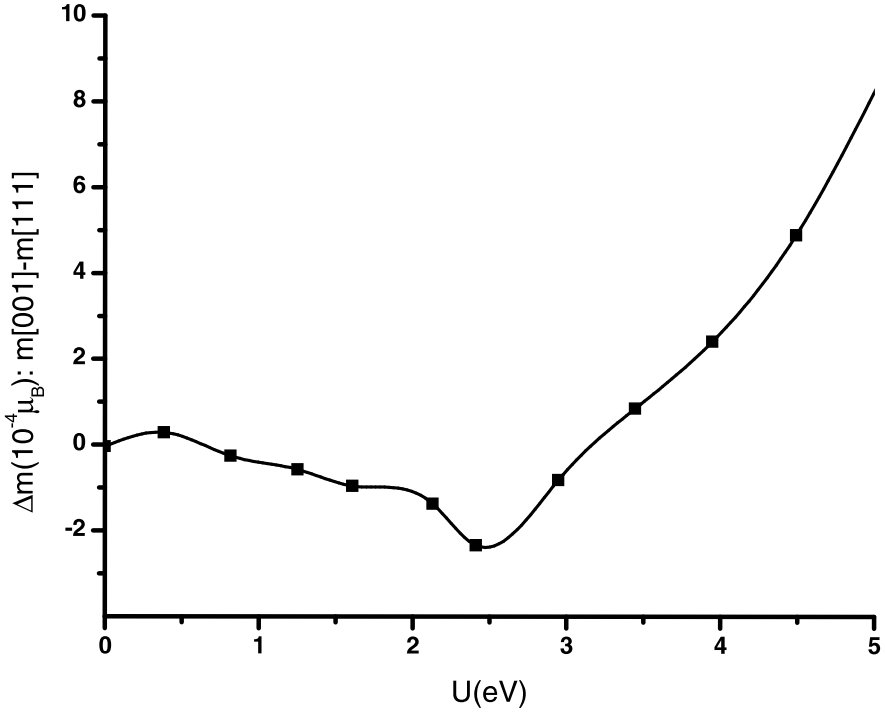

Figure 8.2: Calculated difference of magnetic moment $\Delta M = M(001) - M(111)$ for Fe.

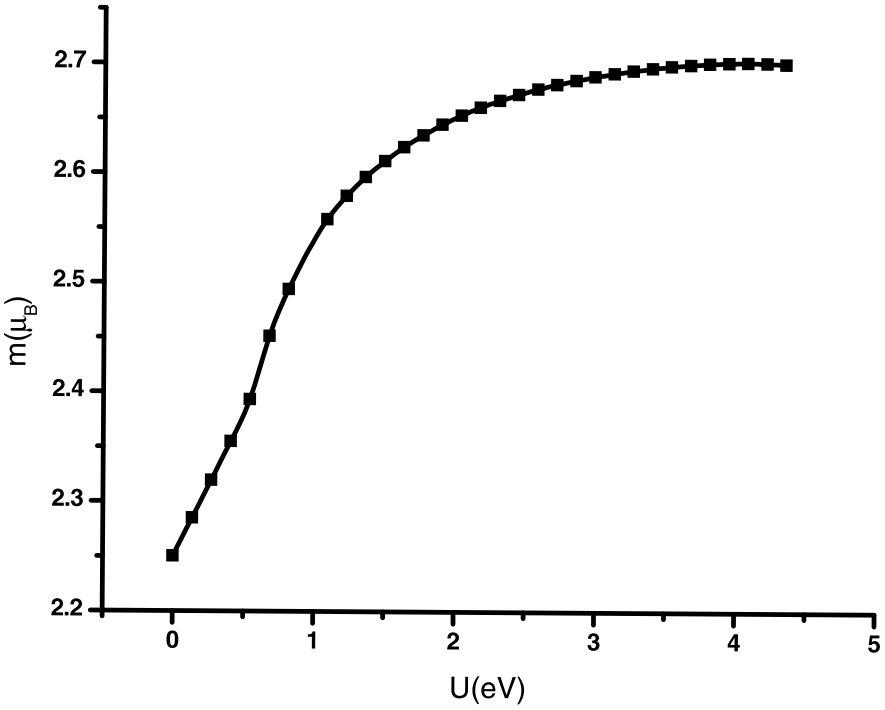

Figure 8.3: Calculated magnetic moment of Fe.

8.3 Ni

We now discuss the calculated MAE of Ni (see Fig. 8.4). The MAE at $U = 0$ is the same as in the case with the old double counting term ($2\ \mu eV$). The change of MAE as U is turned on is fairly different from the case with the old double counting term. As U increases, MAE increases to $9.5\ \mu eV$ till $U = 1.2\ eV$. Then MAE decreases to $3\ \mu eV$ till $U = 2.5\ eV$. MAE increase back to $6\ \mu eV$ till $U = 3.3\ eV$. From the MAE decreases, changing the easy direction from (001) to (111) at $U = 4\ eV$. The experimental value of MAE with the correct easy axis is predicted at $4.2\ eV$. Compared to the case with old double counting term, MAE changes more for U less than $4\ eV$. The magnitude of change is in this range of U is three times larger than that in the case with old double counting term. Moreover, there are fluctuations of MAE in this range. An interesting thing is that the MAE is strictly positive for U less than $4\ eV$. Therefore the correct easy axis is far off from LSDA as in the case with the old double counting term. This explains why it's been so hard to predict the correct easy axis of Ni and why unphysical values of parameters had to be used even

when the correct easy axis is predicted.

The value of $U(4.2\ eV)$ with the correct prediction is near that $(4\ eV)$ of the case with the old double counting. The change from the wrong easy axis to the correct easy axis occurs over the range of $\delta U \sim 0.3eV$, which is again of the order of spin-orbit coupling.

This implies the important of DFSC states in predicting magnetic anisotropy.

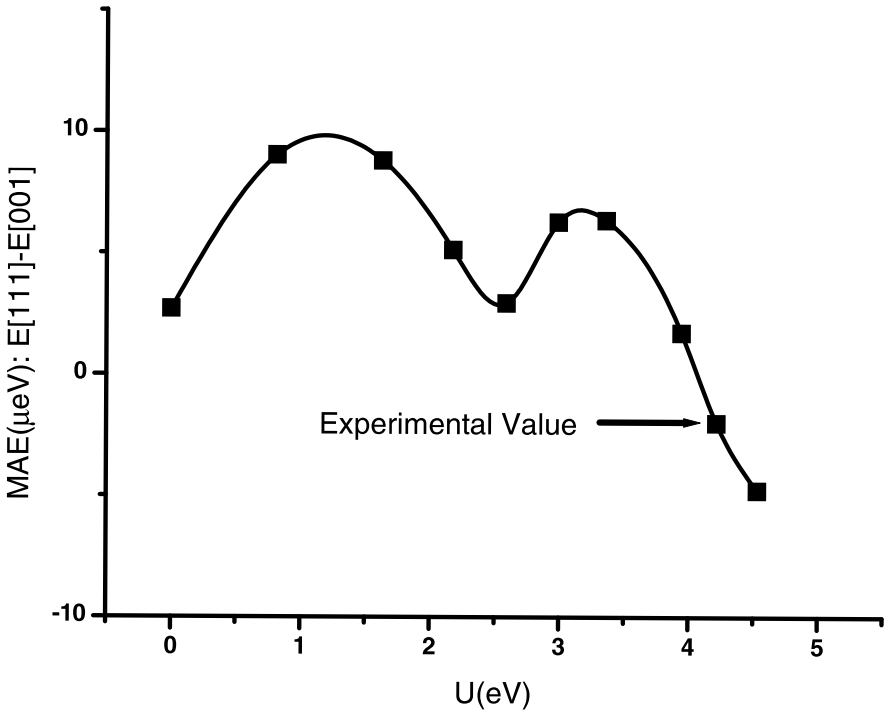

Figure 8.4: Experimental and calculated magnetocrystalline anisotropy energy MAE = $E(111) - E(001)$ for Ni. Experimental MAEs are marked by arrows for Ni $(-2.8\ \mu eV)$.

The difference of magnetic moments (m[001]-m[111]) again shows close relationship with MAE (see Fig. 8.3). It increases till $U = 0.7\ eV$. Then it decreases till $U = 1.8\ eV$. It increases again till $U = 2.7\ eV$. From there, it decreases, changing its sign at $4\ eV$. This concurrent change of MAE and the difference of magnetic moments confirms our claim explaining why previous attempts using force theorem has failed in predicting magnetic anisotropy energy.

Compared to the case with the old double counting term, the difference of magnetic moments changes more for U less than $4\ eV$. Moreover, there are fluctuations of the difference in this range. Here,we observe that the comparison of difference of magnetic moments is also in line with the comparision of MAE. This strengthens the claim that

the magnitude of magnetic moments is a decisive factor in determining magnetic anisotropy.

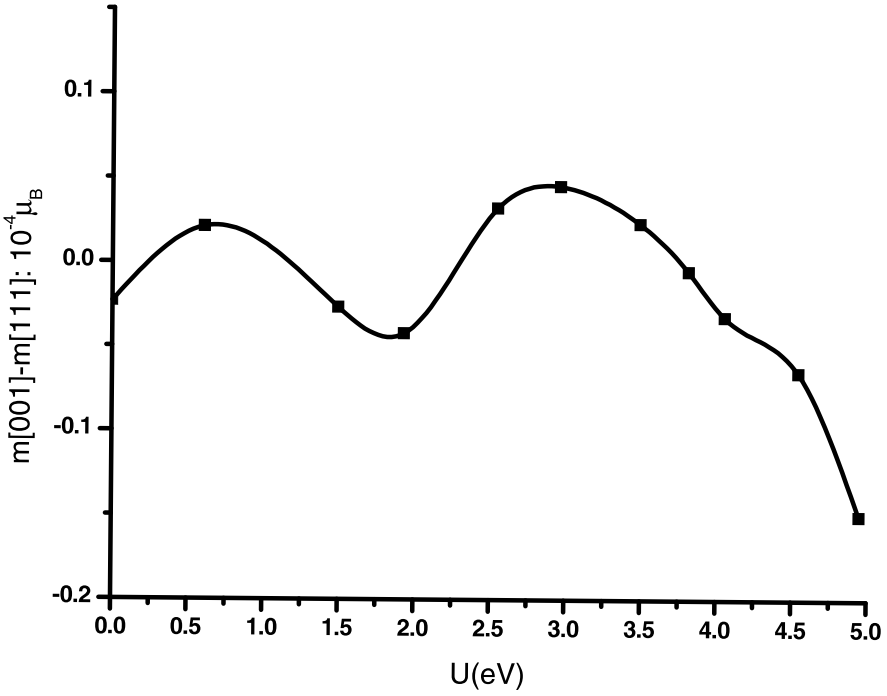

Figure 8.5: Calculated difference of magnetic moment $\Delta M = M(001) - M(111)$ for Ni.

We find that the magnetic moment is within a desired accuracy (see Fig. 8.6). On increasing U, magnetic moment slightly increases till $U = 0.5\ eV$. Then it decreases At $U = 4.2\ eV$, the magnetic moment is 0.589 μ_{B}, which is within 3% off from the experimental value.

With new double counting term, the correct magnetic anisotropy and the correct magnetic moment is predicted at $U = 4.2\ eV$. A remaining question is that there is no theoretical ground on which we prefer the new double counting term. As with other computational approaches, the agreement with experimental values is a compelling reason to choose a method in preference to another method. Though LDA+U with the new double counting term works for Ni, it makes no difference for Fe. It is, therefore, very hard to choose the new double counting term in preference to the old double counting term.

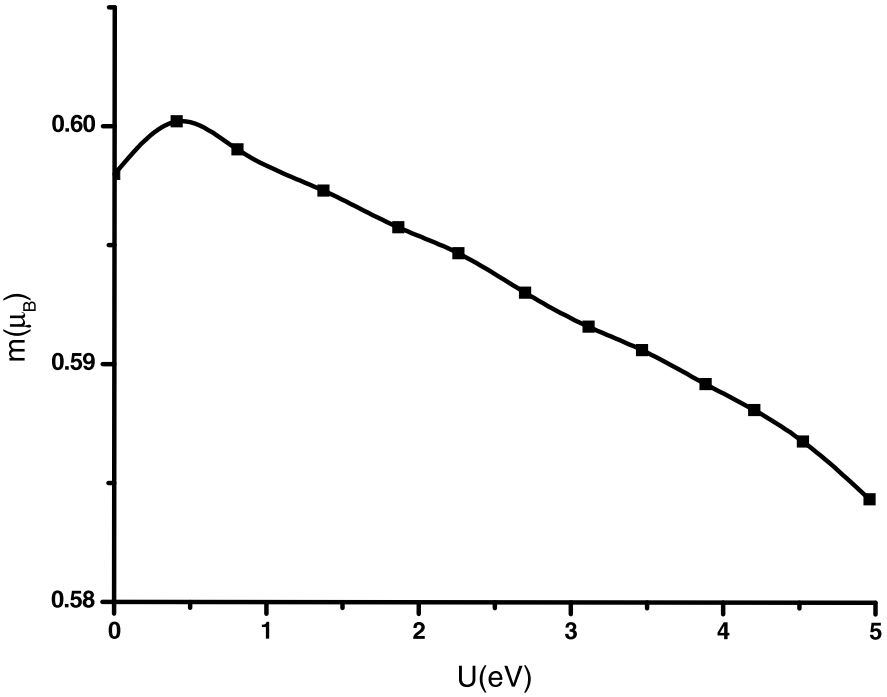

Figure 8.6: Calculated magnetic moment of Fe.

Chapter 9

Effect of Stoner Parameter J: Old Double Counting

9.1 Introduction

We studied the effect of Coulomb parameter U in the last two chapters. We found that the correct magnetic anisotropy with the correct magnetic moment can be predicted simultaneously for Ni. In the case of Fe, however, we could not predict the correct magnetic anisotropy and the correct magnetic moment simultaneously. In this chapter, we remedy this undesirable result incorporating Stoner parameter as well as Coulomb parameter.

We first exam Coulomb interaction between $3d$ electrons. The Coulomb interaction between $3d$ electrons is described by

$$\langle m, m''|v_C|m', m'''\rangle = \sum_k a_k(m, m', m'', m''')F^k, \tag{9.1}$$

$$a_k(m, m', m'', m''') = \frac{4\pi}{2k+1}\sum_{q=-k}^{k}\langle lm|Y_{kq}|lm'\rangle\langle lm''|Y^*_{kq}|lm'''\rangle. \tag{9.2}$$

where $0 \leq k \leq 4$, and m is magnetic moment quantum number of $3d$ electrons . By symmetry, only those $a_k(m, m', m'', m''')$ with odd k have non-zero values. The Coulomb interaction bwteen $3d$ electrons, therefore, can be described by three paramteters F^0, F^2, and F^4. These three parameters be linked to Coulomb and Stoner parameters U and J obtained from LSDA supercell procedures via $U = F^0$ and $J = (F^2 + F^4)/14$. The ratio F^2/F^4 is to a good accuracy a constant ~ 0.625 for d electrons. With this relation between F^2 and F^4, we have two free parameters U and J in describing Coulomb interaction between $3d$ electrons.

We use these two parameters, U and J, to tackle the problem of predicting magnetic anisotropy and magnetic moment at the same time. We use the old double counting

term in this section.

9.2 Fe

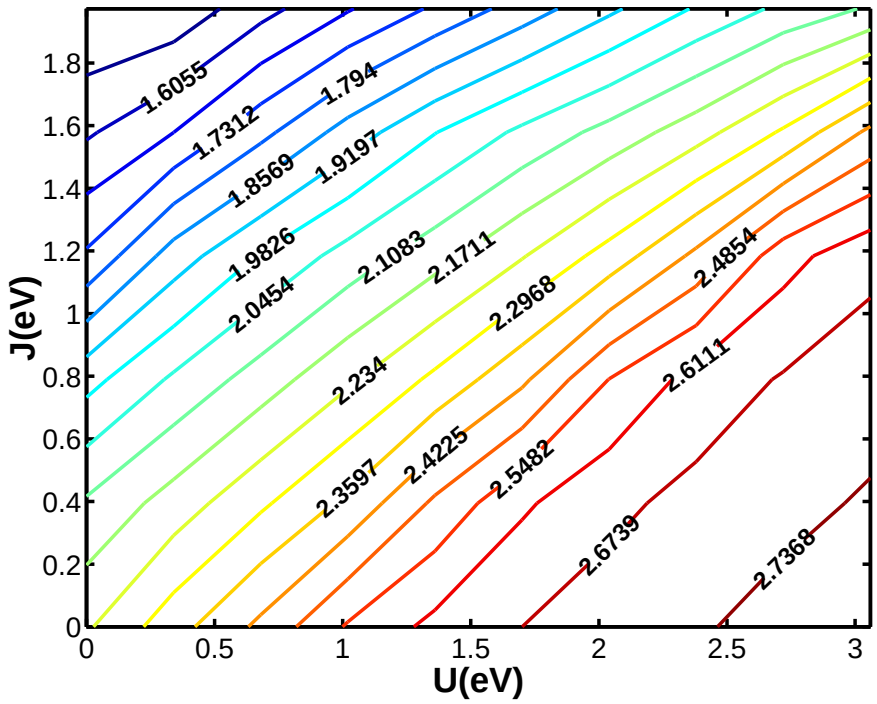

Figure 9.1: Fe. Contour plot of magnetic moment as a function of Coulomb parameter U and Stoner parameter J. The contour is drawn at 0.063 μ_B interval, which is 2.9% of the experimental value of magnetic moment 2.2 μ_B

We first find magnetic moment as a function of U and J (see Fig. 9.1). The magnetic moment changes at similar rates for both U and J. Out of the contours, we pick the contour with experimental magnetic moment 2.2 μ_B, to study magnetic anisotropy. This makes sure of predicting the correct magnetic moment.

Since we expect the magnetic moment a continuous function of U and J at least for small U and J, it is not surprising to have a contour with the experimental magnetic moment. It is, however, very exciting observation that the contour lies within reasonable ranges of U and J. For example, it is possible that the contour is confined within a narrow range of U, say $0 \leq U \leq 1\ eV$ for a reasonable range of J, say $J \leq 2\ eV$, or vice versa. As we see later, this confinement happens in case of Ni.

Magnetic moment increases as U increases, but decreases as J increases. At first

sight, it is counter-intuitive for magnetic moment to decrease as J increases. Note that what we are increasing is F^2 and F^4 at a certain proportion, not J. The sum of F^2 and F^4 is linked to J. This linkage is established by observing their appearance in double counting term. Unlike F^0 that has a tight link with U, the link of F^2 and F^4 to J is very weak. The terminology J must be take with some grains of salt.

We restricted the value of U less than 3 eV and the value of J less than 2 eV. Since the strong correlation effects are described not only by U but also J, we expect that the value of U where the correct magnetic anisotropy is predicted is less than the case with only U. As we seen in short order, this is the case.

We describe the calculated MAE. The MAE is calculated along the contour with magnetic moment 2.2 μ_{B}. At $U = 0$ eV and $J = 0$ eV, the MAE is 0.5 μeV. It increases as we move along the contour in the direction of increasing U and J. Unlike the case with only U, MAE is monotonically increasing to 6 μeV at $U = 3$ eV and $J = 1.8$ eV.

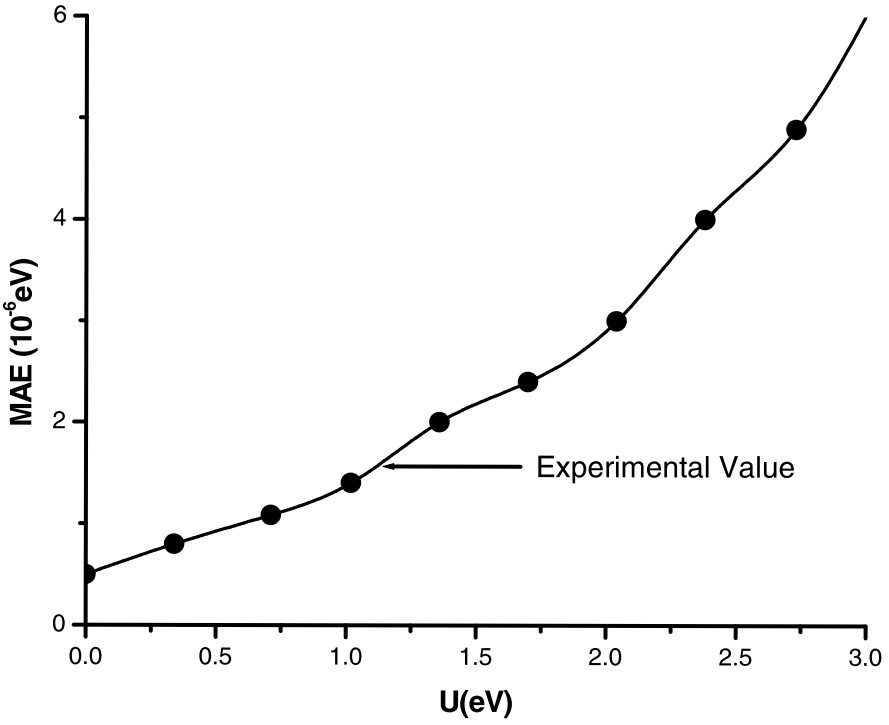

Figure 9.2: Fe. Magnetic Anisotropy Energy, $E(111) - E(001)$. The contour with magnetic moment 2.2 $\mu_{\mathrm{B}}$is followed. The magnetic anisotropy energy is plotted as a function of U. The corresponding value of J can be found in the contour plot Fig. 9.1.

The correct MAE with the correct direction of magnetic moment is predicted at

$$U = 1.2\ eV \text{ and } J = 0.8\ eV.$$

We find concurrent behaviours of MAE and the difference of magnetic moments (See Fig. 9.3). The difference of magnetic moments moderately increases till $U = 2\ eV$ and then rapidly increase. There is no change of increase rate in MAE. If we restrict our interest into physically meaningful range of U $(0 \leq U \leq 2\ eV)$, then we observe the concurrence in good agreement. This again confirms that the magnitude of magnetic moment is a determining factor in magnetic anisotropy.

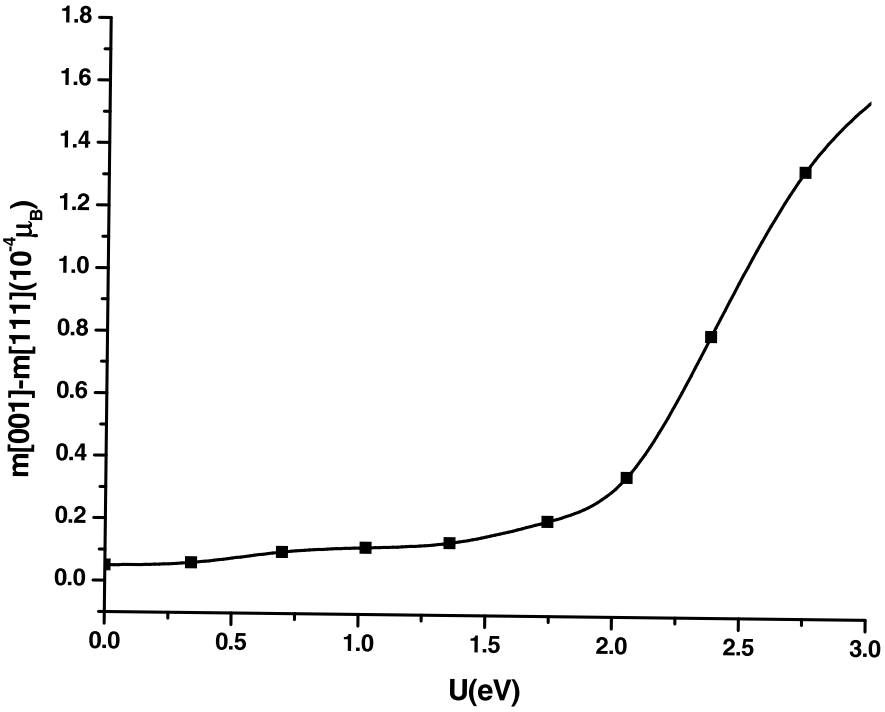

Figure 9.3: Fe. Difference of Magnetic Moments, $m(001) - E(111)$. The contour with magnetic moment 2.2 $\mu_{\mathrm{B}}$is followed. The magnetic anisotropy energy is plotted as a function of U. The corresponding value of J can be found in the contour plot Fig. 9.1.

9.3 Ni

We now discuss the effect of Stoner parameter J as well as U. We first find magnetic moment as a function of U and J (see Fig. 9.4). The magnetic moment changes much faster for J than for U. This situation is quite different form that of Fe, where the magnetic moment changes at similar rates for U and J. Note that for a magnetic

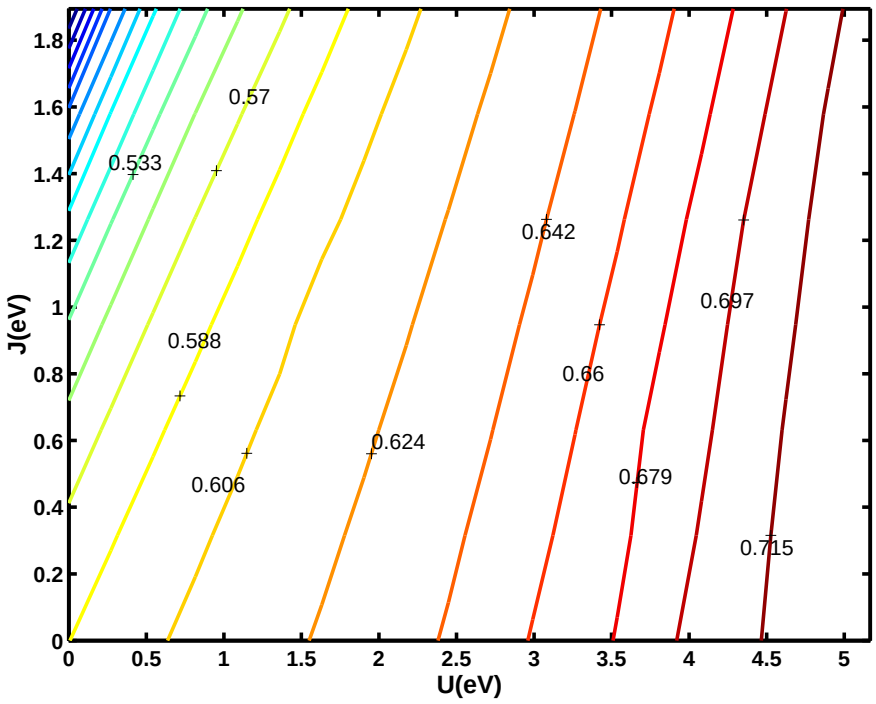

Figure 9.4: Ni. Contour plot of magnetic moment as a function of Coulomb parameter U and Stoner parameter J. The contour is drawn at 0.018 μ_B interval, which is 2.9% of the experimental value of magnetic moment 0.606 μ_B

moment, the available value of U is restricted to $\delta \sim 1\ eV$.

Magnetic moment increases as U increases, but decreases as J increases. Note that what we are increasing is F^2 and F^4 at a certain proportion ($F^4 = 0.526F^2$), not J. We restricted the value of U less than 5 eV and the value of J less than 2 eV.

For magnetic anisotropy, we walked along three paths. We now discuss the results. The first path we walk along is the constant magnetic moment contour passing the origin. MAE increases to 13 μeV as we move along the contour in the direction of increasing U and J till $U = 0.4\ eV$ and $J = 0.25\ eV$. Then it decreases, changing from the wrong easy axis to the correct easy axis at $U = 1.5\ eV$ and $J = 1.2\ eV$. The correct anisotropy energy is predicted at two points. One is at $U = 1.2\ eV$ and $J = 1.3\ eV$, and the other is at $U = 1.6\ eV$ and $J = 1.7\ eV$. As discussed, comparing the absolute values of U and J with experiments need some caution. We can, however, compare relative values with experiments. In experiments, J is much smaller than U. Since, we predicted the correct magnetic anisotropy when U and J are similar, the

result is not desirable. Moreover, we find that there is LDA artificial X_2 pocket.

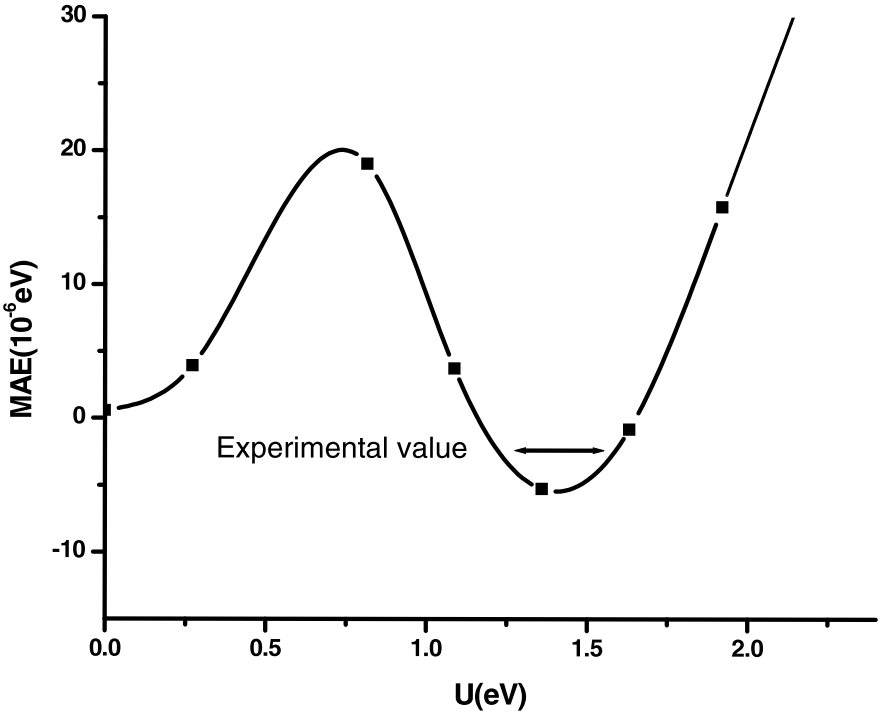

Figure 9.5: Ni. Magnetic Anisotropy Energy, $E(111) - E(001)$. The contour with magnetic moment 0.59 $\mu_{\mathrm{B}}$is followed. The magnetic anisotropy energy is plotted as a function of U. The corresponding value of J can be found in the contour plot Fig. 9.4.

Compared the result with only U, we brought more than solve problems. Therefore we try another path to walk along. This time we walked along another constant J path, where $J = 0.3\ eV$. We learned in case of Fe that larger J would make the necessary value of U smaller to predict the correct magnetic anisotropy. We see this again in the previous case with constant magnetic moment. These are the motivations to walk along the path with $J = 0.3\ eV$.

MAE increases to 15 μeV as we move along the contour in the direction of increasing U and J till $U = 0.7$. Then it wiggle down to 0.3 μeV till $U = 2eV$. From there it slightly increases to 1 μeV and stays around till $U = 3.1\ eV$. It then decreases, changing from the wrong easy axis to the correct easy axis at $U = 3.3\ eV$, to $-14\ \mu eV$ till $U = 3.8\ eV$. From there it increases again, chnageing from the correct easy axis to the wrong easy axis at $U = 4.3\ eV$.

The correct anisotropy energy is predicted at two points. One is at $U = 3.4\ eV$, and

the other is at $U = 4.2\ eV$. For $U = 4.2\ eV$ and $J = 0.3\ eV$ the magnetic moment is larger than that at $U = 4\ eV$ and $J = 0\ eV$. For this reason, we prefer the point $U = 3.4\ eV$ and $J = 0.3\ eV$. The magnetic moment at this point is 0.67 μ_B, off by 11% from the experimental value.

The Fermi surface does not contain the LDA artificial X_2 pocket. However, there are still LDA+U artificial L pockets. In conclusion, turning on a small J improved the result. The Fermi surface is basically the same as that with $J = 0$. The magnetic moment is closer to the experimental value. The magnetic anisotropy is correctly predicted.

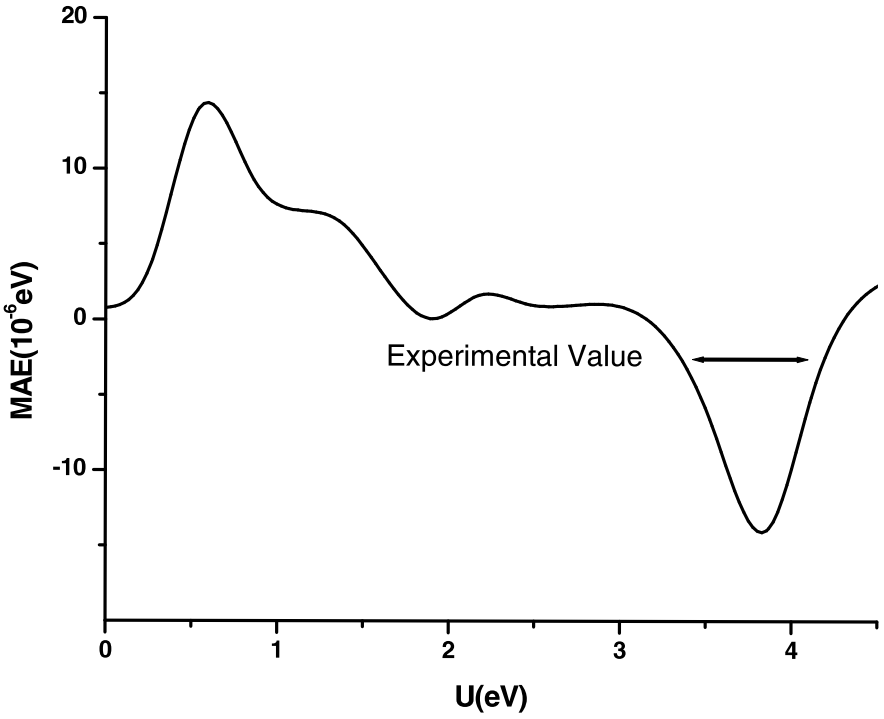

Figure 9.6: Ni. Magnetic Anisotropy Energy, $E(111) - E(001)$. The path with Stoner parameter $J = 0.3\ eV$ is followed.

From the previous two studies, we see that turning on J reduces the necessary U to predict the correct magnetic anisotropy. We also see that small U makes the calculated magnetic moment closer the experimental value. This insight takes us to working on several points with reasonable values of U and J. Form this study, we find the best result at $U = 1.9\ eV$ and $J = 1.2\ eV$. Now we discuss this result.

We walked along a line connecting the origin and the point with $U = 1.9\ eV$ and

$J = 1.2\ eV$. The calculated MAE is plotted in Fig. 9.7. As we walk along the line in increasing J and J direction, MAE increases to 60 μeV till $U = 0.5\ eV$ and $J = 0.3\ eV$, then decreases. While decreasing it makes a flat area from $U = 1.4\ eV$ and $J = 0.9$ to $U = 1.7\ eV$ and $J = 1.1\ eV$ where MAE is positive and around 10 μeV. After the flat area, MAE changes from the wrong easy axis to the correct easy axis. The correct magnetic anisotropy is predicted at $U = 1.9\ eV$ and $J = 1.2\ eV$. At this point the magnetic moment is 0.61 μ_{B}, which is in good agreement with the experimental value 0.606 μ_{B}

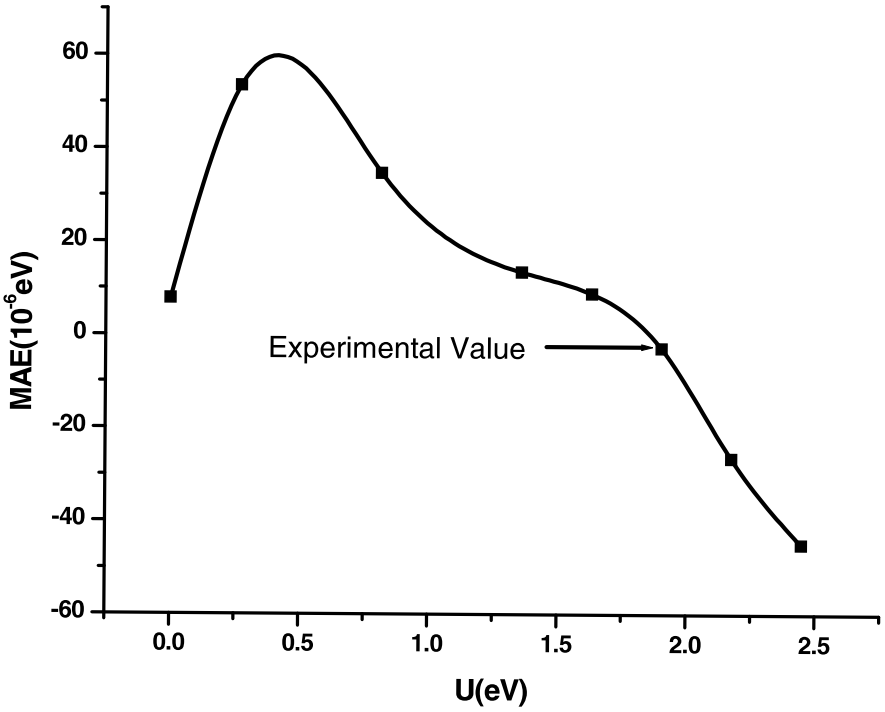

Figure 9.7: Ni. Magnetic Anisotropy Energy, $E(111) - E(001)$. The line connecting the origin and $U = 1.9\ eV$ and $J = 1.2\ eV$ is followed. The corresponding value of magnetic moment can be found in the contour plot Fig. 9.4.

We also study the difference of magnetic moments $(m(001) - m(111))$. We find again the concurrent behaviour of MAE and the difference of magnetic moments. The calculated difference of magnetic moments is plotted in Fig. 9.8. As we walk along the line in increasing J and J direction, the difference increases to till $U = 0.4\ eV$ and $J = 0.2\ eV$, then decreases. While decreasing it makes a flat area from $U = 0.9\ eV$ and $J = 0.6$ to $U = 1.7\ eV$ and $J = 1.1\ eV$. After the flat area, the difference decrease

rapidly. Now, it is clear that the magnitude of magnetic moment is a determining factor in magnetic anisotropy.

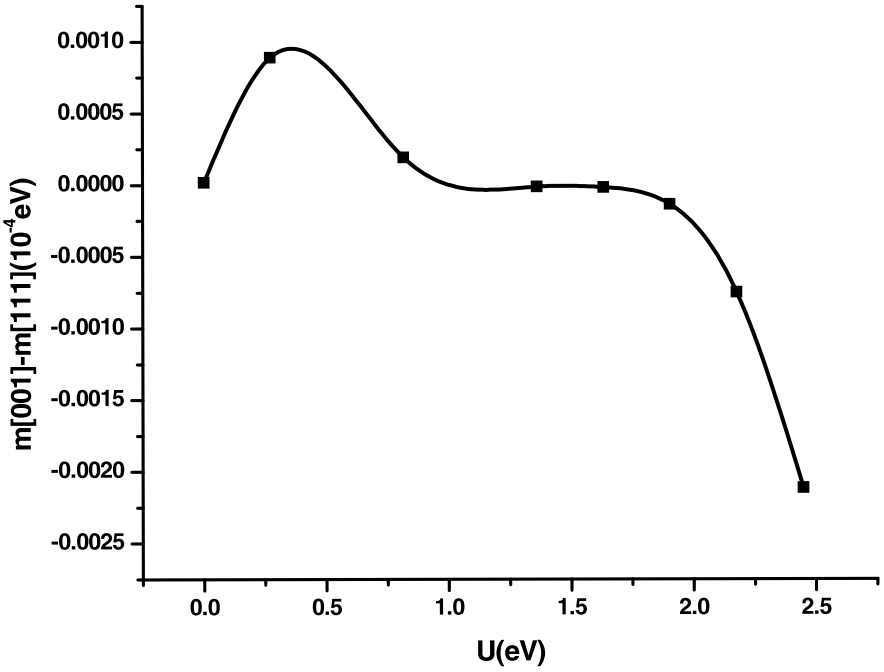

Figure 9.8: Ni. Difference of Magnetic Moments, $m(001) - m(111)$. The line connecting the origin and $U = 1.9\ eV$ and $J = 1.2\ eV$ is followed. The corresponding value of magnetic moment can be found in the contour plot Fig. 9.4.

We now present implications of our results on the calculated electronic structure for the case of Ni. One important feature which emerges from the calculation is the absence of the X_2 pocket (see Fig. 9.9). This has been predicted by LDA but has not been found experimentally [37]. The band corresponding to the pocket is pushed down just below the Fermi level. This is expected since correlation effects are more important for slower electrons and the velocity near the pocket is rather small. It turns out that the whole band is submerged under the Fermi level.

In LDA, we see that five bands are passing through the Fermi level in ΓX direction. Note that two bands are degenerate due to the residual symmetry in the direction. As we move away from the ΓX direction, we see that two bands are submerged below the Fermi level. These two bands are the two X pockets in LDA. Experiments confirm that there is one only X pocket. One of the two X pockets is, therefore, an LDA artifact.

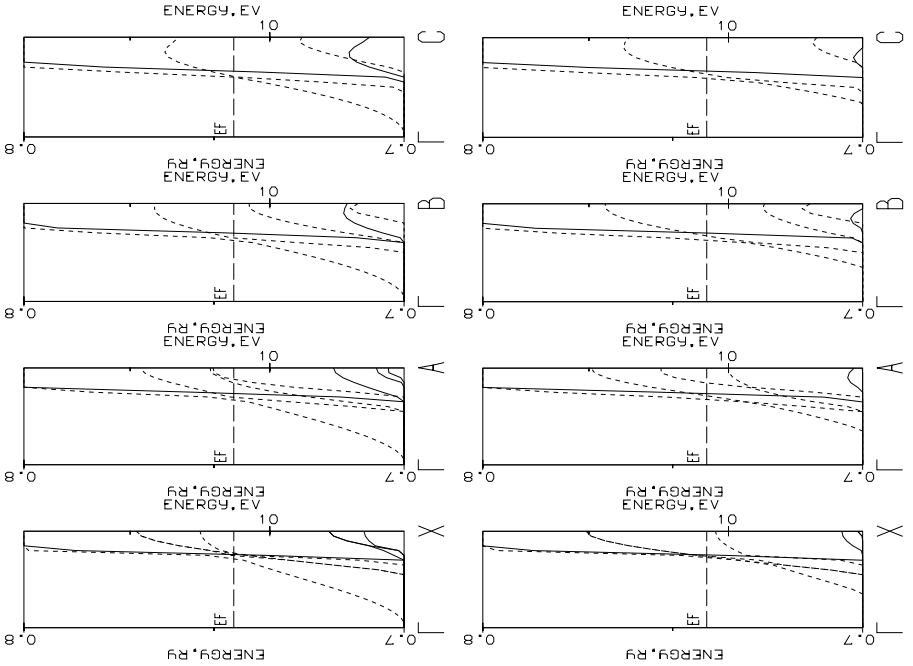

(a) LDA (b) LDA+U

Figure 9.9: The X pockets of LDA+U. Inspecting the figures, we see that there are X_5 and X_2 pockets in LDA and that there is a X_5 pocket in LDA+U. The X_2 pocket was found in LDA, but no experiments has confirmed it. The X_5 pocket, present in both LDA and LDA+U has been confirmed in experiments. The solid lines represent bands with dominating up-spin. The dotted lines represent bands with dominating down-spin. $X = (0, 0, 1)$, $A = (1/16, 1/16, 1)$, $B = (2/16, 2/16, 1)$, $C = (3/16, 3/16, 1)$. .

In LDA+U, we see that four bands are passing through the Fermi level in ΓX direction. Note that two bands are degenerate due to the residual symmetry in the direction. As we move away from the ΓX direction, we see that one band is submerged below the Fermi level. The is the experimentally confirmed X_5 pocket. A very important point to notice is that the band that makes X_2 pocket in LDA is just below the Fermi level. This brings a suspicion that the point $U = 1.9\ eV$ and $J = 1.2\ eV$ is where the X_2 pocket just disappear. For this reason we study the X pockets at $U = 1.7\ eV$ and $J = 1.1\ eV$ (see Fig. 9.10).

At this point we see that five bands are passing through the Fermi level in ΓX direction. As we move away from the ΓX direction, we see that two bands are submerged below the Fermi level. These are X_5 and X_2 pockets.

Notice that the band that makes X_2 pocket is just above the Fermi level in ΓX direction. We we mover away from the ΓX direction, the band is submerged below the Fermi level immediately. This confirms that the point $U = 1.9\ eV$ and $J = 1.2\ eV$ is where the X_2 pocket just disappear.

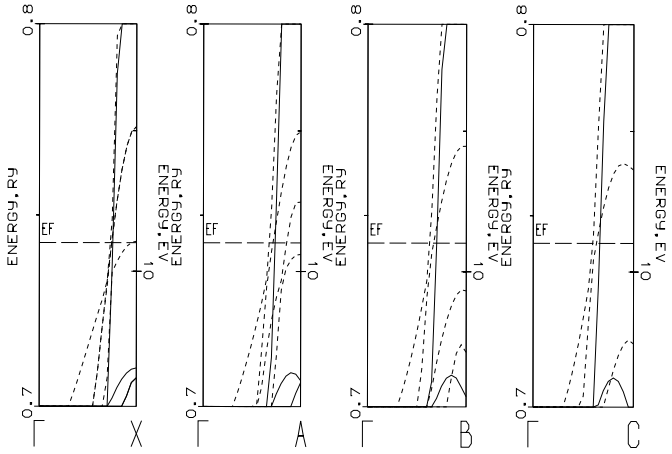

Figure 9.10: The X pockets of LDA+U at $U = 1.7\ eV$ and $J = 1.1\ eV$. Inspecting the figures, we see that there are X_5 and X_2 pockets. Note that the X_2 pocket is extremely small. The solid lines represent bands with dominating up-spin. The dotted lines represent bands with dominating down-spin. $X = (0, 0, 1)$, $A = (1/16, 1/16, 1)$, $B = (2/16, 2/16, 1)$, $C = (3/16, 3/16, 1)$. .

There has been some suspicions that the incorrect position of the X_2 band within LDA was responsible for the incorrect prediction of the easy axis within this theory. Daalderop and coworkers [10] removed the X_2 pocket by increasing the number of valence electrons and found the correct easy axis. We see that the correct magnetic anisotropy with the correct magnetic moment comes when this artificial X_2 pocket just disappear. We therefore conclude that the absence of the pocket is one of the central elements in determining the magnetic anisotropy, and there is no need for any ad-hoc adjustment within a theory which takes into account the correlations.

In the study of the effect of Coulomb parameter, we have found two extra very tiny L pockets as well as L neck in LDA+U (see Figs. 7.8 and 7.6). This L neck has been confirmed by experiments. There is, however, no experimental confirmation on this L pockets. In this study, we see that there is the experimentally confirmed L neck and that there is not these artificial L pockets (see Fig. 9.11.)

We now discuss the L neck. The experimental L neck is a spin-down dominated band.

From the Fig. 9.11, we see one spin-down dominated band is just below the Fermi level in ΓL direction. As we mover away from the ΓL direction, we see that the band is surfacing up above the Fermi level. This is the experimentally confirmed L neck.

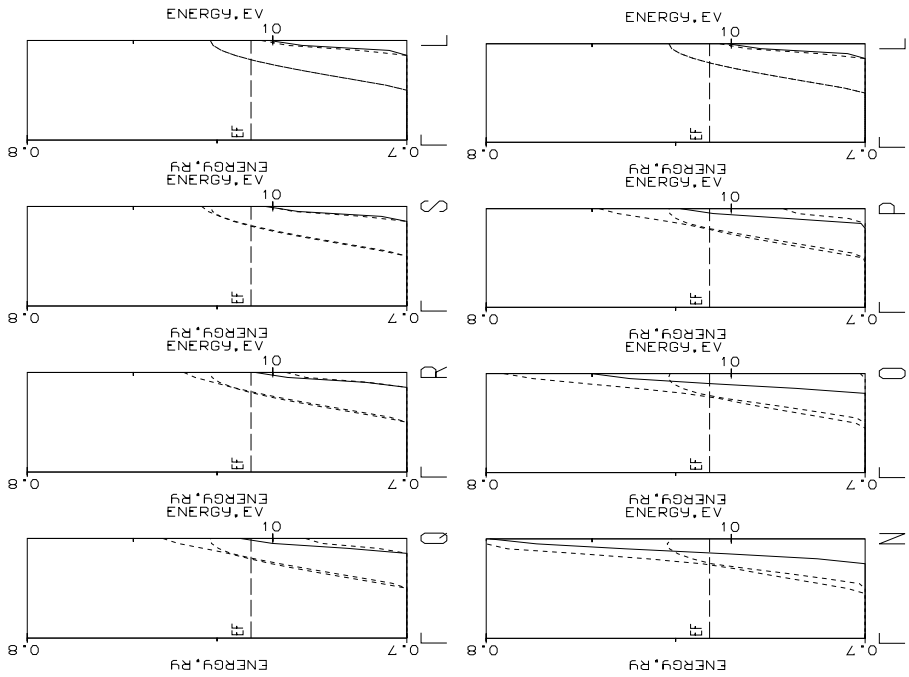

Figure 9.11: The L neck of LDA+U. Notice the absence of L pockets. Inspecting the figures, we see that there is a L neck. The solid lines represent bands with dominating up-spin. The dotted lines represent bands with dominating down-spin. The points are: $N = (29/64, 29/64, 19/32)$, $O = (30/64, 30/64, 18/32)$, $P = (31/64, 31/64, 17/32$, $Q = (125/256, 125/256, 67/128)$, $R = (126/256, 126/256, 66/128)$, $S = (127/256, 127/256, 65/128)$, $L = (128/256, 128/256, 64/128)$.

We now discuss the absence of the artificial L pockets. Notice that there is another band just below the Fermi level in ΓQ direction, ΓR direction, ΓS direction, and ΓL direction. This band was above the Fermi surface in ΓL direction in the study of Coulomb parameter. In this case, we see that the band is below the Fermi surface always and does not form a pocket. Regarding the other artificial L pocket, we see that no other band is near the Fermi surface, this band is well below the Fermi surface and does not form a pocket.

We now describe the effects originated from (near) degenerate states close to the Fermi surface. These have been of primary interest in past analytic studies [6, 7]. We

will call such states *degenerate Fermi surface crossing* (DFSC) states. The importance of the DFSC states leads us to comparative analysis of the LDA and LDA+U band structures near the Fermi level. In LDA, five bands are crossing the Fermi level at

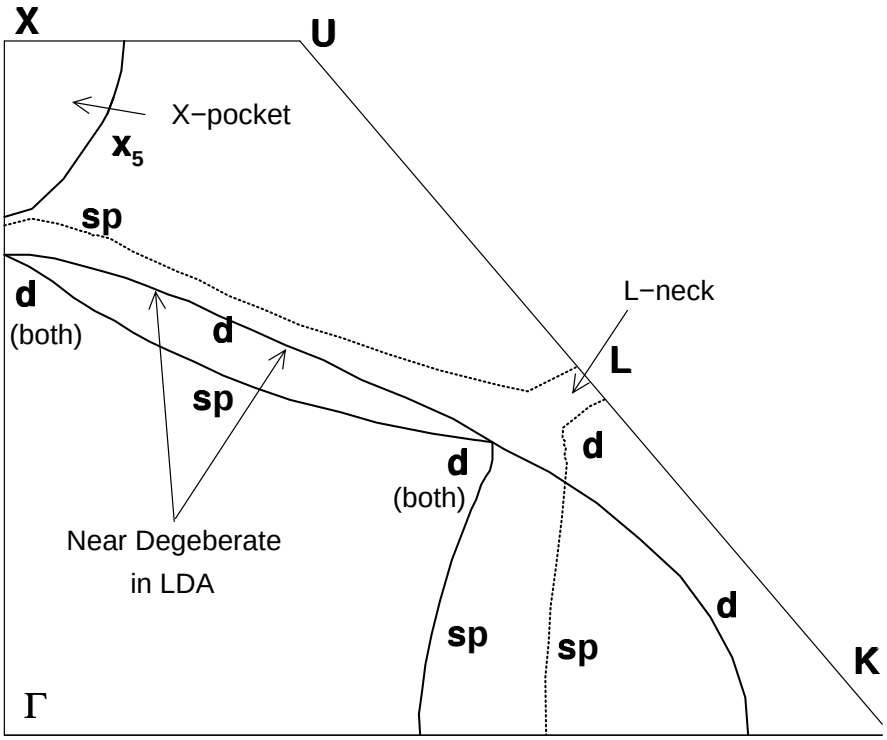

Figure 9.12: Calculated Fermi Surface of Ni with the correlation effects taken into account. The solid and dotted lines correspond to majority and minority dominant spin carriers. Dominant orbital characters are expressed. Both experimentally confirmed X_5 pocket and L neck can be seen. The X_2 pocket is missing, which is in agreement with experiments.

nearly the same points along the ΓX direction. Two of the five bands are degenerate for the residual symmetry and the other three bands accidentally cross the Fermi surface at nearly the same points. There are two *sp* bands with spin up and spin down, respectively. The other three bands are dominated by *d* orbitals. In LDA+U, one of the *d* bands is pushed down below the Fermi surface. The other four bands are divided into two degenerate pieces at the Fermi level (see Fig. 9.12): Two symmetry related degenerate $d_\downarrow$ bands and two near degenerate $sp_\uparrow$ and $sp_\downarrow$ bands. In sum the correlation weakens the effect of degenerate bands along ΓX direction.

In LDA, we found that two bands are accidentally near degenerate along the line on

the Fermi surface within the plane ΓXL. One band is dominated by $d_\downarrow$ orbitals. The other is dominated by $s_\downarrow$ orbitals near X and by $d_\downarrow$ orbitals off X. This accidental DFSC states persist from ΓX direction to ΓL direction. (Along ΓL direction, the degeneracy is for the residual symmetry). In LDA+U, these accidental DFSC states disappear(see Fig. 7.8). With the correlation effect U, this accidental DFCS states along a line on fermi surface move away from the fermi surface leaving only the states along ΓL direction DFSC. This degenerate states' moving away from fermi surface makes the first order perturbation effect sums up to zero as described above. Instead, there is new two-fold DFSC states along ΓL direction, both of which are dominated by $d_\downarrow$ orbitals.

Comparing the bands of LDA and LDA+U, we see that turning on string correlation removes five-fold degeneracy to two two-fold degeneracy along the ΓX direction, and generates a two-fold degeneracy and an effective two-fold degeneracy along the ΓL direction. In other words, strong correlation reduces the effect of splitting along ΓX direction while increase the effect of splitting along ΓL direction. Based on the tight binding model of Mori and coworkers [7], degenerate bands along ΓL direction prefer $(1,1,1)$ direction of magnetic moment and that along ΓX direction prefer $(0,0,1)$. Therefore we can conclude that the change of DFSC states, induced by the strong correlation effect, makes the magnetic moment prefer $(1,1,1)$ direction to $(0,0,1)$ direction.

As we have seen, strong correlation reduces the number of DFSC states along ΓX direction while increasing that of DFSC states along ΓL direction. Based on the tight–binding model, Mori and coworkers [7] have shown that DFSC states along ΓL direction result in the magnetization aligned along $(1,1,1)$ direction and DFSC states along ΓX direction result in the magnetization aligned along $(0,0,1)$ direction. Since the strong correlation does precisely this, we conclude that disappearance of DFSC states along ΓX direction and their appearance along ΓL direction is another important element that determines the easy axis of Ni.

To conclude, we find that the correct magnetic anisotropy and the correct magnetic moment is predicted when we incorporate strong correlation effect. We also find that

the correct Fermi surface is also predicted at the same time. This is the first work predicting the correct magnetic anisotropy, the correct magnetic moment, and the correct Fermi sufcace simultaneously.

Chapter 10

Effect of Stoner Parameter: New Double Counting Term

10.1 Introduction

Our study of the effect of Stoner parameter J as well as the Coulomb parameter U in the last chapter gives the perfect result. In this section, we would like to study the effect of double counting term when both U and J are turned on. Since the old double counting term has been studied in the last chapter, we study the new double counting term in this section with both U and J.

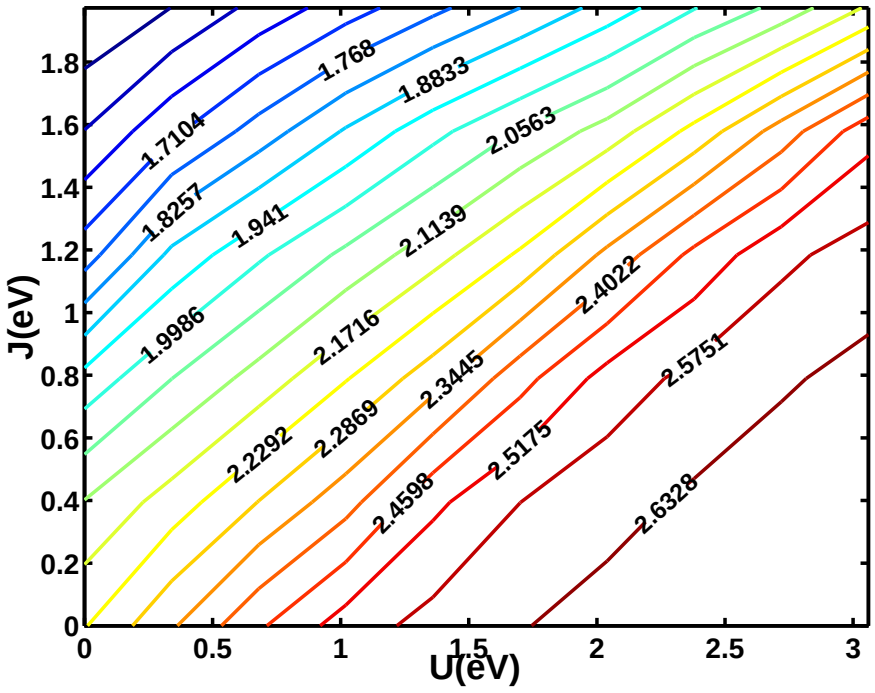

Figure 10.1: Fe. Contour plot of magnetic moment as a function of Coulomb parameter U and Stoner parameter J. The contour is drawn at 0.058 μ_B interval, which is 2.7% of the experimental value of magnetic moment 2.2 μ_B

10.2 Fe

We first find magnetic moment as a function of U and J (see Fig. 10.1). The magnetic moment changes at similar rates for both U and J. Out of the contours, we pick the contour with experimental magnetic moment 2.2 μ_B, to study magnetic anisotropy. This makes sure of predicting the correct magnetic moment.

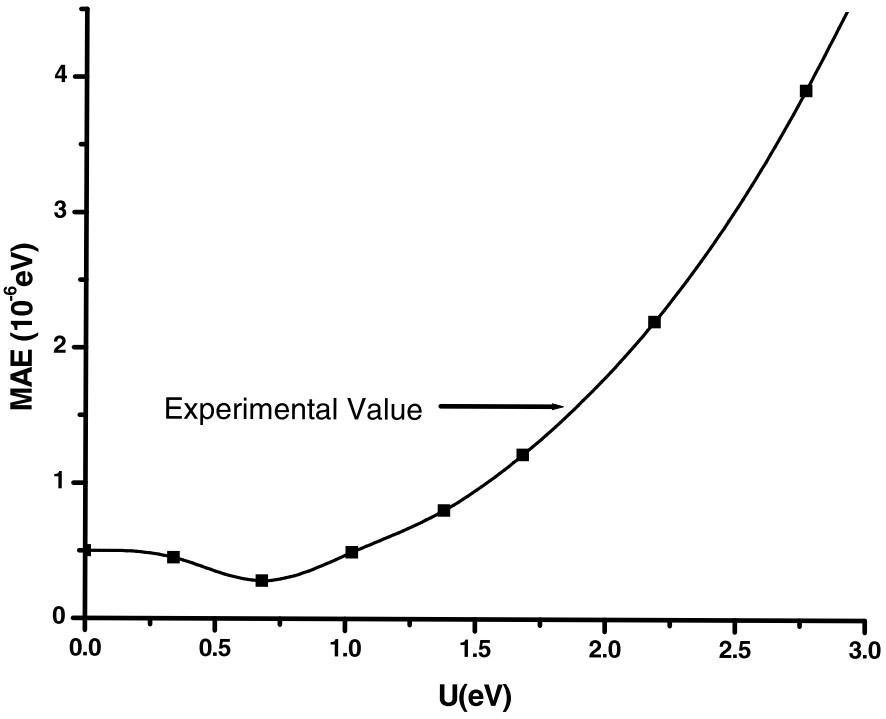

Figure 10.2: Fe. Magnetic Anisotropy Energy, $E(111) - E(001)$. The contour with magnetic moment 2.2 $\mu_B$is followed. The magnetic anisotropy energy is plotted as a function of U. The corresponding value of J can be found in the contour plot Fig. 10.1.

As in the case with the old double counting term, the contour lies within reasonable ranges of U and J. It is not confined within a narrow range of U, say $0 \leq U \leq 1\ eV$ for a reasonable range of J, say $J \leq 2\ eV$, nor vice versa. As we see later, this confinement happens in case of Ni.

Magnetic moment increases as U increases, but decreases as J increases. Note that what we are increasing is F^2 and F^4 at a certain proportion, not J. The sum of F^2 and F^4 is linked to J by observing their appearance in double counting term.

We restricted the value of U less than 3 eV and the value of J less than 2 eV. As we

have seen in the last chapter, the value of U where the correct magnetic anisotropy is predicted is less than the case with only U. This parameter space turns out more than enough for the current study.

We describe the calculated MAE. The MAE is calculated along the contour with magnetic moment 2.2 μ_{B} (see Fig. 10.2) At $U = 0\ eV$ and $J = 0\ eV$, the MAE is 0.5 μeV. we move along the contour in the direction of increasing U and J. MAE first slightly decrease to 0.3 μeV till $U = 0.7\ eV$ and $J = 0.6\ eV$. It then increases. The correct magnetic anisotropy is predicted at $U = 1.9\ eV$ and $J = 1.3\ eV$. Compared to the care with the old double counting, the correct magnetic anisotropy is predicted at larger values of both U and J.

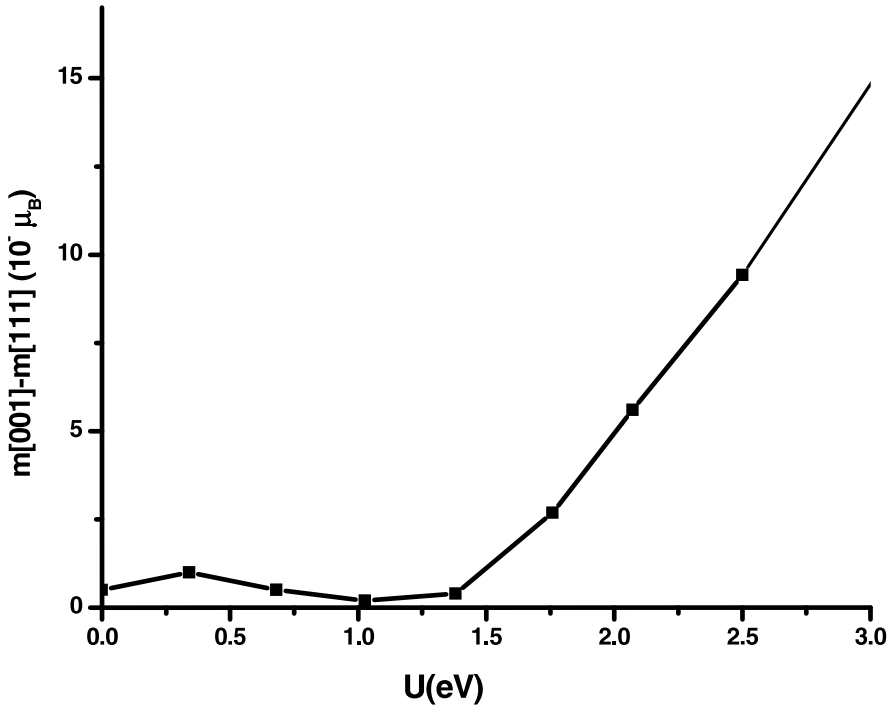

Figure 10.3: Fe. Difference of Magnetic Moments, $m(001) - E(111)$. The contour with magnetic moment 2.2 $\mu_{\mathrm{B}}$is followed. The magnetic anisotropy energy is plotted as a function of U. The corresponding value of J can be found in the contour plot Fig. 10.1.

We find concurrent behaviours of MAE and the difference of magnetic moments (See Fig. 10.3). The difference of magnetic moments moderately slightly increases and then slightly decrease till $U = 1.4\ eV$ and $J = 1\ eV$. From there, it rapidly increase. This again confirms that the magnitude of magnetic moment is a determining factor in

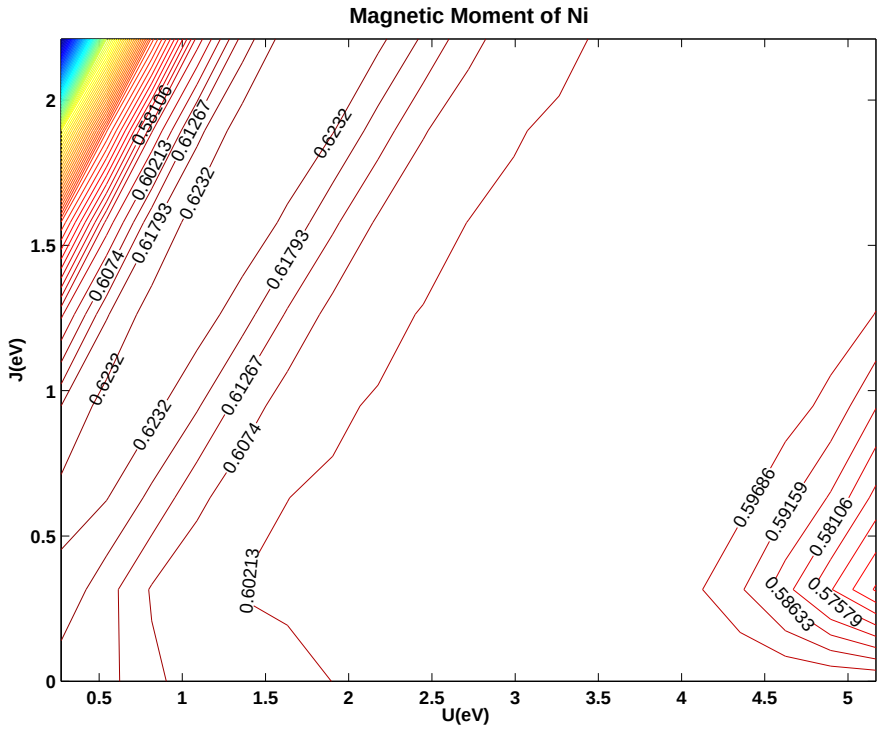

Figure 10.4: Ni. Contour plot of magnetic moment as a function of Coulomb parameter U and Stoner parameter J. The contour is drawn at 0.005 μ_{B} interval, which is 0.9% of the experimental value of magnetic moment 0.606 μ_{B}

magnetic anisotropy.

10.3 Ni

We now discuss the effect of Stoner parameter J as well as U for Ni. We first find magnetic moment as a function of U and J (see Fig. 10.4). We see that the magnetic moment is nearly constant over the parameter space for physically meaningful area, say $0.5969\ \mu_{\mathrm{B}} \leq m0.6232\ \mu_{\mathrm{B}}$.

This result is in accord with the previous studies. With new double counting, we find that the magnetic moment is nearly independent of U in the study of the effect of Coulomb parameter. We also find that magnetic moment does not change much as J changes in the study of the effect of Coulomb parameter U and Stoner parameter J with the old double counting. Here with the new double counting and J, nothing special happened and the result is a combination of the previous studies.

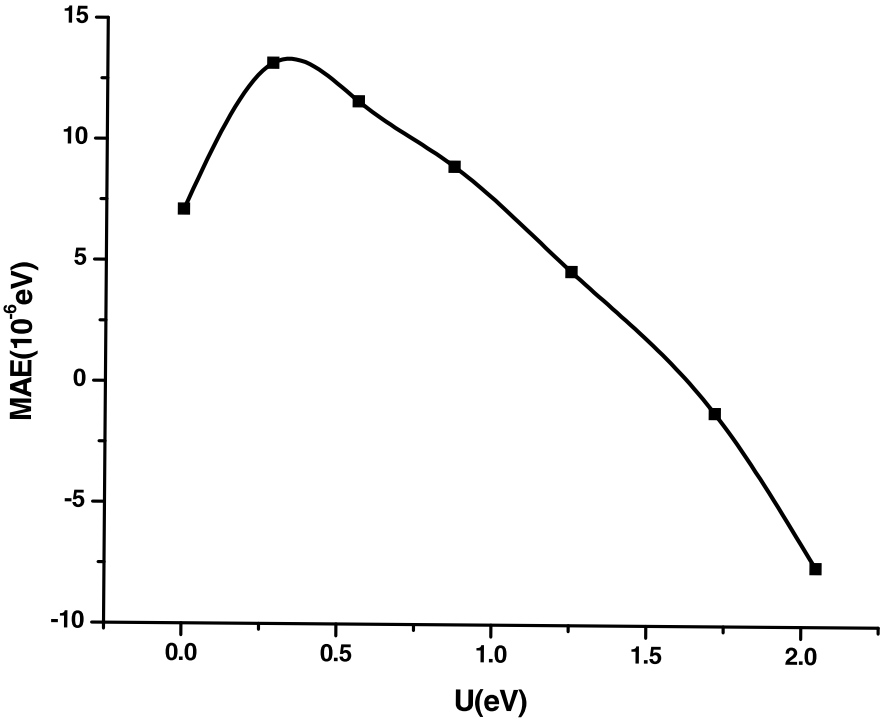

Figure 10.5: Ni. Old Double Counting. On the Curve

For magnetic anisotropy, we walked along two paths. We now discuss the results. The first path we walk along is the constant magnetic moment contour passing the origin. MAE increases to 20 μeV as we move along the contour in the direction of increasing U and J till $U = 0.8$ and $J = 0.8$. Then it decreases, changing from the wrong easy axis to the correct easy axis at $U = 1.1\ eV$ and $J = 1.2\ eV$, to $-5\ \mu eV$ till $U = 1.4\ eV$ and $J = 1.4\ eV$. From there it increases again, chnageing from the correct easy axis to the wrong easy axis at $U = 1.7\ eV$ and $J = 1.5\ eV$.

The correct anisotropy energy is predicted at $U = 1.7\ eV$ and $J = 1.5\ eV$. As discussed, comparing the absolute values of U and J with experiments need some caution. We can, however, compare relative values with experiments. In experiments, J is much smaller than U. Since, we predicted the correct magnetic anisotropy when U and J are similar, the result is not desirable.

We now study the Fermi surface (see Fig. 10.6). We see that four bands are passing through the Fermi level in ΓX direction. Note that two bands are degenerate due to the residual symmetry in the direction. As we move away from the ΓX direction, we

see that one band is submerged below the Fermi level. The is the experimentally confirmed X_5 pocket. A very important point to notice is that the band that makes X_2 pocket in LDA is just below the Fermi level and does not form an pocket.

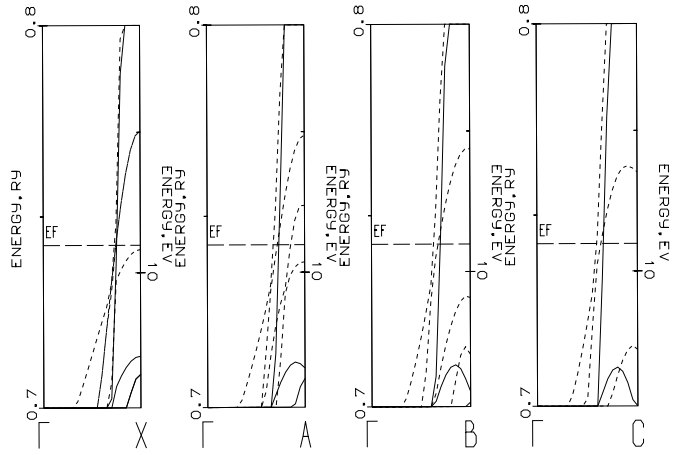

Figure 10.6: The X pockets of LDA+U at $U = 1.7\ eV$ and $J = 1.1\ eV$. Inspecting the figures, we see that there are X_5 pocket. Note that the X_2 is not present. The solid lines represent bands with dominating up-spin. The dotted lines represent bands with dominating down-spin. $X = (0, 0, 1)$, $A = (1/16, 1/16, 1)$, $B = (2/16, 2/16, 1)$, $C = (3/16, 3/16, 1)$. .

We now discuss the L neck. From the Fig. 10.7, we see one spin-down dominated band is just below the Fermi level in ΓL direction. As we mover away from the ΓL direction, we see that the band is surfacing up above the Fermi level. This is the experimentally confirmed L neck.

We now discuss the absence of the artificial L pockets. Notice that there is another band just below the Fermi level in ΓR direction, ΓS direction, and ΓL direction. This band was above the Fermi surface in ΓL direction in the study of Coulomb parameter. In this case, we see that the band is below the Fermi surface always and does not form a pocket. Regarding the other artificial L pocket, we see that no other band is near the Fermi surface, this band is well below the Fermi surface and does not form a pocket. The configuration of Fermi surface and the degenerate states near the Fermi level is the same as in the case with old double counting.

In conclusion, we find the correct magnetic moment, the correct Fermi surface, and the correct magnetic anisotropy simultaneously at $U = 1.7\ eV$ and $J = 1.5\ eV$.

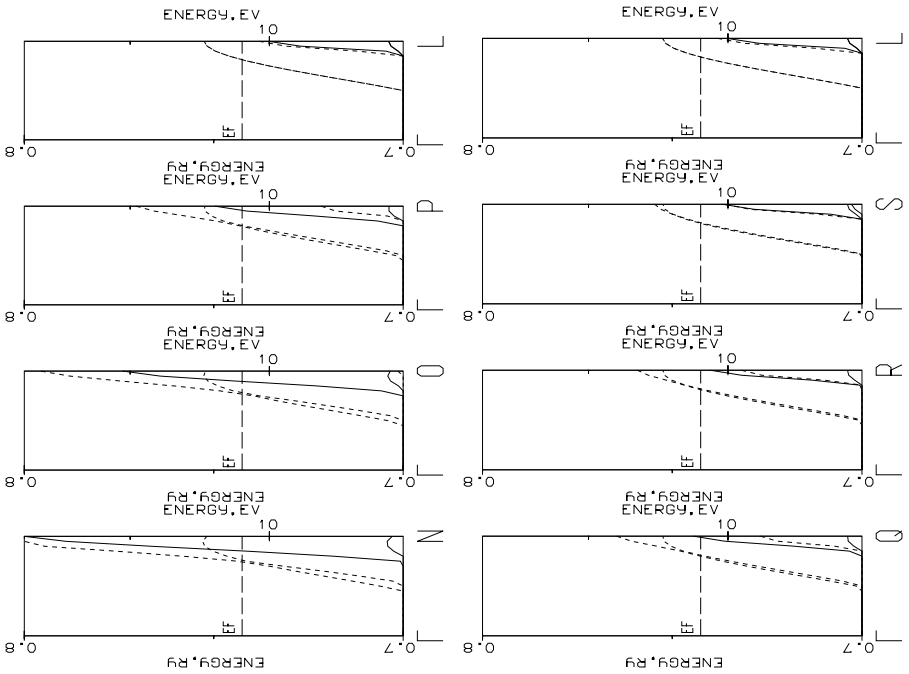

Figure 10.7: The L neck of LDA+U. Notice the absence of L pockets. Inspecting the figures, we see that there is a L neck. The solid lines represent bands with dominating up-spin. The dotted lines represent bands with dominating down-spin. The points are: $N = (29/64, 29/64, 19/32)$, $O = (30/64, 30/64, 18/32)$, $P = (31/64, 31/64, 17/32$, $Q = (125/256, 125/256, 67/128)$, $R = (126/256, 126/256, 66/128)$, $S = (127/256, 127/256, 65/128)$, $L = (128/256, 128/256, 64/128)$.

Except that the value of J is of the same magnitude as U, the result is perfect.

We try another path to walk along. This time we walked along a constant J path, where $J = 0.3\ eV$. MAE increases with a wiggle to 15 μeV as we move along the contour in the direction of increasing U till $U = 1.5$. Then it decreases, changing from the wrong easy axis to the correct easy axis at $U = 3.8\ eV$, The correct anisotropy energy is predicted at $U = 4.2\ eV$.

We now study the Fermi surface (see Fig. 10.9). We see that two bands are passing through the Fermi level in ΓX direction. Notice that there is no X pockets. The two bands, one of which would make a X_5 pocket is way below the Fermi level. The band that makes LDA X_2 pocket is also below the Fermi surface. The LDA+U improved LDA in the sense that it removes the artificial X_2 pocket. However, the improvement is surpassed by the absence of experimentally confirmed X_5 pocket.

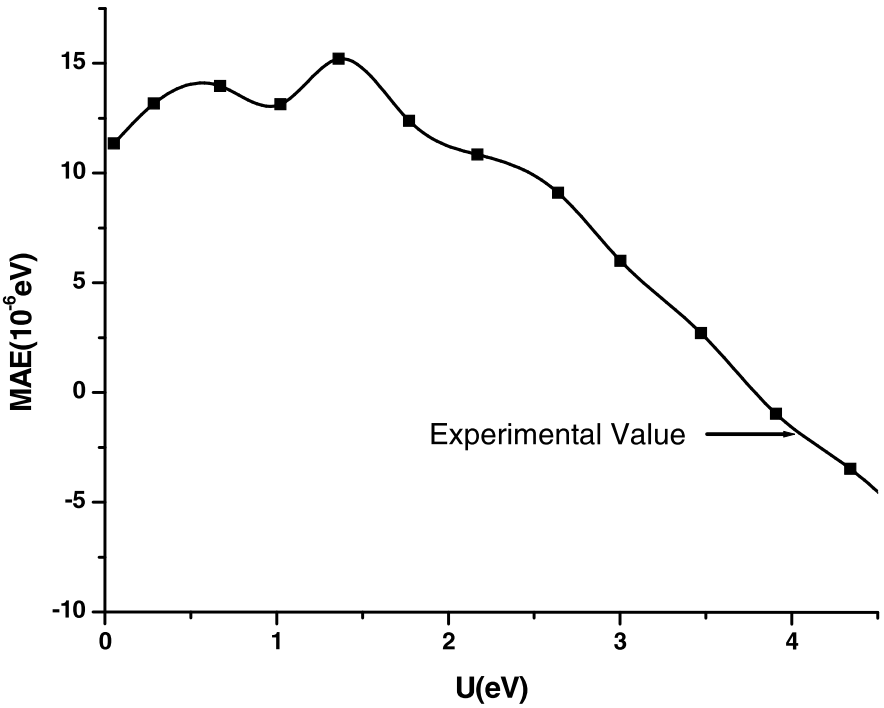

Figure 10.8: Ni. Magnetic Anisotropy Energy, $E(111) - E(001)$. The path with Stoner parameter $J = 0.3\ eV$ is followed.

We now discuss the L neck. From the Fig. 10.10, we see that two bands are crossing the Fermi level. The spin-down dominated bands is the candidate for the L neck. As can be seen from the figure, this band is already above the Fermi level in ΓL direction. It therefore does not form a neck. The other band is the candidate for the L pocket. As can been seen, this band is not submerged as we move away from ΓL direction. It does not make a pocket. The two degenerate bands below the Fermi level is supposed to cross the Fermi level. In sum, the band structure near the L point is not in good agreement with the experiments.

In conclusion, the prediction of the correct magnetic moment and the correct magnetic anisotropy at $U = 4.2\ eV$ and $J = 0.3\ eV$ is an LDA+U artifact. Its Fermi surface is not in accord with the experiments and we discard the result.

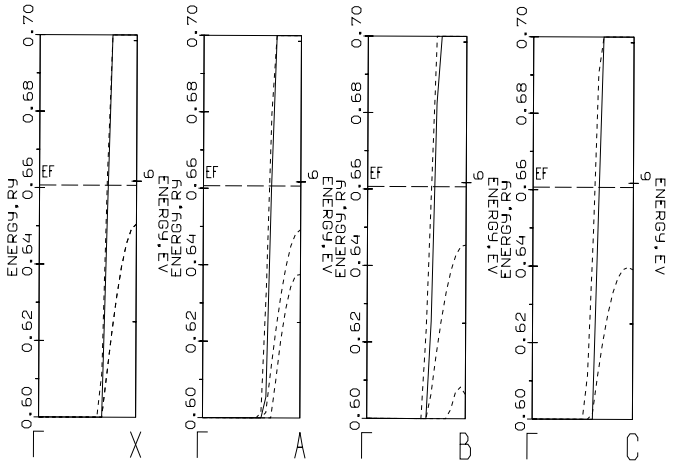

Figure 10.9: The X pockets of LDA+U at $U = 4.2\ eV$ and $J = 0.3\ eV$. Inspecting the figures, we see that there is no X pockets. The solid lines represent bands with dominating up-spin. The dotted lines represent bands with dominating down-spin. $X = (0, 0, 1)$, $A = (1/16, 1/16, 1)$, $B = (2/16, 2/16, 1)$, $C = (3/16, 3/16, 1)$. .

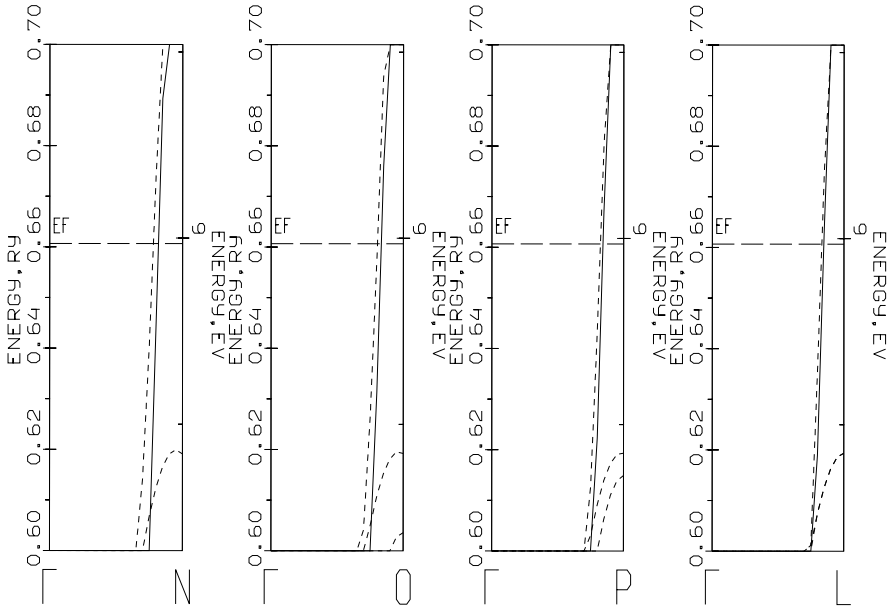

Figure 10.10: The L neck of LDA+U. $N = (29/64, 29/64, 19/32)$, $O = (30/64, 30/64, 18/32)$, $P = (31/64, 31/64, 17/32$, $L = (128/256, 128/256, 64/128)$.

Part II

Beyond One Electron Model

Chapter 11

Introduction

LDA+U is a static limit of dynamic mean field theory (DMFT). The DMFT approach has been extensively used to study model Hamiltonian of correlated electron systems in the weak, strong and intermediate coupling regimes. It has been very successful in describing the physics of realistic systems, like the transition metal oxides and, therefore, is expected to treat properly the materials with d or f electrons.

The model Hamiltonian of DMFT is Hubbard model. Most of the research efforts on Hubbard model have been devoted to single band models. In actual materials, one is frequently faced with the issue of multi-bands. A scheme able to deal with general multiband Hubbard model or its DMFT cousin, general mutiband impurity model, is lacking. This is also a prerequisite for the development of *ab initio* DMFT scheme[49].

Present techniques based on either non-crossing approximation or iterative perturbation theory are unable to provide the solution due to the limited number of regions where these approximation do not break down[15]. Heavy Quantum Monte Carlo technique is the only method that can cope with orbitally degenerate situation, but its applicability is limited singlets at high temperature[50].

A new approach to this problem is suggested[51]. In this approach, two physically different limits are considered: limit of low frequencies, $i\omega \to 0$, and limit of high frequencies, $i\omega \to \infty$. With the Green functions for each limits, an interpolation scheme is used to find the full Green functions.

Green functions in low frequency limit can be obtained using slaveboson method[52, 53]. We study slaveboson method in the next chapter. Green functions in high frequency limit is the topic of the last two chapters.

11.1 The Hubbard model

The Hubbard model was first proposed in 1963 independently by Hubbard [?] and Gutzwiller [44] in an attempt to describe the effects of correlations for d electrons in metals. Transition metals where the d-band is partially full display characteristics which in some circumstances can be best understood in terms of localized atomic-like electrons but in other cases the experimental features are better described in terms of band theory. The Hubbard model is essentially the simplest model that captures this duality and it can be derived from the full electronic Hamiltonian for the metal by keeping only interaction terms between electrons that are situated on the same site, or more specifically between electrons of different spins which are in the same Wannier state. For an s-band the Hubbard Hamiltonian is given by:

$$H = -\sum_{\langle ij\rangle\sigma} t_{ij} c^{+}_{i\sigma} c_{j\sigma} + U \sum_{j} n_{j\uparrow} n_{j\downarrow}. \tag{11.1}$$

Here $c^{+}_{i\sigma}$ creates an electron in a Wannier state localized at site i with spin σ, U is the local on site interaction between different spins and t_{ij} is the hopping integral between sites i and j. For our purposes we will want to generalize this Hamiltonian by increasing the spin degeneracy from 2 to N and since we will be working in the grand canonical ensemble we introduce a chemical potential that we add to the Hamiltonian. Thus we have:

$$H = -\sum_{\langle ij\rangle\sigma} t_{ij} c^{+}_{i\sigma} c_{j\sigma} + \frac{U}{2} \sum_{j\sigma\neq\sigma'} n_{j\sigma} n_{j\sigma'} - \mu \sum_{j\sigma} n_{j\sigma}. \tag{11.2}$$

Here σ runs from $-j$ to j where $2j+1 = N$. This model has a higher spin degeneracy than the original Hamiltonian of Hubbard and can thus be expected to be a better representation of the physics in the materials of interest, i.e. compounds of transition and rare earth metals which have partly filled d and f bands. In spite of being one of the simplest model of correlated electrons on a lattice the Hubbard model has proven to be quite difficult to tackle theoretically. It is only during the last few years that some real progress has been made, especially with the development of the dynamical mean field theory [15].

11.2 An overview of dynamical mean field theory

The dynamical mean field theory can be regarded as the quantum analog of the classical Curie-Weiss mean field theory for magnets. As its classical counterpart it can be shown to be the exact formulation of the model in question in the limit when the number of dimensions or the coordination number of the lattice goes to infinity, with an appropriate scaling of parameters. When the number of neighbors of a given lattice site increases it is reasonable to assume that its interactions with the neighbors can be replaced by an effective interaction with some average field that represents the dynamic state of the neighbors. These ideas can be concretely realized in the following way: A given lattice site is selected, o say, and an effective action is derived for the degrees of freedom living on this site by integrating out the degrees of freedom of the other sites in the lattice. The effective action can be represented in terms of the Green's functions, G^0_{ij}, of the so called cavity Hamiltonian, i.e. the lattice Hamiltonian obtained by deleting the site o and all the bonds associated with it. By scaling the hopping integral such that $z^{|i-j|}t^2_{ij}$ is a constant, where z is the coordination number of the lattice and $|i-j|$ is the Taxi-cab distance between the sites i and j, and then taking the limit when $z \to \infty$ the action simplifies tremendously and we obtain:

$$S_{eff} = -\int_0^\beta d\tau \int_0^\beta d\tau' \sum_\sigma c^+_{o\sigma}\mathcal{G}^{-1}(\tau-\tau')c_{o\sigma} + \frac{U}{2}\int_0^\beta d\tau \sum_{\sigma\neq\sigma'} n_{o\sigma}n_{o\sigma'} \qquad (11.3)$$

where the function $\mathcal{G}$ is the so called Weiss function and plays the role of the Weiss field of the Curie-Weiss theory and is given by,

$$\mathcal{G}^{-1}(i\omega_n) = i\omega_n + \mu - \sum_{\langle ij\rangle} t_{io}t_{jo}G^0_{ij}(i\omega_n). \qquad (11.4)$$

Given an explicit form for the action, the on-site interacting Green's function G can in principle be calculated (in practice this is a nontrivial problem) by evaluating the following expectation value:

$$G(\tau-\tau') = -\langle Tc_o(\tau)c^+_o(\tau')\rangle_{S_{eff}}. \qquad (11.5)$$

The self consistency condition that is now imposed is that this Green's function be the same as the diagonal, on site lattice Green's function, $G_{oo} \equiv G_{loc}$. To compute the

full, lattice Green's function it is useful to switch over to momentum representation and introduce a self energy Σ which is momentum independent in the infinite dimensional limit and given by,

$$\Sigma(i\omega_n) = \mathcal{G}^{-1}(i\omega_n) - G^{-1}(i\omega_n). \tag{11.6}$$

Then the momentum dependent Green's functions are given by,

$$G(k, i\omega_n) = \frac{1}{i\omega_n + \mu - \varepsilon_k - \Sigma(i\omega_n)} \tag{11.7}$$

where ε_k is the dispersion relation of the lattice. The general inter-site lattice Green's function can be computed from this expression by Fourier transform and the diagonal term is of course simply the momentum integral of the expression above. At this point it is useful to stop and look over the equations that we have so far. Let us for a moment assume that we have a guess for the self energy, Σ. From there we can compute the local Green's function by momentum integration over $G(k, i\omega)$ and then the Weiss field can be computed from equation (11.6). We now have all the ingredients to compute the local Green's function from the action, and then we can use equation (11.6) again to get a new solution for the self energy. This process can now be started over and iterated until self consistency is attained. Thus it seems that we have all that is necessary to solve our problem but we still haven't used the cavity Green's function, G^0. In the limit $z \to \infty$ the cavity Green's function, G^0_{ij}, is very simply related to the full lattice Green's function , G_{ij}. This relation is,

$$G^0_{ij} = G_{ij} - \frac{G_{io}G_{jo}}{G_{oo}} \tag{11.8}$$

and it is quite simple to understand: using the interpretation of the Green's function as the likelihood of finding an electron at site j if it is created at i we see that this likelihood is the same in the full lattice as in the lattice with a cavity at o, except that in the cavity lattice we cannot go through the site o and thus we must subtract those contributions off after normalization for processes that start at o and come back to o. Putting this relation into the equation (11.4) and using the form for the momentum dependent Green's functions we end again up with equation (11.6). So, somehow this relation between the cavity Green's function and the full Green's function seems to be

equivalent to the momentum independence of the self energy. Here it is useful to use the representation of the local Green's function in terms of the density of states:

$$G(i\omega_n) = \int \frac{D(\epsilon)d\epsilon}{\zeta - \epsilon} \tag{11.9}$$

where $D(\epsilon)$ is the bare density of states of the lattice and $\zeta = i\omega_n + \mu - \Sigma(i\omega_n)$. We see that G is essentially given by a Hilbert transform over the density of states and if we can invert that we can express the self energy in term of the Green's function and then the Weiss function can be expressed solely in terms of the Green's function through equation (11.6).

In the calculations that follow we will use the Bethe lattice of infinite connectivity with only nearest neighbor hopping given by t_o, $zt_o^2 = t^2$. In that case the self consistency condition becomes especially simple and we get,

$$\mathcal{G}^{-1}(i\omega) = i\omega + \mu - t^2 G_{loc}(i\omega) - G_{loc}^{-1}(i\omega). \tag{11.10}$$

Given the physical picture embodied in the DMFT, i.e. of an electron on a single site interacting with a bath of electrons on the rest of the lattice it is not surprising that a connection can be made between the dynamical mean field theory described above and impurity models like the Anderson impurity model,

$$H^{AIM} = \sum_{k\sigma} \tilde{\varepsilon}_k c_{k\sigma}^+ c_{k\sigma} - \mu \sum_{\sigma} f_\sigma^+ f_\sigma + \sum_{k\sigma} (V_k c_{k\sigma}^+ f_\sigma + h.c.) + \frac{U}{2} \sum_{\sigma \neq \sigma'} n_\sigma n_{\sigma'} \tag{11.11}$$

by noting that if the conduction electrons $c_{k\sigma}$ are integrated out an action of the form (11.3) is obtained with

$$\mathcal{G}^{-1}(i\omega) = i\omega + \mu - \int d\varepsilon \frac{\Delta(\varepsilon)}{i\omega - \varepsilon} \quad \text{where} \quad \Delta(\varepsilon) = \sum_k V_k^2 \delta(\varepsilon - \tilde{\varepsilon}_k) \tag{11.12}$$

is the hybridization function of the Anderson model. The full impurity Green's function will now be equal to G_{loc} provided Δ is chosen such that the self-consistency condition is fulfilled. On the Bethe-lattice that requirement gives us

$$\Delta(\varepsilon) = t^2 \rho_{loc}(\varepsilon) = -\frac{t^2}{\pi} \operatorname{Im} G_{loc}(\varepsilon + i0). \tag{11.13}$$

The impurity model connection is very fortunate since impurity models have been studied intensely in the past, their physics is well known and many tools and methods

exist to deal with such models such as quantum Monte-Carlo methods, exact diagonalization methods, iterated perturbation methods and the so called non-crossing approximation (NCA) which we will mainly focus on here.

Chapter 12

Slaveboson Method

12.1 Introduction

The correlation-driven metal-insulator transition, or Mott transition [38], observed in materials such as V_2O_3 [39, 40] and $NiS_{2-x}Se_x$ [40, 41, 42], is a nonperturbative problem usually tackled within the Hubbard model of strongly correlated electrons. This model describes itinerant electrons subject to an on-site repulsion U comparable or greater than the bare bandwidth $2D$.

In an early work, Brinkman and Rice [43] investigated the Mott transition from the metallic side using Gutzwiller's variational scheme [44, 45]. In this approximation, the metal is described as a strongly renormalized Fermi liquid.

A low-energy scale ZD (Z is the quasiparticle residue) collapses linearly in U as the Mott transition, occuring at a critical U_{BR}, is approached from the metallic side. ZD is a measure for the renormalized Fermi energy.

Kotliar and Ruckenstein devised a slave-boson method in which the approximation of Gutzwiller, Brinkman, and Rice is recovered on the saddle-point level, but which at the same time is open to various generalizations [46].

An example is the subject of this paper: We investigate the possibility and implications of antiferromagnetic long-range order on either side of the Mott transition. To this effect, we introduce magnetic frustration, which helps stabilize an antiferromagnetic metallic phase for not too large degrees of frustration and causes the insulating side to favor antiferromagnetic long-range order.

We also determine the orders of the various transitions involved. We expect our results to be qualitatively correct on the metallic side, for temperatures well below

ZD, and in the limit of large lattice coordination. The reason is, that in the *absence of long-range order*, the Brinkman-Rice scenario for the Mott transition is known to be the correct description of the coherent low-energy excitations in the limit of infinite dimensions [47]. In this limit, the dynamical mean-field theory (DMFT) becomes exact [15] and provides a unified framework for describing the various phases and features of the Mott transition [47]. The influence of antiferromagnetic long-range order on the Mott transition has been recently addressed within DMFT [48].

12.2 Formalism

The single-band Hubbard model is given by

$$\hat{H} = -\sum_{ij\sigma} t_{ij} c_{i\sigma}^{+} c_{j\sigma} + U \sum_{i} \hat{n}_{i\uparrow} \hat{n}_{i\downarrow}, \tag{12.1}$$

where we take the amplitudes t_{ij} to be nonzero only between nearest and next-nearest neighbors, in which cases they equal t and t', respectively. $c_{i\sigma}^{+}$ and $c_{i\sigma}$ are creation and annihilation operators for an electron of spin σ at site i, and $\hat{n}_{i\sigma} \equiv c_{i\sigma}^{+} c_{i\sigma}$. In this work, we consider the two-dimensional cubic lattice and restrict ourselves to half filling and zero temperature.

In the Kotliar-Ruckenstein approach, two aspects of a physical electron are separated: that it is a *fermion* and that it affects the *occupancy* of some site. The first aspect is taken into account by a fermionic field $f_{i\sigma}$, while the possible occupancies of the sites are described by bosonic fields: e_i describes empty, $p_{i\sigma}$ singly occupied, and d_i doubly occupied sites. The physical electron field is represented as $c_{i\sigma} = \tilde{z}_{i\sigma} f_{i\sigma}$ with $\tilde{z}_{i\sigma} = (1 - p_{i\sigma}^{+} p_{i\sigma} - d_i^{+} d_i)^{-1/2} (e_i^{+} p_{i\sigma} + p_{i-\sigma}^{+} d_i^{+})(1 - e_i^{+} e_i - p_{i-\sigma}^{+} p_{i-\sigma})^{-1/2}$, while appropriate constraints eliminate unphysical states [46]. Thus, the problem posed by the Hubbard interaction is shifted to that of keeping track of the backflow of bosonic excitations, $\tilde{z}_{i\sigma}^{+} \tilde{z}_{j\sigma}$, accompanying the itinerant fermions, $f_{i\sigma}^{+} f_{j\sigma}$.

Proceeding along the lines of Ref. [46], we first set up the functional-integral representation of the Hubbard model in terms of the above-mentioned auxiliary fields, integrate out the fermions, and solve the remaining problem in the saddle-point approximation. To describe antiferromagnetism, we divide the lattice into two

sublattices, A and B, and look for solutions satisfying the following relations between the sublattice Bose fields: $e_B = e_A$, $p_{B\sigma} = p_{A-\sigma}$, $d_B = d_A$, and $m = p_{A\uparrow}^2 - p_{A\downarrow}^2$, where m is the staggered magnetization. For our result, we need the dispersion relations

$$\epsilon_{\vec{k}\eta}[X] = -4t' \cos k_x \cos k_y + \eta t \sqrt{X^2 + 4(\cos k_x + \cos k_y)^2}, \tag{12.2}$$

where the lattice spacing has been set equal to one, X is some dynamically generated staggered magnetic field, and $\eta = \pm 1$. The equations for the density per site (which at half filling is equal to one) and the staggered magnetization,

$$\begin{aligned} 1 &= \frac{1}{N} \sum_{\vec{k}\eta} f(\epsilon_{\vec{k}\eta}[X] - \tilde{\mu}), & (12.3) \\ m(X, \tilde{\mu}) &= \frac{1}{N} \sum_{\vec{k}} \frac{X}{\sqrt{X^2 + 4(\cos k_x + \cos k_y)^2}} \\ &\quad \times \left[f(\epsilon_{\vec{k}-}[X] - \tilde{\mu}) - f(\epsilon_{\vec{k}+}[X] - \tilde{\mu}) \right], & (12.4) \end{aligned}$$

can be solved unambiguously for X and the effective chemical potential $\tilde{\mu}$, to yield functions $\tilde{\mu}(m)$ and $X(m)$. In Eqs. (12.3) and (12.4), N is the total number of lattice sites, the sum is over the first Brillouin zone, and $f(\epsilon) = \Theta(-\epsilon)$ is the Fermi function at zero temperature. From the mean-field equation

$$\frac{\partial q(m, d^2)}{\partial d^2} K(m) + U = 0, \tag{12.5}$$

where the functions $q(m, d^2)$ and $K(m)$ are given by

$$\begin{aligned} q(m, d^2) &= \frac{4d^2}{1 - m^2} \left[1 - 2d^2 + \sqrt{(1 - 2d^2)^2 - m^2} \right], & (12.6) \\ K(m) &\equiv \frac{1}{N} \sum_{\vec{k}\eta} \epsilon_{\vec{k}\eta}[X(m)] f(\epsilon_{\vec{k}\eta}[X(m)] - \tilde{\mu}(m)) \\ &\quad + tmX(m), & (12.7) \end{aligned}$$

we obtain the average portion of doubly occupied sites as a function of the staggered magnetization, $d^2(m)$. This function along with Eqs. (12.6) and (12.7) allow to write the ground-state energy per site as a function of the staggered magnetization as

$$e(m) = q(m) K(m) + U d^2(m). \tag{12.8}$$

This result has an intuitive interpretation: $K(m)$ is the kinetic energy of noninteracting lattice fermions with nearest and next-nearest neighbor hopping,

subject to an internal staggered magnetic field $tX(m)$. The renormalization factor $q(m)$ accounts for the reduction of the hopping amplitudes due to the local correlations and is characteristic of the Gutzwiller approximation. In our scheme, q arises from the expectation value $\langle \tilde{z}^{+}_{i\sigma} \tilde{z}_{j\sigma} \rangle$ and thus represents the average effect of the backflowing slave bosons. The second term in Eq. (12.8) is the contribution of the Hubbard interaction to the energy. For $U = 0$, Eqs. (12.5) and (12.6) yield $d^2 = (1 - m^2)/4$ and $q = 1$, so $\epsilon(m) = K(m)$. For $t' = m = 0$, Eqs. (12.2)-(12.7) imply: $X = \tilde{\mu} = 0$; $K = 2 \int_{-\infty}^{0} d\epsilon \, D_0(\epsilon)\epsilon$, where $D_0(\epsilon)$ is the density of states for noninteracting electrons; $d^2 = \frac{1}{4}(1 - \frac{U}{U_c})$ with $U_c = 8|K|$; and $q = 1 - (\frac{U}{U_c})^2$. We thus recover a result of Ref. [46].

We have also considered the Hubbard model in the Hartree-Fock approximation, which turns out to be tantamount to taking $q = 1$ and $d^2(m) = (1 - m^2)/4$ in Eq. (12.8), while the function $K(m)$ is again determined by Eqs. (12.3), (12.4), and (12.7).

12.3 Example

In the following, we determine the ground state for given model parameters U and $\alpha \equiv t'/t$ by minimizing the energy function (12.8). α is a measure for the degree of magnetic frustration and is varied from zero to one. Furthermore, the evolution of $e(m)$ as a function of U and α reveals how the transitions between the various phases take place. Whether the system is metallic or insulating depends on the value of the ground-state magnetization: If it exceeds a certain value, m_{MIT}, a gap opens up in the single-particle spectrum and the system goes insulating. This can be seen from Eq. (12.2) if we use that m increases monotonically as a function of X. Consequently, the insulator is always antiferromagnetically ordered. From Eqs. (12.2)-(12.4), we further infer that m_{MIT} does not depend on U, but on the degree of magnetic frustration: Due to perfect nesting, $\lim_{\alpha \to 0} m_{\mathrm{MIT}} = 0$. As α is turned on, m_{MIT} increases monotonically as a function of α. In the following, we discuss our results. We must distinguish between three regimes of magnetic frustration and may restrict the discussion of $e(m)$ to positive magnetizations. Fig. 12.1 illustrates how $e(m)$ evolves as a function of U and α. The resulting phase diagram is displayed in Fig. 12.2.

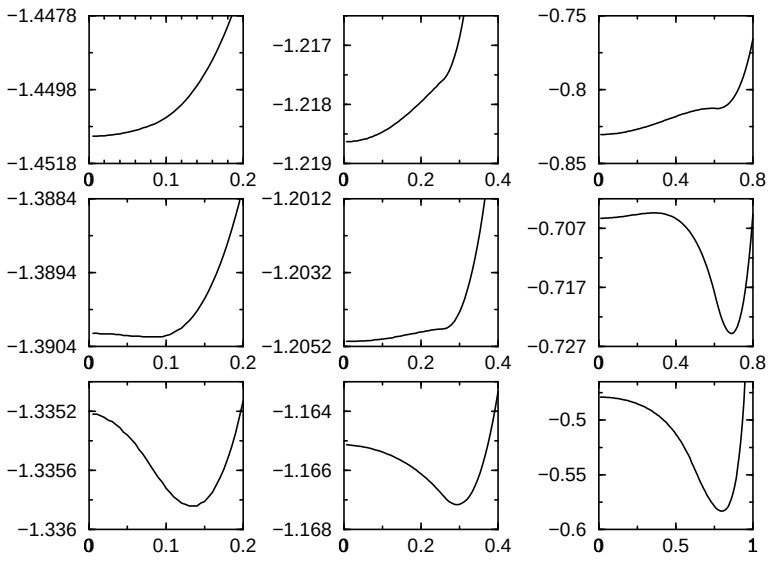

Figure 12.1: The function $e(m)$ as a function of U and the magnetic frustration. The columns from left to right correspond to the small-, intermediate-, and large-α regimes, respectively. The respective values are $\alpha = 0.02$, 0.1, and 0.5, corresponding to $m_{\mathrm{MIT}} = 0.09$, 0.26, and 0.61, respectively. Each column displays how $e(m)$ changes qualitatively upon increasing U, from the paramagnetic metal (top row) to the antiferromagnetic insulator (bottom row). The middle row shows examples in the antiferromagnetic metal (first two plots), and one after the metal-insulator transition has taken place but before the local minimum at $m = 0$ turns over into a local maximum (plot on the right). The plot in the center has its minimum at a nonzero magnetization, which is not discernible.

For *small* degrees of magnetic frustration, $0 < \alpha < 0.06$ (first column of Fig. 12.1), we first find a second-order transition from the paramagnetic to the antiferromagnetic metal at a critical value U_{mag}. Upon further increasing U, the resulting minimum is continuously shifted towards higher magnetizations until it crosses m_{MIT} at a second critical value, U_{MIT}. Consequently, the metal-insulator transition is also of second order. Since m_{MIT} vanishes as $\alpha \to 0$, both transitions coincide in this limit.

For *intermediate* levels of magnetic frustration, $0.06 \leq \alpha < 0.14$ (middle column of Fig. 12.1), m_{MIT} is sufficiently large for the metal-insulator transition to take place differently: Before the ground-state magnetization of the antiferromagnetic metal reaches m_{MIT} upon increasing U, a second minimum at a magnetization above m_{MIT} has emerged and become the absolute minimum of $e(m)$. Consequently, the metal-insulator transition is now of first order. The transition lines $U_{\mathrm{MIT}}(\alpha)$ from the small-α and intermediate-α regimes meet at $\alpha = 0.06$ (full circle in Fig. 12.2). At this

point, the two degenerate minima of the first-order transition merge at $m_{\rm MIT}$. Finally, the antiferromagnetic metallic phase disappears gradually as $\alpha \to 0.14$ (full square in Fig. 12.2).

For *large* degrees of magnetic frustration, $\alpha \geq 0.14$ (right column of Fig. 12.1), the antiferromagnetic and metal-insulator transitions coincide, $U_{\rm MIT} = U_{\rm mag}$, because the second-order transition is now preempted by the first-order one: By the time the minimum at $m = 0$ bifurcates, the one *above* $m_{\rm MIT}$ has already evolved into the absolute one, and remains to be so, as U is further increased.

In Hartree-Fock approximation, the function $e(m)$ evolves, for all values of α and upon increasing U, as follows: After a second-order transition from the paramagnetic to the antiferromagnetic metal, the minimum is continuously displaced towards higher magnetizations, until it exceeds $m_{\rm MIT}$. Thus, both transitions are of second order and never coincide.

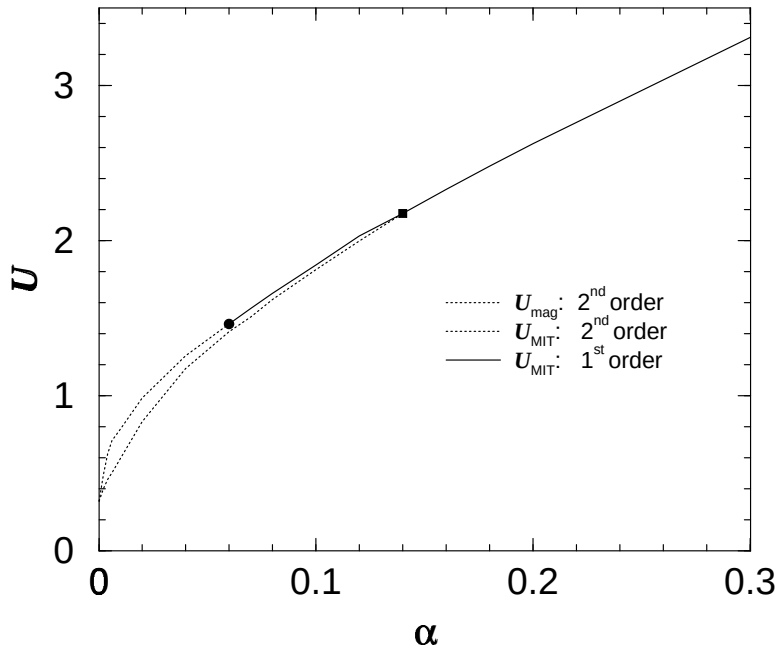

Figure 12.2: The various phases and transitions as a function of $\alpha \equiv t'/t$ and U. The small-U phase is the paramagnetic metal, while the large-U phase is the antiferromagnetic insulator. In between, an antiferromagnetically ordered metallic phase is sandwiched that disappears at a tricritical point (full square). The dotted and full lines indicate second- and first-order transitions, respectively. The full circle marks the point where the metal-insulator transition changes its order.

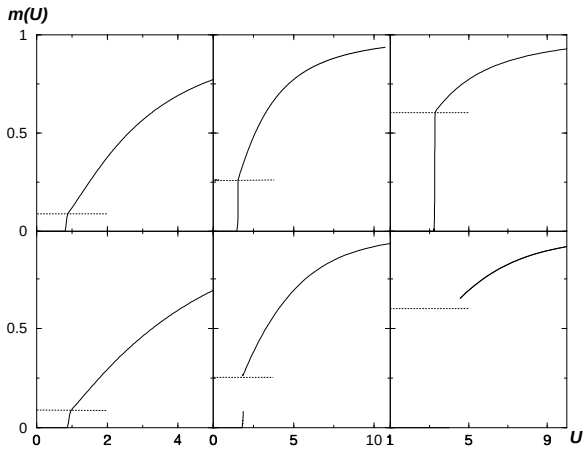

Figure 12.3: The function m as a function of U. The columns from left to right correspond to the small-, intermediate-, and large-α regimes, respectively. The respective values are $\alpha = 0.02$, 0.1, and 0.5, corresponding to $m_{\rm MIT} = 0.09$, 0.26, and 0.61, respectively. shown as dotted lines. Each column displays how m changes qualitatively upon increasing U, within Hartree Fock approximation (top row) and within Slave boson approxiamtion (botton row).

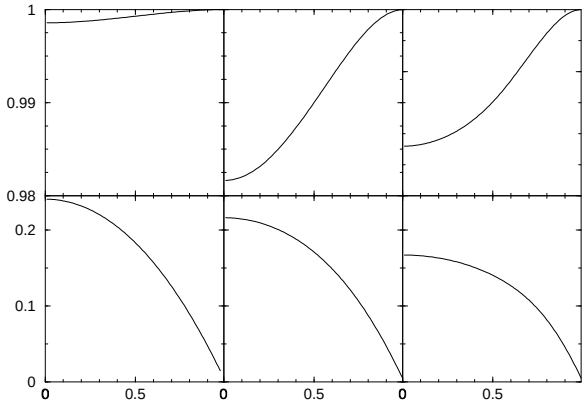

Figure 12.4: The function $q(m)$ (top row) and the function $d^2(m)$ (bottom row) as a function of m at U_{MIT}. The columns from left to right correspond to the small-, intermediate-, and large-α regimes, respectively. The respective values are $\alpha = 0.02$, 0.1, and 0.5.

Chapter 13

Momentum Expansion Method

13.1 Introduction

We develop self consistency equation in high frequency limit. In this chapter we develop self consistency equations using moment expansion method. This method is appealing particularly because of the small matrix size of Green functions. This naive moment expansion method, however, does not yield a self consistency equation up to the desired order. In the next chapter, we use equation of motion method with Hubbard operators that would give those equations.

Consider a Green function of fermion operators, $G(\tau) = -\langle T_\tau f_\alpha(\tau) f_\beta^\dagger(0)\rangle$. Expanding the Fourier transform of this Green function in $1/i\omega_n$, we express the Green function in terms of moments $M^{(n)},\ n = 1, 2, \cdots$:

$$G_{\alpha\beta}(i\omega_n) = \frac{M_{\alpha\beta}^{(1)}}{i\omega_n} + \frac{M_{\alpha\beta}^{(2)}}{(i\omega_n)^2} + \frac{M_{\alpha\beta}^{(3)}}{(i\omega_n)^3} + \frac{M_{\alpha\beta}^{(4)}}{(i\omega_n)^4} + \cdots, \tag{13.1}$$

where the moments can be obtained in the following way[54, 55].

$$M_{\alpha\beta}^{(1)} = \langle\{f_\alpha, f_\beta^\dagger\}\rangle = \delta_{\alpha\beta}, \tag{13.2}$$

$$M_{\alpha\beta}^{(2)} = \langle\{[f_\alpha, H], f_\beta^\dagger\}\rangle, \tag{13.3}$$

$$M_{\alpha\beta}^{(3)} = \langle\{[[f_\alpha, H]H], f_\beta^\dagger\}\rangle, \tag{13.4}$$

$$M_{\alpha\beta}^{(4)} = \langle\{[[[f_\alpha, H], H], H], f_\beta^\dagger\}\rangle. \tag{13.5}$$

When these moments can be expressed in terms of Green functions, the Eq. 13.1 is a self consistency equation with the expression of moments. In general, the moments can be expressed in terms of Green functions up to a certain order n. Then the Eq. 13.1 is a self consistency equation that is exact up to $1/(i\omega_n)^n$.

In following sections, we derive expressions for the moments in terms of Green functions. Two models will be considered: N band impurity model and N band lattice Hubbard model, both with density-density on-site interactions.

13.2 Impurity Model

We consider N-band Anderson impurity model. The Hamiltonian of this impurity model consists of three parts,

$$H = H_{\rm atom} + H_{\rm band} + H_{\rm hyb}, \tag{13.6}$$

where $H_{\rm atom}$ is the Hamiltonian of the impurity, $H_{\rm band}$ is the Hamiltonian of the surrounding bands, and $H_{\rm hyb}$ is the Hamiltonian hybridizing the impurity and the bands. Explicit forms of the component Hamiltonians read

$$H_{\rm atom} = \sum_{\alpha} \epsilon_{\alpha} f^{\dagger}_{\alpha} f_{\alpha} + \sum_{\alpha\beta} U^{\alpha\beta} n_{\alpha} n_{\beta}, \tag{13.7}$$

$$H_{\rm band} = \sum_{\alpha\vec{k}} \epsilon^{\alpha\vec{k}} c^{\dagger}_{\alpha\vec{k}} c_{\alpha\vec{k}}, \tag{13.8}$$

$$H_{\rm hyb} = \sum_{\alpha\beta\vec{k}} V^{\alpha\beta}_{\vec{k}} \left(f^{\dagger}_{\alpha} c_{\beta\vec{k}} + c^{\dagger}_{\alpha\vec{k}} f_{\beta} \right), \tag{13.9}$$

where $V^{\alpha\beta}_{\vec{k}} = \left(V^{\beta\alpha}_{\vec{k}} \right)^{*}$, $U^{\alpha\beta} = U^{\beta\alpha}$, and $U^{\alpha\alpha} = 0$. The band indices α and β run from 0 to N.

We write Green functions as

$$G^{-1}_{\alpha\beta}(i\omega_n) = (i\omega_n - \epsilon_{\alpha})\delta_{\alpha\beta} - \tilde{\Delta}_{\alpha\beta}(i\omega_n) - \Sigma_{\alpha\beta}(i\omega_n), \tag{13.10}$$

where the hybridization matrix is $\tilde{\Delta}_{\alpha\beta}(i\omega_n) = \sum_{\gamma\vec{k}} V^{\alpha\gamma}_{\vec{k}} V^{\gamma\beta}_{\vec{k}} / (i\omega_n - \epsilon^{\gamma\vec{k}})$. We expand the Eq. 13.10 in $1/i\omega_n$, assuming the expansion of the self energy in $1/i\omega_n$ as

$$\Sigma_{\alpha\beta}(i\omega_n) = \Sigma^{(0)}_{\alpha\beta} + \frac{\Sigma^{(1)}_{\alpha\beta}}{i\omega} + \frac{\Sigma^{(2)}_{\alpha\beta}}{(i\omega_n)^2}. \tag{13.11}$$

Identifying this expansion with the Eq. 13.1, the moments of self energy can be

written as

$$\Sigma^{(0)}_{\alpha\beta} = M^{(2)}_{\alpha\beta} - \epsilon_\alpha \delta_{\alpha\beta}, \tag{13.12}$$

$$\begin{aligned}\Sigma^{(1)}_{\alpha\beta} &= M^{(3)}_{\alpha\beta} - \left(M^{(2)}\right)^2_{\alpha\beta} - \Delta_{\alpha\beta}, \\ &= M^{(3)}_{\alpha\beta} - \epsilon_\alpha M^{(2)} - \epsilon_\beta \Sigma^{(0)}_{\alpha\beta} - \left(\Sigma^{(0)}\right)^2_{\alpha\beta} - \Delta_{\alpha\beta},\end{aligned} \tag{13.13}$$

$$\begin{aligned}\Sigma^{(2)}_{\alpha\beta} &= M^{(4)}_{\alpha\beta} - \left(M^{(2)}\right)^3_{\alpha\beta} - \left(M^{(2)}(\Sigma^{(1)}+\Delta) + (\Sigma^{(1)}+\Delta)M^{(2)}\right)_{\alpha\beta} - \sum_{a\vec{k}} \epsilon_{a\vec{k}} V^{\alpha a}_{\vec{k}} V^{a\beta}_{\vec{k}}, \\ &= M^{(4)}_{\alpha\beta} - \epsilon_\alpha M^{(3)} - \left(\Delta M^{(2)}\right)_{\alpha\beta} - \sum_{a\vec{k}} \epsilon_{a\vec{k}} V^{\alpha a}_{\vec{k}} V^{a\beta}_{\vec{k}} \\ &- \left(\Sigma^{(1)} M^{(2)} + M^{(1)} \Sigma^{(2)}\right)_{\alpha\beta},\end{aligned} \tag{13.14}$$

where $\Delta_{\alpha\beta} = \sum_{\gamma\vec{k}} V^{\alpha\gamma}_{\vec{k}} V^{\gamma\beta}_{\vec{k}}$.

Now we derive explicit expressions for $M^{(n)}$ and $\Sigma^{(m)}$. The first moment $M^{(1)}$ is straightforward. The second moment can be calculated as

$$\begin{aligned}M^{(2)} &= \langle\{[f_\alpha, H], f^\dagger_\beta\}\rangle, \\ &= \epsilon_\alpha \delta_{\alpha\beta} + \sum_\gamma U^{\alpha\gamma} \langle\{f_\alpha n_\gamma, f^\dagger_\beta\}\rangle, \\ &= \epsilon_\alpha \delta_{\alpha\beta} + \delta_{\alpha\beta} \sum_\gamma U^{\alpha\gamma} \langle n_\gamma\rangle + U^{\alpha\beta} \langle f_\alpha f^\dagger_\beta\rangle.\end{aligned} \tag{13.15}$$

Then the zeroth moment of self energy $\Sigma^{(0)}_{\alpha\beta}$ follows from the Eq. 13.12:

$$\Sigma^{(0)}_{\alpha\beta} = \delta_{\alpha\beta} \sum_\gamma U^{\alpha\gamma} \langle n_\gamma\rangle + U^{\alpha\beta} \langle f_\alpha f^\dagger_\beta\rangle. \tag{13.16}$$

Since $\langle f_\alpha f^\dagger_\beta\rangle = -G_{\alpha\beta}(\tau = 0^+)$ and $n_\gamma = \langle f^\dagger_\gamma f_\gamma\rangle$, the Eq. 13.1 is a self consistency equation up to $1/(\omega_n)^2$.

For an impurity model with general on-site interactions, It can be shown that the second moment can also be expressed in terms of Green functions . At this order, however, the Green function is in fact the Green function of the atomic Hamiltonian, as can be seen in the Eq. 13.16. Since the Green function is that of atomic Hamiltonian, the many body physics can not be captured. For many body physics, therefore, we need to incorporate the third moment in a self consistency equation.

To calculate the third moment, we need to calculate $\sum_\gamma U^{\alpha\gamma}\langle\{[f_\alpha n_\gamma, H], f_\beta^\dagger\}\rangle$ first:

$$\begin{aligned}\sum_\gamma U^{\alpha\gamma}\langle\{[f_\alpha n_\gamma, H], f_\beta^\dagger\}\rangle &= \epsilon_\alpha \Sigma^{(0)}_{\alpha\beta} + \delta_{\alpha\beta}\sum_{\gamma\delta} U^{\alpha\gamma}U^{\alpha\delta}\langle n_\gamma n_\delta\rangle \\ &+ 2U^{\alpha\beta}\sum_\gamma U^{\alpha\gamma}\langle f_\alpha f_\beta^\dagger n_\gamma\rangle + U^{\alpha\beta}U^{\alpha\beta}\langle f_\alpha f_\beta^\dagger\rangle \\ &+ U^{\alpha\beta}\left(\langle\tilde{C}_\alpha f_\beta^\dagger\rangle - \langle f_\alpha \tilde{C}_\beta^\dagger\rangle\right) \\ &- \delta_{\alpha\beta}\sum_\gamma U^{\alpha\gamma}\left(\langle\tilde{C}_\gamma f_\gamma^\dagger\rangle - \langle f_\gamma \tilde{C}_\gamma^\dagger\rangle\right), \qquad (13.17)\end{aligned}$$

where $\tilde{C}_\alpha = \sum_{a\vec{k}} V^{\alpha a} c_{a\vec{k}}$, $\tilde{C}_\alpha^\dagger = \sum_{a\vec{k}} V^{a\alpha} c_{a\vec{k}}^\dagger$. As shown in the next chapter, $\langle\tilde{C}_\alpha f_\beta^\dagger\rangle$ and $\langle f_\alpha \tilde{C}_\beta^\dagger\rangle$ can be expressed in terms of Green functions using equation of motion method. However, $\langle n_\gamma n_\delta\rangle$ $\langle f_\alpha f_\beta^\dagger n_\gamma\rangle$ can not be expressed in terms of Green functions. To devise a way to express these terms in terms of Green functions, we need to introduce projected Green functions with proper projection operators. A good candidate for the project operators is the project operator formed from the eigenstates of atomic Hamiltonian. This consideration leads us to Hubbard operators. Construction of self consistency equation using Hubbard operators is discussed in the next section.

Here we write down the third moment and the first moment of self energy for completeness. Since Hubbard operators introduce Hilbert space, hence large matrix size, it is important to find a limit where a self consistency equation can be constructed without them. The following equations can be used as a first step toward

such endeavors.

$$
\begin{aligned}
M^{(3)}_{\alpha\beta} &= \langle\{[[f_\alpha, H]H], f^\dagger_\beta\}\rangle, \\
&= \epsilon_\alpha \langle\{[f_\alpha, H], f^\dagger_\beta\}\rangle + \sum_{a\vec{k}} V^{\alpha a}_{\vec{k}} \langle\{[c_{a\vec{k}}, H], f^\dagger_\beta\}\rangle + \sum_\gamma U^{\alpha\gamma} \langle\{[f_\alpha n_\gamma, H], f^\dagger_\beta\}\rangle, \\
&= \epsilon_\alpha M^{(2)}_{\alpha\beta} + \Delta_{\alpha\beta} + \sum_\gamma U^{\alpha\gamma} \langle\{[f_\alpha n_\gamma, H], f^\dagger_\beta\}\rangle, \qquad (13.18) \\
\Sigma^{(1)}_{\alpha\beta} &= M^{(3)}_{\alpha\beta} - \epsilon_\alpha M^{(2)} - \epsilon_\beta \Sigma^{(0)}_{\alpha\beta} - \left(\Sigma^{(0)}\right)^2_{\alpha\beta} - \Delta_{\alpha\beta}, \\
&= \sum_\gamma U^{\alpha\gamma} \langle\{[f_\alpha n_\gamma, H], f^\dagger_\beta\}\rangle - \epsilon_\beta \Sigma^{(0)}_{\alpha\beta} - \left(\Sigma^{(0)}\right)^2_{\alpha\beta}, \qquad (13.19) \\
&= (\epsilon_\alpha - \epsilon_\beta) U^{\alpha\beta} \langle f_\alpha f^\dagger_\beta\rangle \\
&+ \delta_{\alpha\beta} \sum_{\gamma\delta} U^{\alpha\gamma} U^{\alpha\delta} \left(\langle n_\gamma n_\delta\rangle - \langle n_\gamma\rangle\langle n_\delta\rangle\right) \\
&+ U^{\alpha\beta} \sum_\gamma \left(2U^{\alpha\gamma} \langle f_\alpha f^\dagger_\beta n_\gamma\rangle - U^{\alpha\gamma} \langle f_\alpha f^\dagger_\beta\rangle\langle n_\gamma\rangle - U^{\beta\gamma} \langle f_\alpha f^\dagger_\beta\rangle\langle n_\gamma\rangle\right) \\
&+ U^{\alpha\beta} U^{\alpha\beta} \langle f_\alpha f^\dagger_\beta\rangle - \sum_\gamma U^{\alpha\gamma} U^{\gamma\beta} \langle f_\alpha f^\dagger_\gamma\rangle\langle f_\gamma f^\dagger_\beta\rangle \\
&+ U^{\alpha\beta} \left(\langle \tilde{C}_\alpha f^\dagger_\beta\rangle - \langle f_\alpha \tilde{C}^\dagger_\beta\rangle\right) - \delta_{\alpha\beta} \sum_\gamma U^{\alpha\gamma} \left(\langle \tilde{C}_\gamma f^\dagger_\gamma\rangle - \langle f_\gamma \tilde{C}^\dagger_\gamma\rangle\right). \qquad (13.20)
\end{aligned}
$$

Finding the second moment of self energy $\Sigma^{(2)}_{\alpha\beta}$ is important in studying ferromagnetic materials. As we could not set up a self consistency equation for the first moment of self energy, we would not be able to find a way to a self consistency equation for the second moment of self energy. An explicit expression is, however, may find its use in finding a limit where a self consistency equation can be constructed and in understanding the difficulty involved. Similarly to the case of the first moment of self

energy, we need to calculate $\sum_\gamma \langle\{[[f_\alpha n_\gamma, H], H], f_\beta^\dagger\}\rangle$:

$$
\begin{aligned}
&\sum_\gamma \langle\{[[f_\alpha n_\gamma, H], H], f_\beta^\dagger\}\rangle = \qquad (13.21)\\
&\epsilon_\alpha^2 U^{\alpha\beta}\langle f_\alpha f_\beta^\dagger\rangle + \delta_{\alpha\beta}\epsilon_\alpha^2 \sum_\gamma U^{\alpha\gamma}\langle n_\gamma\rangle + 2\delta_{\alpha\beta}\sum_{\gamma\delta}\epsilon_\alpha U^{\alpha\gamma}U^{\alpha\delta}\langle n_\gamma n_\delta\rangle \\
+\;& 4\epsilon_\alpha U^{\alpha\beta}\sum_\gamma U^{\alpha\gamma}\langle f_\alpha f_\beta^\dagger n_\gamma\rangle + 2\epsilon_\alpha U^{\alpha\beta}U^{\alpha\beta}\langle f_\alpha f_\beta^\dagger\rangle \\
+\;& \delta_{\alpha\beta}\sum_{\gamma\delta\epsilon} U^{\alpha\gamma}U^{\alpha\delta}U^{\alpha\epsilon}\langle n_\gamma n_\delta n_\epsilon\rangle + U^{\alpha\beta}U^{\alpha\beta}U^{\alpha\beta}\langle f_\alpha f_\beta^\dagger\rangle \\
+\;& 3U^{\alpha\beta}U^{\alpha\beta}\sum_\gamma U^{\alpha\gamma}\langle f_\alpha f_\beta^\dagger n_\gamma\rangle + 3U^{\alpha\beta}\sum_{\gamma\delta} U^{\alpha\gamma}U^{\alpha\delta}\langle f_\alpha f_\beta^\dagger n_\gamma n_\delta\rangle \\
+\;& \delta_{\alpha\beta}\sum_{\gamma\delta} U^{\alpha\gamma}\left(\Delta_{\gamma\delta}\langle f_\gamma^\dagger f_\delta\rangle + \Delta_{\delta\gamma}\langle f_\delta^\dagger f_\gamma\rangle\right) + \sum_\gamma \Delta_{\alpha\beta}U^{\alpha\gamma}\langle n_\gamma\rangle \\
+\;& \epsilon_\alpha U^{\alpha\beta}\left(\langle\tilde{C}_\alpha f_\beta^\dagger\rangle - \langle f_\alpha\tilde{C}_\beta^\dagger\rangle\right) + \delta_{\alpha\beta}\sum_\gamma \epsilon_\gamma U^{\alpha\gamma}\left(\langle\tilde{C}_\gamma f_\gamma^\dagger\rangle - \langle f_\gamma\tilde{C}_\gamma^\dagger\rangle\right) \\
-\;& 2\delta_{\alpha\beta}\epsilon_\alpha\sum_\gamma U^{\alpha\gamma}\left(\langle\tilde{C}_\gamma f_\gamma^\dagger\rangle - \langle f_\gamma\tilde{C}_\gamma^\dagger\rangle\right) \\
+\;& U^{\alpha\beta}U^{\alpha\beta}\left(\langle\tilde{C}_\alpha f_\beta^\dagger\rangle - \langle f_\alpha\tilde{C}_\beta^\dagger\rangle\right) + 2U^{\alpha\beta}\sum_\gamma U^{\alpha\gamma}\left(\langle\tilde{C}_\alpha f_\beta^\dagger n_\gamma\rangle - \langle f_\alpha\tilde{C}_\beta^\dagger n_\gamma\rangle\right) \\
-\;& 2\delta_{\alpha\beta}\sum_{\gamma\delta} U^{\alpha\gamma}U^{\alpha\delta}\left(\langle\tilde{C}_\gamma f_\gamma^\dagger n_\delta\rangle - \langle f_\gamma\tilde{C}_\gamma^\dagger n_\delta\rangle\right) - 2\delta_{\alpha\beta}\sum_\gamma U^{\alpha\gamma}U^{\alpha\gamma}\left(\langle\tilde{C}_\gamma f_\gamma^\dagger\rangle - \langle f_\gamma\tilde{C}_\gamma^\dagger\rangle\right) \\
-\;& (\epsilon_\alpha+\epsilon_\beta)U^{\alpha\beta}\langle f_\alpha\tilde{C}_\beta^\dagger\rangle - U^{\alpha\beta}\sum_\gamma (U^{\alpha\gamma}+U^{\beta\gamma})\langle f_\alpha\tilde{C}_\beta^\dagger n_\gamma\rangle \\
+\;& \delta_{\alpha\beta}\sum_{\gamma\delta} U^{\alpha\gamma}U^{\gamma\delta}\left(\langle f_\gamma\tilde{C}_\gamma^\dagger n_\delta\rangle + \langle\tilde{C}_\gamma f_\gamma^\dagger n_\delta\rangle\right) - \delta_{\alpha\beta}\sum_{\gamma\delta} U^{\alpha\gamma}U^{\alpha\delta}\left(\langle f_\gamma\tilde{C}_\gamma^\dagger n_\delta\rangle + \langle\tilde{C}_\gamma f_\gamma^\dagger n_\delta\rangle\right) \\
+\;& 2\delta_{\alpha\beta}\sum_\gamma U^{\alpha\gamma}\langle\tilde{C}_\gamma\tilde{C}_\gamma^\dagger\rangle - 2U^{\alpha\beta}\langle\tilde{C}_\alpha\tilde{C}_\beta^\dagger\rangle
\end{aligned}
$$

$$
\begin{aligned}
&+\;\; U^{\alpha\beta}\left(\langle f_\alpha\tilde{\mathcal{C}}_\beta^\dagger\rangle + \langle\tilde{\mathcal{C}}_\alpha f_\beta^\dagger\rangle\right) - \delta_{\alpha\beta}\sum_\gamma U^{\alpha\gamma}\left(\langle f_\gamma\tilde{\mathcal{C}}_\gamma^\dagger\rangle + \langle\tilde{\mathcal{C}}_\gamma f_\gamma^\dagger\rangle\right) \\
&+\;\; 3U^{\alpha\beta}\sum_\gamma U^{\alpha\gamma}\left(\langle f_\alpha f_\beta^\dagger f_\gamma^\dagger\tilde{C}_\gamma\rangle - \langle f_\alpha f_\beta^\dagger\tilde{C}_\gamma^\dagger f_\gamma\rangle\right) \\
&-\;\; \sum_\gamma U^{\alpha\gamma}U^{\gamma\beta}\left(\langle f_\alpha f_\beta^\dagger f_\gamma^\dagger\tilde{C}_\gamma\rangle + \langle f_\alpha f_\beta^\dagger\tilde{C}_\gamma^\dagger f_\gamma\rangle\right),
\end{aligned}
$$

where $\tilde{\mathcal{C}}_\alpha = \sum_{a\vec{k}}\epsilon_{a\vec{k}}V_{\vec{k}}^{\alpha a}c_{a\vec{k}}$, $\tilde{\mathcal{C}}_\alpha^\dagger = \sum_{a\vec{k}}\epsilon_{a\vec{k}}V_{\vec{k}}^{a\alpha}c_{a\vec{k}}^\dagger$. First we meet the same difficulty as in the case of the first moment of self energy. We need to introduce projected Green functions to cope with such terms as $\langle O n_\gamma\rangle$, where O is an operator. Moreover there are four fermion operators such as $\langle f_\alpha f_\beta^\dagger\tilde{C}_\gamma^\dagger f_\gamma\rangle$. We need to find a limit where these terms cancel each other, or Wick-like decomposition is valid. Another challenge is the

presence of operators $\tilde{\mathcal{C}}_\alpha$ and $\tilde{\mathcal{C}}_\alpha^\dagger$. It is very unclear how to cope with these operators. When $\sum_\gamma \langle\{[[f_\alpha n_\gamma, H], H], f_\beta^\dagger\}\rangle$ can be expressed in terms of Green functions, the fourth moment and the second moment of self energy can be found in the following way.

$$\begin{aligned} M^{(4)}_{\alpha\beta} &= \langle\{[[[f_\alpha, H], H], H], f_\beta^\dagger\}\rangle, \\ &= \epsilon_\alpha M^{(3)}_{\alpha\beta} + \sum_{a\vec{k}} \epsilon_{a\vec{k}} V_{\vec{k}}^{\alpha a} V_{\vec{k}}^{a\beta} + \left(\Delta M^{(1)}\right)_{\alpha\beta} + \sum_\gamma \langle\{[[f_\alpha n_\gamma, H], H], f_\beta^\dagger\}\rangle, \quad (13.22) \\ \Sigma^{(2)}_{\alpha\beta} &= \sum_\gamma \langle\{[[f_\alpha n_\gamma, H], H], f_\beta^\dagger\}\rangle - \left(\Sigma^{(1)} M^{(2)} + M^{(3)} \Sigma^{(0)}\right)_{\alpha\beta}. \quad (13.23) \end{aligned}$$

13.3 Impurity Model: Special cases

13.3.1 Diagonal Hybridization

Diagonal hybridization $\Delta_{\alpha\beta} = \Delta_{\alpha\alpha}\delta_{\alpha\beta}$ is a natural candidate for a limit where a self consistency equation can be written down. In this case, the off-diagonal components of the Green function vanish. Since the hybridization matrix is real, we see that $\langle \tilde{C}_\gamma f_\gamma^\dagger\rangle = \langle f_\gamma \tilde{C}_\gamma^\dagger\rangle$. Using these properties, the moments of self energy can be found from the expressions for the case with general hybridization:

$$M^{(2)}_{\alpha\beta} = \epsilon_\alpha \delta_{\alpha\beta} + \Sigma^{(0)}_{\alpha\beta}, \quad \Sigma^{(0)}_{\alpha\beta} = \delta_{\alpha\beta} \sum_\gamma U^{\alpha\gamma} \langle n_\gamma\rangle. \quad (13.24)$$

$$M^{(3)}_{\alpha\beta} = \epsilon_\alpha^2 \delta_{\alpha\beta} + 2\delta_{\alpha\beta}\epsilon_\alpha \sum_\gamma U^{\alpha\gamma}\langle n_\gamma\rangle + \Delta_{\alpha\beta} + \Sigma^{(1)}_{\alpha\beta}, \quad (13.25)$$

$$\begin{aligned} \Sigma^{(1)}_{\alpha\beta} &= \delta_{\alpha\beta} \sum_{\gamma\delta} U^{\alpha\gamma} U^{\alpha\delta} \left(\langle n_\gamma n_\delta\rangle - \langle n_\gamma\rangle\langle n_\delta\rangle\right) \\ &\quad - \delta_{\alpha\beta} \sum_\gamma U^{\alpha\gamma} \left(\langle \tilde{C}_\gamma f_\gamma^\dagger\rangle - \langle f_\gamma \tilde{C}_\gamma^\dagger\rangle\right) \quad (13.26) \\ &= \delta_{\alpha\beta} \sum_{\gamma\delta} U^{\alpha\gamma} U^{\alpha\delta} \left(\langle n_\gamma n_\delta\rangle - \langle n_\gamma\rangle\langle n_\delta\rangle\right). \quad (13.27) \end{aligned}$$

At this order, though it is not possible to express the term $\langle n_\gamma n_\delta\rangle$ in terms of Green functions, the moments can be found using Hartree expression. If Hartree approximation is used, however, the Green function is that of mean field theory and dynamic aspects of the physics can not be captured. Even with diagonal

hybridization, it is not possible to construct a self consistency equation for Green functions able to capture dynamic aspects of physics.

13.3.2 $SU(N)$ case

$SU(N)$ case is the simplest case among the multi-band impurity models. By $SU(N)$, we mean that 1) the hybridization is diagonal and flavor-independent, $\delta_{\alpha\beta} = \Delta\delta_{\alpha\beta}$, and 2) the energies of non-interacting fermions are the same, $\epsilon_\alpha = \epsilon$. For easy comparison with the result of Hubbard operator method, the ϵ_α is rescaled to $\epsilon_\alpha + U$. This amounts to restoring the diagonal on-site interaction $U^{\alpha\alpha} = U$. As in the case of diagonal hybridization, there is no improvement for fourth order moments especially because of the presence of the operators $\tilde{\mathcal{C}}_\alpha$ and $\tilde{\mathcal{C}}^\dagger_\alpha$. Up to the third order, the moments and self energy can be written as

$$M^{(2)}_{\alpha\beta} = \epsilon_\alpha\delta_{\alpha\beta} + \Sigma^{(0)}_{\alpha\beta}, \quad \Sigma^{(0)}_{\alpha\beta} = \delta_{\alpha\beta}U\langle N\rangle \tag{13.28}$$

$$M^{(3)}_{\alpha\beta} = \epsilon^2_\alpha\delta_{\alpha\beta} + 2\delta_{\alpha\beta}\epsilon_\alpha U\langle N\rangle + \delta_{\alpha\beta}U^2\langle N^2\rangle + \Delta_{\alpha\beta} + \Sigma^{(1)}_{\alpha\beta} \tag{13.29}$$

$$\begin{aligned}\Sigma^{(1)}_{\alpha\beta} &= \delta_{\alpha\beta}\sum_{\gamma\delta} U^{\alpha\gamma}U^{\alpha\delta}\left(\langle n_\gamma n_\delta\rangle - \langle n_\gamma\rangle\langle n_\delta\rangle\right) \\ &- \delta_{\alpha\beta}\sum_{\gamma} U^{\alpha\gamma}\left(\langle\tilde{C}_\gamma f^\dagger_\gamma\rangle - \langle f_\gamma\tilde{C}^\dagger_\gamma\rangle\right) \qquad (13.30)\\ &= \delta_{\alpha\beta}U^2\left(\langle N^2\rangle - \langle N\rangle^2\right), \qquad (13.31)\end{aligned}$$

where $N = \sum_\alpha n_\alpha$. As in the case with general hybridization, the term $\langle N^2\rangle$ can not be expressed in terms of Green functions. Using Hartree approximation reduces to mean field theory. Equation of motion method using Hubbard operators open a way to overcome this difficulty. We discuss equation of motion method in the next chapter.

13.4 Lattice Hubbard Model

We consider N-band Lattice model. The Hamiltonian of this model is,

$$H = \sum_{ij\alpha\beta} t^{\alpha\beta}_{ij} f_{i\alpha}f^\dagger_{j\beta} + \sum_{i\alpha\beta}\frac{U^{\alpha\beta}_i}{2}n^i_\alpha n^j_\beta, \tag{13.32}$$

where $i, j, k, \cdots$ are lattice indices and $\alpha, \beta, \gamma, \cdots$ are band indices. We assume that $U^{\alpha\beta}_i = U^{\beta\alpha}_i$, and $U^{\alpha\alpha}_i = 0$. The band indices run from 0 to N. We expand the Fourier

transforms of Green functions $G_{ij\alpha\beta}(\tau) = -\langle T_\tau f_{i\alpha}(\tau) f^\dagger_{j\beta}(0)\rangle$ in $1/i\omega_n$,

$$G_{ij\alpha\beta} = \frac{M^{(1)}_{ij\alpha\beta}}{i\omega_n} + \frac{M^{(2)}_{ij\alpha\beta}}{(i\omega_n)^2} + \frac{M^{(3)}_{ij\alpha\beta}}{(i\omega_n)^3} + \frac{M^{(4)}_{ij\alpha\beta}}{(i\omega_n)^4} + \cdots, \tag{13.33}$$

where the moments can be found by the following equations.

$$M^{(1)}_{ij\alpha\beta} = \langle\{f_{i\alpha}, f^\dagger_{j\beta}\}\rangle = \delta_{ij}\delta_{\alpha\beta}, \tag{13.34}$$

$$M^{(2)}_{ij\alpha\beta} = \langle\{[f_{i\alpha}, H], f^\dagger_{j\beta}\}\rangle, \tag{13.35}$$

$$M^{(3)}_{ij\alpha\beta} = \langle\{[[f_{i\alpha}, H]H], f^\dagger_{j\beta}\}\rangle, \tag{13.36}$$

$$M^{(4)}_{ij\alpha\beta} = \langle\{[[[f_{i\alpha}, H], H], H], f^\dagger_{j\beta}\}\rangle. \tag{13.37}$$

We write the Green function as

$$[G_{ij\alpha\beta}]^{-1} = i\omega_n\delta_{ij}\delta_{\alpha\beta} - t^{\alpha\beta}_{ij} - \Sigma_{ij\alpha\beta}, \tag{13.38}$$

and the self energy as

$$\Sigma_{ij\alpha\beta} = \Sigma^{(0)}_{ij\alpha\beta} + \frac{\Sigma^{(1)}_{ij\alpha\beta}}{i\omega} + \frac{\Sigma^{(2)}_{ij\alpha\beta}}{(i\omega_n)^2} + \cdots \tag{13.39}$$

Expanding the Eq. 13.38 using the Eq. 13.39, the moments of self energy can be written as

$$\Sigma^{(0)}_{ij\alpha\beta} = M^{(2)}_{ij\alpha\beta} - t^{\alpha\beta}_{ij}, \tag{13.40}$$

$$\Sigma^{(1)}_{ij\alpha\beta} = M^{(3)}_{ij\alpha\beta} - (tM^{(2)})_{ij\alpha\beta} - (\Sigma^{(0)}t)_{ij\alpha\beta} - \left(\Sigma^{(0)}\right)^2_{ij\alpha\beta}, \tag{13.41}$$

$$\Sigma^{(2)}_{ij\alpha\beta} = M^{(4)}_{ij\alpha\beta} - (tM^{(3)})_{ij\alpha\beta} - \left(\Sigma^{(0)}M^{(3)} + \Sigma^{(1)}M^{(2)}\right)_{ij\alpha\beta}. \tag{13.42}$$

Now we present the expressions of moments. The first moment is trivial. The second moment can be straightforwardly calculated:

$$M^{(2)}_{ij\alpha\beta} = t^{\alpha\beta}_{ij} + \Sigma^{(0)}_{ij\alpha\beta}, \tag{13.43}$$

$$\begin{aligned}\Sigma^{(0)}_{ij\alpha\beta} &= \delta_{ij}\sum_\gamma U^{\alpha\gamma}_i \langle\{f_{i\alpha}n^i_\gamma, f^\dagger_{i\beta}\}\rangle, \\ &= \delta_{ij}\delta_{\alpha\beta}\sum_\gamma U^{\alpha\gamma}_i\langle n^i_\gamma\rangle + \delta_{ij}U^{\alpha\beta}_i\langle f_{i\alpha}f^\dagger_{i\beta}\rangle.\end{aligned} \tag{13.44}$$

Up to this order, a self consistency equation can be written. However, the Green function is that of atomic Hamiltonian. To capture the many body physics, we need

higher order moments. To calculate the third order moment, we need $\sum_\gamma U_i^{\alpha\gamma}\langle\{[f_{i\alpha}n_\gamma^i, H], f_{j\beta}^\dagger\}\rangle$:

$$\begin{aligned}
\sum_\gamma U_i^{\alpha\gamma}\langle\{[f_{i\alpha}n_\gamma^i, H], f_{j\beta}^\dagger\}\rangle &= t_{ij}^{\alpha\beta}\sum_\gamma U_i^{\alpha\gamma}\langle n_\gamma^i\rangle + \sum_\gamma U_i^{\alpha\gamma}t_{ij}^{\gamma\beta}\langle f_{i\alpha}f_{j\gamma}^\dagger\rangle \\
&+ \delta_{ij}\delta_{\alpha\beta}\sum_{\gamma\delta} U_i^{\alpha\gamma}U_i^{\alpha\delta}\langle n_\gamma^i n_\delta^i\rangle \\
&+ 2\delta_{ij}U_i^{\alpha\beta}\sum_\gamma U_i^{\alpha\gamma}\langle f_{i\alpha}f_{j\beta}^\dagger n_\gamma^i\rangle + \delta_{ij}U_i^{\alpha\beta}U_i^{\alpha\beta}\langle f_{i\alpha}f_{i\beta}^\dagger\rangle \\
&+ \delta_{ij}U_i^{\alpha\beta}\left(\langle\tilde{f}_{i\alpha}f_{j\beta}^\dagger\rangle - \langle f_{i\alpha}\tilde{f}_{j\beta}^\dagger\rangle\right) \\
&- \delta_{ij}\delta_{\alpha\beta}\sum_\gamma U_i^{\alpha\gamma}\left(\langle\tilde{f}_{i\gamma}f_{i\gamma}^\dagger\rangle - \langle f_{i\gamma}\tilde{f}_{i\gamma}^\dagger\rangle\right), \qquad (13.45)
\end{aligned}$$

where $\tilde{f}_{i\alpha} = \sum_{j\beta} t_{ij}^{\alpha\beta}f_{j\beta}$, $\tilde{f}_{i\alpha}^\dagger = \sum_{j\beta} t_{ji}^{\beta\alpha}f_{j\beta}^\dagger$. Here we meet the same problem as that of impurity model: the term $\langle f_{i\alpha}f_{j\beta}^\dagger n_\gamma^i\rangle$ can not be expressed in terms of Green functions. This problem can be overcome by introducing projection operators such as Hubbard operators. We discuss this possibility in the next chapter. Assuming an expression for $\sum_\gamma U_i^{\alpha\gamma}\langle\{[f_{i\alpha}n_\gamma^i, H], f_{j\beta}^\dagger\}\rangle$ is available, the second moments and the first moment of self energy read

$$\begin{aligned}
M_{ij\alpha\beta}^{(3)} &= \langle\{[[f_{i\alpha}, H]H], f_{j\beta}^\dagger\}\rangle, \qquad (13.46)\\
&= \sum_{k\gamma} t_{ik}^{\alpha\gamma}\langle\{[f_{k\gamma}, H], f_{j\beta}^\dagger\}\rangle + \sum_\gamma U_i^{\alpha\gamma}\langle\{[f_{i\alpha}n_\gamma^i, H], f_{j\beta}^\dagger\}\rangle, \qquad (13.47)\\
&= (tM^{(2)})_{ij\alpha\beta} + \sum_\gamma U_i^{\alpha\gamma}\langle\{[f_{i\alpha}n_\gamma^i, H], f_{j\beta}^\dagger\}\rangle, \qquad (13.48)
\end{aligned}$$

$$\begin{aligned}
\Sigma_{\alpha\beta}^{(1)} &= M_{ij\alpha\beta}^{(3)} - (tM^{(2)})_{ij\alpha\beta} - (\Sigma^{(0)}t)_{ij\alpha\beta} - \left(\Sigma^{(0)}\right)_{ij\alpha\beta}^2, \qquad (13.49)\\
&= \sum_\gamma U_i^{\alpha\gamma}\langle\{[f_{i\alpha}n_\gamma^i, H], f_{j\beta}^\dagger\}\rangle - (\Sigma^{(0)}t)_{ij\alpha\beta} - \left(\Sigma^{(0)}\right)_{ij\alpha\beta}^2, \qquad (13.50)\\
&= \delta_{ij}\delta_{\alpha\beta}\sum_{\gamma\delta} U_i^{\alpha\gamma}U_i^{\alpha\delta}\left(\langle n_\gamma^i n_\delta^i\rangle - \langle n_\gamma^i\rangle\langle n_\delta^i\rangle\right) \\
&+ 2\delta_{ij}U_i^{\alpha\beta}\sum_\gamma\left(U_i^{\alpha\gamma}\langle f_{i\alpha}f_{j\beta}^\dagger n_\gamma^i\rangle - U_i^{\alpha\gamma}\langle f_{i\alpha}f_{j\beta}^\dagger\rangle\langle n_\gamma^i\rangle - U_i^{\beta\gamma}\langle f_{i\alpha}f_{j\beta}^\dagger\rangle\langle n_\gamma^i\rangle\right) \\
&+ \delta_{ij}U_i^{\alpha\beta}U_i^{\alpha\beta}\langle f_{i\alpha}f_{i\beta}^\dagger\rangle - \delta_{ij}\sum_\gamma U_i^{\alpha\gamma}U_i^{\gamma\beta}\langle f_{i\alpha}f_{i\gamma}^\dagger\rangle\langle f_{i\gamma}f_{i\beta}^\dagger\rangle \qquad (13.51)\\
&+ \delta_{ij}U_i^{\alpha\beta}\left(\langle\tilde{f}_{i\alpha}f_{j\beta}^\dagger\rangle - \langle f_{i\alpha}\tilde{f}_{j\beta}^\dagger\rangle\right) - \delta_{ij}\delta_{\alpha\beta}\sum_\gamma U_i^{\alpha\gamma}\left(\langle\tilde{f}_{i\gamma}f_{i\gamma}^\dagger\rangle - \langle f_{i\gamma}\tilde{f}_{i\gamma}^\dagger\rangle\right).
\end{aligned}$$

The fourth order moment can be found in a similar way. We need an expression for $\sum_\gamma U_i^{\alpha\gamma}\langle\{[[f_{i\alpha}n_\gamma, H], H], f_{j\beta}^\dagger\}\rangle$:

$$
\begin{aligned}
&\sum_\gamma U_i^{\alpha\gamma}\langle\{[[f_{i\alpha}n_\gamma, H], H], f_{j\beta}^\dagger\}\rangle \qquad (13.52)\\
=\;& \delta_{ij}U_i^{\alpha\beta}\sum_{k\gamma}(t^2)_{ik}^{\alpha\gamma}\langle f_{k\gamma}f_{j\beta}^\dagger\rangle + \sum_\gamma U_i^{\alpha\gamma}(t^2)_{ij}^{\alpha\beta}\langle n_\gamma^i\rangle + 2t_{ij}^{\alpha\beta}\sum_{\gamma\delta}U_i^{\alpha\gamma}U_j^{\beta\delta}\langle n_\gamma^i n_\delta^j\rangle\\
+\;& \delta_{ij}U_i^{\alpha\beta}\sum_{\gamma\delta}t_{ik}^{\alpha\gamma}U_k^{\gamma\delta}\langle f_{k\gamma}f_{j\beta}^\dagger n_\delta^k\rangle + \delta_{ij}U_i^{\alpha\beta}\sum_\gamma\left(t_{ii}^{\alpha\gamma}U_i^{\gamma\beta}\langle f_{i\gamma}f_{i\beta}^\dagger\rangle - U^{\alpha\gamma}t_{ii}^{\gamma\beta}\langle f_{i\alpha}f_{i\gamma}^\dagger\rangle\right)\\
+\;& \sum_{\gamma\delta}U_i^{\alpha\gamma}t_{ij}^{\alpha\delta}U_j^{\delta\beta}\langle f_{j\delta}f_{j\beta}^\dagger n_\gamma^i\rangle + \delta_{ij}U_i^{\alpha\beta}\langle f_{i\alpha}\mathcal{F}_{i\beta}^\dagger\rangle - 2\delta_{ij}U_i^{\alpha\beta}\langle\tilde{f}_{i\alpha}\tilde{f}_{j\beta}^\dagger\rangle\\
+\;& 2\delta_{ij}\delta_{\alpha\beta}\sum_\gamma U_i^{\alpha\gamma}\langle\tilde{f}_{i\gamma}\tilde{f}_{j\gamma}^\dagger\rangle + 2\sum_\gamma U_i^{\alpha\gamma}t_{ij}^{\alpha\beta}\left(\langle f_{i\gamma}\tilde{f}_{i\gamma}^\dagger\rangle - \langle\tilde{f}_{i\gamma}f_{i\gamma}^\dagger\rangle\right)\\
+\;& 2\delta_{ij}U_i^{\alpha\beta}\sum_\gamma U_i^{\alpha\gamma}\langle\tilde{f}_{i\alpha}f_{j\beta}n_\gamma^i\rangle + \delta_{ij}U_i^{\alpha\beta}U_i^{\alpha\beta}\left(\langle\tilde{f}_{i\alpha}f_{j\beta}\rangle - \langle f_{i\alpha}\tilde{f}_{i\beta}^\dagger\rangle\right)\\
+\;& 3\delta_{ij}U_i^{\alpha\beta}U_i^{\alpha\beta}\sum_\gamma U_i^{\alpha\gamma}\langle f_{i\alpha}f_{j\beta}n_\gamma^i\rangle + 3\delta_{ij}U_i^{\alpha\beta}\sum_{\gamma\delta}U_i^{\alpha\gamma}U^{\alpha\delta}\langle f_{i\alpha}f_{j\beta}n_\gamma^i n_\delta^i\rangle\\
+\;& \delta_{ij}\delta_{\alpha\beta}\sum_{\gamma\delta\epsilon}U_i^{\alpha\gamma}U_i^{\alpha\delta}U_i^{\alpha\epsilon}\langle n_\gamma^i n_\delta^i n_\epsilon^i\rangle + \delta_{ij}U_i^{\alpha\beta}U_i^{\alpha\beta}U_i^{\alpha\beta}\langle f_{i\alpha}f_{j\beta}^\dagger\rangle\\
-\;& 3\delta_{ij}\delta_{\alpha\beta}\sum_{\gamma\delta}U_i^{\alpha\gamma}U_i^{\alpha\delta}\left(\langle\tilde{f}_{i\delta}f_{i\delta}^\dagger n_\gamma^i\rangle - \langle f_{i\delta}\tilde{f}_{i\delta}^\dagger n_\gamma^i\rangle\right) + 3\sum_{\gamma\delta}U_i^{\alpha\gamma}U_i^{\alpha\delta}t_{ij}^{\delta\beta}\langle f_{i\alpha}f_{i\delta}^\dagger n_\gamma^i\rangle\\
-\;& 3\delta_{ij}U_i^{\alpha\beta}\sum_\gamma U^{\alpha\gamma}\langle f_{i\alpha}\tilde{f}_{i\beta}^\dagger n_\gamma^i\rangle - 2\delta_{ij}\delta_{\alpha\beta}\sum_\gamma U_i^{\alpha\gamma}U_i^{\alpha\gamma}\left(\langle\tilde{f}_{i\gamma}f_{i\gamma}^\dagger\rangle + \langle f_{i\gamma}\tilde{f}_{i\gamma}^\dagger\rangle\right)\\
+\;& 2\delta_{ij}\delta_{\alpha\beta}\sum_{\gamma\delta}U_i^{\alpha\gamma}U_i^{\alpha\delta}\left(t_{ii}^{\gamma\delta}\langle f_{i\delta}f_{i\gamma}^\dagger\rangle + t_{ii}^{\delta\gamma}\langle f_{i\gamma}f_{i\delta}^\dagger\rangle\right) + 2\sum_\gamma U_i^{\alpha\gamma}U_i^{\alpha\gamma}t_{ij}^{\gamma\beta}\langle f_{i\alpha}f_{i\gamma}^\dagger\rangle\\
-\;& \sum_{\gamma\delta}U_i^{\alpha\gamma}t_{ij}^{\gamma\beta}U_i^{\gamma\delta}\langle f_{i\alpha}f_{i\gamma}^\dagger n_\delta^i\rangle + \delta_{ij}\delta_{\alpha\beta}U_i^{\alpha\gamma}U_i^{\gamma\delta}\left(\langle\tilde{f}_{i\gamma}f_{i\gamma}n_\delta^i\rangle + \langle f_{i\gamma}\tilde{f}_{i\gamma}n_\delta^i\rangle\right)\\
+\;& \delta_{ij}\delta_{\alpha\beta}\sum_{\gamma\delta}U_i^{\alpha\gamma}U_i^{\gamma\delta}(t_{ii}^{\delta\gamma} - t_{ii}^{\gamma\delta})\langle f_{i\delta}f_{i\gamma}^\dagger\rangle - \delta_{ij}U_i^{\alpha\beta}\sum_\gamma U^{\beta\gamma}\langle f_{i\alpha}\tilde{f}_{i\beta}^\dagger n_\gamma^i\rangle
\end{aligned}
$$

$$
\begin{aligned}
- \quad & \delta_{ij}\delta_{\alpha\beta}\sum_{\gamma} U^{\alpha\gamma}\left(\langle \mathcal{F}_{i\gamma} f^{\dagger}_{i\gamma}\rangle + \langle f_{i\gamma}\mathcal{F}^{\dagger}_{i\gamma}\rangle\right) + \sum_{k\gamma\delta} U_i^{\alpha\gamma} t_{ik}^{\gamma\delta} t_{kj}^{\delta\beta}\langle f_{i\alpha} f^{\dagger}_{i\gamma}\rangle \\
- \quad & \delta_{ij}\delta_{\alpha\beta}\sum_{k\gamma\delta\epsilon} U_i^{\alpha\gamma} U_k^{\delta\epsilon}\left(t_{ik}^{\gamma\delta}\langle f_{k\delta} f_{i\gamma} n^k_{\epsilon}\rangle - t_{ki}^{\delta\gamma}\langle f_{i\gamma} f_{k\delta} n^k_{\epsilon}\rangle\right) \\
+ \quad & \sum_{\gamma\delta} U_i^{\alpha\gamma}(t_{ij}^{\gamma\beta} + t_{ji}^{\beta\gamma}) U^{\beta\delta}\langle f_{i\alpha} f_{i\gamma} n^j_{\delta}\rangle + \delta_{ij}\sum_{\gamma} U^{\alpha\gamma} t^{\beta\gamma} U^{\beta\gamma}\langle f_{i\alpha} f^{\dagger}_{i\gamma}\rangle \\
+ \quad & 3\delta_{ij} U_i^{\alpha\beta}\sum_{\gamma}\left(\langle f_{i\alpha} f^{\dagger}_{j\beta} f^{\dagger}_{i\gamma}\tilde{f}_{i\gamma}\rangle - \langle f_{i\alpha} f^{\dagger}_{j\beta}\tilde{f}^{\dagger}_{i\gamma} f_{i\gamma}\rangle\right) \\
- \quad & \delta_{ij}\sum_{\gamma} U_i^{\alpha\gamma} U^{\gamma\beta}\left(\langle f_{i\alpha} f^{\dagger}_{j\beta} f^{\dagger}_{i\gamma}\tilde{f}_{i\gamma}\rangle - \langle f_{i\alpha} f^{\dagger}_{j\beta}\tilde{f}^{\dagger}_{i\gamma} f_{i\gamma}\rangle\right) \\
+ \quad & \sum_{\gamma\delta} U_i^{\alpha\gamma} U^{\delta\beta}\left(t_{\gamma\delta}^{ij}\langle f_{i\alpha} f^{\dagger}_{i\gamma} f_{j\delta} f^{\dagger}_{j\beta}\rangle - t_{\delta\gamma}^{ji}\langle f_{i\alpha} f_{j\delta} f^{\dagger}_{j\beta} f^{\dagger}_{i\gamma}\rangle\right),
\end{aligned}
$$

where $\mathcal{F}_{i\alpha} = \sum_{j\beta}(t^2)_{ij}^{\alpha\beta} f_{j\beta}$. We face similar problems as in impurity models. We need an projections scheme to deal with terms such as $\langle \tilde{f}_{i\alpha} f_{j\beta} n^i_{\gamma}\rangle$ and we need to deal with four fermion terms such as $\langle f_{i\alpha} f_{j\delta} f^{\dagger}_{j\beta} f^{\dagger}_{i\gamma}\rangle$. When an expression of $\sum_{\gamma} U_i^{\alpha\gamma}\langle\{[[f_{i\alpha} n_{\gamma}, H], H], f^{\dagger}_{j\beta}\}\rangle$ is available, the fourth moment and the second moment of self energy can be found by

$$
\begin{aligned}
M^{(4)}_{ij\alpha\beta} &= \langle\{[[[f_{i\alpha}, H], H], H], f^{\dagger}_{j\beta}\}\rangle & (13.53)\\
&= \sum_{k\gamma} t_{ik}^{\alpha\gamma}\langle\{[[f_{k\gamma}, H], H], f^{\dagger}_{j\beta}\}\rangle + \sum_{\gamma} U_i^{\alpha\gamma}\langle\{[[f_{i\alpha} n_{\gamma}, H], H], f^{\dagger}_{j\beta}\}\rangle & (13.54)\\
&= (tM^{(3)})_{ij\alpha\beta} + \sum_{\gamma} U_i^{\alpha\gamma}\langle\{[[f_{i\alpha} n_{\gamma}, H], H], f^{\dagger}_{j\beta}\}\rangle & (13.55)\\
\Sigma^{(2)}_{\alpha\beta} &= \sum_{\gamma} U_i^{\alpha\gamma}\langle\{[[f_{i\alpha} n_{\gamma}, H], H], f^{\dagger}_{j\beta}\}\rangle - \left(\Sigma^{(0)} M^{(3)} + \Sigma^{(1)} M^{(2)}\right)_{\alpha\beta}. & (13.56)
\end{aligned}
$$

Chapter 14

Equation of Method

14.1 Multi-band Hubbard Model

As seen in the previous chapter, finding a scheme able to construct self consistency equations of Green functions for general multi-band model is important. In this chapter, we use equation of motion method with Hubbard operators. Unlike the moment expansion method, we successfully construct self consistency equations for both multi-band models: multi-band lattice Hubbard model and multi-band impurity model.

We consider N-band Hubbard model with Hamiltonian,

$$H = \sum_i H^i_{\rm atom} + H_{\rm hop}, \tag{14.1}$$

where $H^i_{\rm atom}$ is the Hamiltonian of an atom at site i, and $H_{\rm hop}$ is the Hamiltonian describing fermion hopping between sites. Explicit forms of the component Hamiltonians read

$$H^i_{\rm atom} = \sum_\alpha \epsilon^i_\alpha n^i_\alpha + \sum_{\alpha\beta\gamma\delta} \Gamma^{\alpha\beta\gamma\delta}_i f^\dagger_{i\alpha} f^\dagger_{i\beta} f_{i\gamma} f_{i\delta}, \tag{14.2}$$

$$H_{\rm hop} = \sum_{ij\alpha\beta} V^{\alpha\beta}_{ij} \left(f^\dagger_{i\alpha} f_{j\beta} + f^\dagger_{j\beta} f_{i\alpha} \right), \tag{14.3}$$

where $f_{i\alpha}(f^\dagger_{i\alpha})$ is a fermion annihilation(creation) operator of flavor α at site i and $V^{\alpha\beta}_{ij}$ is a hopping amplitude between flavor α at site i and flavor β at site j. The on-site interaction satisfies $U^{\alpha\beta\gamma\delta} = \left(U^{\delta\gamma\beta\alpha}\right)^*$. The flavor (band) indices α, β, γ, and δ run from 0 to N.

In DMFT, the lattice model maps into an impurity model with Hamiltonian

$$H = H_{\rm atom} + H_{\rm band} + H_{\rm hyb}, \tag{14.4}$$

where

$$H_{\text{atom}} = \sum_{\alpha} \epsilon_{\alpha} n_{\alpha} + \sum_{\alpha\beta\gamma\delta} \Gamma^{\alpha\beta\gamma\delta} f^{\dagger}_{i\alpha} f^{\dagger}_{i\beta} f_{i\gamma} f_{i\delta}, \tag{14.5}$$

$$H_{\text{hyb}} = \sum_{\alpha\beta\vec{k}} V^{\alpha\beta}_{\vec{k}} \left(f^{\dagger}_{\alpha} c_{\beta\vec{k}} + c^{\dagger}_{\alpha\vec{k}} f_{\beta} \right), \tag{14.6}$$

$$H_{\text{band}} = \sum_{\alpha\vec{k}} \epsilon^{\alpha\vec{k}} c^{\dagger}_{\alpha\vec{k}} c_{\alpha\vec{k}}. \tag{14.7}$$

The annihilation(creation) operators $c_{\alpha\vec{k}}(c_{\alpha\vec{k}})$ describe band fermions. The hybridization amplitude $V^{\alpha\beta}_{\vec{k}}$ satisfies $V^{\alpha\beta}_{\vec{k}} = \left(V^{\beta\alpha}_{\vec{k}}\right)^{*}$.

In this section, we present self consistency equations for Green functions applying equation of motion method to Hubbard operators. We find Green functions for atomic Hamiltonian first to introduce the method and set up notations. Then we find a self consistency equation of Green functions for lattice model. This is only possible in DMFT limit in the sense that the coordination number z approaches to infinity. Finally, a self consistency equation of Green function for impurity model is presented.

14.2 Atomic Case

To see how the Hubbard operator approach works, we solve the atomic case with Hamiltonian

$$H_{\text{atom}} = \sum_{\alpha} \epsilon_{\alpha} n_{\alpha} + \sum_{\alpha\beta\gamma\delta} \Gamma^{\alpha\beta\gamma\delta} f^{\dagger}_{\alpha} f^{\dagger}_{\beta} f_{\gamma} f_{\delta}, \tag{14.8}$$

where α runs over the band index from 1 to N, and $\Gamma^{\alpha\beta\gamma\delta}$ satisfies the relation to make the Hamiltonian self conjugate. A bases can be setup as the set of states $|n, \mathcal{I}\rangle$, where

$$|n, \mathcal{I}\rangle = \prod_{k=1}^{n} f^{\dagger}_{\alpha_k} |0\rangle, \quad \alpha_k < \alpha_l \text{ for } k < l, \quad n = 0, 1, 2, \cdots, N \tag{14.9}$$

Since the atomic Hamiltonian conserves the number of electrons, an eigenstates is a linear combinations of the states $|n, \mathcal{I}\rangle$ with the same number of electrons n,

$$H_{\text{atom}}|n, I\rangle = \epsilon_{nI}|n, I\rangle, \quad |n, I\rangle = \sum_{\mathcal{I}=1}^{{}^{N}C_{n}} c^{n}_{I\mathcal{I}} |n, \mathcal{I}\rangle, \tag{14.10}$$

where $c^{n}_{I\mathcal{I}}$ are constants.

The Hubbard operators are defined as

$$X_{IJ}^{nm} = |n, I\rangle\langle m, J|. \tag{14.11}$$

A subset of the Hubbard operators, $\{X_{II}^{nn}\}$ is a complete set of projection operators summing to the identity, $\sum_{nI} X_{II}^{nn} = 1$. Using these operators, the creation and annihilation operators can be projected into eigenstates of the atomic Hamiltonian,

$$\begin{aligned} f_\alpha &= \sum_{nmIJ} X_{II}^{mm} f_\alpha X_{JJ}^{nn} = \sum_{nIJ} F_{IJ}^{\alpha nn+1} X_{IJ}^{nn+1}, \quad F_{IJ}^{\alpha nn+1} = \langle n, I|f_\alpha|n+1, J\rangle \\ f_\alpha^\dagger &= \sum_{nmIJ} X_{II}^{mm} f_\alpha^\dagger X_{JJ}^{nn} = \sum_{nIJ} F_{IJ}^{\alpha n+1n} X_{IJ}^{n+1n}, \quad F_{IJ}^{\alpha n+1n} = \langle n+1, I|f_\alpha^\dagger|n, J\rangle. \end{aligned}$$

Since the Hubbard operator X_{IJ}^{mn} is fermionic (bosonic) when $m-n$ is odd (even), we use different commutators for different Hubbard operators depending on their statistical nature:

$$\{X_{IJ}^{mn}, X_{KL}^{op}\}_\pm = X_{IJ}^{mn} X_{KL}^{op} - (-1)^{(m-n)(o-p)} X_{KL}^{op} X_{IJ}^{mn}. \tag{14.12}$$

14.2.1 General On-site Interaction

In terms of the Hubbard operator, the Hamiltonian reads

$$H_{\text{atom}} = \sum_{nI} \epsilon_{nI} X_{II}^{nn}. \tag{14.13}$$

Green functions of Hubbard operators, $G_{IJKL}^{mnop}(\tau) = -\langle T_\tau X_{IJ}^{mn}(\tau) X_{KL}^{op}(0)\rangle$, can be calculated by taking time derivative of Green functions,

$$\begin{aligned} \frac{\partial}{\partial\tau} G_{IJKL}^{mnop}(\tau) &= -\delta(\tau)\langle\{X_{IJ}^{mn}, X_{KL}^{op}\}_\pm\rangle - \langle T_\tau \frac{\partial}{\partial\tau} X_{IJ}^{mn}(\tau) X_{KL}^{op}(0)\rangle & (14.14) \\ &= -\delta(\tau)\langle\{X_{IJ}^{mn}, X_{KL}^{op}\}_\pm\rangle \\ &- \langle T_\tau [X_{IJ}^{mn}(\tau), H_{\text{atom}}(\tau)] X_{KL}^{op}(0)\rangle & (14.15) \end{aligned}$$

The commutator of a Hubbard operator and the Hamiltonian is found straightforwardly,

$$[X_{IJ}^{mn}, H_{\text{atom}}] = (\epsilon_{nJ} - \epsilon_{mI}) X_{IJ}^{mn}. \tag{14.16}$$

Substituting the eq. 14.16 to the eq. 14.15, we obtain

$$\frac{\partial}{\partial\tau} G_{IJKL}^{mnop}(\tau) = -\delta(\tau)\langle\{X_{IJ}^{mn}, X_{KL}^{op}\}_\pm\rangle - (\epsilon_{nJ} - \epsilon_{mI}) G_{IJKL}^{mnop}(\tau). \tag{14.17}$$

Taking Fourier transform of eq. 14.17 yields the Green functions of Hubbard operators,

$$G^{mnop}_{IJKL}(\omega_n) = \frac{\langle\{X^{mn}_{IJ}, X^{op}_{KL}\}_{\pm}\rangle}{\omega_n - (\epsilon_{nJ} - \epsilon_{mI})}. \tag{14.18}$$

The Green functions of fermion operators $G_{\alpha\beta}(\tau) = \langle T_\tau f_\alpha(\tau) f^\dagger_\beta(0)\rangle$ can be obtained by summing the Green functions of Hubbard operators

$$G_{\alpha\beta}(i\omega_n) = \sum_{mIJ}\sum_{nJK} F^{\alpha mm+1}_{IJ} F^{\alpha n+1n}_{KL} G^{mm+1n+1n}_{IJKL}(i\omega_n), \tag{14.19}$$

where $G^{mm+1n+1n}_{IJKL}(i\omega_n)$ can be easily evaluated to

$$G^{mm+1n+1n}_{IJKL}(i\omega_n) = \delta_{nm}\delta_{JK}\delta_{IL}\frac{e^{-\beta\epsilon_{nI}} + e^{-\beta\epsilon_{n+1J}}}{i\omega_n - (\epsilon_{nJ} - \epsilon_{mI})}. \tag{14.20}$$

14.2.2 Density-Density On-site Interaction

When the on-site interaction has the form of $\sum_{\alpha\beta} U^{\alpha\beta} n_\alpha n_\beta$, the states $|n, \mathcal{I}\rangle$ are the eigenstates by themselves. In this case, the index for the number of fermions n does not give an extra information. We drop out the index and let the index $\mathcal{I}$ scan all the eigenstates. Introducing new notations $|\mathcal{I} + \alpha\rangle = f^\dagger_\alpha|\mathcal{I}\rangle$, the fermion operators can be expressed as

$$f_\alpha = \sum_{\mathcal{I}} X_{\mathcal{I}\mathcal{I}+\alpha}, \quad f^\dagger_\alpha = \sum_{\mathcal{I}} X_{\mathcal{I}+\alpha\mathcal{I}} \tag{14.21}$$

The Green functions of fermion operators read

$$G_{\alpha\beta}(i\omega_n) = \sum_{\mathcal{I}\mathcal{J}} G_{\mathcal{I}\mathcal{I}+\alpha\mathcal{J}+\alpha\mathcal{J}}(i\omega_n), \qquad \alpha \notin \mathcal{I}, \quad \beta \notin \mathcal{J} \tag{14.22}$$

where the Green functions of Hubbard operators are evaluated, similarly to those of General on-site interaction case, to

$$G_{\mathcal{I}\mathcal{I}+\alpha\mathcal{J}+\alpha\mathcal{J}}(i\omega_n) = \frac{\langle\{X_{\mathcal{I}\mathcal{I}+\alpha}, X_{\mathcal{J}+\alpha\mathcal{J}}\}_{\pm}\rangle}{i\omega_n - (\epsilon_J - \epsilon_I)} \tag{14.23}$$

$$= \delta_{\mathcal{I}\mathcal{J}}\frac{e^{-\beta\epsilon_{\mathcal{I}}} + e^{-\beta\epsilon_{\mathcal{I}+\alpha}}}{i\omega_n - (\epsilon_{\mathcal{I}+\alpha} - \epsilon_{\mathcal{I}})}. \tag{14.24}$$

14.3 Lattice Model

14.3.1 Generic on-site interaction

Self consistency equation

We consider N-band Hubbard model with Hamiltonian,

$$H = \sum_i H^i_{\rm atom} + H_{\rm hop}, \tag{14.25}$$

where $H^i_{\rm atom}$ is the Hamiltonian of an atom at site i, and $H_{\rm hop}$ is the Hamiltonian describing fermion hopping between sites. Explicit forms of the component Hamiltonians read

$$H^i_{\rm atom} = \sum_\alpha \epsilon^i_\alpha n^i_\alpha + \sum_{\alpha\beta\gamma\delta} \Gamma^{\alpha\beta\gamma\delta}_i f^\dagger_{i\alpha} f^\dagger_{i\beta} f_{i\gamma} f_{i\delta}, \tag{14.26}$$

$$H_{\rm hyb} = \sum_{ij\alpha\beta} V^{\alpha\beta}_{ij} \left(f^\dagger_{i\alpha} f_{j\beta} + f^\dagger_{j\beta} f_{i\alpha} \right), \tag{14.27}$$

The site indices i and j run over the lattice and the flavor indices α and β run over the N bands. The Hubbard operators $X^{mn}_{iIJ} \equiv |i,m,I\rangle\langle i,n,J|$, where $|i,m,I\rangle$ is an eigenstate with energy ϵ^i_{mI} of the atomic Hamiltonian at site i with n particles, are defined at each site similarly to those of atomic case except that the operators act as the identity operator on all the other sites. The fermion Green functions can be expressed as a sum over the Green functions of Hubbard operators,

$$G^{ij}_{\alpha\beta}(i\omega_n) = \sum_{mIJ} \sum_{nKL} F^{\alpha mm+1}_{iIJ} F^{\beta n+1n}_{jKL} G^{mm+1n+1n}_{iIJjKL}(i\omega_n), \tag{14.28}$$

where

$$G^{mm+1n+1n}_{iIJjKL}(\tau) = -\langle T_\tau X^{mm+1}_{iIJ}(\tau) X^{n+1n}_{jKL}(0)\rangle, \tag{14.29}$$

$$F^{\alpha nn+1}_{iIJ} = \langle i,n,I|f_{i\alpha}|i,n+1,J\rangle, \quad F^{\alpha n+1n}_{jIJ} = \langle j,n+1,I|f^\dagger_{j\alpha}|j,n,J\rangle. \tag{14.30}$$

Since the coefficients $F^{\alpha nn+1}_{iIJ}$ and $F^{\alpha n+1n}_{jIJ}$ are fixed once the atomic problem is solved, we concentrate on finding the Green functions of Hubbard operators $G^{mm+1n+1n}_{iIJjKL}(\tau)$.

Taking time derivative of the Eq. 14.29, we obtain

$$\begin{aligned}\frac{\partial}{\partial\tau}G^{mm+1n+1n}_{iIJjKL}(\tau) &= -\delta(\tau)\langle\{X^{mm+1}_{iIJ}, X^{n+1n}_{jKL}\}\rangle - \langle T_\tau[X^{mm+1}_{iIJ}, H](\tau)X^{n+1n}_{jKL}(0)\rangle \\ &= -\delta(\tau)\langle\{X^{mm+1}_{iIJ}, X^{n+1n}_{jKL}\}\rangle - (\epsilon^i_{m+1J} - \epsilon^i_{mI})\langle T_\tau X^{mm+1}_{iIJ}(\tau)X^{n+1n}_{jKL}(0)\rangle \\ &- \langle T_\tau[X^{mm+1}_{iIJ}, H_{\rm hop}](\tau)X^{n+1n}_{jKL}(0)\rangle.\end{aligned} \tag{14.31}$$

We approximate $[X^{mm+1}_{iIJ}, H_{\rm hop}]$ by a linear combination of X^{pp+1}_{kLM}:

$$[X^{mm+1}_{iIJ}, H_{\rm hop}] = \sum_{kpMN} Y^{mm+1pp+1}_{iIJkMN} X^{pp+1}_{kMN}. \tag{14.32}$$

Substituting the Eq. 14.32 to the Eq. 14.31 yields

$$\begin{aligned}\frac{\partial}{\partial\tau}G^{mm+1n+1n}_{iIJjKL}(\tau) &= -\delta(\tau)\langle\{X^{mm+1}_{iIJ}, X^{n+1n}_{jKL}\}\rangle \\ &- (\epsilon^i_{m+1J} - \epsilon^i_{mI})\langle T_\tau X^{mm+1}_{iIJ}(\tau)X^{n+1n}_{jKL}(0)\rangle \\ &- \sum_{kpMN} Y_{iIJpMN}\langle T_\tau X^{pp+1}_{pMN}(\tau)X^{n+1n}_{jKL}(0)\rangle.\end{aligned} \tag{14.33}$$

Using the definition of the Green functions of Hubbard operator and Fourier transform, we obtain

$$\begin{aligned}&\langle\{X^{mm+1}_{iIJ}, X^{n+1n}_{jKL}\}\rangle = \\ &\sum_{kpMN}[(i\omega_n - (\epsilon^i_{m+1J} - \epsilon^i_{mI}))\delta_{ik}\delta_{mp}\delta_{IM}\delta_{JN} - Y^{mm+1pp+1}_{iIJkMN}]G^{pp+1n+1n}_{kMNjKL}(i\omega_n).\end{aligned} \tag{14.34}$$

Taking anticommutator the Eq. 14.32 with X^{n+ln}_{jKL}, we obtain

$$\langle\{[X^{mm+1}_{iIJ}, H_{\rm hop}], X^{n+1n}_{jKL}\}\rangle = \sum_{kpMN} Y^{mm+1pp+1}_{iIJkMN}\langle\{X^{pp+1}_{kMN}, X^{n+1n}_{jKL}\}\rangle. \tag{14.35}$$

Solving this equation gives the Y matrix.

Introducing matrix notation

$$G_{\{imIJ\}\{jnLK\}} \equiv G^{mm+1n+1n}_{iIJjKL} \tag{14.36}$$

$$Y_{\{imIJ\}\{jnLK\}} \equiv Y^{mm+1nn+1}_{iIJjLK} \tag{14.37}$$

$$\tilde{Y}_{\{imIJ\}\{jnLK\}} \equiv \langle\{[X^{mm+1}_{iIJ}, H_{\rm hop}], X^{n+1n}_{jKL}\}\rangle \tag{14.38}$$

$$Z_{\{imIJ\}\{jnLK\}} \equiv \langle\{X^{mm+1}_{iIJ}, X^{n+1n}_{jKL}\}\rangle \tag{14.39}$$

$$= \delta_{ij}\delta_{nm}(\delta_{JK}\langle X^{mm}_{iIL}\rangle + \delta_{IL}\langle X^{m+1m+1}_{jKJ}\rangle) \tag{14.40}$$

$$\delta\epsilon_{\{imIJ\}\{jnLK\}} \equiv (\epsilon^{i}_{m+1J} - \epsilon^{i}_{mI})\delta_{ij}\delta_{mn}\delta_{IL}\delta_{JK} \tag{14.41}$$

$$\mathbf{1}_{\{imIJ\}\{jnLK\}} \equiv \delta_{ij}\delta_{mn}\delta_{IL}\delta_{JK}, \tag{14.42}$$

the Eq. 14.34 can be written in matrix form as

$$[G^{-1}] = Z^{-1}[i\omega_n\mathbf{1} - \delta\epsilon - Y] \tag{14.43}$$

or

$$G = \frac{Z}{i\omega_n\mathbf{1} - \delta\epsilon - Y}, \tag{14.44}$$

where the division implies matrix inversion.

The expectation value of a 0-particle Hubbard operator can be found from a corresponding Green function at $\tau = 0$:

$$\langle X^{mm}_{iIL}\rangle = -G^{mm+1m+1m}_{iIMiML}(\tau = 0), \tag{14.45}$$

where M is a state with $m+1$-particles. To complete a self consistency equation for the Green functions of Hubbard operators, we need to express $\tilde{Y}$ matrix in terms of the Green functions. For site diagonal $\tilde{Y}$ matrix, this expression can be obtained without further approximation. For site off-diagonal $\tilde{Y}$ matrix, we need to take a DMFT lmit to express the $\tilde{Y}$ matrix in terms of the Green functions of Hubbard operators. In DMFT limit, the site off-diagonal $\tilde{Y}$ matrix is given by

$$\langle\{[X^{mm+1}_{iIJ}, H_{\rm hop}], X^{n+1n}_{jKL}\}\rangle = \sum_{\alpha\beta}(V^{\alpha\beta}_{ij} + V^{\beta\alpha}_{ji})q^{mm+1}_{iIL}q^{n+1n}_{jKL}, \tag{14.46}$$

where

$$q^{mm+1}_{iIJ} \equiv \sum_C F^{\alpha m+1m}_{iJC}\langle X^{mm}_{iIC}\rangle + \sum_C F^{\alpha m+1m}_{iCI}\langle X^{m+1m+1}_{iCJ}\rangle \tag{14.47}$$

$$q^{n+1n}_{KL} \equiv \sum_C F^{\beta nn+1}_{jLC}\langle X^{n+1n+1}_{jKC}\rangle + \sum_C F^{\beta nn+1}_{jCK}\langle X^{nn}_{jCL}\rangle. \tag{14.48}$$

The site diagonal $\tilde{Y}$ matrix is given by

$$
\begin{aligned}
&\langle\{[X^{mm+1}_{iIJ}, H_{\rm hop}\,], X^{n+1n}_{iKL}\}\rangle \\
&= \sum_{j\alpha\beta}\sum_{qCD} \delta_{m+1n} F^{\alpha m+1m}_{iLI} F^{\beta qq+1}_{jCD} (V^{\alpha\beta}_{ij} + V^{\beta\alpha}_{ji}) G^{qq+1m+2m+1}_{jCDiKJ}(\tau = 0^+) \\
&- \sum_{j\alpha\beta}\sum_{qCD} \delta_{mn+1} F^{\alpha m+1m}_{iJK} F^{\beta qq+1}_{jCD} (V^{\alpha\beta}_{ij} + V^{\beta\alpha}_{ji}) G^{qq+1n+1n}_{jCDiIL}(\tau = 0^+) \\
&+ \sum_{j\alpha\beta}\sum_{qCD}\sum_{M} \delta_{mn}\delta_{IL} F^{\alpha m+1m}_{iJM} F^{\beta qq+1}_{jCD} (V^{\alpha\beta}_{ij} + V^{\beta\alpha}_{ji}) G^{qq+1n+1n}_{jCDiKM}(\tau = 0^+) \\
&- \sum_{j\alpha\beta}\sum_{qCD}\sum_{M} \delta_{mn}\delta_{JK} F^{\alpha m+1m}_{iMI} F^{\beta qq+1}_{jCD} (V^{\alpha\beta}_{ij} + V^{\beta\alpha}_{ji}) G^{qq+1n+1n}_{jCDiML}(\tau = 0^+) \\
&- \sum_{j\alpha\beta}\sum_{qCD} \delta_{m+1n} F^{\alpha m+1m+2}_{iJK} F^{\beta q+1q}_{jCD} (V^{\alpha\beta}_{ij} + V^{\beta\alpha}_{ji}) G^{mm+1q+1q}_{iILjCD}(\tau = 0^+) \\
&+ \sum_{j\alpha\beta}\sum_{qCD} \delta_{mn+1} F^{\alpha nn+1}_{iLI} F^{\beta q+1q}_{jCD} (V^{\alpha\beta}_{ij} + V^{\beta\alpha}_{ji}) G^{mm+1q+1q}_{iKJjCD}(\tau = 0^+) \\
&- \sum_{j\alpha\beta}\sum_{qCD}\sum_{M} \delta_{mn}\delta_{JK} F^{\alpha m-1m}_{iMI} F^{\beta q+1q}_{jCD} (V^{\alpha\beta}_{ij} + V^{\beta\alpha}_{ji}) G^{m-1mq+1q}_{iMLjCD}(\tau = 0^+) \\
&+ \sum_{j\alpha\beta}\sum_{qCD}\sum_{M} \delta_{mn}\delta_{IL} F^{\alpha m+1m+2}_{iJM} F^{\beta q+1q}_{jCD} (V^{\alpha\beta}_{ij} + V^{\beta\alpha}_{ji}) G^{m+1m+2q+1q}_{iKMjCD}(\tau = 0^+).
\end{aligned}
\tag{14.49}
$$

This expression for site diagonal $\tilde{Y}$ matrix holds without DMFT approximation.

Derivation of $\tilde{Y}$ matrix

Site off-diagonal $\tilde{Y}$ matrix is given by

$$\tilde{Y}^{mm+1n+1n}_{iIJjKL} = \langle\{[X^{mm+1}_{iIJ}, H_{\rm hop}], X^{n+1n}_{jKL}\}\rangle. \tag{14.50}$$

A straightforward but tedious calculation yields for $\neq j$

$$\begin{aligned}
\tilde{Y}^{mm+1n+1n}_{iIJjKL} &= \sum_{\alpha\beta}\sum_{CD} F^{\alpha m+1m}_{iJC} F^{\beta nn+1}_{jDK}(V^{\alpha\beta}_{ij} + V^{\beta\alpha}_{ji})\langle X^{mm}_{iIC} X^{nn}_{jDL}\rangle \\
&+ \sum_{\alpha\beta}\sum_{CD} F^{\alpha m+1m}_{iJC} F^{\beta nn+1}_{jLD}(V^{\alpha\beta}_{ij} + V^{\beta\alpha}_{ji})\langle X^{mm}_{iIC} X^{n+1n+1}_{jKD}\rangle \\
&+ \sum_{\alpha\beta}\sum_{CD} F^{\alpha m+1m}_{iCI} F^{\beta nn+1}_{jDK}(V^{\alpha\beta}_{ij} + V^{\beta\alpha}_{ji})\langle X^{m+1m+1}_{iCJ} X^{nn}_{jDL}\rangle \\
&+ \sum_{\alpha\beta}\sum_{CD} F^{\alpha m+1m}_{iCI} F^{\beta nn+1}_{jLD}(V^{\alpha\beta}_{ij} + V^{\beta\alpha}_{ji})\langle X^{m+1m+1}_{iCJ} X^{n+1n+1}_{jKD}\rangle \\
&- \sum_{\alpha\beta}\sum_{CD} F^{\alpha m+1m+2}_{iJC} F^{\beta n+ln}_{jKD}(V^{\alpha\beta}_{ij} + V^{\beta\alpha}_{ji})\langle X^{mm+2}_{iIC} X^{n+2n}_{jDL}\rangle \\
&- \sum_{\alpha\beta}\sum_{CD} F^{\alpha m+1m+2}_{iJC} F^{\beta nn-1}_{jLD}(V^{\alpha\beta}_{ij} + V^{\beta\alpha}_{ji})\langle X^{mm+2}_{iIC} X^{n+1n-1}_{jKD}\rangle \\
&- \sum_{\alpha\beta}\sum_{CD} F^{\alpha m-1m}_{iCI} F^{\beta n+1n}_{jKD}(V^{\alpha\beta}_{ij} + V^{\beta\alpha}_{ji})\langle X^{m-1m+1}_{iCJ} X^{n+2n}_{jDL}\rangle \\
&- \sum_{\alpha\beta}\sum_{CD} F^{\alpha m-1m}_{iCI} F^{\beta nn-1}_{jLD}(V^{\alpha\beta}_{ij} + V^{\beta\alpha}_{ji})\langle X^{m-1m+1}_{iCJ} X^{n+1n-1}_{jKD}\rangle.
\end{aligned} \tag{14.51}$$

In DMFT limit, the only components that are of the first order in V_{ij} are relevant for $\tilde{Y}$ matrix. Since all the terms in the Eq. 14.51 contain $V_{ij} + V_{ji}$, we only need to take zeroth order expectation values of two Hubbard operators into consideration. In this limit, the expectation value of two Hubbard operators at different sites decomposes into product of two expectation values of each Hubbard operator:

$$\langle X^{mm}_{iIJ} X^{nn}_{jKL}\rangle = \langle X^{mm}_{iIJ}\rangle\langle X^{nn}_{jKL}\rangle, \quad i \neq j \tag{14.52}$$

Using these two properties, we can write site off diagonal $\tilde{Y}$ matrix in DMFT limit as

$$\begin{aligned}
\tilde{Y}^{mm+1n+1n}_{iIJjKL} &= \sum_{\alpha\beta}\sum_{CD} F^{\alpha m+1m}_{iJC} F^{\beta nn+1}_{jDK}(V^{\alpha\beta}_{ij} + V^{\beta\alpha}_{ji})\langle X^{mm}_{iIC}\rangle\langle X^{nn}_{jDL}\rangle \\
&+ \sum_{\alpha\beta}\sum_{CD} F^{\alpha m+1m}_{iJC} F^{\beta nn+1}_{jLD}(V^{\alpha\beta}_{ij} + V^{\beta\alpha}_{ji})\langle X^{mm}_{iIC}\rangle\langle X^{n+1n+1}_{jKD}\rangle \\
&+ \sum_{\alpha\beta}\sum_{CD} F^{\alpha m+1m}_{iCI} F^{\beta nn+1}_{jDK}(V^{\alpha\beta}_{ij} + V^{\beta\alpha}_{ji})\langle X^{m+1m+1}_{iCJ}\rangle\langle X^{nn}_{jDL}\rangle \\
&+ \sum_{\alpha\beta}\sum_{CD} F^{\alpha m+1m}_{iCI} F^{\beta nn+1}_{jLD}(V^{\alpha\beta}_{ij} + V^{\beta\alpha}_{ji})\langle X^{m+1m+1}_{iCJ}\rangle\langle X^{n+1n+1}_{jKD}\rangle.
\end{aligned} \tag{14.53}$$

Arranging terms in the Eq. 14.53, we obtain

$$\tilde{Y}^{mm+1n+1n}_{iIJjKL} = \sum_{\alpha\beta}(V^{\alpha\beta}_{ij} + V^{\beta\alpha}_{ji})q^{mm+1}_{iIL}q^{n+1n}_{jKL}, \quad i \neq j, \tag{14.54}$$

where

$$q^{mm+1}_{iIJ} \equiv \sum_C F^{\alpha m+1m}_{iJC}\langle X^{mm}_{iIC}\rangle + \sum_C F^{\alpha m+1m}_{iCI}\langle X^{m+1m+1}_{iCJ}\rangle, \tag{14.55}$$

$$q^{n+1n}_{KL} \equiv \sum_C F^{\beta nn+1}_{jLC}\langle X^{n+1n+1}_{jKC}\rangle + \sum_C F^{\beta nn+1}_{jCK}\langle X^{nn}_{jCL}\rangle. \tag{14.56}$$

The site diagonal Y matrix is defined by

$$\tilde{Y}^{mm+1n+1n}_{iIJiKL} = \langle\{[X^{mm+1}_{iIJ}, H_{\rm hop}], X^{n+1n}_{iKL}\}\rangle. \tag{14.57}$$

A straightforward calculation yields

$$\begin{aligned}
\tilde{Y}^{mm+1n+1n}_{iIJiKL} &= \sum_{j\alpha\beta}\sum_{qCD}\delta_{m+1n}F^{\alpha m+1m}_{iLI}F^{\beta qq+1}_{jCD}(V^{\alpha\beta}_{ij} + V^{\beta\alpha}_{ji})\langle X^{m+2m+1}_{iKJ}X^{qq+1}_{jCD}\rangle \\
&- \sum_{j\alpha\beta}\sum_{qCD}\delta_{mn+1}F^{\alpha n+2n+1}_{iJK}F^{\beta qq+1}_{jCD}(V^{\alpha\beta}_{ij} + V^{\beta\alpha}_{ji})\langle X^{n+1n}_{iIL}X^{qq+1}_{jCD}\rangle \\
&+ \sum_{j\alpha\beta}\sum_{qCD}\sum_M\delta_{mn}\delta_{IL}F^{\alpha m+1m}_{iJM}F^{\beta qq+1}_{jCD}(V^{\alpha\beta}_{ij} + V^{\beta\alpha}_{ji})\langle X^{n+1n}_{iKM}X^{qq+1}_{jCD}\rangle \\
&- \sum_{j\alpha\beta}\sum_{qCD}\sum_M\delta_{mn}\delta_{JK}F^{\alpha m+1m}_{iMI}F^{\beta qq+1}_{jCD}(V^{\alpha\beta}_{ij} + V^{\beta\alpha}_{ji})\langle X^{n+1n}_{iML}X^{qq+1}_{jCD}\rangle \\
&+ \sum_{j\alpha\beta}\sum_{qCD}\delta_{m+1n}F^{\alpha m+1m+2}_{iJK}F^{\beta q+1q}_{jCD}(V^{\alpha\beta}_{ij} + V^{\beta\alpha}_{ji})\langle X^{mm+1}_{iIL}X^{q+1q}_{jCD}\rangle \\
&- \sum_{j\alpha\beta}\sum_{qCD}\delta_{mn+1}F^{\alpha nn+1}_{iLI}F^{\beta q+1q}_{jCD}(V^{\alpha\beta}_{ij} + V^{\beta\alpha}_{ji})\langle X^{n+1n+2}_{iKJ}X^{q+1q}_{jCD}\rangle \\
&+ \sum_{j\alpha\beta}\sum_{qCD}\sum_M\delta_{mn}\delta_{JK}F^{\alpha m-1m}_{iMI}F^{\beta q+1q}_{jCD}(V^{\alpha\beta}_{ij} + V^{\beta\alpha}_{ji})\langle X^{m-1m}_{iML}X^{q+1q}_{jCD}\rangle \\
&- \sum_{j\alpha\beta}\sum_{qCD}\sum_M\delta_{mn}\delta_{IL}F^{\alpha m+1m+2}_{iJM}F^{\beta q+1q}_{jCD}(V^{\alpha\beta}_{ij} + V^{\beta\alpha}_{ji})\langle X^{m+1m+2}_{iKM}X^{q+1q}_{jCD}\rangle.
\end{aligned}$$

Using

$$\langle X^{m+2m+1}_{iKJ}X^{qq+1}_{jCD}\rangle = G^{qq+1m+2m+1}_{iCDjKJ}(\tau = 0^+), \tag{14.58}$$

we express $\tilde{Y}_{ii}$ in terms of the Green function of Hubbard operators.

14.3.2 Density-density on-site interaction

Self consistency equation

We consider N-band Hubbard model on lattice with Hamiltonian,

$$H = \sum_i H^i_{\rm atom} + H_{\rm hop}, \tag{14.59}$$

$$H_{\rm hop} = \sum_{ij\alpha\beta} V_{ij}^{\alpha\beta} \left(f^\dagger_{i\alpha} f_{j\beta} + f^\dagger_{j\beta} f_{i\alpha} \right), \tag{14.60}$$

$$H^i_{\rm atom} = \sum_\alpha \epsilon^i_\alpha n^i_\alpha + \sum_{\alpha\beta} U_i^{\alpha\beta} n_{i\alpha} n_{i\beta}. \tag{14.61}$$

The site indices i and j run over the lattice and the flavor indices α and β run over the N bands. The Hubbard operators $X^{mn}_{iIJ} \equiv |i,m,I\rangle\langle i,n,J|$, where $|i,m,I\rangle$ is an eigenstate with energy ϵ^i_{mI} of atomic Hamiltonian at site i with n particles, are defined at each site similarly to that of atomic case except that the operators act as the identity operator on all the other sites. Due to the simple on-site interaction, the eigenstate of atomic Hamiltonian can be found easily as $|i,n,\mathcal{I}\rangle = f^\dagger_{i\alpha_1} \cdots f^\dagger_{i\alpha_n} |0\rangle$. In this basis the F numbers of general Hubbard model reduce to delta functions $F^{\alpha m m+1}_{iIJ} = \delta_{\mathcal{I}-\alpha\mathcal{J}}$ and $F^{\alpha m+1 m}_{jIJ} = \delta_{\mathcal{I}+\alpha\mathcal{J}}$, where $|i,m,\mathcal{I}+\alpha\rangle = f^\dagger_{i\alpha}|i,m,\mathcal{I}\rangle$. This property simplifies the expression of Green functions and it is better not to keep track of number of particles.

The fermion Green functions can be expressed as sums over the Green functions of Hubbard operators,

$$G^{ij}_{\alpha\beta}(i\omega_n) = \sum_{\mathcal{I}\mathcal{J}} G_{i\mathcal{I}\mathcal{I}+\alpha j\mathcal{J}+\beta\mathcal{J}}(i\omega_n), \tag{14.62}$$

where

$$G_{i\mathcal{I}\mathcal{I}+\alpha j\mathcal{J}+\beta\mathcal{J}}(\tau) = -\langle T_\tau X^i_{\mathcal{I}\mathcal{I}+\alpha}(\tau) X^j_{\mathcal{J}+\alpha\mathcal{J}}(0)\rangle. \tag{14.63}$$

A self consistency equation for $G_{i\mathcal{I}\mathcal{I}+\alpha j\mathcal{J}+\beta\mathcal{J}}(i\omega_n)$ requires much smaller matrix size than a self consistency equation for $G^{mm+1n+1n}_{iIJjKL}(i\omega_n)$. However, expressing expectation values of Hubbard operators need extra care since such states as $|i,\mathcal{I}-\alpha\rangle$ appear. In this situation, we need to take care of the sign of the state $|i,\mathcal{I}-\alpha\rangle$ in

expressing in terms of a representative state. Moreover, there are Green functions in need that are not of type $G_{i\mathcal{I}\mathcal{I}+\alpha j\mathcal{J}+\beta\mathcal{J}}(i\omega_n)$. It, therefore, is safer to use the self consistency equation of general Hubbard model. In what following, we formulate a self consistency equation for $G_{i\mathcal{I}\mathcal{I}+\alpha j\mathcal{J}+\beta\mathcal{J}}(i\omega_n)$, but the expectation values of Hubbard operator are not expressed in terms of Green function for these problems.

We approximate $[X_{i\mathcal{I}\mathcal{I}+\alpha}, H_{\rm hop}]$ by a linear combination of $X_{k\mathcal{J}\mathcal{J}+\gamma}$:

$$[X_{i\mathcal{I}\mathcal{I}+\alpha}, H_{\rm hop}] = \sum_{k\mathcal{J}\gamma} Y_{i\mathcal{I}\mathcal{I}+\alpha k\mathcal{J}\mathcal{J}+\gamma} X_{k\mathcal{J}\mathcal{J}+\gamma}. \tag{14.64}$$

Using the definition of the Green functions of Hubbard operator and Fourier transform, we obtain

$$\sum_{k\mathcal{K}\gamma}[(i\omega_n - (\epsilon^i_{m+1\mathcal{I}+\alpha} - \epsilon^i_{m\mathcal{I}}))\delta_{ik}\delta_{mp}\delta_{\mathcal{I}\mathcal{J}}\delta_{\alpha\beta} - Y_{i\mathcal{I}\mathcal{I}+\alpha k\mathcal{K}\mathcal{K}+\gamma}]G_{k\mathcal{K}\mathcal{K}+\gamma j\mathcal{J}\mathcal{J}+\beta}(i\omega_n) = \langle\{X_{i\mathcal{I}\mathcal{I}+\alpha}, X_{j\mathcal{J}+\beta\mathcal{J}}\}\rangle. \tag{14.65}$$

Taking anticommutator the Eq. 14.64 with $X_{j\mathcal{J}+\beta\mathcal{J}}$, we obtain

$$\langle\{[X_{i\mathcal{I}\mathcal{I}+\alpha}, H_{\rm hop}], X_{j\mathcal{J}+\beta\mathcal{J}}\}\rangle = \sum_{k\mathcal{K}\gamma} Y_{i\mathcal{I}\mathcal{I}+\alpha k\mathcal{K}\mathcal{K}+\gamma}\langle\{X_{k\mathcal{K}\mathcal{K}+\gamma}, X_{j\mathcal{J}+\beta\mathcal{J}}\}\rangle. \tag{14.66}$$

Solving this equation gives the Y matrix.

Introducing matrix notation

$$G_{\{i\mathcal{I}\alpha\}\{j\mathcal{J}\beta\}} \equiv G_{i\mathcal{I}\mathcal{I}+\alpha j\mathcal{J}+\beta\mathcal{J}} \tag{14.67}$$

$$Y_{\{i\mathcal{I}\alpha\}\{k\mathcal{K}\gamma\}} \equiv Y_{i\mathcal{I}\mathcal{I}+\alpha k\mathcal{K}\mathcal{K}+\gamma} \tag{14.68}$$

$$\tilde{Y}_{\{i\mathcal{I}\alpha\}\{j\mathcal{J}\beta\}} \equiv \langle\{[X_{i\mathcal{I}\mathcal{I}+\alpha}, H_{\rm hop}], X_{j\mathcal{J}+\beta\mathcal{J}}\}\rangle \tag{14.69}$$

$$Z_{\{i\mathcal{I}\alpha\}\{j\mathcal{J}\beta\}} \equiv \langle\{X_{i\mathcal{I}\mathcal{I}+\alpha}, X_{j\mathcal{J}+\beta\mathcal{J}}\}\rangle \tag{14.70}$$

$$= \delta_{ij}(\delta_{\mathcal{I}\mathcal{J}}\langle X_{i\mathcal{J}+\beta\mathcal{I}+\alpha}\rangle + \delta_{\mathcal{I}+\alpha\mathcal{J}+\beta}\langle X_{j\mathcal{I}\mathcal{J}}\rangle) \tag{14.71}$$

$$\delta\epsilon_{\{i\mathcal{I}\alpha\}\{j\mathcal{J}\beta\}} \equiv (\epsilon^i_{\mathcal{I}+\alpha} - \epsilon^i_{\mathcal{I}})\delta_{ij}\delta_{\mathcal{I}\mathcal{J}}\delta_{\alpha\beta} \tag{14.72}$$

$$\mathbf{1}_{\{i\mathcal{I}\alpha\}\{j\mathcal{J}\beta\}} \equiv \delta_{ij}\delta_{\mathcal{I}\mathcal{J}}\delta_{\alpha\beta}, \tag{14.73}$$

the Eq. 14.65 can be written in matrix form as

$$[G^{-1}] = Z^{-1}[i\omega_n\mathbf{1} - \delta\epsilon - Y], \tag{14.74}$$

or

$$G = \frac{Z}{i\omega_n \mathbf{1} - \delta\epsilon - Y}, \tag{14.75}$$

where the division implies matrix inversion.

The expectation value of a 0-particle Hubbard operator can be found from a corresponding Green function at $\tau = 0$:

$$\langle X_{i\mathcal{I}\mathcal{J}} \rangle = -G_{i\mathcal{I}\mathcal{I}+\delta i J+\delta J}(\tau = 0^+), \tag{14.76}$$

where δ is a flavored not included in $|i\mathcal{I}\rangle$ state. To complete a self consistency equation for the Green functions of Hubbard operators, we need to express $\tilde{Y}$ matrix in terms of the Green functions. For site diagonal $\tilde{Y}$ matrix, this expression can be obtained without further approximation. For site off-diagonal $\tilde{Y}$ matrix, we need to take a DMFT lmit to express the $\tilde{Y}$ matrix in terms of the Green functions of Hubbard operators. In DMFT limit, the site off-diagonal $\tilde{Y}$ matrix is given by

$$\tilde{Y}_{i\mathcal{I}\mathcal{I}+\alpha j\mathcal{J}\mathcal{J}+\beta} = \sum_{\gamma\delta} (V_{ij}^{\gamma\delta} + V_{ji}^{\delta\gamma}) q_{i\mathcal{I}\mathcal{I}+\alpha\gamma} q_{j\mathcal{J}+\beta\mathcal{J}\delta}, \quad i \neq j \tag{14.77}$$

where

$$q_{i\mathcal{I}\mathcal{I}+\alpha\gamma} \equiv \langle X_{iI\mathcal{I}+\alpha-\gamma} \rangle + \langle X_{i\mathcal{I}+\gamma\mathcal{I}+\gamma} \rangle, \tag{14.78}$$

$$q_{i\mathcal{J}+\beta\mathcal{J}\gamma} \equiv \langle X_{i\mathcal{J}+\beta-\delta\mathcal{J}} \rangle + \langle X_{i\mathcal{J}+\beta\mathcal{J}+\delta} \rangle. \tag{14.79}$$

The site diagonal $\tilde{Y}$ matrix is given by

$$\begin{aligned}
\tilde{Y}_{\{i\mathcal{I}\alpha\}\{j\mathcal{J}\beta\}} &= \sum_{j\gamma\delta}\sum_{qC}\delta_{\mathcal{J}\mathcal{I}+\gamma}(V_{ij}^{\gamma\delta}+V_{ji}^{\delta\gamma})\langle X_{i\mathcal{J}+\beta\mathcal{I}+\alpha}X_{j\mathcal{C}\mathcal{C}+\delta}\rangle \\
&- \sum_{j\gamma\delta}\sum_{qC}\delta_{\mathcal{I}+\alpha\mathcal{J}+\beta+\gamma}(V_{ij}^{\gamma\delta}+V_{ji}^{\delta\gamma})\langle X_{i\mathcal{I}\mathcal{J}}X_{j\mathcal{C}\mathcal{C}+\delta}\rangle \\
&+ \sum_{j\gamma\delta}\sum_{qC}\delta_{\mathcal{I}\mathcal{J}}(V_{ij}^{\gamma\delta}+V_{ji}^{\delta\gamma})\langle X_{i\mathcal{J}+\beta\mathcal{I}+\alpha-\gamma}X_{j\mathcal{C}\mathcal{C}+\delta}\rangle \\
&- \sum_{j\gamma\delta}\sum_{qC}\delta_{\mathcal{I}+\alpha\mathcal{J}+\beta}(V_{ij}^{\gamma\delta}+V_{ji}^{\delta\gamma})\langle X_{i\mathcal{I}+\gamma\mathcal{J}}X_{j\mathcal{C}\mathcal{C}+\delta}\rangle \\
&+ \sum_{j\gamma\delta}\sum_{qC}\delta_{\mathcal{I}+\alpha+\gamma\mathcal{J}+\beta}(V_{ij}^{\gamma\delta}+V_{ji}^{\delta\gamma})\langle X_{i\mathcal{I}\mathcal{J}}X_{j\mathcal{C}+\delta\mathcal{C}}\rangle \\
&- \sum_{j\gamma\delta}\sum_{qC}\delta_{\mathcal{J}+\gamma\mathcal{I}}(V_{ij}^{\gamma\delta}+V_{ji}^{\delta\gamma})\langle X_{i\mathcal{J}+\beta\mathcal{I}+\alpha}X_{j\mathcal{C}+\delta\mathcal{C}}\rangle \\
&+ \sum_{j\gamma\delta}\sum_{qC}\delta_{\mathcal{I}+\alpha\mathcal{J}+\beta}(V_{j}^{\gamma\delta}+V_{ji}^{\delta\gamma})\langle X_{i\mathcal{I}-\gamma\mathcal{J}}X_{j\mathcal{C}+\gamma\mathcal{C}}\rangle \\
&- \sum_{j\gamma\delta}\sum_{qC}\delta_{\mathcal{I}\mathcal{J}}(V_{ij}^{\gamma\delta}+V_{ji}^{\delta\gamma})\langle X_{i\mathcal{J}+\beta\mathcal{I}+\alpha+\gamma}X_{j\mathcal{C}+\delta\mathcal{C}}\rangle. \qquad (14.80)
\end{aligned}$$

This expression for site diagonal $\tilde{Y}$ matrix holds without approximation.

Derivation Site off-diagonal $\tilde{Y}$ matrix

A straightforward calculation yields

$$\begin{aligned}
\langle\{[X_{i\mathcal{I}\mathcal{I}+\alpha},H_{\rm hop}],X_{j\mathcal{J}+\beta\mathcal{J}}\}\rangle &= \sum_{\gamma\delta}(V_{ij}^{\gamma\delta}+V_{ji}^{\delta\gamma})\langle X_{i\mathcal{I}\mathcal{I}+\alpha-\gamma}X_{j\mathcal{J}+\beta-\delta\mathcal{J}}\rangle \\
&+ \sum_{\gamma\delta}(V_{ij}^{\gamma\delta}+V_{ji}^{\delta\gamma})\langle X_{i\mathcal{I}\mathcal{I}+\alpha-\gamma}X_{j\mathcal{J}+\beta\mathcal{J}+\delta}\rangle \\
&+ \sum_{\gamma\delta}(V_{ij}^{\gamma\delta}+V_{ji}^{\delta\gamma})\langle X_{i\mathcal{I}+\gamma\mathcal{I}+\alpha}X_{j\mathcal{J}+\beta-\delta\mathcal{J}}\rangle \\
&+ \sum_{\gamma\delta}(V_{ij}^{\gamma\delta}+V_{ji}^{\delta\gamma})\langle X_{i\mathcal{I}+\gamma\mathcal{I}+\alpha}X_{j\mathcal{J}+\beta\mathcal{J}+\delta}\rangle \\
&- \sum_{\gamma\delta}(V_{ij}^{\gamma\delta}+V_{ji}^{\delta\gamma})\langle X_{i\mathcal{I}\mathcal{I}+\alpha+\gamma}X_{j\mathcal{J}+\beta+\delta\mathcal{J}}\rangle \\
&-^{l} \sum_{\gamma\delta}(V_{ij}^{\gamma\delta}+V_{ji}^{\delta\gamma})\langle X_{i\mathcal{I}\mathcal{I}+\alpha+\gamma}X_{j\mathcal{J}+\beta\mathcal{J}-\delta}\rangle \\
&-^{l} \sum_{\gamma\delta}(V_{ij}^{\gamma\delta}+V_{ji}^{\delta\gamma})\langle X_{i\mathcal{I}-\gamma\mathcal{I}+\alpha}X_{j\mathcal{J}+\beta+\delta\mathcal{J}}\rangle \\
&- \sum_{\gamma\delta}(V_{ij}^{\gamma\delta}+V_{ji}^{\delta\gamma})\langle X_{i\mathcal{I}-\gamma\mathcal{I}+\alpha}X_{j\mathcal{J}+\beta\mathcal{J}-\delta}\rangle. \qquad (14.81)
\end{aligned}$$

In DMFT limit, $\langle X_{i\mathcal{I}\mathcal{I}+\alpha} X_{j\mathcal{J}+\beta\mathcal{J}}\rangle = \langle X_{i\mathcal{I}\mathcal{I}+\alpha}\rangle\langle X_{j\mathcal{J}+\beta\mathcal{J}}\rangle$ and only the terms with 0-particle Hubbard operators survive.

$$\begin{aligned}\langle\{[X_{i\mathcal{I}\mathcal{I}+\alpha}, H_{\rm hop}], X_{j\mathcal{J}+\beta\mathcal{J}}\}\rangle &= \sum_{\gamma\delta}(V_{ij}^{\gamma\delta}+V_{ji}^{\delta\gamma})\langle X_{i\mathcal{I}\mathcal{I}+\alpha-\gamma}\rangle\langle X_{j\mathcal{J}+\beta-\delta\mathcal{J}}\rangle \\ &+ \sum_{\gamma\delta}(V_{ij}^{\gamma\delta}+V_{ji}^{\delta\gamma})\langle X_{i\mathcal{I}\mathcal{I}+\alpha-\gamma}\rangle\langle X_{j\mathcal{J}+\beta\mathcal{J}+\delta}\rangle \\ &+ \sum_{\gamma\delta}(V_{ij}^{\gamma\delta}+V_{ji}^{\delta\gamma})\langle X_{i\mathcal{I}+\gamma\mathcal{I}+\alpha}\rangle\langle X_{j\mathcal{J}+\beta-\delta\mathcal{J}}\rangle \\ &+ \sum_{\gamma\delta}(V_{ij}^{\gamma\delta}+V_{ji}^{\delta\gamma})\langle X_{i\mathcal{I}+\gamma\mathcal{I}+\alpha}\rangle\langle X_{j\mathcal{J}+\beta\mathcal{J}+\delta}\rangle \quad (14.82)\end{aligned}$$

Arranging terms in the Eq. 14.82 , we obtain

$$\tilde{Y}_{i\mathcal{I}\mathcal{I}+\alpha j\mathcal{J}\mathcal{J}+\beta} = \sum_{\gamma\delta}(V_{ij}^{\gamma\delta}+V_{ji}^{\delta\gamma}) q_{i\mathcal{I}\mathcal{I}+\alpha\gamma} q_{j\mathcal{J}+\beta\mathcal{J}\delta}, \quad i \neq j \qquad (14.83)$$

where

$$q_{i\mathcal{I}\mathcal{I}+\alpha\gamma} \equiv \langle X_{iI\mathcal{I}+\alpha-\gamma}\rangle + \langle X_{i\mathcal{I}+\gamma\mathcal{I}+\gamma}\rangle, \qquad (14.84)$$

$$q_{i\mathcal{J}+\beta\mathcal{J}\gamma} \equiv \langle X_{i\mathcal{J}+\beta-\delta\mathcal{J}}\rangle + \langle X_{i\mathcal{J}+\beta\mathcal{J}+\delta}\rangle. \qquad (14.85)$$

14.3.3 Diagonal hybridization with density-density on-site interaction

Self consistency equation

When the hybridization is diagonal and the on-site interaction is a density-density interaction, there is no flavor change. Hence, flavor off-diagonal Green functions vanish. The hopping Hamiltonian reads

$$H_{\rm hop} = \sum_{ij\alpha} V_{ij}^{\alpha\alpha}\left(f_{i\alpha}^{\dagger} f_{j\alpha} + f_{j\alpha}^{\dagger} f_{i\alpha}\right). \qquad (14.86)$$

Due to the simple on-site interaction, the eigenstates of atomic Hamiltonian can be found easily as $|i,n,\mathcal{I}\rangle = f_{i\alpha_1}^{\dagger}\cdots f_{i\alpha_n}^{\dagger}|0\rangle$. In this basis the F numbers of general Hubbard model reduced to delta functions $F_{iIJ}^{\alpha m m+1} = \delta_{\mathcal{I}-\alpha\mathcal{J}}$ and $F_{jIJ}^{\alpha m+1 m} = \delta_{\mathcal{I}+\alpha\mathcal{J}}$, where $|i,m,\mathcal{I}+\alpha\rangle = f_{i\alpha}^{\dagger}|i,m,\mathcal{I}\rangle$. This property with flavor conservation simplifies the expression of Green functions and it is better not to keep track of number of particles.

The fermion Green functions can be expressed as sums over the Green functions of Hubbard operators,

$$G^{ij}_{\alpha\alpha}(i\omega_n) = \sum_{\mathcal{I}\mathcal{J}} G_{i\mathcal{I}\mathcal{I}+\alpha j\mathcal{J}+\alpha\mathcal{J}}(i\omega_n), \tag{14.87}$$

where

$$G_{i\mathcal{I}\mathcal{I}+\alpha j\mathcal{J}+\beta\mathcal{J}}(\tau) = -\langle T_\tau X^i_{\mathcal{I}\mathcal{I}+\alpha}(\tau) X^j_{\mathcal{J}+\alpha\mathcal{J}}(0)\rangle. \tag{14.88}$$

We approximate $[X_{i\mathcal{I}\mathcal{I}+\alpha}, H_{\rm hop}]$ by a linear combination of $X_{k\mathcal{J}\mathcal{J}+\alpha}$:

$$[X_{i\mathcal{I}\mathcal{I}+\alpha}, H_{\rm hop}] = \sum_{k\mathcal{J}} Y_{i\mathcal{I}\mathcal{I}+\alpha k\mathcal{J}\mathcal{J}+\alpha} X_{k\mathcal{J}\mathcal{J}+\alpha}. \tag{14.89}$$

Using the definition of the Green functions of Hubbard operator and Fourier transform, we obtain

$$\begin{aligned}\sum_{k\mathcal{K}}[(i\omega_n - (\epsilon^i_{m+1\mathcal{I}+\alpha} - \epsilon^i_{m\mathcal{I}}))\delta_{ik}\delta_{\mathcal{I}\mathcal{K}} - Y_{i\mathcal{I}\mathcal{I}+\alpha k\mathcal{K}\mathcal{K}+\alpha}]G_{k\mathcal{K}\mathcal{K}+\alpha j\mathcal{J}\mathcal{J}+\alpha}(i\omega_n) \\ = \langle\{X_{i\mathcal{I}\mathcal{I}+\alpha}, X_{j\mathcal{J}+\alpha\mathcal{J}}\}\rangle.\end{aligned} \tag{14.90}$$

Taking anticommutator the Eq. 14.89 with $X_{j\mathcal{J}+\alpha\mathcal{J}}$, we obtain

$$Y_{i\mathcal{I}\mathcal{I}+\alpha j\mathcal{J}\mathcal{J}+\alpha} = \frac{\langle\{[X_{i\mathcal{I}\mathcal{I}+\alpha}, H_{\rm hop}], X_{j\mathcal{J}+\alpha\mathcal{J}}\}\rangle}{\langle\{X_{j\mathcal{I}\mathcal{I}+\alpha}, X_{j\mathcal{J}+\alpha\mathcal{J}}\}\rangle}. \tag{14.91}$$

Solving this equation gives the Y matrix.

Introducing matrix notation

$$G^\alpha_{\{i\mathcal{I}\}\{j\mathcal{J}\}} \equiv G_{i\mathcal{I}\mathcal{I}+\alpha j\mathcal{J}+\alpha\mathcal{J}} \tag{14.92}$$

$$Y^\alpha_{\{i\mathcal{I}\}\{k\mathcal{J}\}} \equiv Y_{i\mathcal{I}\mathcal{I}+\alpha k\mathcal{J}\mathcal{J}+\alpha} \tag{14.93}$$

$$\tilde{Y}^\alpha_{\{i\mathcal{I}\}\{j\mathcal{J}\}} \equiv \frac{\langle\{[X_{i\mathcal{I}\mathcal{I}+\alpha}, H_{\rm hop}], X_{j\mathcal{J}+\alpha\mathcal{J}}\}\rangle}{\langle\{X_{i\mathcal{I}\mathcal{I}+\alpha}, X_{i\mathcal{I}+\alpha\mathcal{I}}\}\rangle\langle\{X_{j\mathcal{J}\mathcal{J}+\alpha}, X_{j\mathcal{J}+\alpha\mathcal{J}}\}\rangle} \tag{14.94}$$

$$Z^\alpha_{\{i\mathcal{I}\}\{j\mathcal{J}\}} \equiv \langle\{X_{i\mathcal{I}\mathcal{I}+\alpha}, X_{j\mathcal{J}+\alpha\mathcal{J}}\}\rangle \tag{14.95}$$

$$= \delta_{ij}\delta_{\mathcal{I}\mathcal{J}}(\langle X_{i\mathcal{I}+\alpha\mathcal{I}+\alpha}\rangle + \langle X_{j\mathcal{I}\mathcal{I}}\rangle) \tag{14.96}$$

$$\delta\epsilon^\alpha_{\{i\mathcal{I}\}\{j\mathcal{J}\}} \equiv (\epsilon^i_{\mathcal{I}+\alpha} - \epsilon^i_{\mathcal{I}})\delta_{ij}\delta_{\mathcal{I}\mathcal{J}} \tag{14.97}$$

$$\mathbf{1}_{\{i\mathcal{I}\alpha\}\{j\mathcal{J}\beta\}} \equiv \delta_{ij}\delta_{\mathcal{I}\mathcal{J}}, \tag{14.98}$$

the Eq. 14.90 can be written in matrix form as

$$[G^{-1}_\alpha] = Z^{-1}_\alpha[i\omega_n\mathbf{1} - \delta\epsilon_\alpha] - \tilde{Y}_\alpha \tag{14.99}$$

or

$$G_\alpha = \frac{Z_\alpha}{i\omega_n \mathbf{1} - \delta\epsilon_\alpha - Y_\alpha}, \tag{14.100}$$

where the division implies matrix inversion.

The expectation value of a 0-particle Hubbard operator can be found from a corresponding Green function at $\tau = 0$:

$$\langle X_{i\mathcal{I}\mathcal{J}} \rangle = -G_{i\mathcal{I}\mathcal{I}+\delta iJ+\delta J}(\tau = 0), \tag{14.101}$$

where δ is a flavor not included in $|i\mathcal{I}\rangle$ state. To complete a self consistency equation for the Green functions of Hubbard operators, we need to express $\tilde{Y}$ matrix in terms of the Green functions. For site diagonal $\tilde{Y}$ matrix, this expression can be obtained without further approximation. For site off-diagonal $\tilde{Y}$ matrix, we need to take a DMFT lmit to express the $\tilde{Y}$ matrix in terms of the Green functions of Hubbard operators. In DMFT limit, the site off-diagonal $\tilde{Y}$ matrix is given by

$$\tilde{Y}^{\alpha}_{\{i\mathcal{I}\}\{j\mathcal{J}\}} = (V^{\alpha\alpha}_{ij} + V^{\alpha\alpha}_{ji}), \quad i \neq j. \tag{14.102}$$

The site diagonal $\tilde{Y}$ matrix is given by

$$\tilde{Y}^{\alpha}_{\{i\mathcal{I}\}\{i\mathcal{J}\}} = \frac{\langle\{[X_{i\mathcal{I}\mathcal{I}+\alpha}, H_{\rm hop}], X_{i\mathcal{J}+\alpha\mathcal{J}}\}\rangle}{\langle\{X_{i\mathcal{I}\mathcal{I}+\alpha}, X_{i\mathcal{I}+\alpha\mathcal{I}}\}\rangle\langle\{X_{i\mathcal{J}\mathcal{J}+\alpha}, X_{i\mathcal{J}+\alpha\mathcal{J}}\}\rangle}, \tag{14.103}$$

where

$$\begin{aligned}
\langle\{[X_{i\mathcal{I}\mathcal{I}+\alpha}, H_{\rm hop}], X_{i\mathcal{J}+\alpha\mathcal{J}}\}\rangle &= -\sum_{j\gamma}\sum_{qC} \delta_{\mathcal{J}\mathcal{I}+\gamma}(V^{\gamma\gamma}_{ij} + V^{\gamma\gamma}_{ji})\langle X_{i\mathcal{I}+\alpha+\gamma\mathcal{I}+\alpha} X_{j\mathcal{C}\mathcal{C}+\gamma}\rangle \\
&+ \sum_{j\gamma}\sum_{qC} \delta_{\mathcal{I}+\alpha\mathcal{J}+\alpha+\gamma}(V^{\gamma\gamma}_{ij} + V^{\gamma\gamma}_{ji})\langle X_{i\mathcal{J}+\gamma\mathcal{J}} X_{j\mathcal{C}\mathcal{C}+\gamma}\rangle \\
&+ \sum_{j\gamma}\sum_{qC} \delta_{\mathcal{I}\mathcal{J}}(V^{\gamma\gamma}_{ij} + V^{\gamma\gamma}_{ji})\langle X_{i\mathcal{I}+\alpha\mathcal{I}+\alpha-\gamma} X_{j\mathcal{C}\mathcal{C}+\gamma}\rangle \\
&- \sum_{j\gamma}\sum_{qC} \delta_{\mathcal{I}\mathcal{J}}(V^{\gamma\gamma}_{ij} + V^{\gamma\gamma}_{ji})\langle X_{i\mathcal{I}+\gamma\mathcal{I}} X_{j\mathcal{C}\mathcal{C}+\gamma}\rangle \\
&- \sum_{j\gamma}\sum_{qC} \delta_{\mathcal{I}+\alpha+\gamma\mathcal{J}+\alpha}(V^{\gamma\gamma}_{ij} + V^{\gamma\gamma}_{ji})\langle X_{i\mathcal{I}\mathcal{I}+\gamma} X_{j\mathcal{C}+\gamma\mathcal{C}}\rangle \\
&+ \sum_{j\gamma}\sum_{qC} \delta_{\mathcal{J}+\gamma\mathcal{I}}(V^{\gamma\gamma}_{ij} + V^{\gamma\gamma}_{ji})\langle X_{i\mathcal{J}+\alpha\mathcal{J}+\alpha+\gamma} X_{j\mathcal{C}+\gamma\mathcal{C}}\rangle \\
&+ \sum_{j\gamma}\sum_{qC} \delta_{\mathcal{I}\mathcal{J}}(V^{\gamma\gamma}_{j} + V^{\gamma\gamma}_{ji})\langle X_{i\mathcal{I}-\gamma\mathcal{J}} X_{j\mathcal{C}+\gamma\mathcal{C}}\rangle \\
&- \sum_{j\gamma}\sum_{qC} \delta_{\mathcal{I}\mathcal{J}}(V^{\gamma\gamma}_{ij} + V^{\gamma\gamma}_{ji})\langle X_{i\mathcal{J}+\alpha\mathcal{I}+\alpha+\gamma} X_{j\mathcal{C}+\gamma\mathcal{C}}\rangle
\end{aligned} \tag{14.104}$$

This expression for site diagonal $\tilde{Y}$ matrix holds without approximation.

Derivation Site off-diagonal $\tilde{Y}$ matrix

A straightforward calculation yields

$$\begin{aligned}
\langle\{[X_{i\mathcal{I}\mathcal{I}+\alpha}, H_{\rm hop}], X_{j\mathcal{J}+\alpha\mathcal{J}}\}\rangle = &\sum_{\gamma}(V_{ij}^{\gamma\gamma}+V_{ji}^{\gamma\gamma})\langle X_{i\mathcal{I}\mathcal{I}+\alpha-\gamma}X_{j\mathcal{J}+\alpha-\gamma\mathcal{J}}\rangle \\
&+\sum_{\gamma}(V_{ij}^{\gamma\gamma}+V_{ji}^{\gamma\gamma})\langle X_{i\mathcal{I}\mathcal{I}+\alpha-\gamma}X_{j\mathcal{J}+\alpha\mathcal{J}+\gamma}\rangle \\
&+\sum_{\gamma}(V_{ij}^{\gamma\gamma}+V_{ji}^{\gamma\gamma})\langle X_{i\mathcal{I}+\gamma\mathcal{I}+\alpha}X_{j\mathcal{J}+\alpha-\gamma\mathcal{J}}\rangle \\
&+\sum_{\gamma}(V_{ij}^{\gamma\gamma}+V_{ji}^{\gamma\gamma})\langle X_{i\mathcal{I}+\gamma\mathcal{I}+\alpha}X_{j\mathcal{J}+\alpha\mathcal{J}+\gamma}\rangle \\
&-\sum_{\gamma}(V_{ij}^{\gamma\gamma}+V_{ji}^{\gamma\gamma})\langle X_{i\mathcal{I}\mathcal{I}+\alpha+\gamma}X_{j\mathcal{J}+\alpha+\gamma\mathcal{J}}\rangle \\
&-\sum_{\gamma}(V_{ij}^{\gamma\gamma}+V_{ji}^{\gamma\gamma})\langle X_{i\mathcal{I}\mathcal{I}+\alpha+\gamma}X_{j\mathcal{J}+\alpha\mathcal{J}-\gamma}\rangle \\
&-^{l}\sum_{\gamma}(V_{ij}^{\gamma\gamma}+V_{ji}^{\gamma\gamma})\langle X_{i\mathcal{I}-\gamma\mathcal{I}+\alpha}X_{j\mathcal{J}+\alpha+\gamma\mathcal{J}}\rangle \\
&-\sum_{\gamma}(V_{ij}^{\gamma\gamma}+V_{ji}^{\gamma\gamma})\langle X_{i\mathcal{I}-\gamma\mathcal{I}+\alpha}X_{j\mathcal{J}+\alpha\mathcal{J}-\gamma}\rangle.
\end{aligned} \tag{14.105}$$

In DMFT limit $\langle X_{i\mathcal{I}\mathcal{I}+\alpha}X_{j\mathcal{J}+\beta\mathcal{J}}\rangle = \langle X_{i\mathcal{I}\mathcal{I}+\alpha}\rangle\langle X_{j\mathcal{J}+\beta\mathcal{J}}\rangle$ and only the terms with 0-particle Hubbard operators survive.

$$\begin{aligned}
\langle\{[X_{i\mathcal{I}\mathcal{I}+\alpha}, H_{\rm hop}], X_{j\mathcal{J}+\alpha\mathcal{J}}\}\rangle &= (V_{ij}^{\alpha\alpha}+V_{ji}^{\alpha\alpha})\langle X_{i\mathcal{I}\mathcal{I}}\rangle\langle X_{j\mathcal{J}\mathcal{J}}\rangle \\
&+ (V_{ij}^{\alpha\alpha}+V_{ji}^{\alpha\alpha})\langle X_{i\mathcal{I}\mathcal{I}}\rangle\langle X_{j\mathcal{J}+\alpha\mathcal{J}+\alpha}\rangle \\
&+ (V_{ij}^{\alpha\alpha}+V_{ji}^{\alpha\alpha})\langle X_{i\mathcal{I}+\alpha\mathcal{I}+\alpha}\rangle\langle X_{j\mathcal{J}\mathcal{J}}\rangle \\
&+ (V_{ij}^{\alpha\alpha}+V_{ji}^{\alpha\alpha})\langle X_{i\mathcal{I}+\alpha\mathcal{I}+\alpha}\rangle\langle X_{j\mathcal{J}+\alpha\mathcal{J}+\alpha}\rangle.
\end{aligned} \tag{14.106}$$

Arranging terms in the Eq. 14.106 , we obtain

$$\langle\{[X_{i\mathcal{I}\mathcal{I}+\alpha}, H_{\rm hop}], X_{j\mathcal{J}+\alpha\mathcal{J}}\}\rangle = (V_{ij}^{\alpha\alpha}+V_{ji}^{\alpha\alpha})q_{i\mathcal{I}\alpha}q_{j\mathcal{J}\alpha}, \quad i\neq j, \tag{14.107}$$

where

$$q_{i\mathcal{I}\alpha} \equiv \langle X_{i\mathcal{I}\mathcal{I}}\rangle + \langle X_{i\mathcal{I}+\alpha\mathcal{I}+\alpha}\rangle. \tag{14.108}$$

Therefore

$$\tilde{Y}^{\alpha}_{\{i\mathcal{I}\}\{j\mathcal{J}\}} = V^{\alpha\alpha}_{ij} + V^{\alpha\alpha}_{ji}. \tag{14.109}$$

14.3.4 $SU(N)$

Self consistency equation

For $SU(N)$, the fermion Green functions are flavor diagonal and independent of flavors. Therefore we only need to find $G_{\{i\alpha\}\{j\alpha\}}$ with a fixed α. Throught this section, α means a pre-fixed favor. Using Hubbard operator the Green function can be found by

$$G_{\{i\alpha\}\{j\alpha\}} = \sum_{mn}\sum_{\mathcal{I}\mathcal{J}} -\langle T_\tau X^{mm+1}_{i\mathcal{I}\mathcal{I}+\alpha}(\tau) X^{n+1n}_{j\mathcal{J}+\alpha\mathcal{J}}(0)\rangle, \tag{14.110}$$

where $\mathcal{I}$ and $\mathcal{J}$ scan C^{N-1}_m m-particle state without particle α and C^{N-1}_n n-particle state without particle α, respectively.

We need to see the Hubbard operator Green function as a matrix. The appropriate index consists of site i and number of particles n. The Hubbard operators under consideration are of type $X^{mm+1}_{\mathcal{I}\mathcal{I}+\alpha}$ and $X^{m+1m}_{\mathcal{I}+\alpha\mathcal{I}}$. The matrices under consideration are

$$G_{\{im\}\{jn\}}(\tau) \equiv \sum_{\mathcal{I}\mathcal{J}} -\langle T_\tau X^{mm+1}_{i\mathcal{I}\mathcal{I}+\alpha}(\tau) X^{n+1n}_{j\mathcal{J}+\alpha\mathcal{J}}(0)\rangle, \tag{14.111}$$

$$Z_{\{im\}\{jn\}} \equiv \delta_{ij}\delta_{mn}\sum_{\mathcal{I}}\langle\{X^{mm+1}_{i\mathcal{I}\mathcal{I}+\alpha}, X^{m+1m}_{i\mathcal{I}+\alpha\mathcal{I}}\}\rangle \tag{14.112}$$

$$\delta\epsilon_{\{im\}\{jn\}} \equiv \delta_{ij}\delta_{mn}(\epsilon^i_{m+1} - \epsilon^i_m) \tag{14.113}$$

$$Y_{\{im\}\{jn\}} \equiv \frac{\sum_{\mathcal{I}\mathcal{J}}\langle\{[X^{mm+1}_{i\mathcal{I}\mathcal{I}+\alpha}, H_{\rm hop}], X^{n+1n}_{j\mathcal{J}+\alpha\mathcal{J}}\}\rangle}{\sum_{\mathcal{I}}\langle\{X^{nn+1}_{j\mathcal{I}\mathcal{I}+\alpha}, X^{n+1n}_{j\mathcal{I}+\alpha\mathcal{I}}\}\rangle}. \tag{14.114}$$

It is convenient to introduce new notations X^{mm+1}_i and X^{m+1m}_i, where

$$X^{mm+1}_i = \sum_{\mathcal{I}} X^{mm+1}_{i\mathcal{I}\mathcal{I}+\alpha}, \quad X^{m+1m}_i = \sum_{\mathcal{I}} X^{m+1m}_{i\mathcal{I}+\alpha\mathcal{I}}. \tag{14.115}$$

The Green function reads

$$[G^{-1}]_{\{im\}\{jn\}}(i\omega_n) = \frac{i\omega_n\mathbf{1} - \delta\epsilon^i}{\langle\{X^{mm+1}_i, X^{m+1m}_i\}\rangle}\delta_{ij}\delta_{mn} - \tilde{Y}_{\{im\}\{jn\}}, \tag{14.116}$$

where

$$\tilde{Y}_{\{im\}\{jn\}} = \frac{\langle\{[X^{mm+1}_i, H_{\rm hop}], X^{n+1n}_j\}\rangle}{\langle\{X^{mm+1}_i, X^{m+1m}_i\}\rangle\langle\{X^{nn+1}_j, X^{n+1n}_j\}\rangle}. \tag{14.117}$$

The renormailzation constant $\langle\{X_i^{mm+1}, X_i^{m+1m}\}\rangle$ can be found from site-diagonal Habbard operator Green function by

$$\langle\{X_i^{mm+1}, X_i^{m+1m}\}\rangle = -C_m^{N-1}(\langle X_{i\mathcal{K}\mathcal{K}}^{mm}\rangle + \langle X_{i\mathcal{K}+\alpha\mathcal{K}+\alpha}^{m+1m+1}\rangle), \tag{14.118}$$

where $\mathcal{K}$ is a m-particle state without the particle α. For a state $\mathcal{K}$, The expectation values $\langle X_{i\mathcal{K}\mathcal{K}}^{mm}\rangle$ and $\langle X_{i\mathcal{K}+\alpha\mathcal{K}+\alpha}^{m+1m+1}\rangle$ are

$$\langle X_{i\mathcal{K}\mathcal{K}}^{mm}\rangle = -\frac{1}{C_m^{N-1}} G_{\{im\}\{im\}}(\tau = 0^+) \tag{14.119}$$

$$\langle X_{i\mathcal{K}+\alpha\mathcal{K}+\alpha}^{m+1m+1}\rangle = -\frac{1}{C_{m+1}^{N-1}} G_{\{im+1\}\{im+1\}}(\tau = 0^+). \tag{14.120}$$

For site off-diagonal $\tilde{Y}$, it can be shown that

$$\tilde{Y}_{\{im\}\{jn\}} = V_{ij} + V_{ji}, \quad i \neq j. \tag{14.121}$$

For site diagonal $\tilde{Y}$, we need to evaluate $\langle\{[X_i^{mm+1}, H_{\rm hop}], X_i^{n+1n}\}\rangle$ using

$$\begin{aligned}
\langle\{[X_i^{mm+1}, H_{\rm hop}], X_i^{n+1n}\}\rangle &= -\sum_{jq} \delta_{m+1n}(V_{ij} + V_{ji}) n G_{\{jq\}\{in\}}(\tau = 0^+) \\
&+ \sum_{jq} \delta_{mn+1}(V_{ij} + V_{ji})(N - n - 1) G_{\{jq\}\{in\}}(\tau = 0^+) \\
&+ \sum_{jq} \delta_{mn}(V_{ij} + V_{ji})(n) G_{\{jq\}\{in\}}(\tau = 0^+) \\
&- \sum_{jq} \delta_{mn}(V_{ij} + V_{ji})(N - n - 1) G_{\{jq\}\{in\}}(\tau = 0^+) \\
&+ \sum_{jq} \delta_{m+1n}(V_{ij} + V_{ji})(N - m - 1) G_{\{im\}\{jq\}}(\tau = 0^+) \\
&- \sum_{jq} \delta_{mn+1}(V_{ij} + V_{ji}) m G_{\{im\}\{jq\}}(\tau = 0^+) \\
&- \sum_{jq} \delta_{mn}(V_j + V_{ji})(N - m) G_{\{im-1\}\{jq\}}(\tau = 0^+) \\
&+ \sum_{jq} \delta_{mn}(V_{ij} + V_{ji})(m + 1) G_{\{im+1\}\{jq\}}(\tau = 0^+).
\end{aligned} \tag{14.122}$$

The fermion Green function $G_{\{i\alpha\}\{j\alpha\}}(i\omega_n)$ can be found by summing all the Hubbard operator Green function:

$$G_{\{i\alpha\}\{j\alpha\}}(i\omega_n) = \sum_{mn} G_{\{im\}\{jn\}}(i\omega_n) \tag{14.123}$$

As an example, we consider $N = 2$ and $U = \infty$ case. Then the fermion Green function $G_{\{i\sigma\}\{j\sigma\}}(\tau)$, where $\sigma = \pm 1$ is the flavor index, is

$$G_{\{i\sigma\}\{j\sigma\}} = -\langle T_\tau X^{01}_{i0\sigma}(\tau) X^{10}_{j\sigma 0}(0)\rangle = G_{\{i0\}\{j0\}}(\tau). \tag{14.124}$$

The Hubbard operator Green function can be found by Fourier transform of $G_{\{i0\}\{j0\}}(i\omega_n)$ that can be found by inverting $[G^{-1}]_{\{i0\}\{j0\}}(i\omega_n)$ given by

$$[G^{-1}]_{\{i0\}\{j0\}}(i\omega_n) = \frac{i\omega_n - {\epsilon_\sigma}^i}{\langle X^{00}_i + X^{\sigma\sigma}_i\rangle}\delta_{ij} - \tilde{Y}_{\{i0\}\{j0\}}. \tag{14.125}$$

The components of $\tilde{Y}_{\{i0\}\{j0\}}$ matrix are

$$\begin{aligned}
\tilde{Y}_{\{in\}\{jm\}} &= (V_{ij} + V_{ji}), \quad i \neq j, \\
\tilde{Y}_{\{i0\}\{i0\}} &= -\sum_j \frac{(V_{ij} + V_{ji})\langle X^{\sigma 0}_i X^{0\sigma}_j\rangle}{\langle X^{00}_i + X^{\sigma\sigma}_i\rangle\langle X^{00}_i + X^{\sigma\sigma}_i\rangle}.
\end{aligned}$$

Derivation of Y matrix

The Y matrix for $SU(N)$ case can be calculated from the Y matrix for diagonal hybridization with density-density on-site interaction case taking flavor independent hopping amplitudes.

In DMFT limit, summing $\langle\{[X^{mm+1}_{i\mathcal{I}\mathcal{I}+\alpha}, H_{\rm hop}], X^{n+1n}_{j\mathcal{J}+\alpha\mathcal{J}}\}\rangle$ over C^{N-1}_m m-particle states $\mathcal{I}$ and C^{N-1}_n n-particle states $\mathcal{J}$ we obtain

$$\begin{aligned}
\sum_{\mathcal{I}\mathcal{J}}\langle\{[X^{mm+1}_{i\mathcal{I}\mathcal{I}+\alpha}, H_{\rm hop}], X^{n+1n}_{j\mathcal{J}+\alpha\mathcal{J}}\}\rangle &= \sum_{\mathcal{I}\mathcal{J}}\sum_\beta (V_{ij}+V_{ji})\langle X^{mm}_{i\mathcal{I}\mathcal{I}+\alpha-\beta}\rangle\langle X^{nn}_{j\mathcal{J}+\alpha-\beta\mathcal{J}}\rangle \\
&+ \sum_{\mathcal{I}\mathcal{J}}\sum_\beta (V_{ij}+V_{ji})\langle X^{mm}_{i\mathcal{I}\mathcal{I}+\alpha-\beta}\rangle\langle X^{n+1n+1}_{j\mathcal{J}+\alpha\mathcal{J}+\beta}\rangle \\
&+ \sum_{\mathcal{I}\mathcal{J}}\sum_\beta (V_{ij}+V_{ji})\langle X^{m+1m+1}_{i\mathcal{I}+\beta\mathcal{I}+\alpha}\rangle\langle X^{nn}_{j\mathcal{J}+\alpha-\beta\mathcal{J}}\rangle \\
&+ \sum_{\mathcal{I}\mathcal{J}}\sum_\beta (V_{ij}+V_{ji})\langle X^{m+1m+1}_{i\mathcal{I}+\beta\mathcal{I}+\alpha}\rangle\langle X^{n+1n+1}_{j\mathcal{J}+\alpha\mathcal{J}+\beta}\rangle, \quad i \neq j.
\end{aligned} \tag{14.126}$$

Since $\langle X_{\mathcal{K}\mathcal{L}}\rangle = \delta_{\mathcal{K}\mathcal{L}}\langle X_{\mathcal{K}\mathcal{L}}\rangle$, we see that the summation over β in the Eq. 14.126 is

restricted to $\beta = \alpha$. The Eq. 14.126 now reads

$$\begin{aligned}\sum_{\mathcal{I}\mathcal{J}}\langle\{[X^{mm+1}_{i\mathcal{I}\mathcal{I}+\alpha}, H_{\rm hop}], X^{n+1n}_{j\mathcal{J}+\alpha\mathcal{J}}\}\rangle &= \sum_{\mathcal{I}\mathcal{J}}(V_{ij}+V_{ji})\langle X^{mm}_{i\mathcal{I}\mathcal{I}}\rangle\langle X^{nn}_{j\mathcal{J}\mathcal{J}}\rangle \\ &+ \sum_{\mathcal{I}\mathcal{J}}(V_{ij}+V_{ji})\langle X^{mm}_{i\mathcal{I}\mathcal{I}}\rangle\langle X^{n+1n+1}_{j\mathcal{J}+\alpha\mathcal{J}+\alpha}\rangle \\ &+ \sum_{\mathcal{I}\mathcal{J}}(V_{ij}+V_{ji})\langle X^{m+1m+1}_{i\mathcal{I}+\alpha\mathcal{I}+\alpha}\rangle\langle X^{nn}_{j\mathcal{J}\mathcal{J}}\rangle \qquad (14.127) \\ &+ \sum_{\mathcal{I}\mathcal{J}}(V_{ij}+V_{ji})\langle X^{m+1m+1}_{i\mathcal{I}+\alpha\mathcal{I}+\alpha}\rangle\langle X^{n+1n+1}_{j\mathcal{J}+\alpha\mathcal{J}+\alpha}\rangle, \quad i\neq j.\end{aligned}$$

Summing over $\mathcal{I}$ and $\mathcal{J}$ yields

$$\langle\{[X^{mm+1}_{i}, H_{\rm hop}], X^{n+1n}_{j}\}\rangle = (V_{ij}+V_{ji})\langle\{X^{mm+1}_{i}, X^{m+1m}_{i}\}\rangle\langle\{X^{nn+1}_{j}, X^{n+1n}_{j}\}\rangle, \quad i\neq j. \qquad (14.128)$$

Dividing the Eq. 14.128 by $\langle\{X^{mm+1}_{i}, X^{m+1m}_{i}\}\rangle\langle\{X^{nn+1}_{j}, X^{n+1n}_{j}\}\rangle$, we obtain

$$\begin{aligned}\tilde{Y}_{\{im\}\{jn\}} &= \frac{\langle\{[X^{mm+1}_{i}, H_{\rm hop}], X^{n+1n}_{j\mathcal{J}}\}\rangle}{\langle\{X^{mm+1}_{i}, X^{m+1m}_{i}\}\rangle\langle\{X^{nn+1}_{j}, X^{n+1n}_{j}\}\rangle} \qquad (14.129) \\ &= V_{ij}+V_{ji}, \quad i\neq j. \qquad (14.130)\end{aligned}$$

Summing $\langle\{[X^{mm+1}_{i\mathcal{I}\mathcal{I}+\alpha}, H_{\rm hop}], X^{n+1n}_{i\mathcal{J}+\alpha\mathcal{J}}\}\rangle$ of diagonal hybridization with density-density on-site interaction case over C^{N-1}_{m} m-particle states $\mathcal{I}$ and C^{N-1}_{n} n-particle states $\mathcal{J}$ with favor independent hopping amplitudes, we obtain

$$\begin{aligned}\langle\{[X^{mm+1}_{i}, H_{\rm hop}], X^{n+1n}_{i}\}\rangle &= -\sum_{\mathcal{I}}\sum_{j\beta}\sum_{qC}\delta_{m+1n}(V_{ij}+V_{ji})\langle X^{n+1n}_{i\mathcal{I}+\alpha+\beta\mathcal{I}+\alpha}X^{qq+1}_{j\mathcal{C}\mathcal{C}+\beta}\rangle \\ &+ \sum_{\mathcal{J}}\sum_{j\beta\neq\alpha}\sum_{qC}\delta_{mn+1}(V_{ij}+V_{ji})\langle X^{n+1n}_{i\mathcal{J}+\beta\mathcal{J}}X^{qq+1}_{j\mathcal{C}\mathcal{C}+\beta}\rangle \\ &+ \sum_{\mathcal{I}}\sum_{j\beta}\sum_{qC}\delta_{mn}(V_{ij}+V_{ji})\langle X^{n+1n}_{i\mathcal{I}+\alpha\mathcal{I}+\alpha-\beta}X^{qq+1}_{j\mathcal{C}\mathcal{C}+\beta}\rangle \\ &- \sum_{\mathcal{I}}\sum_{j\beta}\sum_{qC}\delta_{mn}(V_{ij}+V_{ji})\langle X^{n+1n}_{i\mathcal{I}+\beta\mathcal{I}}X^{qq+1}_{j\mathcal{C}\mathcal{C}+\beta}\rangle \\ &- \sum_{\mathcal{I}}\sum_{j\beta\neq\alpha}\sum_{qC}\delta_{m+1n}(V_{ij}+V_{ji})\langle X^{mm+1}_{i\mathcal{I}\mathcal{I}+\beta}X^{q+1q}_{j\mathcal{C}+\beta\mathcal{C}}\rangle \\ &+ \sum_{\mathcal{J}}\sum_{j\alpha}\sum_{qC}\delta_{mn+1}(V_{ij}+V_{ji})\langle X^{mm+1}_{i\mathcal{J}+\alpha\mathcal{J}+\alpha+\beta}X^{q+1q}_{j\mathcal{C}+\beta\mathcal{C}}\rangle \\ &+ \sum_{\mathcal{I}}\sum_{i\beta}\sum_{qC}\delta_{mn}(V_{j}+V_{ji})\langle X^{m-1m}_{i\mathcal{I}-\beta\mathcal{I}}X^{q+1q}_{j\mathcal{C}+\beta\mathcal{C}}\rangle \qquad (14.131) \\ &- \sum_{\mathcal{I}}\sum_{j\beta}\sum_{qC}\delta_{mn}(V_{ij}+V_{ji})\langle X^{m+1m+2}_{i\mathcal{I}+\alpha\mathcal{J}+\alpha+\beta}X^{q+1q}_{j\mathcal{C}+\beta\mathcal{C}}\rangle.\end{aligned}$$

Using a $SU(N)$ property that $\langle X^{n+1n}_{i\mathcal{I}+\beta\mathcal{I}} X^{qq+1}_{j\mathcal{C}\mathcal{C}+\beta}\rangle$ is independent of $\mathcal{I}$ and $\mathcal{C}$, the summation in the Eq. 14.131 over $\mathcal{I}$, $\mathcal{J}$ and β can be carried on to yield

$$\begin{aligned}
\langle\{[X_i^{mm+1}, H_{\rm hop}], X_i^{n+1n}\}\rangle &= -\sum_{\mathcal{K}}\sum_{j}\sum_{qC}\delta_{m+1n}(V_{ij}+V_{ji})n\langle X^{n+1n}_{i\mathcal{K}+\alpha\mathcal{K}} X^{qq+1}_{j\mathcal{C}\mathcal{C}+\alpha}\rangle \\
&+ \sum_{\mathcal{K}}\sum_{j}\sum_{qC}\delta_{mn+1}(V_{ij}+V_{ji})(N-n-1)\langle X^{n+1n}_{i\mathcal{K}+\alpha\mathcal{K}} X^{qq+1}_{j\mathcal{C}\mathcal{C}+\alpha}\rangle \\
&+ \sum_{\mathcal{K}}\sum_{j}\sum_{qC}\delta_{mn}(V_{ij}+V_{ji})n\langle X^{n+1n}_{i\mathcal{K}+\alpha\mathcal{K}} X^{qq+1}_{j\mathcal{C}\mathcal{C}+\alpha}\rangle \\
&- \sum_{\mathcal{K}}\sum_{j}\sum_{qC}\delta_{mn}(V_{ij}+V_{ji})(N-n-1)\langle X^{n+1n}_{i\mathcal{K}+\alpha\mathcal{K}} X^{qq+1}_{j\mathcal{C}\mathcal{C}+\alpha}\rangle \\
&- \sum_{\mathcal{K}}\sum_{j}\sum_{qC}\delta_{m+1n}(V_{ij}+V_{ji})(N-m-1)\langle X^{mm+1}_{i\mathcal{K}\mathcal{K}+\alpha} X^{q+1q}_{j\mathcal{C}+\alpha\mathcal{C}}\rangle \\
&+ \sum_{\mathcal{K}}\sum_{j}\sum_{qC}\delta_{mn+1}(V_{ij}+V_{ji})m\langle X^{mm+1}_{i\mathcal{K}\mathcal{K}+\alpha} X^{q+1q}_{j\mathcal{C}+\alpha\mathcal{C}}\rangle \quad (14.132) \\
&+ \sum_{\mathcal{K}}\sum_{i}\sum_{qC}\delta_{mn}(V_{j}+V_{ji})(N-m)\langle X^{m-1m}_{i\mathcal{K}\mathcal{K}+\alpha} X^{q+1q}_{j\mathcal{C}+\alpha\mathcal{C}}\rangle \\
&- \sum_{\mathcal{K}}\sum_{j}\sum_{qC}\delta_{mn}(V_{ij}+V_{ji})(m+1)\langle X^{m+1m+2}_{i\mathcal{K}\mathcal{K}+\alpha} X^{q+1q}_{j\mathcal{C}+\alpha\mathcal{C}}\rangle,
\end{aligned}$$

where $\mathcal{K}$ restricted to states with corresponding number of particles without particle α.

Rewriting the Eq. 14.132, we obtain

$$\begin{aligned}
\langle\{[X_i^{mm+1}, H_{\rm hop}], X_i^{n+1n}\}\rangle &= -\sum_{jq}\delta_{m+1n}(V_{ij}+V_{ji})n\langle X_i^{n+1n} X_j^{qq+1}\rangle \\
&+ \sum_{jq}\delta_{mn+1}(V_{ij}+V_{ji})(N-n-1)\langle X_i^{n+1n} X_j^{qq+1}\rangle \\
&+ \sum_{jq}\delta_{mn}(V_{ij}+V_{ji})n\langle X_i^{n+1n} X_j^{qq+1}\rangle \\
&- \sum_{jq}\delta_{mn}(V_{ij}+V_{ji})(N-n-1)\langle X_i^{n+1n} X_j^{qq+1}\rangle \\
&- \sum_{jq}\delta_{m+1n}(V_{ij}+V_{ji})(N-m-1)\langle X_i^{mm+1} X_j^{q+1q}\rangle \\
&+ \sum_{jq}\delta_{mn+1}(V_{ij}+V_{ji})m\langle X_i^{mm+1} X_j^{q+1q}\rangle \\
&+ \sum_{jq}\delta_{mn}(V_{j}+V_{ji})(N-m)\langle X_i^{m-1m} X_j^{q+1q}\rangle \quad (14.133) \\
&- \sum_{jq}\delta_{mn}(V_{ij}+V_{ji})(m+1)\langle X_i^{m+1m+2} X_j^{q+1q}\rangle.
\end{aligned}$$

Dividing the Eq. 14.133 by $\langle\{X_i^{mm+1}, X_i^{m+1m}\}\rangle\langle\{X_i^{nn+1}, X_i^{n+1n}\}\rangle$, we obtain site

diagonal Y matrix:

$$\tilde{Y}_{\{im\}\{jn\}} = \frac{\langle\{[X_i^{mm+1}, H_{\rm hop}], X_j^{n+1n}\}\rangle}{\langle\{X_i^{mm+1}, X_i^{m+1m}\}\rangle\langle\{X_i^{nn+1}, X_i^{n+1n}\}\rangle}, \tag{14.134}$$

An explicit expression of $\langle\{[X_i^{mm+1}, H_{\rm hop}], X_i^{n+1n}\}\rangle$ in terms of site off-diagonal Green function is

$$\begin{aligned}
\langle\{[X_i^{mm+1}, H_{\rm hop}], X_i^{n+1n}\}\rangle &= -\sum_{jq}\delta_{m+1n}(V_{ij}+V_{ji})nG_{\{jq\}\{in\}}(\tau=0^+) \\
&+ \sum_{jq}\delta_{mn+1}(V_{ij}+V_{ji})(N-n-1)G_{\{jq\}\{in\}}(\tau=0^+) \\
&+ \sum_{jq}\delta_{mn}(V_{ij}+V_{ji})nG_{\{jq\}\{in\}}(\tau=0^+) \\
&- \sum_{jq}\delta_{mn}(V_{ij}+V_{ji})(N-n-1)G_{\{jq\}\{in\}}(\tau=0^+) \\
&+ \sum_{jq}\delta_{m+1n}(V_{ij}+V_{ji})(N-m-1)G_{\{im\}\{jq\}}(\tau=0^+) \\
&- \sum_{jq}\delta_{mn+1}(V_{ij}+V_{ji})mG_{\{im\}\{jq\}}(\tau=0^+) \\
&- \sum_{jq}\delta_{mn}(V_{j}+V_{ji})(N-m)G_{\{im-1\}\{jq\}}(\tau=0^+) \\
&+ \sum_{jq}\delta_{mn}(V_{ij}+V_{ji})(m+1)G_{\{im+1\}\{jq\}}(\tau=0^+).
\end{aligned} \tag{14.135}$$

14.4 Impurity Model

14.4.1 General On-site Interaction

The Hamiltonian of the model reads

$$H = H_{\rm atom} + \sum_{k\alpha}\epsilon_{k\alpha}c_{k\alpha}^\dagger c_{k\alpha} + \sum_{k\alpha\beta}V_k^{\alpha\beta}\left(f_\alpha^\dagger c_{k\beta} + c_{k\alpha}^\dagger f_\beta\right). \tag{14.136}$$

The Hubbard operators are defined similarly to that of atomic case except that the operators act as the identity operator on the band states. The Green functions of fermion operators can be expressed as sums over the Green functions of Hubbard operators,

$$G_{\alpha\beta}(i\omega_n) = \sum_{mIJ}\sum_{nJK}F_{IJ}^{\alpha mm+1}F_{KL}^{\beta n+1n}G_{IJKL}^{mm+1n+1n}(i\omega_n), \tag{14.137}$$

where

$$G^{mm+1n+1n}_{IJKL}(\tau) = -\langle T_\tau X^{mm+1}_{IJ}(\tau) X^{n+1n}_{KL}(0)\rangle \tag{14.138}$$

The Greend functions of Hubbard operators in Eq. 14.137 can be obtained by taking Fourier transform from the following equation,

$$\begin{aligned}
\frac{\partial}{\partial\tau} G^{mm+1n+1n}_{IJKL}(\tau) &= -\delta(\tau)\langle T_\tau X^{mm+1}_{IJ}(0) X^{n+1n}_{KL}(0)\rangle - \langle T_\tau \frac{\partial}{\partial\tau} X^{mm+1}_{IJ}(\tau) X^{n+1n}_{KL}(0)\rangle \\
&= -\delta(\tau)\langle\{X^{mm+1}_{IJ}, X^{n+1n}_{KL}\}\rangle - \langle T_\tau [X^{mm+1}_{IJ}(\tau), H_{\rm atom}(\tau)] X^{n+1n}_{KL}(0)\rangle \\
&= -\delta(\tau)\langle\{X^{mm+1}_{IJ}, X^{n+1n}_{KL}\}\rangle - (\epsilon_{m+1J} - \epsilon_{mI})\langle T_\tau X^{mm+1}_{IJ}(\tau) X^{n+1n}_{KL}(0)\rangle \\
&\quad -\langle T_\tau [X^{mm+1}_{IJ}(\tau), H_{\rm hyb}(\tau)] X^{n+1n}_{KL}(0)\rangle.
\end{aligned} \tag{14.139}$$

In static limit, we approximate $[X^{mm+1}_{IJ}, H_{\rm hyb}]$ by linear combination of X^{nn+1}_{KL} and $c_{k\alpha}$:

$$[X^{mm+1}_{IJ}, H_{\rm hyb}] = \sum_{nKL} Y^{mm+1nn+1}_{IJKL} X^{nn+1}_{KL} + \sum_{k\alpha} A^{mm+1}_{IJk\alpha} c_{k\alpha}. \tag{14.140}$$

Then the Eq. 14.139 reads

$$\begin{aligned}
\frac{\partial}{\partial\tau} G^{mm+1n+1n}_{IJKL}(\tau) &= -\delta(\tau)\langle\{X^{mm+1}_{IJ}, X^{n+1n}_{KL}\}\rangle - (\epsilon_{m+1J} - \epsilon_{mI}) G^{mm+1n+1n}_{IJKL}(\tau) \\
&\quad - \sum_{pMN} Y^{mm+1pp+1}_{IJMN} G^{pp+1n+1n}_{MNKL}(\tau) \\
&\quad - \sum_{k\alpha} A^{mm+1}_{IJk\alpha} \langle T_\tau c_{k\alpha}(\tau) X^{n+1n}_{KL}(0)\rangle.
\end{aligned} \tag{14.141}$$

The coefficient matrices $Y^{mm+1nn+1}_{IJKL}$ and $A^{mm+1}_{IJk\alpha}$ can be obtained by taking commutator of the Eq. 14.140 with X^{n+1n}_{KL} and $c^\dagger_{k\alpha}$, respectively,

$$\langle\{[X^{mm+1}_{IJ}, H_{\rm hyb}], X^{n+1n}_{KL}\}\rangle = \sum_{pMN} Y^{mm+1pp+1}_{IJMN} \langle\{X^{pp+1}_{MN}, X^{n+1n}_{KL}\}\rangle, \tag{14.142}$$

$$\langle\{[X^{mm+1}_{IJ}, H_{\rm hyb}], c^\dagger_{k\alpha}\}\rangle = A^{mm+1}_{IJk\alpha}. \tag{14.143}$$

To find a self-consistency equation for the Green function of Hubbard operator, we need to know the Green function of a Hubbard operator and a band fermion (mixed Green function). This Green function can be expressed in terms of the Green functions of Hubbard operators. Taking time derivative of mixed Green function

$$G^{n+1n}_{k\beta KL} \equiv -\langle T_\tau c_{k\beta}(\tau) X^{n+1n}_{KL}(0)\rangle \text{ , we have}$$

$$\begin{aligned}
\frac{\partial}{\partial\tau} G^{n+1n}_{k\beta KL} &= -\delta(\tau)\langle\{c_{k\beta}, X^{n+1n}_{KL}\}\rangle - \langle T_\tau \frac{\partial}{\partial\tau} c_{k\beta}(\tau) X^{n+1n}_{KL}(0)\rangle \\
&= -\langle T_\tau \frac{\partial}{\partial\tau} c_{k\beta}(\tau) X^{n+1n}_{KL}(0)\rangle \\
&= -\epsilon_{k\beta}\langle T_\tau c_{k\beta}(\tau) X^{n+1n}_{KL}(0)\rangle - V^{\beta\gamma}_k \langle T_\tau f_\gamma(\tau) X^{n+1n}_{KL}(0)\rangle \\
&= -\epsilon_{k\alpha} G^{n+1n}_{k\beta KL} - \sum_{\beta mIJ} V^{\beta\gamma}_k F^{\gamma mm+1}_{IJ} \langle T_\tau X^{mm+1}_{IJ}(\tau) X^{n+1n}_{KL}(0)\rangle
\end{aligned} \tag{14.144}$$

Taking Fourier transform of Eq. 14.144, multiplying hybridization amplitude $V^{\alpha\beta}_k$, and summing over all the intermediate band states k and β yields

$$G^{n+1n}_{\alpha KL}(i\omega_n) = \sum_{\gamma mIJ} \tilde{\Delta}_{\alpha\gamma}(i\omega_n) F^{\gamma mm+1}_{IJ} G^{mm+1n+1n}_{IJKL}(i\omega_n), \tag{14.145}$$

where $G^{mm+1}_{\alpha KL}(\tau) \equiv -\langle T_\tau \tilde{C}_\alpha(\tau) X^{n+1n}_{KL}\rangle$ and $\Delta_{\alpha\gamma}(i\omega_n) = \sum_{k\beta} V^{\alpha\beta} V^{\beta\gamma}/(i\omega_n - \epsilon_{k\beta})$.

Using these equations, Eq. 14.141 reads after Fourier transform

$$\begin{aligned}
&(i\omega_n - (\epsilon_{n+1J} - \epsilon_{nI})) G^{mm+1n+1n}_{IJKL} \\
&\qquad = \langle\{X^{mm+1}_{IJ}, X^{n+1n}_{KL}\}\rangle + \sum_{pMN} Y^{mm+1pp+1}_{IJMN} G^{pp+1n+1n}_{MNKL}(i\omega_n) \\
&\qquad + \sum_{k\alpha} \sum_{\gamma pMN} A^{mm+1}_{IJk\alpha} \tilde{\Delta}_{\alpha\gamma}(i\omega_n) F^{\gamma pp+1}_{MN} G^{pp+1n+1n}_{MNKL}(i\omega_n).
\end{aligned} \tag{14.146}$$

The equation 14.143 can be solved easily to $A^{mm+1}_{IJk\alpha} = \sum_{pMN} F^{\alpha p+1p}_{MN} \langle\{X^{mm+1}_{IJ}, X^{p+1p}_{MN}\}\rangle$. Then the equation 14.146 reads

$$\begin{aligned}
&(i\omega_n - (\epsilon_{n+1J} - \epsilon_{nI})) G^{mm+1n+1n}_{IJKL} \\
&\qquad = \langle\{X^{mm+1}_{IJ}, X^{n+1n}_{KL}\}\rangle + \sum_{pMN} Y^{mm+1pp+1}_{IJMN} G^{pp+1n+1n}_{MNKL} \\
&\qquad + \sum_{\alpha\beta} \sum_{qOP} \sum_{pMN} \tilde{\Delta}_{\alpha\beta} F^{\alpha p+1p}_{MN} F^{\beta qq+1}_{OP} \langle\{X^{mm+1}_{IJ}, X^{p+1p}_{MN}\}\rangle G^{qq+1n+1n}_{OPKL}.
\end{aligned} \tag{14.147}$$

Introducing matrix notation

$$G_{\{mIJ\}\{nLK\}} \equiv G^{mm+1n+1n}_{IJKL} \tag{14.148}$$

$$Y_{\{mIJ\}\{nLK\}} \equiv Y^{mm+1nn+1}_{IJLK} \tag{14.149}$$

$$\tilde{Y}_{\{mIJ\}\{nLK\}} \equiv \langle\{[X^{mm+1}_{IJ}, H_{\rm hyb}], X^{n+1n}_{KL}\}\rangle \tag{14.150}$$

$$\tilde{\Delta}_{\{mIJ\}\{nLK\}} = \sum_{\alpha\beta}\sum_{pMN} \tilde{\Delta}_{\alpha\beta} F^{\alpha p+1p}_{MN} F^{\beta nn+1}_{LK} \langle\{X^{mm+1}_{IJ}, X^{p+1p}_{MN}\}\rangle \tag{14.151}$$

$$Z_{\{mIJ\}\{nLK\}} \equiv \langle\{X^{mm+1}_{IJ}, X^{n+1n}_{KL}\}\rangle \tag{14.152}$$

$$= \delta_{nm}(\delta_{JK}\langle X^{mm}_{IL}\rangle + \delta_{IL}\langle X^{m+1m+1}_{KJ}\rangle) \tag{14.153}$$

$$\delta\epsilon_{\{mIJ\}\{nLK\}} \equiv (\epsilon_{m+1J} - \epsilon_{mI})\delta_{mn}\delta_{IL}\delta_{JK} \tag{14.154}$$

$$\mathbf{1}_{\{mIJ\}\{nLK\}} \equiv \delta_{mn}\delta_{IL}\delta_{JK}, \tag{14.155}$$

the Eq. 14.147 can be written in matrix form as

$$[G^{-1}] = Z^{-1}[i\omega_n \mathbf{1} - \delta\epsilon - \tilde{\Delta} - Y] \tag{14.156}$$

or

$$G = \frac{Z}{i\omega_n \mathbf{1} - \delta\epsilon - \tilde{\Delta} - Y}, \tag{14.157}$$

where the division implies matrix inversion.

The expectation value of $\langle X^{mm}_{IJ}\rangle$ can be found from a corresponding Green function at $\tau = 0$:

$$\langle X^{mn}_{IJ}\rangle = -\sum_{\omega_n} G^{mm+1m+1m}_{IKKJ}(i\omega_n) e^{-i\omega_n 0^+}. \tag{14.158}$$

To complete a self consistency equation for the Green functions of Hubbard operators, we need to express Y matrix in terms of the Green functions. The Y matrix is given

by $Y = \tilde{Y}Z^{-1}$, where $\tilde{Y}$ is given by

$$\begin{aligned}\tilde{Y}_{\{mIJ\}\{nLK\}} &= \delta_{mn+1}\sum_{\gamma}\left(F^{\gamma m+1m}_{JK}\langle\tilde{C}_{\gamma}X^{n+1n}_{IL}\rangle - \delta_{m+1n}F^{\gamma m+1m}_{LI}\langle\tilde{C}_{\gamma}X^{n+1n}_{KJ}\rangle\right)\\ &+ \delta_{nm}\sum_{\gamma}\sum_{M}\left(\delta_{JK}F^{\gamma m+1m}_{MI}\langle\tilde{C}_{\gamma}X^{m+1m}_{ML}\rangle - \delta_{IL}F^{\gamma m+1m}_{JM}\langle\tilde{C}_{\gamma}X^{m+1m}_{KM}\rangle\right)\\ &+ \delta_{mn+1}\sum_{\gamma}\left(F^{\gamma nn+1}_{LI}\langle\tilde{C}^{\dagger}_{\gamma}X^{mm+1}_{KJ}\rangle - \delta_{m+1n}F^{\gamma mm+1}_{JK}\langle\tilde{C}^{\dagger}_{\gamma}X^{mm+1}_{IL}\right)\rangle\\ &+ \delta_{nm}\sum_{\gamma}\sum_{M}\left(\delta_{IL}F^{\gamma m+1m+2}_{JM}\langle\tilde{C}^{\dagger}_{\gamma}X^{m+1m+2}_{KM}\rangle - \delta_{JK}F^{\gamma m-1m}_{MI}\langle\tilde{C}^{\dagger}_{\gamma}X^{m-1m}_{ML}\rangle\right),\end{aligned} \tag{14.159}$$

where

$$\langle\tilde{C}_{\alpha}X^{n+1n}_{IL}\rangle = -\sum_{i\omega_n}\sum_{\gamma mMN}\tilde{\Delta}_{\alpha\gamma}(i\omega_n)F^{\gamma mm+1}_{MN}G^{mm+1n+1n}_{MNIL}(i\omega_n), \tag{14.160}$$

$$\langle\tilde{C}^{\dagger}_{\alpha}X^{nn+1}_{LI}\rangle = \sum_{i\omega_n}\sum_{\gamma mMN}\tilde{\Delta}_{\gamma\alpha}(i\omega_n)F^{\gamma m+1m}_{MN}G^{m+1mnn+1}_{MNLI}(i\omega_n). \tag{14.161}$$

14.4.2 Density-Density On-site Interaction

As seen from the atomic case, the eigenstates for density-density on-site interaction case are $|\mathcal{I}\rangle = \prod_{k=1}^{n} f^{\dagger}_{\alpha_k}|0\rangle, \quad n = 0, 1, 2, \cdots, N$. Introducing new notation $|\mathcal{I}+\alpha\rangle = f^{\dagger}_{\alpha}|\mathcal{I}\rangle$, fermion Green function can be written as

$$G_{\alpha\beta}(i\omega_n) = \sum_{\mathcal{I}\mathcal{J}} G^{\alpha\beta}_{\mathcal{I}\mathcal{J}}(i\omega_n), \tag{14.162}$$

where

$$G^{\alpha\beta}_{\mathcal{I}\mathcal{J}}(\tau) = -\langle T_{\tau}X_{\mathcal{I}\mathcal{I}+\alpha}(\tau), X_{\mathcal{J}+\beta\mathcal{J}}(0)\rangle. \tag{14.163}$$

We approximate $[X_{\mathcal{I}\mathcal{I}+\alpha}, H_{\rm hyb}]$,

$$[X_{\mathcal{I}\mathcal{I}+\alpha}, H_{\rm hyb}] = \sum_{\mathcal{J}\beta} Y^{\mathcal{J}\mathcal{J}+\beta}_{\mathcal{I}\mathcal{I}+\alpha}X_{\mathcal{J}\mathcal{J}+\beta} + \sum_{k\beta} A^{\mathcal{I}\alpha}_{k\beta}c_{k\beta}, \tag{14.164}$$

where

$$A^{\mathcal{I}\alpha}_{k\beta} = \langle\{[X_{\mathcal{I}\mathcal{I}+\alpha}, H_{\rm hyb}], c^{\dagger}_{k\beta}\}\rangle, \tag{14.165}$$

$$\langle\{[X_{\mathcal{I}\mathcal{I}+\alpha}, H_{\rm hyb}], X_{\mathcal{J}+\beta\mathcal{J}}\}\rangle = \sum_{\mathcal{K}\gamma} Y^{\mathcal{K}\mathcal{K}+\gamma}_{\mathcal{I}\mathcal{I}+\alpha}\langle\{X_{\mathcal{K}\mathcal{K}+\gamma}, X_{\mathcal{J}+\beta\mathcal{J}}\}\rangle. \tag{14.166}$$

Using

$$G_{\alpha\mathcal{J}\beta}(i\omega_n) = \sum_{\mathcal{K}\gamma} \tilde{\Delta}_{\alpha\gamma} G^{\gamma\beta}_{\mathcal{K}\mathcal{J}}(i\omega_n), \tag{14.167}$$

where $G_{\alpha\mathcal{J}\beta}(\tau) = -\langle T_\tau \tilde{C}_\alpha(\tau) X_{\mathcal{J}+\beta\mathcal{J}}(0)\rangle$, a self-consistency equation for the Green functions can be written down as

$$\begin{aligned}(i\omega_n - (\epsilon_{\mathcal{I}+\alpha} - \epsilon_{\mathcal{I}}))\, G_{\mathcal{I}\mathcal{I}+\alpha\mathcal{J}+\beta\mathcal{J}} = \langle\{X_{\mathcal{I}\mathcal{I}+\alpha}, X_{\mathcal{J}+\beta\mathcal{J}}\}\rangle + \sum_{\mathcal{K}\gamma} Y^{\mathcal{K}\mathcal{K}+\gamma}_{\mathcal{I}\mathcal{I}+\alpha} G_{\mathcal{K}\mathcal{K}+\gamma\mathcal{J}+\beta\mathcal{J}} \\ + \sum_{\gamma\delta}\sum_{\mathcal{K}\mathcal{L}} \tilde{\Delta}_{\gamma\delta}\langle[X_{\mathcal{I}\mathcal{I}+\alpha}, X_{\mathcal{K}+\gamma\mathcal{K}}]\rangle G_{\mathcal{L}\mathcal{L}+\delta\mathcal{J}+\beta\mathcal{J}},\end{aligned} \tag{14.168}$$

where $Y^{\mathcal{K}\mathcal{K}+\gamma}_{\mathcal{I}\mathcal{I}+\alpha}$ can be obtained by solving Eq. 14.166, which involves evaluating $\langle\{[X_{\mathcal{I}\mathcal{I}+\alpha}, H_{\rm hyb}], X_{\mathcal{J}+\beta\mathcal{J}}\}\rangle$ in terms of the Green functions.

Introducing matrix notation

$$G_{\{\mathcal{I}\alpha\}\{\mathcal{J}\beta\}} \equiv G_{\mathcal{I}\mathcal{I}+\alpha\mathcal{J}+\beta\mathcal{J}} \tag{14.169}$$

$$Y_{\{\mathcal{I}\alpha\}\{\mathcal{K}\gamma\}} \equiv Y^{\mathcal{K}\mathcal{K}+\gamma}_{\mathcal{I}\mathcal{I}+\alpha} \tag{14.170}$$

$$\tilde{Y}_{\{\mathcal{I}\alpha\}\{\mathcal{J}\beta\}} \equiv \langle\{[X_{i\mathcal{I}\mathcal{I}+\alpha}, H_{\rm hyb}], X_{j\mathcal{J}+\beta\mathcal{J}}\}\rangle \tag{14.171}$$

$$\tilde{\Delta}_{\{\mathcal{I}\alpha\}\{\mathcal{J}\beta\}} \equiv \sum_{\mathcal{K}\gamma} \tilde{\Delta}_{\gamma\beta}\langle\{X_{\mathcal{I}\mathcal{I}+\alpha}, X_{\mathcal{K}+\beta\mathcal{K}}\}\rangle \tag{14.172}$$

$$Z_{\{\mathcal{I}\alpha\}\{\mathcal{J}\beta\}} \equiv \langle\{X_{\mathcal{I}\mathcal{I}+\alpha}, X_{\mathcal{J}+\beta\mathcal{J}}\}\rangle \tag{14.173}$$

$$= (\delta_{\mathcal{I}\mathcal{J}}\langle X_{i\mathcal{J}+\beta\mathcal{I}+\alpha}\rangle + \delta_{\mathcal{I}+\alpha\mathcal{J}+\beta}\langle X_{j\mathcal{I}\mathcal{J}}\rangle) \tag{14.174}$$

$$\delta\epsilon_{\{\mathcal{I}\alpha\}\{\mathcal{J}\beta\}} \equiv (\epsilon_{\mathcal{I}+\alpha} - \epsilon_{\mathcal{I}})\delta_{\mathcal{I}\mathcal{J}}\delta_{\alpha\beta} \tag{14.175}$$

$$\mathbf{1}_{\{\mathcal{I}\alpha\}\{\mathcal{J}\beta\}} \equiv \delta_{\mathcal{I}\mathcal{J}}\delta_{\alpha\beta}, \tag{14.176}$$

the Eq. 14.168 can be written in matrix form as

$$[G^{-1}] = Z^{-1}[i\omega_n \mathbf{1} - \tilde{\Delta} - \delta\epsilon - Y] \tag{14.177}$$

or

$$G = \frac{Z}{i\omega_n \mathbf{1} - \tilde{\Delta} - \delta\epsilon - Y}, \tag{14.178}$$

where the division implies matrix inversion.

The Y matrix is given by $Y = \tilde{Y} Z^{-1}$, where $\tilde{Y}$ is given by

$$\begin{aligned}\tilde{Y}_{\{\mathcal{I}\alpha\}\{\mathcal{J}\beta\}} = &\sum_{\gamma} \left(\delta_{\mathcal{I}+\alpha\mathcal{J}+\beta+\gamma} \langle \tilde{C}_\gamma X_{\mathcal{I}\mathcal{J}} \rangle - \delta_{\mathcal{I}+\gamma\mathcal{J}} \langle \tilde{C}_\gamma X_{\mathcal{J}+\beta\mathcal{I}+\alpha} \rangle \right) \\ &+ \sum_{\gamma} \left(\delta_{\mathcal{I}+\alpha\mathcal{J}+\beta} \langle \tilde{C}_\gamma X_{\mathcal{I}+\gamma\mathcal{J}} \rangle - \sum_{\mathcal{M}} \delta_{\mathcal{I}\mathcal{J}} \delta_{\mathcal{I}+\alpha\mathcal{M}+\gamma} \langle \tilde{C}_\gamma X_{\mathcal{J}+\beta\mathcal{M}} \rangle \right) \\ &+ \sum_{\gamma} \left(\delta_{\mathcal{I}\mathcal{J}} \langle \tilde{C}^\dagger_\gamma X_{\mathcal{J}+\beta\mathcal{I}+\alpha+\gamma} \rangle - \delta_{\mathcal{I}+\alpha+\gamma\mathcal{J}+\beta} \langle \tilde{C}^\dagger_\gamma X_{\mathcal{I}\mathcal{J}} \rangle \right) \\ &+ \sum_{\gamma} \left(\delta_{\mathcal{J}+\gamma\mathcal{I}} \langle \tilde{C}^\dagger_\gamma X_{\mathcal{J}+\beta\mathcal{I}+\alpha} \rangle - \sum_{\mathcal{M}} \delta_{\mathcal{M}+\gamma\mathcal{I}} \delta_{\mathcal{I}+\alpha\mathcal{J}+\beta} \langle \tilde{C}^\dagger_\gamma X_{\mathcal{M}\mathcal{J}} \rangle \right),\end{aligned} \tag{14.179}$$

where

$$\langle \tilde{C}_\alpha X_{\mathcal{I}+\beta\mathcal{I}} \rangle = - \sum_{i\omega_n} \sum_{\gamma\mathcal{J}} \tilde{\Delta}_{\alpha\gamma}(i\omega_n) G_{\mathcal{J}\mathcal{J}+\gamma\mathcal{I}+\beta\mathcal{I}}(i\omega_n), \tag{14.180}$$

$$\langle \tilde{C}^\dagger_\alpha X_{\mathcal{I}\mathcal{I}+\beta} \rangle = \sum_{i\omega_n} \sum_{\gamma\mathcal{J}} \tilde{\Delta}_{\gamma\alpha}(i\omega_n) G_{\mathcal{J}\mathcal{J}+\gamma\mathcal{I}+\beta\mathcal{I}}(i\omega_n). \tag{14.181}$$

We extended the meaning of delta function to

$$\delta_{\mathcal{I}+\alpha\mathcal{J}} \equiv \langle \mathcal{I} + \alpha | \mathcal{J} \rangle = \pm 1, 0. \tag{14.182}$$

For example $\delta_{\mathcal{I}+\alpha+\beta\mathcal{I}+\beta+\alpha} = -1$.

14.4.3 Diagonal Hybridization With Density-Density On-site Interaction

When the hybridization is diagonal, there is no flavor change. The off-diagonal Green functions vanish. We concentrate only on diagonal Green functions.

$$G_{\alpha\alpha}(i\omega_n) = \sum_{\mathcal{I}\mathcal{J}} G_{\mathcal{I}\mathcal{I}+\alpha\mathcal{J}+\alpha\mathcal{J}}(i\omega_n), \tag{14.183}$$

where

$$G_{\mathcal{I}\mathcal{I}+\alpha\mathcal{J}+\beta\mathcal{J}}(\tau) = -\langle T_\tau X_{\mathcal{I}\mathcal{I}+\alpha}(\tau), X_{\mathcal{J}+\alpha\mathcal{J}}(0) \rangle. \tag{14.184}$$

We approximate $[X_{\mathcal{I}\mathcal{I}+\alpha}, H_{\rm hyb}]$,

$$[X_{\mathcal{I}\mathcal{I}+\alpha}, H_{\rm hyb}] = \sum_{\mathcal{J}} Y^{\mathcal{J}\mathcal{J}+\alpha}_{\mathcal{I}\mathcal{I}+\alpha} X_{\mathcal{J}\mathcal{J}+\alpha} + \sum_{k\beta} A^{\mathcal{I}}_k c_{k\alpha}, \tag{14.185}$$

where

$$A_k^{\mathcal{I}} = \langle\{[X_{\mathcal{I}\mathcal{I}+\alpha}, H_{\rm hyb}], c_{k\alpha}^\dagger\}\rangle, \tag{14.186}$$

$$Y_{\mathcal{I}\mathcal{I}+\alpha}^{\mathcal{J}\mathcal{J}+\alpha} = \frac{\langle\{[X_{\mathcal{I}\mathcal{I}+\alpha}, H_{\rm hyb}], X_{\mathcal{J}+\alpha\mathcal{J}}\}\rangle}{\langle\{X_{\mathcal{I}\mathcal{I}+\alpha}, X_{\mathcal{J}+\alpha\mathcal{J}}\}\rangle}. \tag{14.187}$$

Using

$$G_{\alpha\mathcal{I}\alpha}(i\omega_n) = \tilde{\Delta}_{\alpha\alpha}\sum_{\mathcal{K}} G^{\alpha\alpha}_{\mathcal{K}\mathcal{K}+\alpha\mathcal{J}+\alpha\mathcal{J}}(i\omega_n), \tag{14.188}$$

where $G_{\alpha\mathcal{I}\alpha}(\tau) = -\langle T_\tau \tilde{C}_\alpha(\tau) X_{\mathcal{J}+\alpha\mathcal{J}}(0)\rangle(i\omega_n)$, a self-consistency equation for the Green functions can be written down as

$$\begin{aligned}(i\omega_n - (\epsilon_{\mathcal{I}+\alpha} - \epsilon_{\mathcal{I}}))\, G_{\mathcal{I}\mathcal{I}+\alpha\mathcal{J}+\alpha\mathcal{J}} = \langle\{X_{\mathcal{I}\mathcal{I}+\alpha}, X_{\mathcal{J}+\alpha\mathcal{J}}\}\rangle + \sum_{\mathcal{K}} Y_{\mathcal{I}\mathcal{I}+\alpha}^{\mathcal{K}\mathcal{K}+\alpha} G_{\mathcal{K}\mathcal{K}+\alpha\mathcal{J}+\alpha\mathcal{J}} \\ + \sum_{\mathcal{K}} \tilde{\Delta}^{\alpha\alpha}\langle[X_{\mathcal{I}\mathcal{I}+\alpha}, X_{\mathcal{I}+\alpha\mathcal{I}}]\rangle G_{\mathcal{K}\mathcal{K}+\alpha\mathcal{J}+\alpha\mathcal{J}}.\end{aligned} \tag{14.189}$$

Introducing matrix notation

$$G^\alpha_{\{\mathcal{I}\}\{\mathcal{J}\}} \equiv G_{\mathcal{I}\mathcal{I}+\alpha\mathcal{J}+\alpha\mathcal{J}} \tag{14.190}$$

$$Y^\alpha_{\{\mathcal{I}\}\{\mathcal{K}\}} \equiv Y_{\mathcal{I}\mathcal{I}+\alpha}^{\mathcal{K}\mathcal{K}+\alpha} \tag{14.191}$$

$$\tilde{Y}^\alpha_{\{\mathcal{I}\alpha\}\{\mathcal{J}\alpha\}} \equiv \langle\{[X_{\mathcal{I}\mathcal{I}+\alpha}, H_{\rm hop}], X_{\mathcal{J}+\alpha\mathcal{J}}\}\rangle \tag{14.192}$$

$$\tilde{\Delta}^\alpha_{\{\mathcal{I}\}\{\mathcal{J}\}} \equiv \tilde{\Delta}^{\alpha\alpha}\langle\{X_{\mathcal{I}\mathcal{I}+\alpha}, X_{\mathcal{I}+\alpha\mathcal{I}}\}\rangle \tag{14.193}$$

$$Z^\alpha_{\{\mathcal{I}\}\{\mathcal{J}\}} \equiv \langle\{X_{\mathcal{I}\mathcal{I}+\alpha}, X_{\mathcal{J}+\alpha\mathcal{J}}\}\rangle \tag{14.194}$$

$$= \delta_{\mathcal{I}\mathcal{J}}(\langle X_{i\mathcal{I}+\alpha\mathcal{I}+\alpha}\rangle + \langle X_{j\mathcal{I}\mathcal{I}}\rangle) \tag{14.195}$$

$$\delta\epsilon^\alpha_{\{\mathcal{I}\}\{\mathcal{J}\}} \equiv (\epsilon_{\mathcal{I}+\alpha} - \epsilon_{\mathcal{I}})\delta_{\mathcal{I}\mathcal{J}} \tag{14.196}$$

$$\mathbf{1}_{\{\mathcal{I}\}\{\mathcal{J}\}} \equiv \delta_{\mathcal{I}\mathcal{J}}, \tag{14.197}$$

the Eq. 14.168 can be written in matrix form as

$$[G_\alpha^{-1}] = Z_\alpha^{-1}[i\omega_n \mathbf{1} - -\delta\epsilon_\alpha \tilde{\Delta}_\alpha] - \tilde{Y}_\alpha \tag{14.198}$$

or

$$G_\alpha = \frac{Z_\alpha}{i\omega_n \mathbf{1} - \delta\epsilon_\alpha - \tilde{\Delta}_\alpha - Y_\alpha}, \tag{14.199}$$

where the division implies matrix inversion.

The Y_α matrix is given by $Y_\alpha = \tilde{Y}_\alpha Z_\alpha^{-1}$, where $\tilde{Y}_\alpha$ is given by

$$\begin{aligned}\tilde{Y}^{\alpha}_{\{\mathcal{I}\}\{\mathcal{J}\}} = &-\sum_\gamma \Big(\delta_{\mathcal{I}\mathcal{J}+\gamma}\langle \tilde{C}_\gamma X_{\mathcal{J}+\gamma\mathcal{J}}\rangle - \delta_{\mathcal{I}+\gamma\mathcal{J}}\langle \tilde{C}_\gamma X_{\mathcal{I}+\alpha+\gamma\mathcal{I}+\alpha}\rangle\Big)\\ &+\sum_\gamma \Big(\delta_{\mathcal{I}\mathcal{J}}\langle \tilde{C}_\gamma X_{\mathcal{I}+\gamma\mathcal{J}}\rangle - \delta_{\mathcal{I}\mathcal{J}}\langle \tilde{C}_\gamma X_{\mathcal{I}+\alpha\mathcal{I}+\alpha-\gamma}\rangle\Big)\\ &+\sum_\gamma \Big(\delta_{\mathcal{I}\mathcal{J}}\langle \tilde{C}^\dagger_\gamma X_{\mathcal{I}+\alpha\mathcal{I}+\alpha+\gamma}\rangle + \delta_{\mathcal{I}+\alpha+\gamma\mathcal{J}+\alpha}\langle \tilde{C}^\dagger_\gamma X_{\mathcal{I}\mathcal{I}+\gamma}\rangle\Big)\\ &-\sum_\gamma \Big(\delta_{\mathcal{J}+\gamma\mathcal{I}}\langle \tilde{C}^\dagger_\gamma X_{\mathcal{J}+\alpha\mathcal{J}+\alpha+\gamma}\rangle + \delta_{\mathcal{I}\mathcal{J}}\langle \tilde{C}^\dagger_\gamma X_{\mathcal{I}-\gamma\mathcal{J}}\rangle\Big),\end{aligned} \tag{14.200}$$

where

$$\langle \tilde{C}_\alpha X_{\mathcal{I}+\alpha\mathcal{I}}\rangle = -\sum_{i\omega_n}\sum_{\mathcal{J}} \tilde{\Delta}_{\alpha\alpha}(i\omega_n) G_{\mathcal{J}\mathcal{J}+\alpha\mathcal{I}+\alpha\mathcal{I}}(i\omega_n), \tag{14.201}$$

$$\langle \tilde{C}^\dagger_\alpha X_{\mathcal{I}\mathcal{I}+\alpha}\rangle = \sum_{i\omega_n}\sum_{\mathcal{J}} \tilde{\Delta}_{\alpha\alpha}(i\omega_n) G_{\mathcal{J}\mathcal{J}+\alpha\mathcal{I}+\alpha\mathcal{I}}(i\omega_n). \tag{14.202}$$

14.4.4 SU(N)

For $SU(N)$, the fermion Green function is flavor diagonal and independent of flavor.

We concentrate only a diagonal Green functions with representative flavor α.

$$G_{\alpha\alpha}(i\omega_n) = \sum_{mn} G_{mn}(i\omega_n), \tag{14.203}$$

where

$$G_{mn}(\tau) = -\sum_{\mathcal{I}\mathcal{J}} \langle T_\tau X^{mm+1}_{\mathcal{I}\mathcal{I}+\alpha}(\tau), X^{n+1n}_{\mathcal{J}+\beta\mathcal{J}}(0)\rangle. \tag{14.204}$$

$\mathcal{I}$ and $\mathcal{J}$ scan C_m^{N-1} m-particle state without particle α and C_n^{N-1} n-particle state without particle α, respectively.

It is convenient to introduce new notations X_i^{mm+1} and X_i^{m+1m}, where

$$X_i^{mm+1} = \sum_{\mathcal{I}} X^{mm+1}_{i\mathcal{I}\mathcal{I}+\alpha}, \quad X_i^{m+1m} = \sum_{\mathcal{I}} X^{m+1m}_{i\mathcal{I}+\alpha\mathcal{I}}. \tag{14.205}$$

We approximate $[X^{mm+1}, H_{\rm hyb}]$,

$$[X^{mm+1}, H_{\rm hyb}] = Y_{mn} X^{n+1n} + \sum_k A_{nk} c_{k\alpha}, \tag{14.206}$$

where

$$A_{nk} = \langle\{[X^{nn+1}, H_{\rm hyb}], c^\dagger_{k\alpha}\}\rangle, \tag{14.207}$$

$$Y_{mn} = \frac{\langle\{[X^{mm+1}, H_{\rm hyb}], X^{n+1n}\}\rangle}{\langle\{X^{nn+1}, X^{n+1n}\}\rangle} \tag{14.208}$$

Using

$$G_{\alpha\mathcal{I}}(i\omega_n) = \tilde{\Delta}_{\alpha\alpha}\sum_{\mathcal{K}} G^{\alpha\alpha}_{\mathcal{K}\mathcal{I}}(i\omega_n), \tag{14.209}$$

where $G_{\alpha\mathcal{I}}(\tau) = -\langle T_\tau \tilde{C}_\alpha(\tau) X_{\mathcal{I}+\alpha\mathcal{I}}(0)\rangle(i\omega_n)$. A self-consistency equation for the Green functions can be written down as

$$\left(i\omega_n - (\epsilon^{m+1} - \epsilon^m)\right) G_{mn} = \langle\{X^{mm+1}, X^{n+1n}\}\rangle + \sum_l Y_{ml} G_{ln} \tag{14.210}$$

$$+ \sum_l \tilde{\Delta}^{\alpha\alpha}\langle\{X^{mm+1}, X^{m+1m}\}\rangle G_{ln}. \tag{14.211}$$

Introducing new notation $\tilde{\Delta}_{mn} = \tilde{\Delta}^{\alpha\alpha}\langle\{X^{mm+1}, X^{m+1m}\}$ and $\tilde{Y}_{mn} = Y_{mn}/\langle\{X^{mm+1}, X^{m+1m}\}\rangle$ the eq. 14.211 can be written in matrix form as

$$[G^{-1}] = Z^{-1}[i\omega_n \mathbf{1} - \delta\epsilon - \tilde{\Delta}] - \tilde{Y} \tag{14.212}$$

or

$$G = \frac{Z}{i\omega_n \mathbf{1} - \delta\epsilon - \tilde{\Delta} - Y}, \tag{14.213}$$

where the division implies matrix inversion.

The $\tilde{Y}$ matrix is given by

$$\tilde{Y}_{nm} = \frac{(\delta_{n+1m} - \delta_{nm})\tilde{Y}^{(1)}_n + (\delta_{n-1m} - \delta_{nm})\tilde{Y}^{(2)}_n)}{\langle\{X^{mm+1}, X^{m+1m}\}\rangle\langle\{X^{nn+1}, X^{n+1n}\}\rangle} \tag{14.214}$$

$$\tilde{Y}^{(1)}_n = (n+1)Y_{n+1} - (N-n-1)Y_n \tag{14.215}$$

$$\tilde{Y}^{(2)}_n = nY_n - (N-n)Y_{n-1} \tag{14.216}$$

$$Y_n = -T\sum_{i\omega}\tilde{\Delta}(i\omega)\sum_m G_{nm}(i\omega)e^{-i\omega 0^+}. \tag{14.217}$$

Appendix A

Pictures of Band Structures

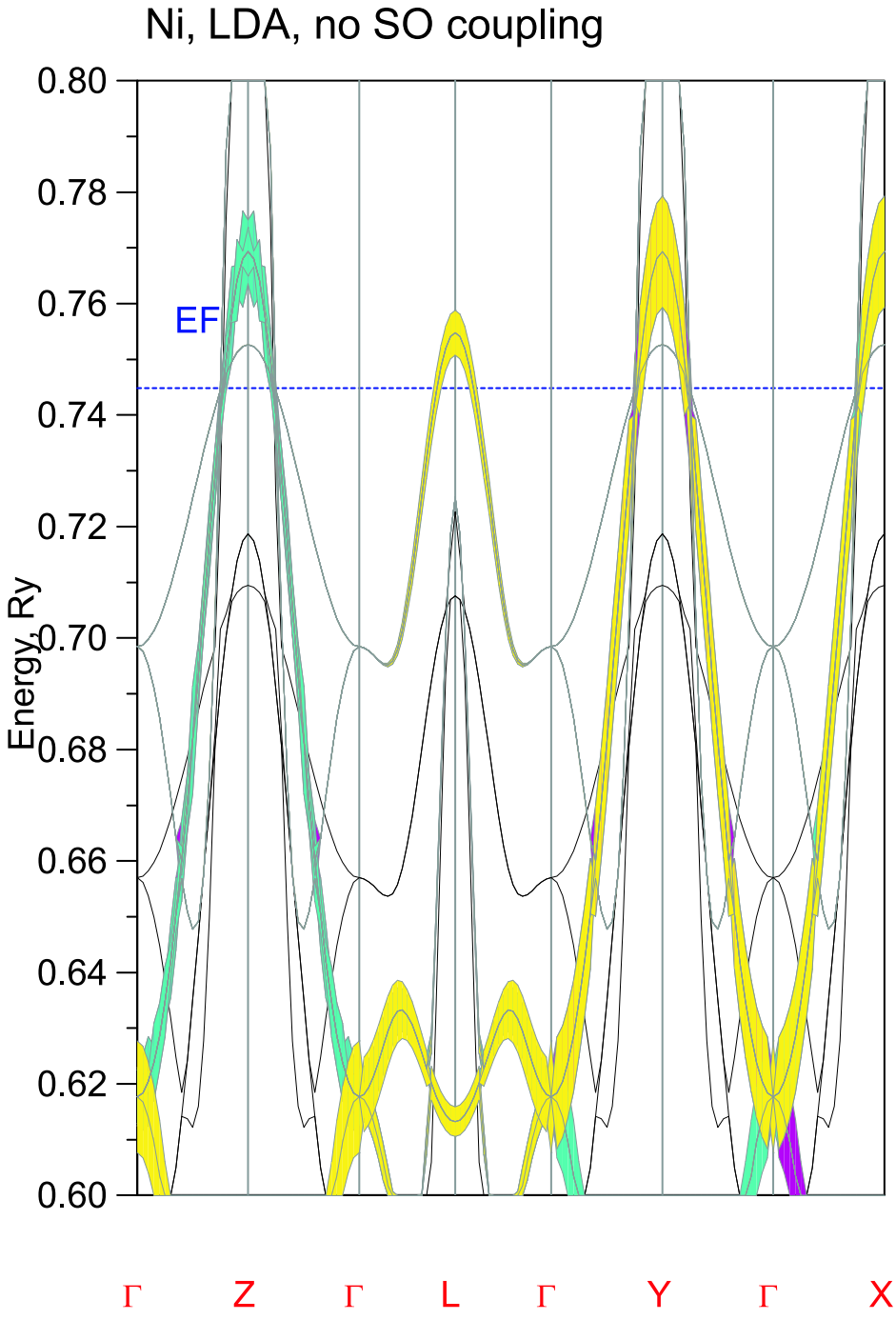

Figure A.1: Fat Band

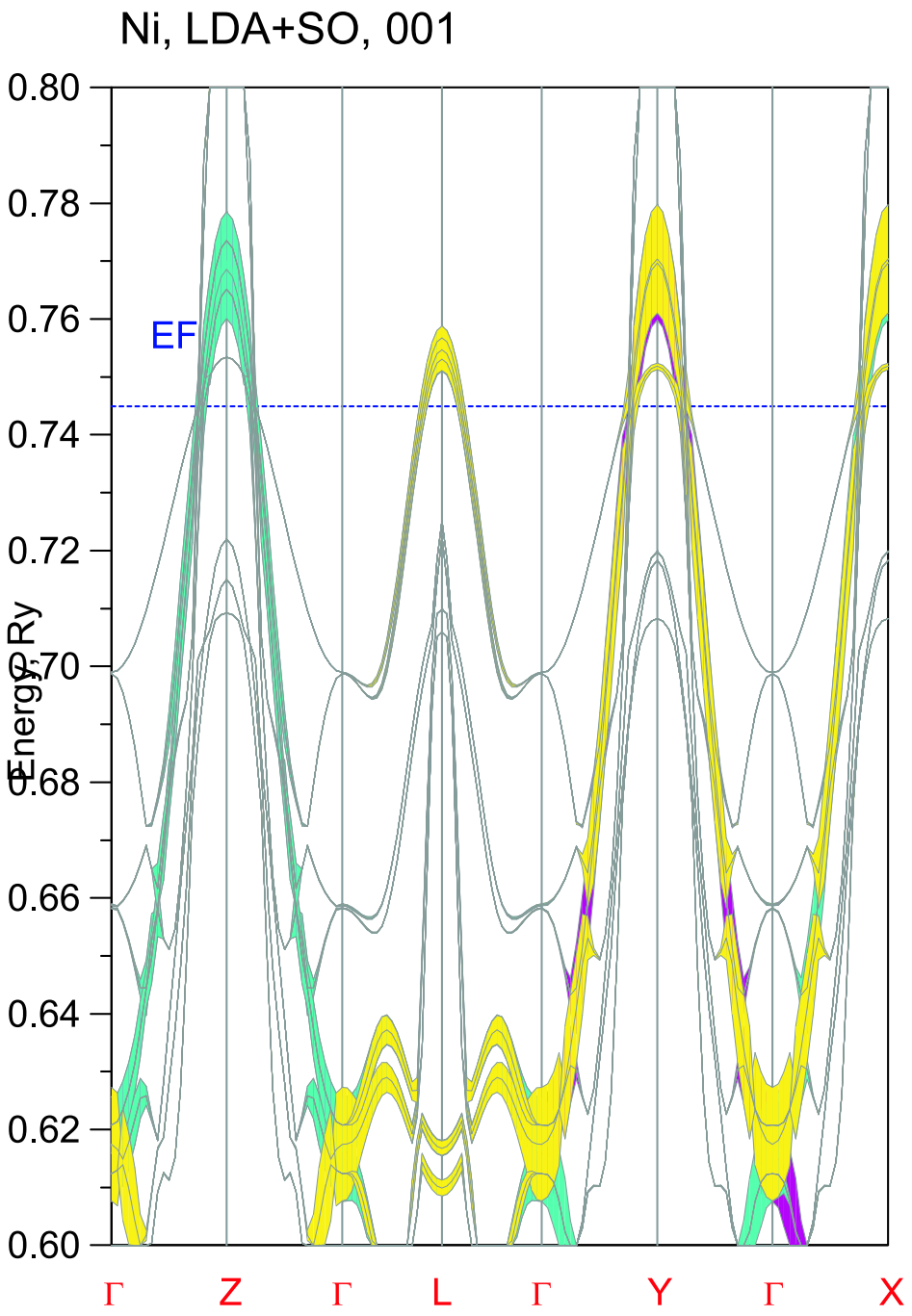

Figure A.2: Fat Band

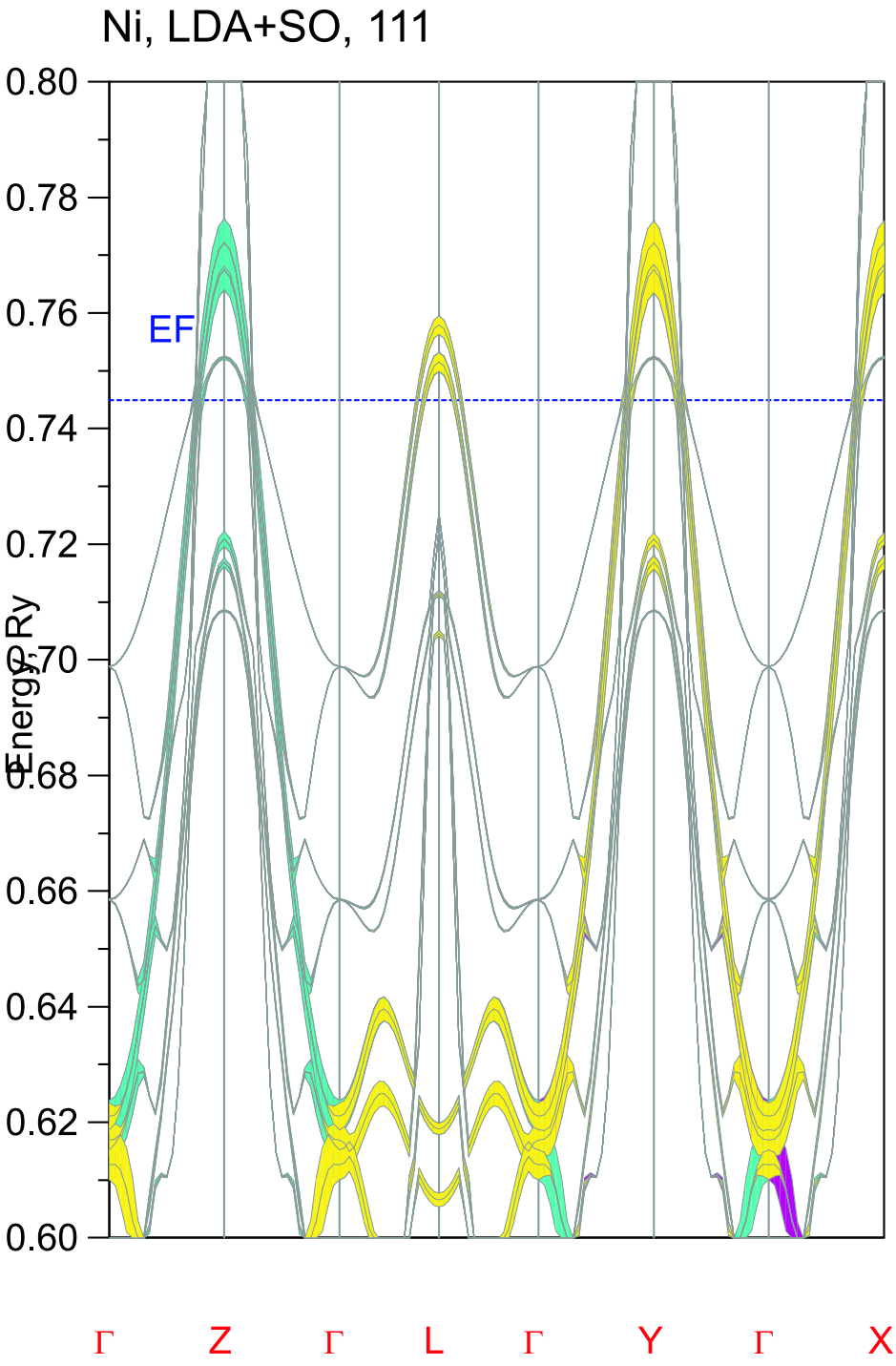

Figure A.3: Fat Band

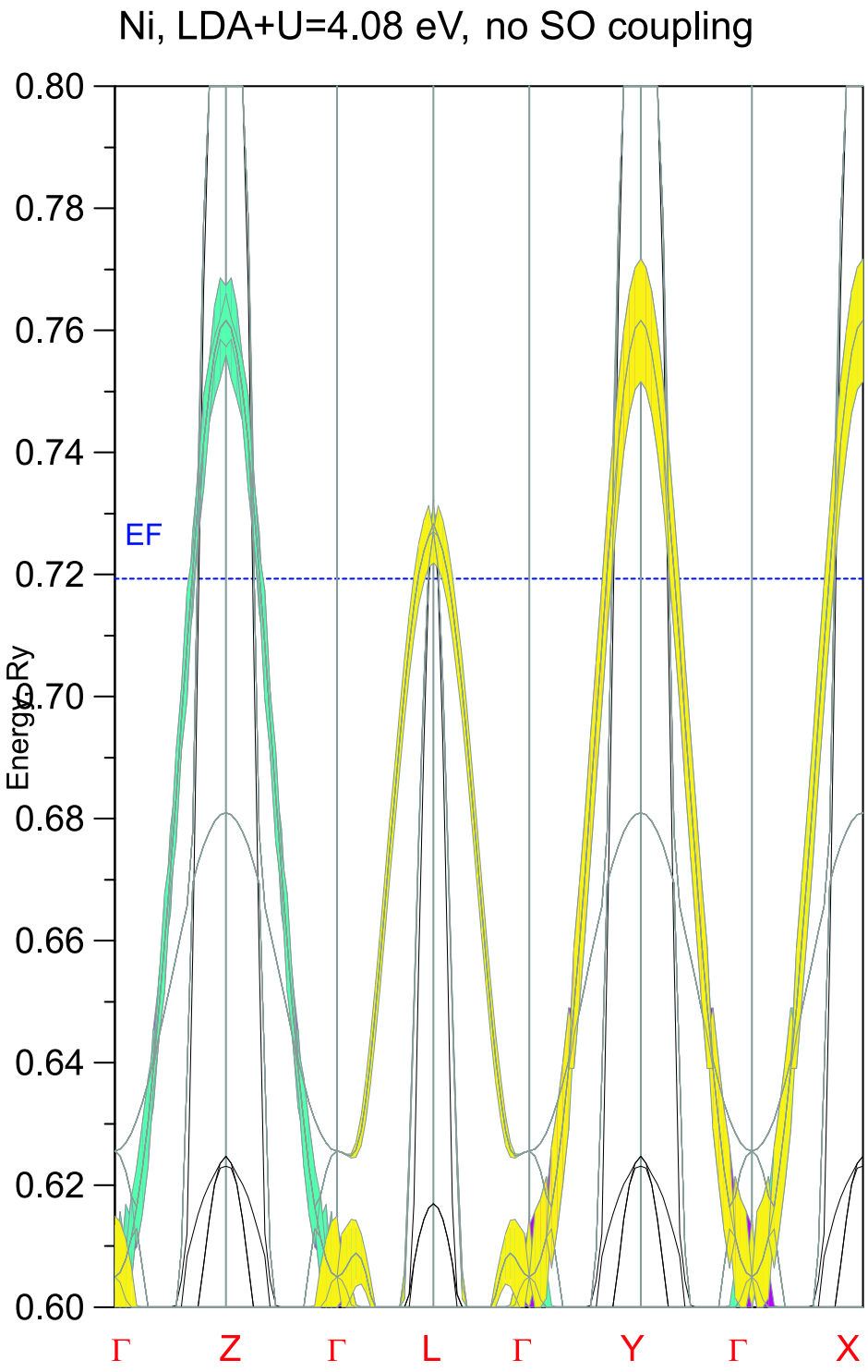

Figure A.4: Fat Band

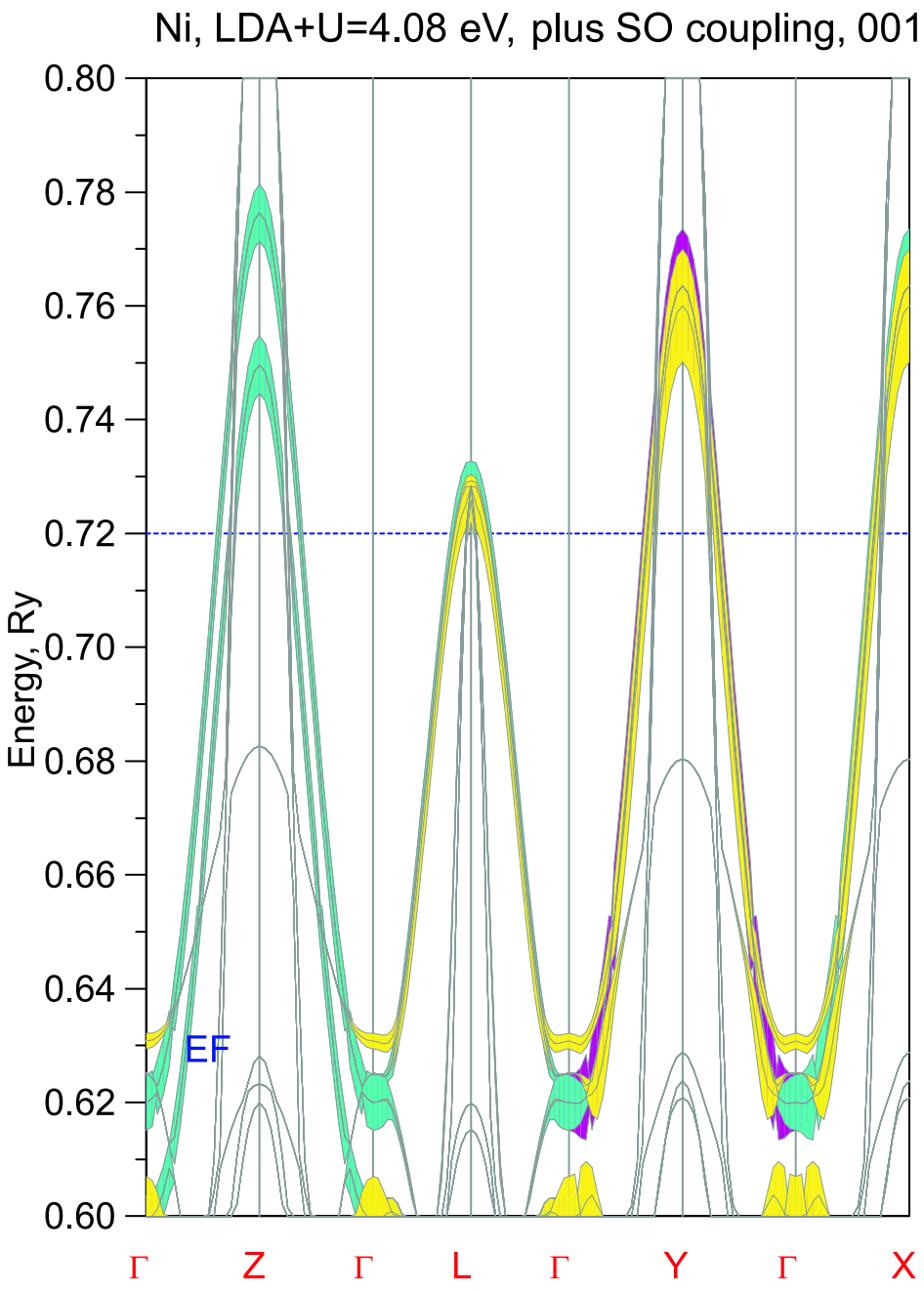

Figure A.5: Fat Band

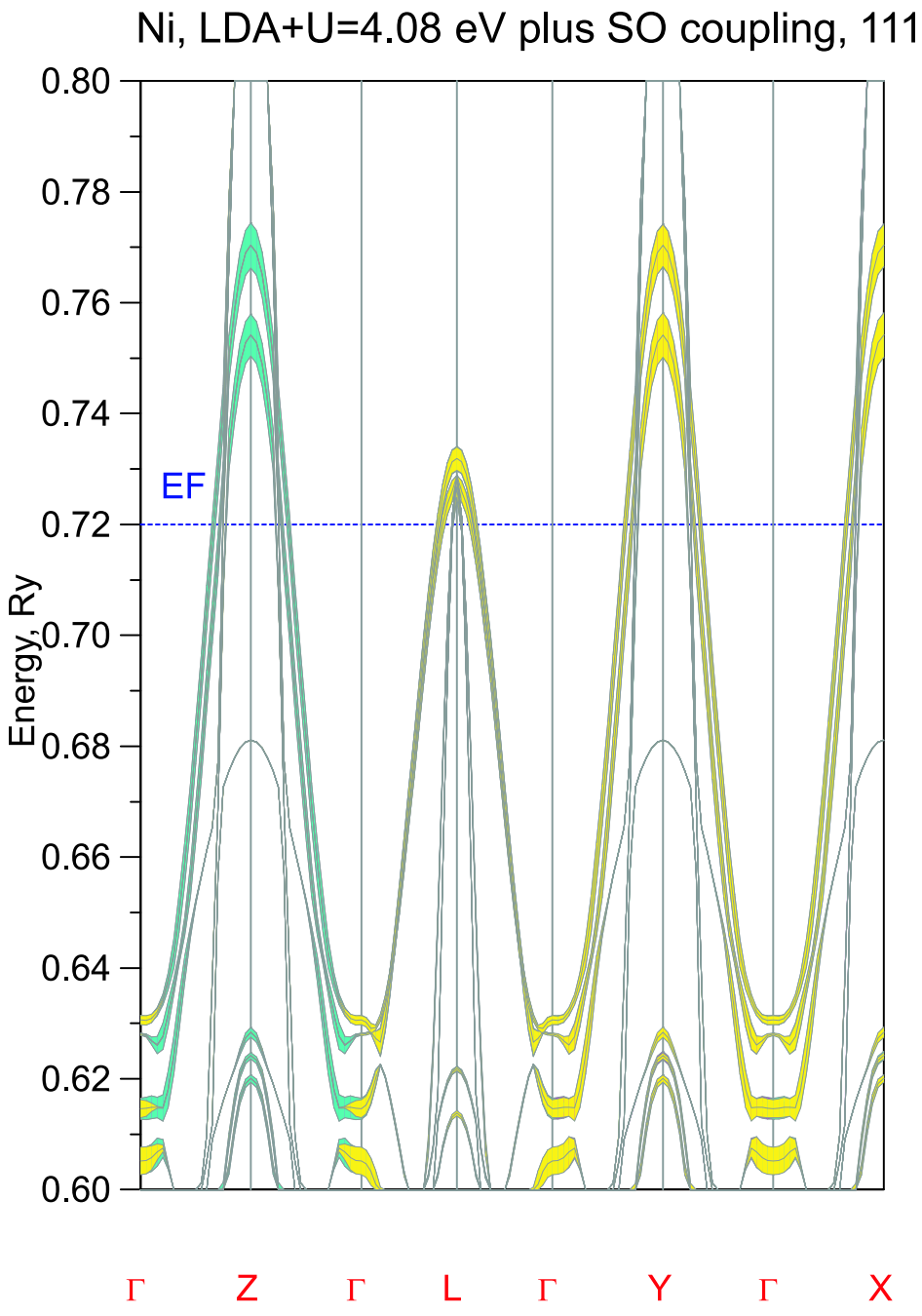

Figure A.6: Fat Band

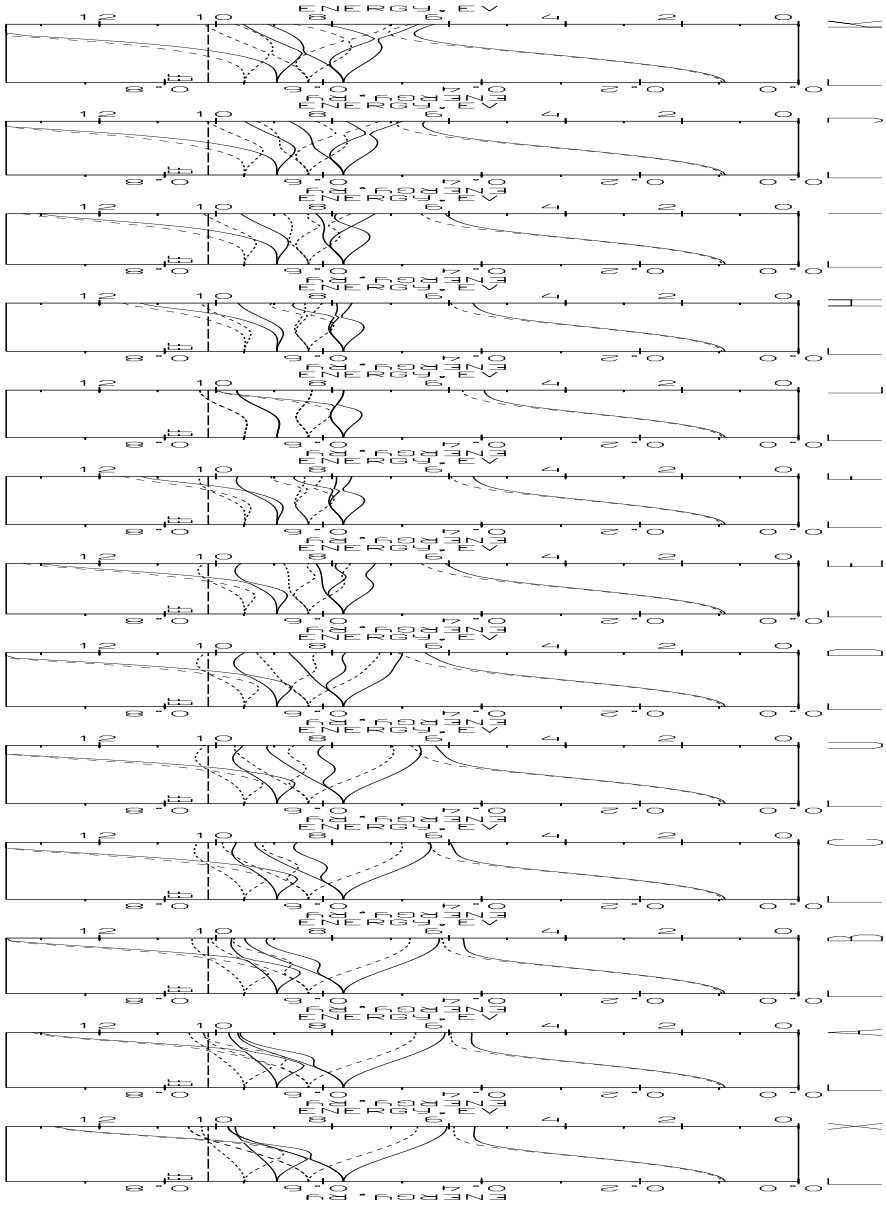

Figure A.7: The LDA Band structure. The direction of the wave vector moves from ΓX, through ΓU and ΓL, to ΓK. The other sheets are directions between them. The first sheet ΓX shows accidentally degenerate five bands on the fermi surface. From the nine sheets from ΓX to ΓL, the accidental DFSC states along a line on the fermi surface can be seen. From the three sheets from ΓX to ΓB, the two pockets X_2 and X_5 can be identified. From the three sheets from ΓF to ΓH, the L neck can be identified.

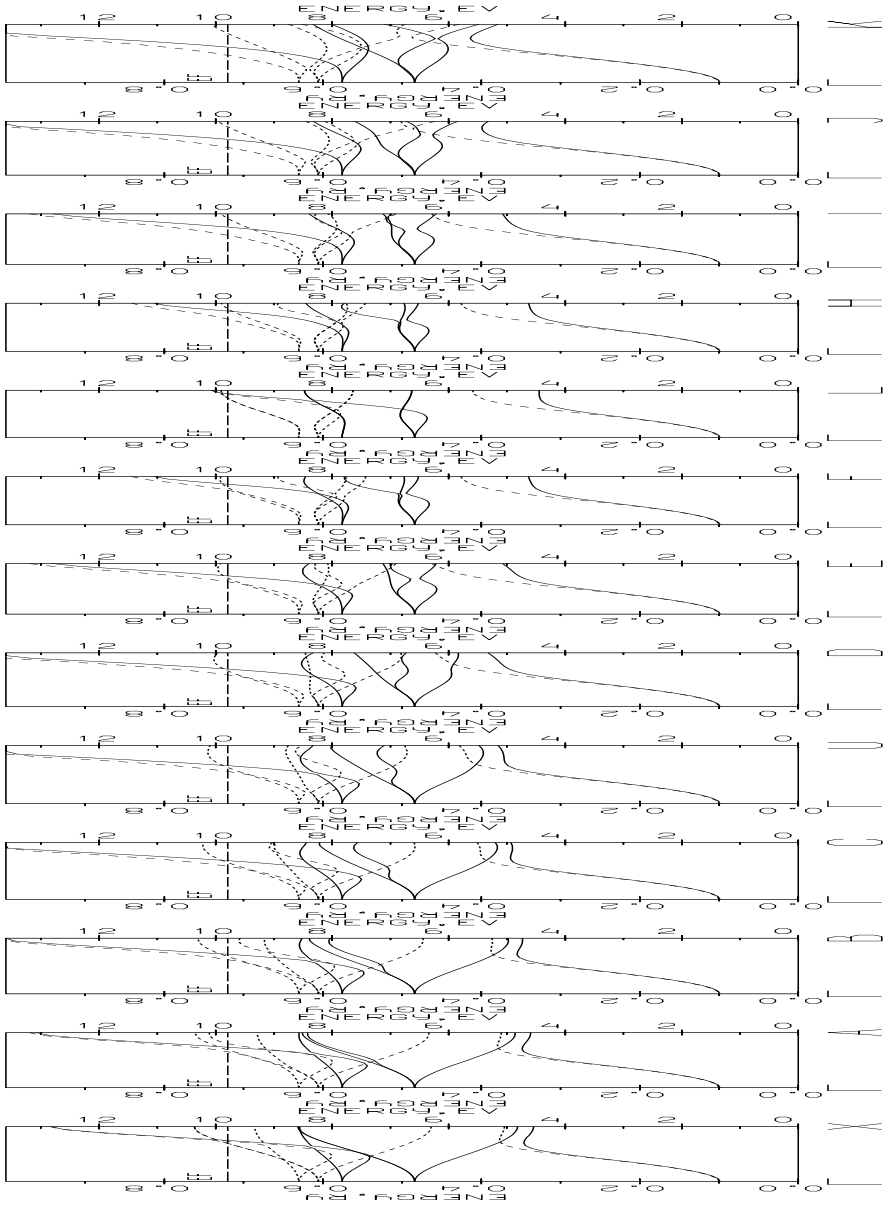

Figure A.8: The LDA+U Band structure. The direction of the wave vector moves from ΓX, through ΓU and ΓL, to ΓK. The other sheets are directions between them. The first sheet ΓX shows accidentally degenerate four bands off the fermi level. From the nine sheets from ΓX to ΓL, we see that the accidental DFSC states of LDA along a line on the fermi surface moves off the fermi level leaving no accidental degeneracy. From the three sheets from ΓX to ΓB, We see that the two X_2 pocket is removed.

Vita

Imseok Yang

1989 - 1995	**Attended Department of Physics, Seoul National University, Seoul, Korea.** Majors: Physics and Mathematics.
1993	**Bachelor of Science** in Physics.
1995	**Master of Science** in Physics.
1995 - present	**Graduate Studies in Physics, Rutgers University, New Brunswick, New Jersey.**
1996 - 2000	Teaching Assistant.
2000 - 2001	Graduate Assistant.
2001	**Ph.D. in Physics.**

Publications

2000	Impact of magnetic frustration on the Mott transition within a slave-boson mean-field theory I. Yang, E. Lange, and G. Kotliar, *Physical Review* , **41B** , 11919 (2000).
2001	Importance of Correlation Effects on Magnetic Anisotropy in Fe and Ni I. Yang, S. Savrasov, and G. Kotliar , submitted to *Physical Review Letters*.

References

[1] J. H. van Vleck, Phys. Rev. **52**, 1178 (1937).

[2] H. Brooks, Phys. Rev. **58**, 909 (1940).

[3] G. C. Fletcher, Proc. R. Soc. London **67A**, 505 (1954).

[4] J. C. Sloncewskij, J. Phys. Soc. Jpn. **17**, Suppl. B (1962).

[5] M. Asdente and M. Delitala, Phys. Rev. **163**, 497 (1967).

[6] E. I. Kondorskii and E. Straube, Sov. Phys.-JETP **36**, 188 (1973).

[7] N. Mori, Y. Fukuda, and T. Ukai, J. Phys. Soc. Jpn. **37**, 1263 (1974).

[8] P. Hohenberg and W. Kohn, Phys. Rev. **136**, 864 (1964).

[9] H. Eckardt, L. Fritsche, and J. Noffke, J. Phys. F **17**, 943 (1987).

[10] G. H. O. Daalderop, P. J. Kelly, and M. F. H. Schuurmans, Phys. Rev. B **41**, 11 919 (1990).

[11] A. Mackintosh and O. K. Andersen, in *Electronsat Fermi Surface*, edited by M. Springford (Cambridge University Press, Cambridge, England, 1980).

[12] J. Trygg, B. Johansson, O. Eriksson, and J. M. Willis, Phys. Rev. Lett. **75**, 2871 (1995).

[13] H. J. F. Jansen, J. Appl. Phys. **67**, 4555 (1990).

[14] G. Schneider, R. P. Erickson, and H. J. F. Jansen, J. Appl. Phys. **81**, 3869 (1997).

[15] A. Georges, G. Kotliar, W. Krauth, and M. Rozenberg, Rev. Mod. Phys. **68**, 13 (1996).

[16] *Strong Correlations in electronic structure calculations*, edited by V. I. Anisimov (Gordon and Breach Science Publishers, Amsterdam, 2000).

[17] L. Nordstrom and D. Singh, Phys. Rev. Lett. **76**, 4420 (1996).

[18] G. Unimin and W. Brenig, cond-mat/9905039 (1999).

[19] W. Kohn and L. J. Sham, Phys. Rev. **140**, 1133 (1965).

[20] O. Gunnarson and B. I. Lundqvist, Phys. Rev. B **13**, 4274 (1976).

[21] O. K. Andersen, Phys. Rev. B **12**, 3060 (1975).

[22] D. D. Koelling and B. N. Harmon, J. Phys. C: Solid State Phys. **10**, 3107 (1977).

[23] V. I. Anisimov, J. Zaanen, and O. K. Andersen, Phys. Rev. B **44**, 943 (1991).

[24] V. I. Anisimov, F. Aryastiawan, and A. I. Lichtenstein, J. Phys.: Condensed Matter **9**, 767 (1997).

[25] B.Brandow, Adv. Phys. **26**, 651 (1977).

[26] S. Savrasov and G. Kotliar, Phys. Rev. Lett. **84**, 3670 (2000).

[27] S. Halilov and *et al.*, Phys. Rev. B **57**, 9557 (1998).

[28] A. I. Liechtenstein, V. I. Anisimov, and J. Zaanen, Phys. Rev. B **12**, 3060 (1975).

[29] I. Y. Solovyev, A. I. Liechtenstein, and K. Terakura, Phys. Rev. Lett. **80**, 5758 (1999).

[30] M. R. Pederson and S. N. Khanna, Phys. Rev. **B 60**, 9566 (1999).

[31] S. Y. Savrasov, Phys. Rev. B **54**, 16470 (1996).

[32] S. Froyen, Phys. Rev. B **39**, 3168 (1989).

[33] M. Methfessel and A. T. Paxton, Phys. Rev. B **40**, 3616 (1989).

[34] M. B. Stearns, in *Landolt Börnstein New Series*, edited by K. H. Hellewege and O. Madelung (Springer-Verlag, Berlin, 1987), Vol. III.

[35] M. Katsenelson and A. Lichtenstein, J. Phys. Cond. Matt. **11**, 1037 (1999).

[36] M. Katsenelson and A. Lichtenstein, Phys. Rev. B **61**, 8906 (2000).

[37] C. S. Wang and J. Callaway, Phys. Rev. B **9**, 4897 (1973).

[38] N. F. Mott, Philos. Mag. **6**, 287 (1961).

[39] S. A. Carter *et al.*, Phys. Rev. B **48**, 16841 (1993).

[40] M. Imada, A. Fujimori, and Y. Tokura, Rev. Mod. Phys. **70**, 1039 (1998).

[41] F. Gautier *et al.*, Phys. Lett. A **53**, 31 (1975).

[42] S. Sudo, J. Magn. Magn. Mater. **114**, 57 (1992).

[43] W. F. Brinkman and T. M. Rice, Phys. Rev. B **2**, 4302 (1970).

[44] M. C. Gutzwiller, Phys. Rev. Lett. **10**, 159 (1963).

[45] M. C. Gutzwiller, Phys. Rev. **137**, A1726 (1965).

[46] G. Kotliar and A. E. Ruckenstein, Phys. Rev. Lett. **57**, 1362 (1986).

[47] G. Kotliar, cond-mat/9903188.

[48] R. Chitra and G. Kotliar, cond-mat/9811144.

[49] G. Kotliar and S. Y. Savrasov, To be published .

[50] M. J. Rozenberg, Phys. Rev. B **55**, R4885 (1997).

[51] S. Y. Savrasov, D. Villani, and G. Kotliar, Private Communication .

[52] R. Fresard and G. Kotliar, Phys. Rev. B **56**, 12909 (1997).

[53] J. Buenemann, W. Weber, and F. Gebhard, Phys. Rev. B **57**, 6896 (1998).

[54] W. Nolting and W. Borgiel, Phys. Rev. B **39**, 6962 (1989).

[55] M. Potthoff, T. Wegnerand, and W. Nolting, Phys. Rev. B **55**, 16132 (1997).